SDC
SOLENOIDAL DETECTOR NOTES

SDC MODULAR STRAW OUTER TRACKING SYSTEM CONCEPTUAL DESIGN REPORT

November 7, 1991

B. Adrian, D. Alexander, B. Corliss, F. Ells, E. Erdos, W.T. Ford, D. Johnson, M. Lohner, P. Rankin, G. Schultz and J.G. Smith
University of Colorado

R. Foster. G. Hanson, F. Luehring, B. Martin, H. Ogren, D.R. Rust and E. Wente
Indiana University

Y. Arai
Kek

J.W. Chapman, A. Dunn and J. Mann
University of Michigan

J. Mayhall, T. Ryan and J. Shaffer
Oak Ridge National Laboratory

H.M. Newcomer, R. Van Berg and H.H. Williams
University of Pennsylvania

R.L. Swensrud and D.T. Hackworth
Westinghouse Science and Technology Center

IUHEE-91-10
SDC-91-00125
November 7, 1991

SDC

MODULAR STRAW

OUTER TRACKING SYSTEM

CONCEPTUAL DESIGN REPORT

B. Adrian, D. Alexander, B. Corliss, F. Ells, E. Erdos, W. T. Ford, D. Johnson, M. Lohner, P. Rankin, G. Schultz and J. G. Smith
University of Colorado

R. Foster, G. Hanson, F. Luehring, B. Martin, H. Ogren, D. R. Rust and E. Wente
Indiana University

Y. Arai
KEK

J. W. Chapman, A. Dunn and J. Mann
University of Michigan

J. Mayhall, T. Ryan and J. Shaffer
Oak Ridge National Laboratory

H. M. Newcomer, R. Van Berg and H. H. Williams
University of Pennsylvania

R. L. Swensrud and D. T. Hackworth
Westinghouse Science and Technology Center

DRAFT

TABLE OF CONTENTS

I. EXECUTIVE SUMMARY

We present the conceptual design of the straw module outer tracking system for the SDC detector. The outer barrel tracking system covers pseudorapidity $|\eta| < 1.6$ with all five superlayers, although the lengths of the superlayers will be adjusted to accommodate the intermediate angle tracking system. In conjunction with the silicon inner tracker and the intermediate angle tracker, this combined tracking system should satisfy the requirements for the SDC tracking system up to and above the SSC design luminosity.

The tracking system conceptual design is given in Section II.2. The outer tracking system is composed of five superlayers of straw tube modules. The modules consist of about two hundred straws enclosed in a carbon fiber composite outer shell. Each module is a complete drift chamber with its own electronics, high voltage and gas connections. Two axial superlayers are used for the high-p_T track segment trigger. A third inner axial superlayer is used primarily for pattern recognition in linking to the silicon tracking system. The coordinate along the beam direction is measured by two small-angle stereo superlayers. It might be possible to include the outer stereo superlayer in the trigger, although this has not yet been studied.

The tracking system requirements are summarized in Section II.1. The physics requirements that the tracking system must meet are rather stringent given the need to reduce costs. The tracking system described in this report should be able to meet the alignment requirements needed to meet the physics goals, as discussed in Sections IV and VI. We have paid careful attention to minimizing the material in the tracking volume. The conceptual design described here has only 3.5% X_0 at 90° incidence. However, the silicon system and beam pipe contribute about 8% X_0, and some reduction may need to be made to reduce the effects of electron bremsstrahlung, which is the most serious problem. The lifetime, rate and occupancy requirements, reviewed in Section II.1, can be met, as discussed in Section III.1. Simulations of the performance of the tracking system, although not complete at this time, are given in Section II.3.

We have made considerable progress during the past year in straw module design and construction, as described in Section IV. The module shell is composed of a carbon fiber composite and foam laminate, which is very rigid with low mass. The first one-meter

shell of this design is being built now, and a four-meter shell will be completed by the end of this year. Six short modules of an earlier design, containing 64 straws, were built and are now being tested at several institutions.

The modules are supported on cylinders of a design similar to the module shells, so that they too have excellent structural properties with low material. Section VI presents the tracking system support structure and assembly procedures for the tracking system. The cylinders are supported by a carbon composite space frame. Results of finite element analyses are given.

The conceptual designs of the front end and trigger electronics are summarized from the individual conceptual design reports in Section V.

Integration of the tracking system with the rest of the detector is described in Section VII. The items discussed are the material in the tracking system design, access and maintenance, risk assessment, safety, and utilities.

The schedule for construction and checkout of the tracking system and a not-yet-final cost estimate are presented in Section VIII.

II. TRACKING SYSTEM DESIGN OVERVIEW

II.1. TRACKING SYSTEM REQUIREMENTS

II.1.1. Summary of Physics Requirements

The tracking system referred to in this report comprises the components of the SDC detector inside the volume defined by the solenoid coil and the faces of the endcap calorimeter, whose purpose is to measure the trajectories of charged particles from the collision. Bending of these particles by the solenoidal magnetic field is directly related to their momentum component transverse to the field direction. Thus the measured three-dimensional trajectories may be converted to momentum vectors for the charged particles, with assignment of the sign of electric charge.

The ideal tracking detector would cover the whole sphere centered on the interaction point. It would sample the tracks nearly continuously along their path length, revealing all particle decays and determining momenta with high precision at all momentum values up to the kinetic limit. It would introduce very little material, so that scattering, energy loss, and interactions of the particles would be negligible.

In the context of the entire SDC detector, the tracking system is to be used in conjunction with the electromagnetic calorimeter to identify electrons, and with tracking detectors outside the hadron calorimeter (muon system) to detect muons. It is also expected to contribute information in real time toward the formation of the Level 1 and Level 2 triggers for the data acquisition.

Thus the tracking system enters into the detection of isolated and non-isolated muons and electrons, low-multiplicity decays of heavy gauge bosons, τ's, J/ψ's, etc., and (as a veto detector) photons. It distinguishes tracks from secondary vertices to help identify b-quark jets, and measures jet multiplicities. It gives a detailed picture of each event that may provide critical insight for the unexpected. It is called upon to provide precisely momentum analyzed electron tracks for calibration of the electromagnetic calorimeter, and to provide a trigger sensitive to charged tracks above a well-defined p_T threshold.

Known examples of important potential physics processes include rare low-multiplicity reactions such as Higgs production and decay $H^0 \rightarrow Z^0 Z^0 \rightarrow l^+ l^- l'^+ l'^-$ or heavy gauge boson $Z' \rightarrow l^+ l^-$. More complicated events will be those involving t-quark production and decay, where the final state may include b-quark jets with detached vertices, isolated W-decay leptons, non-isolated b-decay leptons, and W^- and H^+-decay jets.

Based upon an analysis of the properties of these and other reactions, discussed in detail in the Tracking Design Requirements document,[1] we deduce the following specifications:

(1) $|\eta|$ coverage out to $|\eta| \leq 2.5$, implying $H^0 \rightarrow 4$ charged lepton geometrical efficiency $\geq 60\%$ for $m_H \geq 200$ GeV.

(2) Reconstruction efficiency $\geq 90\%$ (for $|\eta| \leq 2.5$) for each lepton from $H^0 \rightarrow 4$ charged leptons having $p_T \geq 5$ GeV, at design luminosity (exclusive of lepton identification and trigger cuts), but assuming twice the occupancy calculated by Monte Carlo for $pp \rightarrow X$. Number of false tracks of $p_T \geq 5$ GeV to be ≤ 0.1 per event of this class.

(3) Reconstruction efficiency for same as in (2) $\geq 75\%$ at $10 \times$ design luminosity.

(4) Reconstructed (as opposed to parametric) vertex constrained momentum resolution of $\sigma_{p_T}/p_T^2 \leq 20\%$ (100%) TeV^{-1} for $|\eta| \leq (\geq)$ 1.8 for isolated charged tracks.

(5) Efficiency contribution from tracking to lepton identification of $\geq 85\%$ for electrons with $p_T \geq 10$ GeV and $\geq 95\%$ for muons with $p_T \geq 10$ GeV.

(6) Position resolution at the calorimeter of ≤ 1 mm in $r\phi$ or z (want error $\leq \sigma/2$ of calorimeter position accuracy).

(7) Position resolution relative to the muon system of 100 μm in $r\phi$ and 1 mm in z.

(8) Jet charged multiplicity measurement within 15% for jets up to $p_T = 1$ TeV.

(9) B single tagging efficiency $\geq 50\%$ for 125 GeV $\leq m_{top} \leq$ 250 GeV, with $\leq 10\%$ purity. .

(10) First level trigger with momentum resolution $\sigma_{p_T}/p_T^2 \leq 10$ TeV^{-1} -- implies a 10% error for a 10 GeV lepton.

(11) Second-level trigger with momentum resolution $\sigma_{p_T}/p_T^2 = 5$ TeV^{-1}. Gives a 20% error for a 40 GeV lepton for triggering on $Z \rightarrow e^+ e^-$, $W \rightarrow e \nu$ -- needed for calorimeter calibration.

(12) Discovery potential -- hard to quantify. In general, want maximum capabilities from detector. Based on history, highest priority (other than isolated lepton of Higgs case above) would be reconstruction and impact parameter measurement of leptons within jets up to the largest jet p_T possible (at least $\geq$ 500 GeV). Desired reconstruction efficiency $\geq 50\%$.

(13) Measurement of jet fragmentation at modest luminosity for QCD studies and for modelling backgrounds from jets.

(14) Survivability at standard L for $\geq$ 10 years.

(15) Allows a natural path for upgrading to a system with survivability of $\geq$ 10 years at 10 $\times$ standard L with emphasis (e.g., momentum resolution, pattern recognition, isolated track efficiency) to be decided based on what is learned during initial running.

II.1.2. Alignment

Alignment requirements for the SDC tracking system have been discussed by Seiden[2] and Ogren.[3] The maximum uncorrelated systematic positioning errors of the inner and outer tracking systems were given by Seiden as:

Silicon:	Circumferential	5 μm
	Radial	80 μm
	Longitudinal	250 μm
Straws:	Circumferential	35 μm
	Radial	1200 μm
	Longitudinal	250 μm.

The maximum correlated alignment errors for the inner relative to the outer tracking systems were:

Rotational alignment:	10^{-5} radians
Radial alignment:	600 μm
Longitudinal coordinate:	250 μm
Displacement of detector centroids:	15 μm.

Ogren examined these requirements in terms of support structure stability and straw placement. In terms of a modular design, there are three elements to wire placement errors:

1. Displacement of the wires relative to the modules (it is the location of the wires that is crucial, not the location of the straw walls).
2. Positioning errors of the modules relative to the support structure.
3. Alignment of the support structure.

It has been shown that wires can be positioned within modules (short modules, not 4-meter-long modules yet) to about 30 μm in both coordinates transverse to the long dimension of the module.[4] The intrinsic wire resolution is about 100 μm. The superlayer error due to the wires is then 43 μm for six wires in a superlayer. The error in module position is due to placement errors at the attachment points on the support structure

(assumed to be 80 cm apart) and straightness of the module between the attachment points. Errors in each of these quantities of less than 50 μm should be achievable. The total superlayer error, including wire and module positioning, should then conservatively be less than 83 μm, which is the same value used by Seiden for the statistical error of each straw superlayer measurement. Systematic errors due to alignment of the support structure need to be kept small relative to this value. The most difficult requirements to meet are those for relative rotational alignment (10^{-5} radians) and displacement of detector centroids (15 μm). These will have to be monitored continuously.

II.1.3. Material in Tracking Volume

The impact of material in the SDC tracking volume has been studied by the Task Force on Impact of Material in Tracking Volume.[5] The Report of this Task Force gave an estimate of the amount of material in a model SDC tracking system consisting of:

1. Contribution from (typical) internal bremsstrahlung

2. Thin but realistic beam pipe

3. Descoped silicon inner tracking system

4. Axial outer tracking system (i.e., no intermediate tracking for electrons).

The SDC tracking system contains more material than previous conventional tracking systems because the segmentation needed to cope with the high rates requires more tracking elements and thus more material, and because the physics dictates coverage over the rapidity interval $|\eta| < 2.5$, which means that some mechanical support material must be included in the tracking volume. The material in the simple model studied in this Report is listed in Table II.1. Most of the material is located in the inner tracking system. The outer tracking system that we will describe will in fact have less material at $\eta \approx 0$ than this simple model. The most serious requirements on material in the outer tracking system occur at the ends, or wherever there is a wall or connection to break the basic axial structure.

Table II.1. Material Model for SDC Tracking System

	Radius (cm)	$\|\eta\|$ Range	Thickness (X_0)
Internal Bremsstrahlung	0	all	2.5%
Beam pipe	5	all	0.2%
Silicon tracker	10–45	<1	5.0%/sin θ
	"	>1	5.0%/cosθ
	60	all	0.5%/sin θ
Outer tracker	70–165	<1.5	6.0%/sin θ
Average		<2.5	17-18%

The issues are:

1. Tracking. The increase in the outer tracker straw tube occupancy due to interactions in the inner silicon tracker and beam pipe is a small effect and should not degrade tracking in the outer tracking system (see Section II.3). In simulation studies completed so far, track reconstruction efficiency is not degraded by the nominal amount of material. Multiple scattering for low-p_T particles is not a problem. The most serious problem for tracking is due to bremsstrahlung of electrons in the material, mainly in the silicon inner tracker. This results in a change in curvature for the electrons as measured in the outer tracking system and subsequent degradation of the momentum resolution.

2. Triggering. Electron bremsstrahlung will put some high-p_T electrons below the track segment trigger threshold. Multiple scattering would have a similar effect for other particles. In addition, bremsstrahlung will alter the transverse shower profiles in the calorimeter. Pair production from photons will result in extra high-p_T electrons that will pass the Level 1 electron trigger and may result in a loss of high-p_T photons at the trigger level. Studies done by the Task Force showed that if the material before the trigger superlayers was less than 10% X_0, the track trigger efficiency for electrons was > 90% for electrons with p_T > twice the trigger threshold. Multiple scattering in the tracking system was found not to be an issue for the trigger. The rates for isolated electrons from QCD prompt photons, relative to $W \rightarrow e^{\pm}$, $top \rightarrow e^{\pm}$, etc., are expected to be tolerable with 10% X_0 effective radiator in the silicon detector.

3. Electron/photon identification. Electron identification is affected by bremsstrahlung in the material in the tracking volume, as described above. E/p and isolation cuts are very sensitive to the amount of material. The momentum will often be measured to be significantly less than the calorimeter energy because the radiated photon is included in the calorimetric measurement. Isolation can be affected by extra clusters in the calorimeter from the radiated photon. For isolation, the electron efficiency is reduced at low p_T (~ 10 GeV) due to bremsstrahlung occurring at or near the beam pipe. The studies suggested that the material in the silicon tracker should not be greater than ~ 5% X_0. For track-shower match, with ~ 11.5% X_0 at $\eta \approx 0$, approximately 94% of electrons pass a "tight" track-shower cut at shower maximum (10 mm in the bend plane and 5 mm in the non-bend plane). The E/p cut is probably the most problematic. E/p efficiencies ~ 95% for $E/p < 1.5$ were obtained for a silicon system with 6.8% X_0 at $\eta \approx 0$. Highest efficiencies were obtained using only the inner tracking system for the momentum measurement, since the inner tracking system contains most of the material, which degrades the momentum resolution in the outer tracking system.

4. Electron/photon energy measurement. The calorimeter will be calibrated using electrons from Z decays. The material in the tracking volume does not seriously impair the calibration of the calorimeter. The amount of material preceding each tower must be known to within 5% X_0 to establish the correct peak value for E/p. The calorimeter is calibrated by ensuring that the average E/p is correct for each tower individually. The number of electrons required increases exponentially with the amount of material, but remains at a reasonable level (~ one month at SSC design luminosity for ~ 16% X_0 in the tracking system) for up to 0.5 X_0, the maximum thickness in the model considered.

II.1.4. Chamber Occupancy, Rates and Lifetime

Limitations placed on wire chambers by radiation damage and rate requirements are one of the central concerns in tracking at the SSC. The design luminosity of the SSC is 10^{33} cm^{-2} s^{-1}, and higher values are expected. The inelastic cross section at the SSC is expected to be about 100 mb, which gives an interaction rate of 10^8 per second at the design luminosity. An added problem is the small bunch spacing of 16 ns. The last two numbers give 1.6 interactions per bunch crossing, again, at the design luminosity. At a luminosity of 10^{34} cm^{-2} s^{-1}, we would have to deal with 16 interactions per crossing. Most of these interactions are not of interest for physics studies. Instead, they contribute a

background of minimum bias or low-p_T hard scattering events, in which the average charged particle multiplicity per unit of rapidity is 7.5, over the pseudorapidity range $|\eta| < 6$.[6] Figure II.1 shows the charged particle flux and resulting annual radiation dose as a function of perpendicular distance from the beam for standard SSC operating conditions. At a distance of about 70 cm from the beam, the radiation dose is about 10^4 rads/year at the SSC design luminosity; this decreases by about an order of magnitude at a distance of 170 cm. For ten years at a luminosity of 10^{34} cm^{-2} s^{-1}, the dose would be about a Mrad at the smallest radius for the outer tracking system. In addition, there are contributions from photons and neutrons.

The charged particles from "minimum bias" background events produce ionization and signals in wire tracking devices. The amount of current drawn by a wire is proportional to the height and width of the drift cell, the gas gain, the luminosity, and the length of the wire, and is inversely proportional to the square of the radius. At a gas gain of 2×10^4 in a 4 mm symmetrical cell covering half the tracking length at a radius of 70 cm, the current draw would be about 0.5 μA.[7] This number includes the effects of looping tracks in the magnetic field and photon conversions in the material of the tracking system. The collected charge over five years at design luminosity would be about 0.1 C/cm. The current draw per wire and the charge collected decrease substantially for the same size cell at larger radii. Chamber lifetimes of about 1.0 C/cm have been measured in clean laboratory conditions. Aging and radiation damage studies are discussed in more detail in Section III.2.

Another effect of the minimum bias background is a large hit rate per wire. The hit rate per wire is proportional to the rapidity coverage of the wire, the width of the cell, and the number of interactions per second, and inversely proportional to the distance from the beam. Hit rates in the range of several Mhz at design luminosity will occur for wires at radii less than about 120 cm, with rates less than 1 Mhz at larger radii.

A well-known limitation for wire chambers at the SSC is occupancy - the fraction of bunch crossings in which a wire has a hit due to the minimum bias background. This is a serious problem for wire chambers as envisaged for the SSC because a hit causes a small cell to be dead for the width of the pulse and until the electronics has recovered sufficiently to accept another hit. In addition, even with fast gases (drift velocity of about 100 μm/ns), the resolving time of a cell is longer than the time between bunch crossings. This latter effect results in occupancy due to charged particles from earlier bunch crossings. The first

guess is that occupancy at the level of 10% is reasonable, provided the tracking system has enough redundancy. However, underestimates of the occupancy at the level of a factor of three or more could result in a poorly performing tracking system. Estimates of occupancy from computer simulations and their effects on tracking are discussed in Section II.3.

II.2. TRACKING SYSTEM OVERVIEW

II.2.1. Outer Tracking System Concept

The central outer tracking system is composed of cylindrically concentric superlayers of straw tubes. Each superlayer is made up of 6-8 layers of straw tubes. The straw tubes are arranged in modules of approximately trapezoidal cross section, each containing about 200 straws. Each straw module is essentially an independent tracking chamber with its own gas and power connections and its own electronics. The superlayers have straws running either parallel to the beam direction (axial superlayers) or at a small angle to this direction (stereo superlayers) in order to measure the coordinate (z) along the wire.

Although an independent outer tracking system would probably need more superlayers, the SDC outer tracker discussed in this Report is part of an integrated system including a silicon inner tracker. The minimum number of superlayers needed in the outer tracking system can be determined from the following requirements:

1. The outer tracking system must provide a high-p_T track segment trigger

2. The outer tracking system, in conjunction with the silicon inner tracking system, must meet the requirements for momentum measurement

3. There must be sufficient pattern recognition capability to link track segments in the inner and outer tracking systems

4. The outer tracking system must provide measurements of the coordinate along the beam direction (z), in conjunction with the silicon tracker.

In order to provide the high-p_T track segment trigger, we need at least one axial superlayer at the outer radius. At higher luminosities we may require two axial superlayers for the trigger. There is also the possibility of including one of the stereo superlayers so as to obtain the z-coordinate for a high-p_T track in the trigger. *Therefore we have placed two axial superlayers at large radius for the trigger.*

Momentum measurement is accomplished by using both the inner and outer tracking systems in an integrated manner. In order to do this, track segments have to be linked between the two systems. Indications from simulation studies are that we will need an axial superlayer relatively close to the silicon tracker. This inner superlayer might be upgraded to scintillating fibers at high luminosity. *We have therefore placed a third axial superlayer at a radius between 70 cm and 1 m.*

The minimum number of stereo superlayers is two, one with wires running at about +3° to the beam direction, the other at -3°. The best choice would probably be to have both of them at large radius so as to obtain the best resolution in angle and the best coordinate measurement for linking to the calorimeter and muon system. However, some information about the z-coordinate may prove useful in linking to the silicon tracker, since it also provides z information. The exact location of this superlayer is being determined using simulation studies. The stereo superlayer at the larger radius could be used to obtain z information for the high-p_T track segment trigger. *There are thus two stereo superlayers, one between the outer two axial superlayers and one at an intermediate radius.*

The conclusion is that *five superlayers* would provide a minimal system with reasonable performance and essentially no redundancy, especially for the z measurement.

II.2.2. Proposed Outer Tracking System Design

Table II.2 lists the components of the proposed outer tracking system, which consists of five superlayers of straw tubes, three axial superlayers and two stereo. The superlayers are divided in half at $z \approx 0$. The design is also shown in Fig. II.2. The three outer superlayers are placed as in the engineering baseline design,[8] which was defined to provide a basis for earlier mechanical engineering studies. The inner superlayer is placed at about 70 cm radius, consistent with the envelope for the outer tracking system. The second superlayer is equidistant from the inner superlayer and the three outer superlayers. The radial positions of the superlayers and the exact arrangement (axial *vs.* stereo) are rather

arbitrary here and are the subject of ongoing simulation studies. The lengths of the superlayers are in agreement with the η coverage as in the engineering baseline design and would be adjusted to accommodate the intermediate angle tracking system. The two outer axial superlayers are trigger layers and have 8 straws per superlayer. The other superlayers have 6 straws per superlayer. The amount of material in the outer tracking system at 90° is 3.5% of a radiation length including all supports (but not including the last superlayer). (A detailed description of the material in the tracking volume is given in Section VII.1.) There are a total of 1.30×10^5 straws.

Table II.2. Central Outer Tracker Design

Superlayer	Mean Radius (m)	Straws/Layer	Modules	Layers/Superlayer	z_{max} (m)	Stereo Angle (°)
1	0.7096	1060	80	6	2.00	0
2	1.0670	1590	120	6	3.20	+3
3	1.3510	2014	152	8 (trigger)	3.90	0
4	1.4877	2226	168	6	3.95	-3
5	1.6315	2438	184	8 (trigger)	3.95	0

II.2.3. Upgrades/Staging

The central outer tracking system design presented here forms, with the silicon inner tracker, a complete tracking system that should perform well at luminosities up to at least the design value. However, scintillating fibers offer an advantage at high luminosity because of their finer segmentation and therefore lower occupancy. An affordable all-fiber outer tracker may not have enough layers for adequate pattern recognition and stereo measurement. Since fibers introduce more material per superlayer, they are best used where really needed in regions of high occupancy for straws at high luminosity. A system of both fibers and straws could offer some advantages, but the cost would be higher than for an all-straw system because of carrying out both technologies.

We would like to maintain the capability of upgrading to scintillating fibers for the inner superlayer(s) if needed for high luminosity, either later in the design of the detector so that we could have scintillating fibers at turn-on, or a few years after turn-on. We envision

a "vector" scintillating fiber superlayer, with both axial and stereo measurements. It is expected that it will take two to three years for the SSC to reach design luminosity. Meanwhile straw inner superlayers should perform well. It seems likely that the SSC will reach a maximum luminosity of $\sim 5 \times 10^{33}$ cm^{-2} s^{-1} rather than 10^{34} cm^{-2} s^{-1}, and in any case that will take several years.

II.3. SIMULATION RESULTS

II.3.1. Introduction

A detailed GEANT-based model of the central region straw tube tracking system has been developed. This simulation effort was initially made using GEANT only, but now the GEANT models have been successfully incorporated into the SDC standard simulation/analysis program, SDCSIM. SDCSIM is intended to provide an organizing superstructure for both the GEANT simulation and the online/offline analysis code for the SDC detector. Fixed versions of SDCSIM are distributed to the entire collaboration via electronic computer networks to insure that a detailed simulation of the entire detector is rapidly available to the entire collaboration. The simulation now incorporates the following details: a model of the central straw tube tracker, a model of the silicon inner tracker, a model of the adjacent parts of the SDC detector (beam pipe and magnet coil), a description of the cylindrical carbon support structures for each superlayer, an accurate model of the materials within the straw tube system, properly distributed background (minimum bias) events, stereo detector layers, and a detailed model of the readout of the detector based on the timing of hits within the system. Preliminary occupancy, segment finding, and pattern recognition studies have been made in the central region using the improved simulation. Much progress has been made to integrate the outer barrel tracker with the inner silicon tracking system and to study pattern recognition algorithms that take advantage of the integrated tracking system. We are now studying the descoping issues related to the central tracker particularly in the context of a combined silicon-straw system. The straw tube simulation has also been used as the basis for studies of the first level straw tube trigger, as described in Section V.9.

II.3.2. Details of the Simulation

The simulation of the overall SDC detector is now run as part of SDCSIM, and consequently we automatically have access to the geometries of parts of the detector located near the central tracking system: the beam pipe, the silicon tracker, and the magnet coil (see Fig. II.2 for a picture of the combined system). Each SDC detector subsystem group has created a model of their detector compatible with the other detector subsystem models and the rules of SDCSIM. Use of SDCSIM automatically includes the effects of the materials in the other parts of the SDC detector. Also for explicitly studying the effects of materials, a simple set of commands can be used to turn on and off the use of the model of each part of the SDC detector (within SDCSIM).

The proposed straw tube detector tracking geometry consists of a number of cylindrical detectors made from a support cylinder covered with a layer of straw tube modules that detect the charged particles. These structures are called superlayers and are spaced radially throughout the outer tracking volume. For simplicity and to reduce computer time consumption, the simulation does not introduce individual straws and modules; instead, the simulation uses a homogeneous volume of material with appropriate density to represent the modules. Within the simulation, the superlayer is divided into layers and during the tracking of the simulated particles, user-written code records which straws were struck. A layer is the smallest volume introduced. The detector is divided into two halves along the beam directions. See Figs. II.3(a) and II.3(b) for end and oblique views of this geometry. For the straw tube system, a detailed description of the detector material and geometry is read from an external file. The wires in straw tubes run parallel or nearly parallel to the central axis of the detector and therefore provide an azimuthal measurement (ϕ) of the track. The support cylinder is made of a carbon fiber material and is modeled using the GEANT material "carbon" to match the parameters given in the straw tube placement report.[9] The straw tube layers also contain an accurate allowance of material for the straws and the carbon fiber outer shells of the straw modules. This amount of material can be set within the geometry file. The geometry file inputs define the number of superlayers (five in this proposal) and the number of layers within the superlayer (6 for nontrigger and 8 for trigger layers). Since the straw tube detector description is read from a file, testing of multiple geometries for descoping and material studies is easily possible. The external file can also contain statements that activate debugging code. The external file can also contain a command to turn off the straw tube hit recording algorithm; this allows

other subsystems to use our geometry as material only, without requiring a full straw tube hit analysis.

The geometry description includes the full use of both stereo and axial layers. Axial layers have their wires running exactly parallel to the central axis of the support cylinder, while stereo layers have their wires tilted at a 3° angle to the central axis of the superlayer. When axial and stereo layers are analyzed in conjunction with each other, the z position of the track along the superlayer can be calculated. The use of stereo layers required the introduction into GEANT of a new volume shape, the "HYPE." The HYPE is the surface created by rotating a hyperbola around a cylindrical axis that is the geometrical shape of an ideal stereo layer. The superlayer description can have any amount of support material (including none). The straw tube geometry file allows any layer to be defined with any stereo angle or to be axial.

When a track crosses a superlayer, hits are recorded at the point of closest approach of the track to each wire. The distance of closest approach is converted to a drift time. Geometrical inefficiencies due to dead spaces between straws are included by requiring that the point of closest approach of a track to a wire be within a straw. The path of hits in each superlayer (a track segment) contains information about the track momentum. While a track follows a curved path, the curvature of the tracks with rather high transverse momenta (p_T) is small over the thin (2-3 cm) superlayers, and the hits recorded fall on essentially straight lines within the superlayer. The angle of the segment relative to the superlayer cylinder depends on the curvature of the track, which in turn depends on the p_T of the track. High p_T tracks produce segments that are perpendicular to the superlayer, and lower p_T tracks produce smaller angle segments. Each high p_T (stiff) track passes through several superlayers so that a redundant measure of track momentum is obtained, and the process of assigning detector hits to tracks is facilitated.

The simulation includes a detailed model of the way the straw system records the hits caused by the combined effect of an event of interest and background minimum bias events occurring in crossings before, during, and after the event of interest. Low energy tracks both from the event of interest and the minimum bias events can spend hundreds of nanoseconds spiraling through the detector and affect the readout of events tens of crossings after the track was generated. Figure II.4(a) contains a time distribution for the hits caused by 25 minimum bias events in an accurate model of the SDC detector, and for comparison Fig. II.4(b) shows the time distribution of hits with a very low mass SDC

detector. Clearly while the mass of the detector causes a slight increase in the number of hits, it also has the desirable effect of clipping the long tail of late hits. The late hits are caused by low energy tracks that helically spiral (loop) around in limited areas of the detector and are consequently known as loopers. Loopers will drastically interfere with the readout of the detector along their trajectories. It is important to note that these looper hits are not uncorrelated because the loopers affect groups of closely spaced straws. The background hits can either mask or supersede the hits from the event of interest and also produce legitimate stiff tracks which are not related to the event of interest. As the luminosity of the SSC increases, the detector experiences an increasing level of minimum bias hits, and the probability of losing a track or creating a false track from unrelated hits grows.

To study the effect of loopers, our simulation records the hits over a wide time window (as wide as -20 to +4 beam crossings) and models how hits would be recorded. The minimum bias events are modeled using the programs PYTHIA 5.4 and JETSET 7.3 to generate minimum bias tracks with an accurate rapidity distribution. The simulation stores all hits generated over this wide time region (in addition to the hits from the event of interest) and calculates which hits would be recorded by the front end electronics. The recording algorithm is blind to whether the hits it records are from the event of interest or a minimum bias event. The hits that are recorded must be within a 50 ns gate defined by the timing of the event of interest. The recorded hits must also not be blocked by a hit just before the event of interest because the front end electronics does not respond to the second of two closely-spaced signals. A realistic 40 ns dead-time for this effect is included. The hit recording algorithm considers the time offset (from the event of interest) of the bunch crossing producing the particle, the flight time of the particle producing the track, the drift time of the electrons to the sense wire, and the propagation time of the resulting signal to the front end electronics. Kinematical information about the track causing each hit is recorded for later use in understanding how well event reconstruction algorithms worked.

We have used the simulation described above to study the occupancy of an eight-superlayer straw tube system for "minimum bias" background events at the design luminosity. The silicon is used here only as material. The occupancy results as a function of superlayer radius for an eight-superlayer system are shown in Fig. II.5(a) (straws with no other material) and Fig. II.5(b) (a full system of beam pipe, silicon, coil, and straws). Even with a full set of material (except pixels) within the straw tube system, the innermost layer has an occupancy of about 10%. Conversions from the beam pipe/silicon slightly

raise the occupancy of the inner superlayers. The greatest increase in occupancy caused by material is in the outer superlayers of the straw tube system. In this outer region, the occupancy almost doubles (going from the 1.5% to 2.5%) when the material of the coil is included. (However, these results must be considered preliminary because the magnetic field was taken to be uniform over the entire thickness of the coil.)

II.3.3. Event Reconstruction Algorithms

The event reconstruction algorithms consist of three steps: (1) locating clusters of hits (segments) produced by individual tracks within a superlayer, (2) linking the segments into tracks, and (3) fitting the tracks to assign ϕ, p_T, p_Z, and impact parameter to each track.

One of the segment-finding methods is based on a "road" algorithm. In a road algorithm, hits are searched for along a set of trajectories within the detector. The test trajectories are calculated using a set of predefined curvatures (essentially p_T's). This type of algorithm can be used both to find segments and to link segments from one layer to the next. In the segment finding case, hits in the outer layers of a superlayer are used as starting points for the roads. The starting hits are known as anchor hits. The anchor hit has the effect of defining the azimuthal position (ϕ) of the segment. For each of the curvature bins, the algorithm calculates using a straight line (segments from high-p_T tracks are locally straight lines) which straws would be hit based on the track passing through the anchor hit; these sets of straws form the roads. Each road is examined to see if the straws in the road are hit. Provided a minimum number of hits are found (4 for a 6-layer superlayer or 5 for an 8-layer superlayer), a new segment is recorded for the path with the most hits. The ϕ and curvature for the segment are also recorded using the hit drift time to improve spatial resolution of the hit.

Next, the segments from both the straw and silicon superlayers are linked to form tracks. The silicon inner tracker, included in Fig. II.2, consists of eight double-sided cylindrical superlayers in the barrel region.[10] Each wafer has strips with a stereo angle of 5 mrad on one side. Track segments are found in the silicon tracker by associating hits between layers. The silicon segments usually contain z information. We use a global reconstruction algorithm to link the segments in both tracking systems. Zones in curvature/ϕ_0/tan λ space are defined for test tracks (ϕ_0 is the azimuthal angle at which the track originates, and λ is the "dip angle" = $\pi/2$ - θ, where θ is the polar angle). This

algorithm has the advantage that separate tracks do not have to be found in any one system. It will also be easy to extend it to a planer intermediate angle geometry; it has already been used for the end planes of the barrel silicon inner tracker. For each zone, we search in each superlayer for segments at the appropriate ϕ, defined by the curvature and ϕ_0 of the zone and the radius of the superlayer. If there are at least one segment in enough superlayers, we form a track. Stereo superlayers in the straw system are included as well. The zone is broadened for the stereo superlayers to account for the range of possible ϕ offsets. The polar angle bin for the track is determined from the z information from the silicon segments and the ϕ offsets of the stereo straw segments.

Once the segments are associated into tracks, a track fit[11] is performed for the points in the segments. Before fitting, the left-right ambiguity and time offset are determined for each hit, and the drift time and wire number are converted to a position in r, ϕ. z is determined from the stereo superlayers and from the silicon segments. In cases where there is more than one segment in a superlayer, the one giving the best χ^2 for the track is chosen.

A second segment finding algorithm starts a search for hits with the outermost and innermost layers of a superlayer, proceeding from pairs that would give a reasonable crossing angle. For all left-right ambiguity combinations with these hits, it searches each remaining layer in turn for a compatible hit. For either ambiguity choice of the candidate hit, a fit of a line tangent to all of the drift isochrons is made. Solutions meeting a χ^2 test are used to interpolate to the next layer to continue the search for new hits. The code works its way through the superlayer until all layers are exhausted, updating the segment fit with all accumulated information at each stage.

Track segments found by the second algorithm are then linked with one another and with hits in the inner silicon detectors using an algorithm developed by ALEPH. Starting from the outermost superlayer, this algorithm uses the vector quality of a found segment to point to a location in the next inner superlayer. If a track segment there has similar parameters, the algorithm looks inward for segments. It continues in this fashion until all superlayers of the straw tracker and all layers in the inner silicon have been searched. The final track fit then comes from fitting the segment parameters. Ultimately, the final track fit will have to be a refit of all the individual hits found to belong to the same track. The maximum number of superlayers that can be skipped while searching for segments to link together is controlled by a parameter, currently set to one.

II.3.4. Performance of the Tracking System

In this section we present preliminary performance studies from the first of the reconstruction algorithms described in the previous section. We have studied 10 events from 300 GeV Higgs bosons decaying to four muons, in the presence of minimum bias background corresponding to the design luminosity. The efficiency for finding the muon tracks (there were 12 within the silicon barrel tracker η range) is 100% for muon tracks within the rapidity coverage of the barrel silicon inner tracker. Figure V.6(a) shows the hits for such an event in the five superlayer straw and descoped silicon tracking system. The track segments found from these hits are shown in Fig. V.6(b), and the fitted tracks are shown in Fig. V.6(c). Figure V.7(a) and (b) show the resolutions in p_T and ϕ, defined to be the differences between the values for the original tracks and the values from the track fits. We show in Figs. V.8 (a)-(c) the resolutions in θ for tracks with segments found in the silicon inner tracker and both stereo superlayers, with one stereo superlayer, and with no stereo superlayers, respectively.

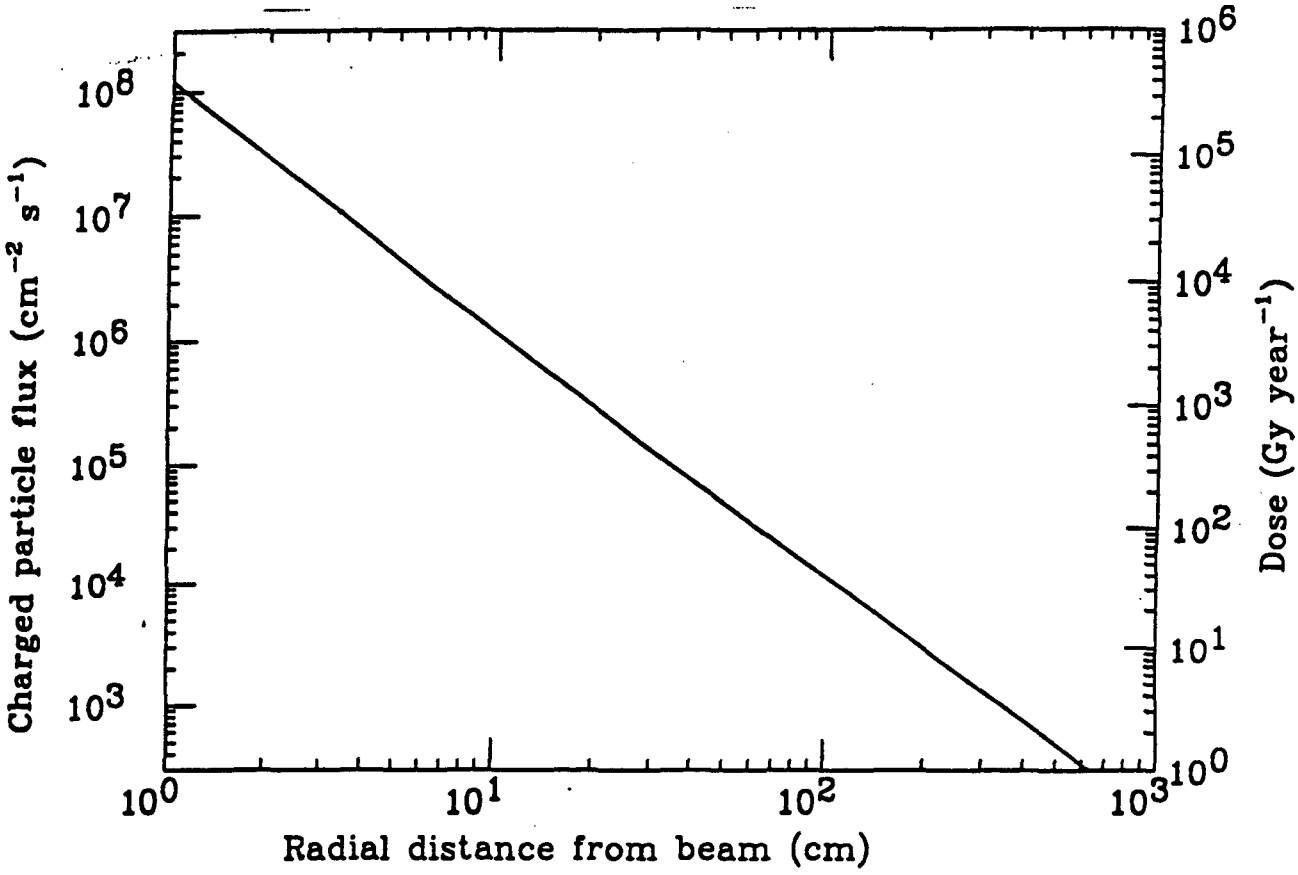

Fig. II.1. The charged particle flux and annual radiation dose as a function of perpendicular distance from the beam under standard SSC operating conditions (from Ref. 6).

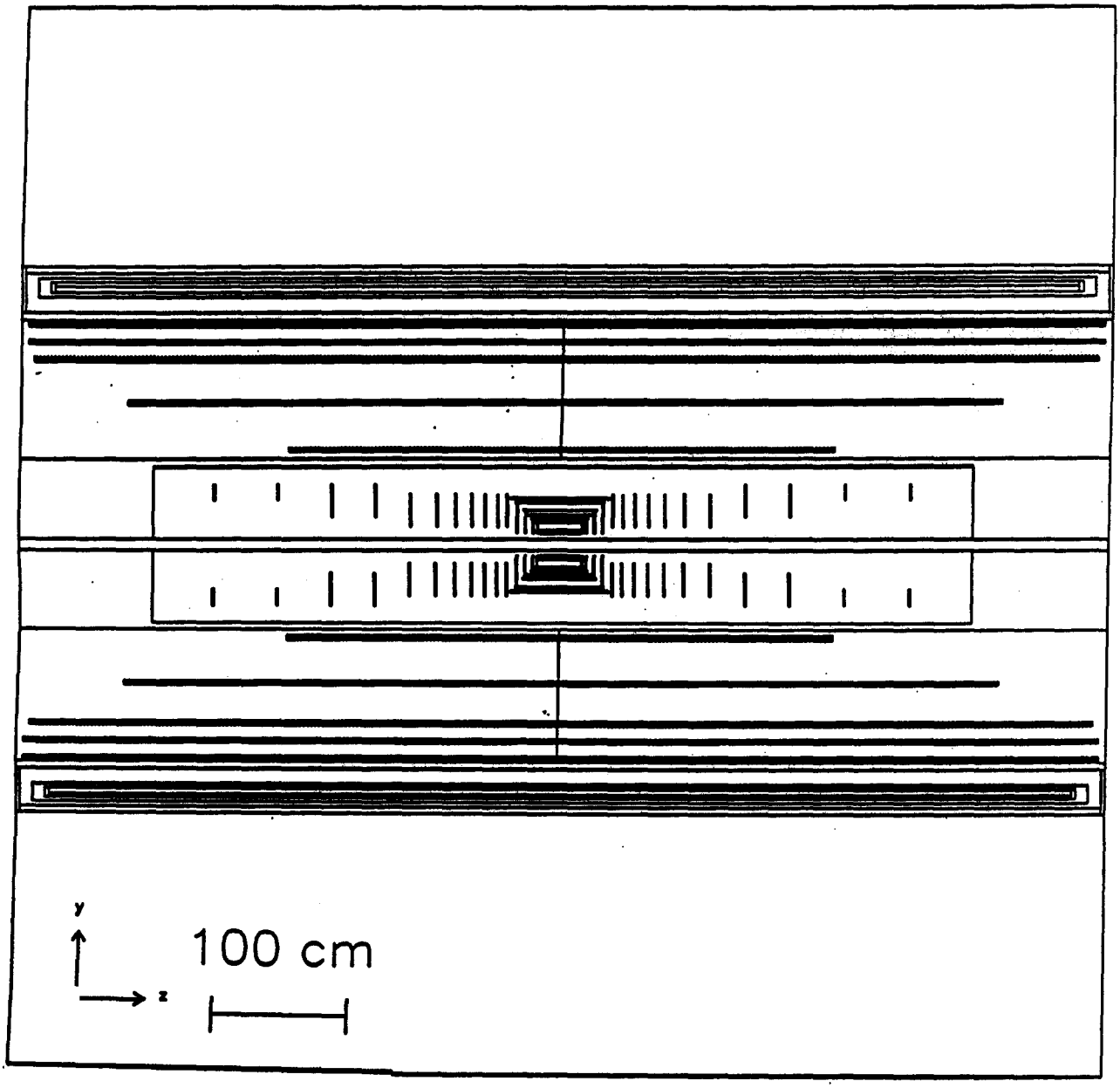

Fig. II.2. A side view of the proposed tracking system design. The figure shows the beam pipe, the descoped silicon tracker, a five superlayer straw tube system, and the solenoidal magnet.

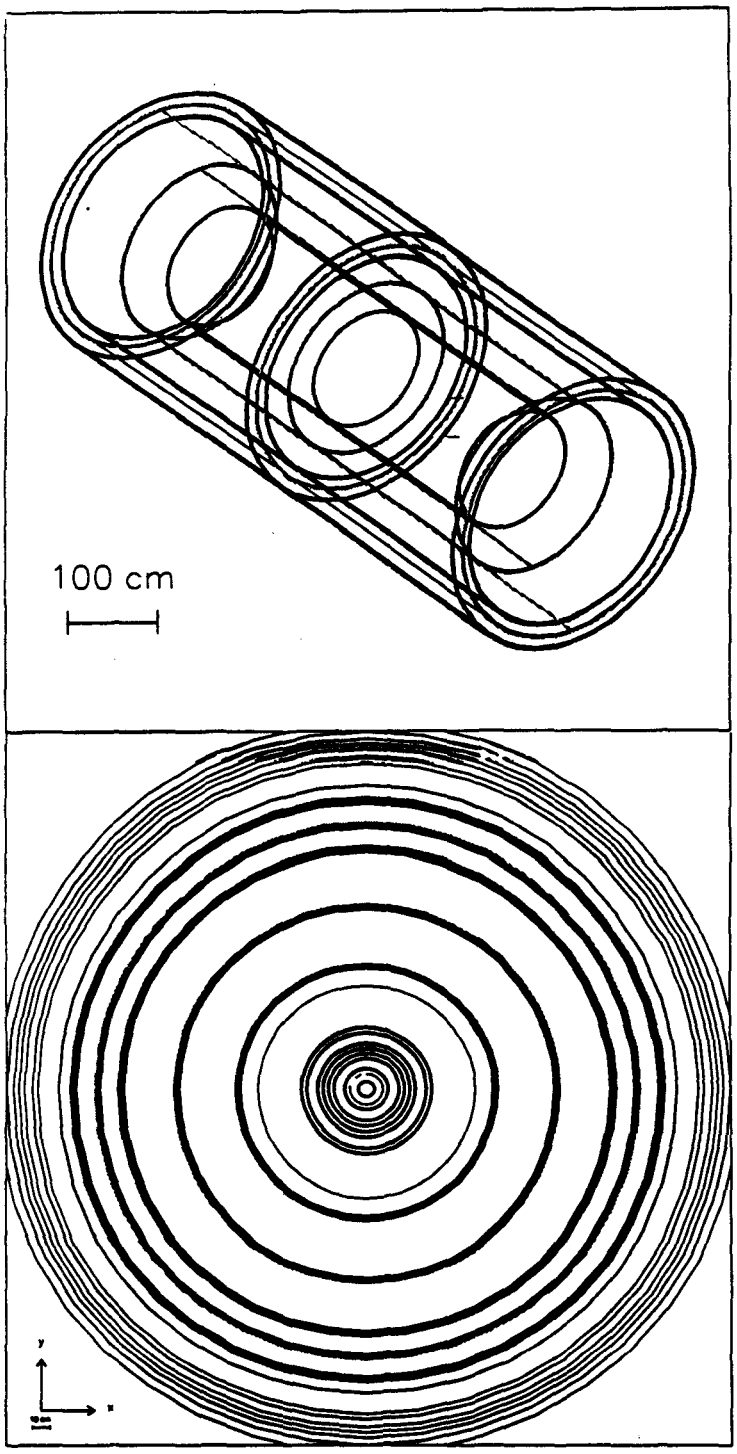

Fig. II.3. (a) An oblique view of the proposed straw tube outer tracker. While not visible because of the scale of the drawing, this geometry includes individual volumes for each layer half and carbon support cylinder.

(b) An end view of the proposed straw tube outer tracking system.

(a)

(b)

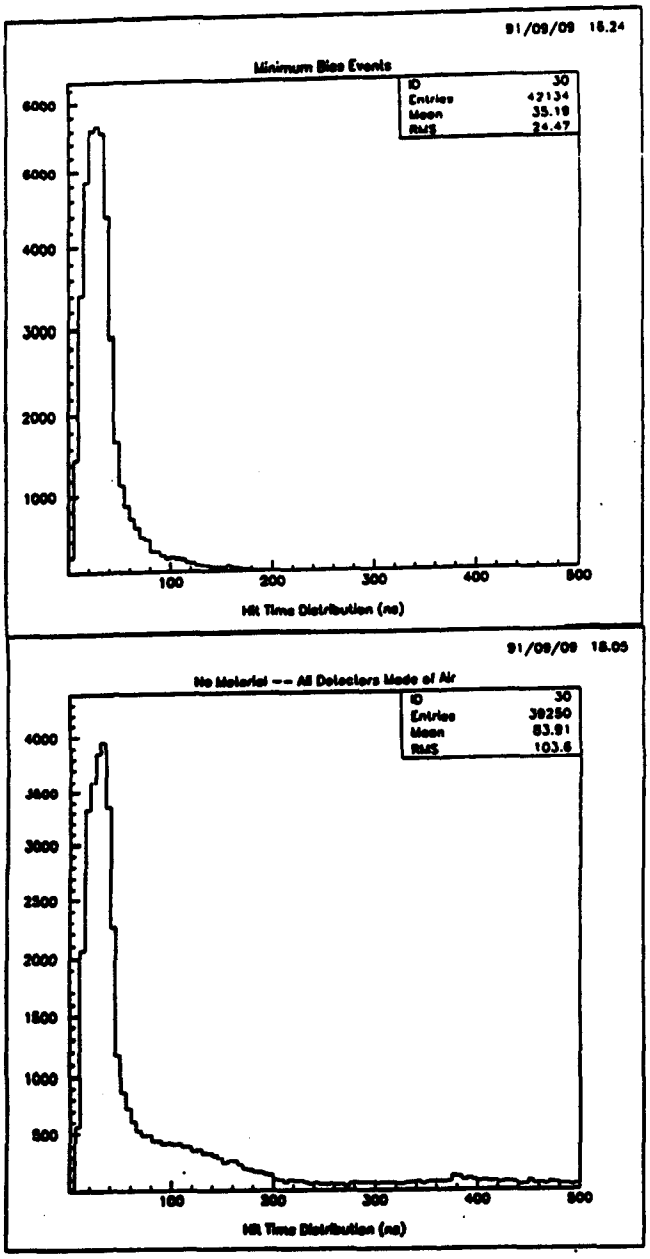

Fig. II.4. (a) The distribution of hit times recorded in an eight layer straw tube tracker (LoI design). The plot shows the hit times recorded for 25 PYTHIA minimum bias events tracked through a full simulation of the SDC tracker system including beam pipe, a full silicon detector, and magnet coil.

(b) The distribution of hit times for a simulated SDC tracker identical to the one in Fig. II.4(a) except all parts of the detector are made of air (essentially a zero mass detector). Again, hit times are recorded for 25 PYTHIA minimum bias events. Note: Fig. II.4(b) shows fewer total hits but more late hits than Fig. II.4(a).

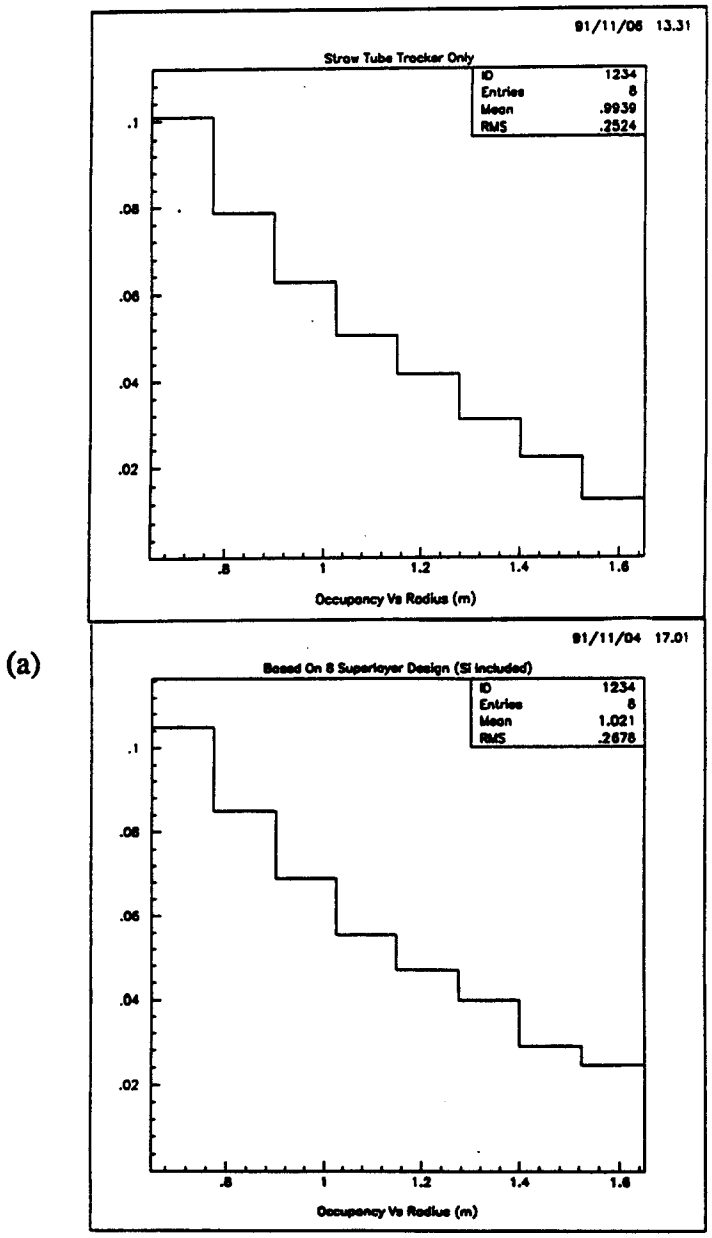

(a)

(b)

Fig. II.5. (a) The occupancy fraction (fraction of wires with a hit) vs. radius of superlayer in a simulation of an eight-superlayer straw tube tracker (LoI design) by itself. The innermost superlayer is at a radius of about 0.7 m and the outermost is at 1.6 m. The occupancy is calculated using minimum bias events only and considers in-time hits from the previous 20 and the next 4 beam crossings.

(b) The same plot as Fig. II.5(a), except that the material of the beam pipe, silicon tracker, and magnet coil is included. The occupancy rises slightly except in the outer superlayer, where backscatters from the magnet coil increase the occupancy considerably (see the text).

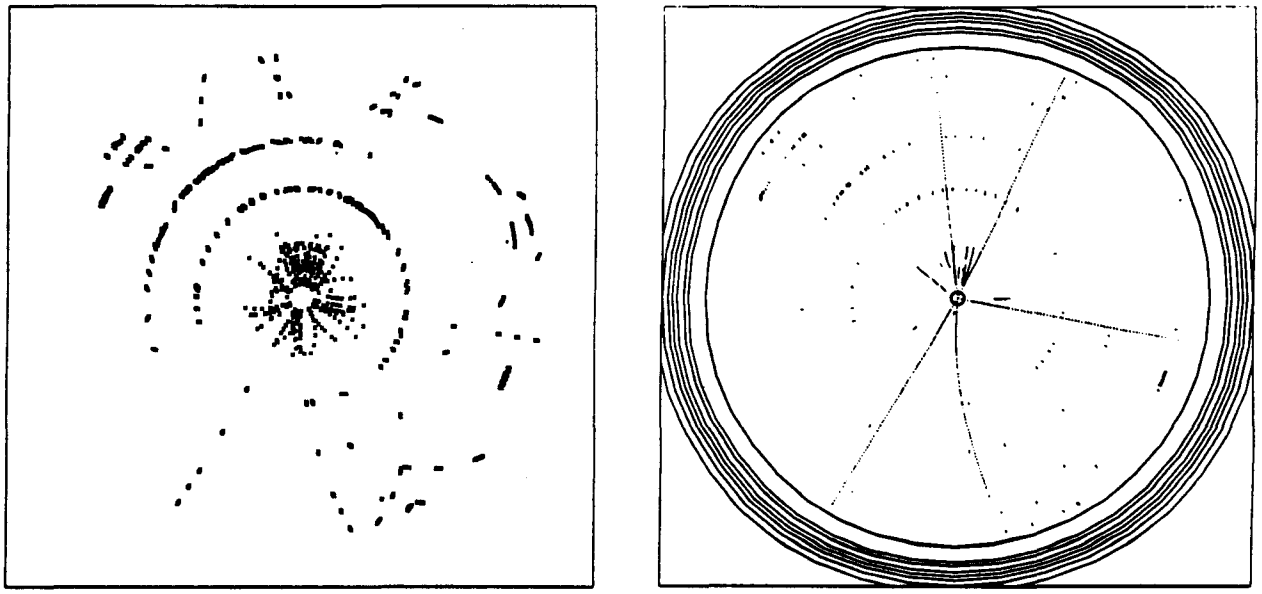

(a) (b)

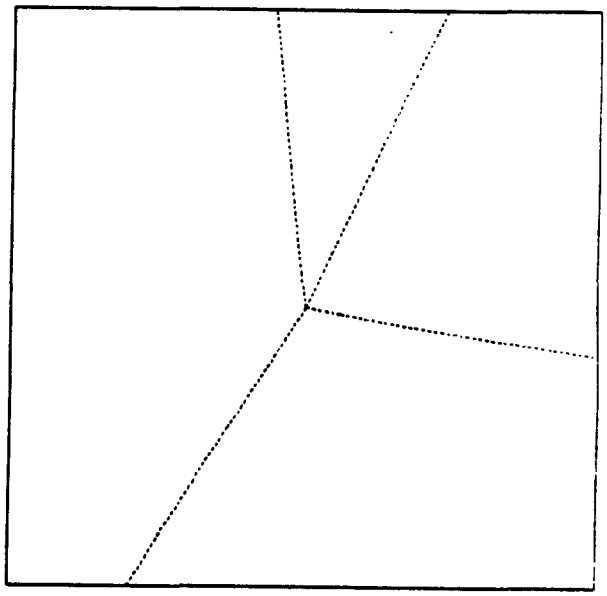

(c)

Fig. II.6. (a) End view of the hits for a 300 GeV Higgs event in a tracking system with five straw tube superlayers and the descoped silicon inner tracker.

(b) Track segments and reconstructed tracks found for the event shown in Fig. II.6(a).

(c) Original Monte Carlo tracks for the event shown in Fig. II.6(a).

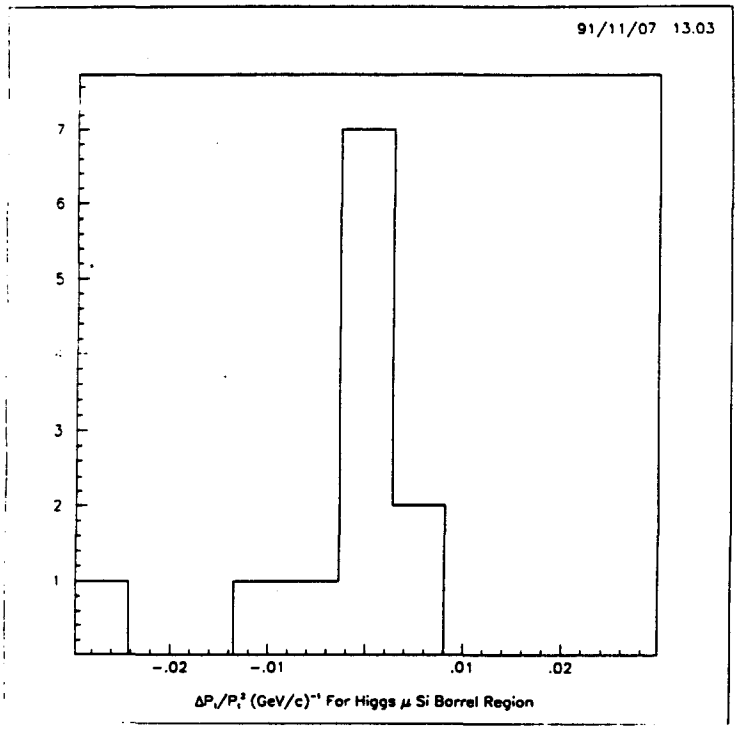

(a)

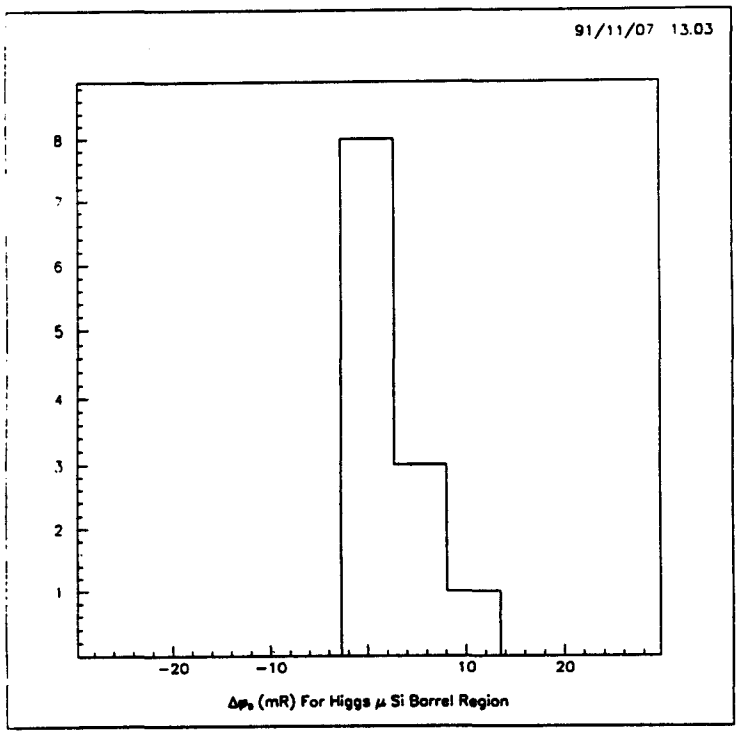

(b)

Fig. II.7. Resolutions in (a) p_T and (b) ϕ for muons from Higgs decay in a minimum bias background corresponding to the design luminosity.

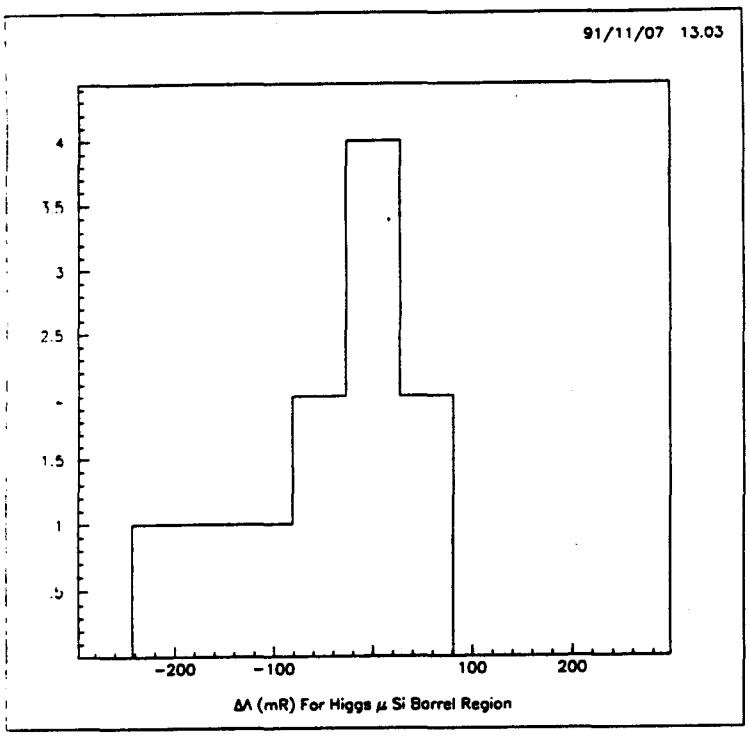

(a) (b)

(c)

Fig. II.8. Resolutions in polar angle for muons from Higgs decay in a minimum bias background corresponding to the design luminosity for tracks with segments in (a) silicon and two stereo straw superlayers, (b) silicon and one stereo straw superlayer, and (c) silicon only.

III. STRAW DRIFT TUBES

III.1. INTRODUCTION

Small drift cell structures have found many applications over many years especially in small high precision chambers. One way of providing a cathode structure to surround the anode wire is with an array of wires. There are several examples of this method of construction.[12] Commonly this is a hexagonal array so that many cells can be packed together in a hexagonally close packed pattern with each successive layer offset from the preceding one by one half of a cell. Another way to provide a cathode is to make a very thin metal tube to surround the anode wire These tubes may be packed together in a close packed structure, and there are examples of drift chambers that are constructed in this way[13]. If the metal tube is in fact a very thin metal coating deposited on a plastic substrate, the mass of the cathode structure is reduced to the point where it is similar to the mass of the wire structure of a drift cell of that design. A drift cell composed of a central anode wire and a metal-coated plastic cathode is referred to as a straw tube drift cell. Arrays of these drift cells have been operating successfuliy in detectors in high energy physics over the course of the last ten years,[14] although all of the examples so far have been small high precision chambers.

There are some important advantages of the tube structure over a cell design with wire cathodes. One is its greater ease of construction and the greater isolation between cells both electrically and mechanically. Also the amount of tension which needs to be supported is reduced by a large factor because it is unnecessary to support the cathode wires. These considerations were discussed thoroughly in the 1986 Snowmass report.[15]

In Section II.1.4 the basic parameters of the SSC are given. In particular, the time between bunch crossings is 16 ns, and there are on the average 1.6 interactions at design luminosity. A straw tube with a diameter of 4 mm operated with a gas in which the drift velocity is ≈0.1 mm/ns is compatible with the bunch crossing time in the sense that the electrons from the passage of charged particles through the tube in one bunch crossing will mostly be collected before the next bunch crossing occurs. Thus at least in this important way a straw tube system is recommended for use at the SSC.

The time separation of events could, of course, be maintained easily by a detector system without drift time. The drift tube system, however, is of lower complexity because

the number of detector elements is reduced by the ratio of the tube radius to the measurement resolution of the drift cell, which is roughly an order of magnitude. This reduction in the complexity of the system by using drift cells is partly counterbalanced by the need to use more complex electronic circuits to measure the drift time, but there still remains a decided advantage in using drift chambers for a large detector over using a device where the resolution depends on the size of the sensitive element. The drift cell parameters are a good match to the SSC requirements. In addition, the experience of the last 10 years plus the ease of manufacture of straw tube drift cells compared to other small cell designs recommend their use for the SDC detector at the SSC.

The rest of this section is devoted to a discussion of the studies which have been carried out to discover whether various extensions of the techniques of the past can be applied to develop a system of straw drift tubes of the magnitude which is required for the SDC. Here is a list of ways in which the tracking system for the SDC will significantly expand the technology that has already been applied to straw drift tube chambers:

1) The straw tube diameter must be reduced from the usual 7-8 mm to 4 mm.
2) The wall thickness must be reduced to minimize material.
3) The length of the tubes must be increased from less than 1 m to 4 m.
4) More tubes are required than have been used in such a system before.
5) Fast gases must be used instead of the usual argon-based gases or slow gases.
6) The tubes will be exposed to a higher radiation dose over their lifetime than other detectors of this type.
7) The tubes will operate with higher occupancy and higher current per unit length than before.

Section III.2 will discuss points 6) and 7). Section III.3 will address one of the problems associated with point 3) Section III.4 on the wire supports will address one of the problems posed by 1), 2) and 3) together. Section III.5 will describe the operation of tubes as described in points 5) and 7). Some of the mechanical specifications deriving from these extensions will also be discussed in other sections of this report.

III.2. AGING AND RADIATION DAMAGE STUDIES

III.2.1. Introduction

There are two important sources of radiation which contribute to the radiation dose experienced by the tubes while in operation and indeed just sitting idle while beam collisions are taking place. One is of course the SSC beam interaction region in the center of the SDC detector while the other is the heavy material, especially the calorimeter, in the detector. The former is the source mainly of charged particles and photons while the latter is the source of neutrons which are able to travel through the walls of the calorimeter and through the magnet to interact in the walls and the gas of the straw tubes.

III.2.2. Radiation Damage to Materials

The radiation damage to the materials of the tubes themselves is not significant. Calculations of the total dose of radiation expected in 10 years of operation at design luminosity produce values in the 10-100 krad range. The materials from which the straws are constructed (Mylar, Kapton and glue) have been tested up to 10 Mrad with no significant structural weakening. Moreover there is very little stress on the tubes themselves in the design which is developed in this report. Other materials used in the construction of the whole system, for example the wire support material, are known also to be tolerant to much higher radiation radiation doses than expected. In short, with a minimum of care to avoid especially sensitive materials, such as Teflon, there is no difficulty in making a structure sufficiently radiation hard for the SDC detector at the SSC.

The radiation hardness of the amplifier circuit is discussed in Section V.6.2. Those electronic components mounted on the chambers include capacitors and resistors. These components not very sensitive to radiation and should be able to stand about 1 Mrad of damage. The cables will be chosen to be resistant to the same level of radiation.

III.2.3. Damage to the Tube during Operation in a Radiation Flux

The limits to the lifetime of a straw tube tracking system come from the action of the electric currents on the anode and the cathode during operation. Studies have been performed to determine this lifetime, and also to discover ways to extend it to the point

where there is no danger of failure from extended operation with electron and ion currents which are relatively large compared to previous experience.

The flux of charged particles from the interaction region is fairly easy to calculate at least in comparison to the flux of neutrons. There is a concerted effort to simulate the events expected at the SSC and evaluate how well they will be tracked in a detector. A byproduct of this is a calculation of the charged particle rate in different parts of the detector. The occupancy, defined as the probability of having a hit in a typical straw tube in a given 50 ns time interval, is shown in Fig. II.5 as a function of the radial position of a layer from the interaction point. These occupancies are for the geometry of Table II.2 and include particles from conversions in the inner tracking system. The occupancies can be converted to current per unit length in a tube at a given gain for a given gas. This is given in Table. III.1 for a gain of 2×10^4 in CF_4 (tetrafluoromethane). It is assumed that 180 electrons are released per cm by a minimum ionizing particle in CF_4.[16] It is a fact that the current per unit length is a constant for a uniform distribution of particles in rapidity. One can convert to charge per unit length expected from 10 years of running by multiplying by 10^8 seconds, which is the number of seconds in 10 SSC years. (1 SSC year is 10^7 seconds because the SSC will not run all year; one third of a year is a good guess for the amount of operation per year.)

The amount of current to be expected from the interaction of neutrons directly with the isobutane in the gas and also with the hydrogen in the plastic straw material can be estimated. It is necessary to know what the neutron flux is in the tracking volume and also some idea of the energy spectrum. Some calculations have been done to determine these parameters.[17 18] Groom's number for the annual fluence at design luminosity of $1.2\times10^{12}/cm^2$ is for no reflections from a uranium-scintillator calorimeter. Adding reflections increases the number by about a factor of two but the lead-scintillator calorimeter, which has recently been adopted, should have about a factor of two less neutrons than the one with uranium. So the two factors cancel. Groom's number is for a spherical calorimeter of radius 2 m around a hollow space where the neutron flux is estimated. The SDC is not spherical, however, but elongated along the beam. Sadrozinski shows that this reduces the annual fluence to about $0.45\times10^{12}/cm^2$. In addition there is probably some room for moderator and absorber on the inside faces of the end cap calorimeters, which would reduce the annual fluence to $0.3\times10^{12}/cm^2$. The fluence is nearly uniform over the tracking volume, at least within a factor of two, which is the approximate accuracy of these estimates. The spectrum calculated by Groom is

approximately Gaussian in the variable logE and centered at about 1 MeV. Moreover, he asserts that this spectrum is almost universally valid for the spectrum of neutrons generated by hadronic interactions.

The next step to calculate the current from the neutrons depends on the gas and the plastic. The ionization current comes mainly from neutron interactions in the gas and the hydrogen in the plastic. Interactions with the other nuclei generate approximately an order of magnitude less ionization because the energy loss per collision is lower. If there is 20% i-C_4H_{10} in CF_4, and the value for the n-p cross section is taken as 4.5 b at 1 MeV, the interaction rate in the hydrogen is about 1/sec/cm for a flux of $3\times10^4/cm^2$, corresponding to the design luminosity. The interaction rate in carbon is about 0.4/cm/sec and in fluorine 1/sec/cm. Using the average energy transfer for 1 MeV neutrons on these elements, a gain of 2×10^4 and an ionization potential of 32 eV, the current drawn is 0.08 na/cm of which 0.06 na/cm is from the hydrogen alone. The knockon protons from 1 MeV neutrons in the plastic have a range of about 1 mg/cm^2 or about 7 μm of plastic. Thus it is only the neutrons above about 1 MeV that will produce knockon protons with sufficient energy to enter the gas. Using this observation, the fact that the hydrogen in the plastic is 5% of the weight and a supplementary geometric acceptance of about 0.5, the current drawn as a result of neutrons interacting in the straw walls is estimated to be 0.15 na/cm.

The total current per unit length from both charged particles and neutrons (see Table. III.1) can be as high as 2.1 na/cm for the layer at 70 cm from the beam and this leads to 0.21 C/cm integrated charge on the wire and the cathode. This is more charge than has been experienced in similar chambers that have operated in the past. Tests have been performed to measure deterioration over time of the wire and also the cathode as described in the following paragraphs.

A considerable amount of trouble has been experienced in the past with anode wire aging. This could take the form of a coating on the wire, which reduces the gain substantially and also initiates Malter breakdown. Or whiskers could grow which would act as discharge paths. Recent studies have shown that CF_4 gas especially when mixed with isobutane is substantially free from these problems.[19] In fact, operation of an aged anode in CF_4 with 20% isobutane resulted in a cleaning effect so that the gain recovered.[20] There is apparently some change in gain from a completely clean state in CF_4 isobutane, but of the order of only 10%.[21] This change would hardly be noticed in a tracking chamber where the pulse height is not measured.

Table III.1. Occupancy and Current Draw

Superlayer	Radius(m)	Length(m)	Occupancy	I(Ch. Part) na/cm	I(Total) na/cm
1	.708	2.00	0.105	1.9	2.1
2	1.04	3.20	0.07	0.8	1.0
3	1.35	3.90	0.04	0.37	0.6
4	1.48	3.95	0.03	0.27	0.5
5	1.61	3.95	0.02	0.18	0.4

Since there seems to be very little concern about deterioration of the anode surface, attention has been focused on the survivability of the cathode. It soon appeared after irradiating the prototype tubes with aluminum coating that there was a problem of damage to the cathode. The symptom was that after a certain amount of radiation the chamber would start to break down at the normal operating voltage. There have been some observations of breakdowns occurring in chambers with aluminum cathodes operating in fairly large radiation fluxes.[22] After this problem was recognized, some studies were done to try to understand and ameliorate it.

The breakdowns which were observed depended on three conditions: a sufficiently high gas gain, a sufficiently large accumulated dose and the presence of a sufficiently large radiation flux. An increase in the dose over time finally resulted in a decrease in the values of radiation flux or gain that could be sustained without breakdown. Even in this state, however, the gain could be raised well above the operating point if the radiation source was weakened sufficiently. Another factor was the level of water contamination in the gas. If the water contamination was increased, the gain could be raised as long as the other factors remained constant.

In all of these studies it was recognized that if a breakdown did occur and continued for time intervals of about 10^2 seconds or more, the tube would be damaged in such a way that it would break down even with the radiation source removed. A breakdown therefore must be quenched immediately when it occurs. Some observation of the aluminum surface after breakdown occurred showed a white powder. This is not present even during extended operation with large radiation induced currents. Apparently there was serious

erosion of the aluminum during breakdown. This was confirmed by electron microscopy of the surface.

The extent of the problem in relation to the levels of dose and radiation level expected at the SSC was investigated. Although it appeared that the radiation levels were sufficiently low that radiation induced breakdown was unlikely, there is an incentive to try to avoid the problem. It has been suggested that other metals would not have the problem that aluminum exhibits. A likely explanation for the behavior of aluminum is that the ion currents create in some way a very thin insulating coating on the cathode. The charge then builds up on this coating to the point where it will pull electrons through with enough energy to be released into the gas and travel to the anode where gas amplification occurs (Malter effect). The process becomes self sustaining if the gain is sufficiently high. It is very difficult to form an insulating coating on copper by the same mechanism because most copper compounds are at least slightly conductive. Both gold and copper tubes were irradiated in the same way as aluminum. Both showed no tendency to break down even with two or three times longer exposures than caused aluminum to break down very easily. Copper also has advantages in its electrical conductivity as explained in the next section. It costs about the same as aluminum and does not increase the amount of material in the tracking system significantly. Copper appears to be the best choice for the cathode material.

Beyond the problem of breakdown, which is solved by using a copper coating on the tubes, there is the problem of the gradual erosion of the cathode surface by the ion current. It is because the coating is so thin that this becomes a concern at all. Measurements were made of the change in resistance of cathodes during the course of radiation exposures. The rate of ablation appears to be no worse than 0.1 μm/C/cm. This means that 0.02 μm would be lost in about 10 years. There would be no difficulty in applying a little extra coating at the beginning to make up for that expected loss.

III.3. SIGNAL ATTENUATION IN LONG STRAWS

The signal attenuation arises almost entirely from resistive losses in the anode wire and the cathode coating. It becomes significant in long chambers and a straw tube chamber is no exception. Given the resistivity of the conductive materials in the anode and the

cathode and the dominant frequency components of the signal, the attenuation can be calculated and compared to the measured value.

A choice has to be made of the material for the cathode coating. There are only five elements with excellent conductivity (<3 μΩ-cm): aluminum, chromium, copper, silver and gold. There is a limit to the thickness that can be applied by vacuum deposition so that an element with excellent conductivity must be used to minimize the resistance. Of these, aluminum has most frequently been used in the past, but the conductivity of an aluminum coating is only about half of its bulk value whereas the conductivity of coatings of the other elements appear to maintain the bulk value (only copper and gold have been tested). The difference could be in the extreme reactivity of aluminum which might therefore combine with residual gas during the vacuum deposition process to produce a coating with inferior conductivity. Of the remaining elements, copper is sufficiently more conductive than chromium that it can be applied in a thinner coating to achieve comparable conductivity with a smaller amount of material. Silver and gold contribute more radiation lengths than copper. The best choice therefore for a coating, based on conductivity and conductivity compared to the amount of material, is copper.

A thickness of 1500 Å of copper with resistivity 1.72 μΩ-cm has a surface resistivity of 0.11 Ω/square, which for a 4 mm diameter tube gives a resistance of 10.5 Ω/m of tube length after correcting for the fact that a straw tube cathode is really a helical strip with a length about 1.15 times the length of the tube and with no conductivity between the windings.

The anode wire must be made of a material with very high tensile strength so that the tension can be large enough to maintain electrostatic stability while keeping the wire radius small enough to generate the intense electric fields necessary for gas amplification. Tungsten, molybdenum and high-strength beryllium-copper have been used in the past. The resistivity of high-strength beryllium-copper is inferior to the other two,and the tensile strength of molybdenum is inferior to tungsten, so that tungsten is the material of choice. Its measured resistivity as a drawn wire is about 5.9 μΩ-cm or 116 Ω/m for 25.4 mm wire.

Clearly the anode wire contributes the major part of the resistance if it is 25.4 μm in diameter. If the diameter is increased, the resistance will decrease, but the skin depth will limit the effective thickness of conductor. At 160 MHz, a frequency characteristic of the leading edge of the signal pulse, the skin depth in the tungsten is 10.6 μm. Thus as far as

signal propagation is concerned, the resistance is already larger than its DC value by about 10%. For wire diameters greater than about 38 μm, the resistance per unit length is inversely proportional to the first power of the diameter because the inner part of the wire carries no current. This provides some motivation for not increasing the wire diameter any more. A 38 μm tungsten wire has an effective resistance of 62 Ω/m, still the major part of the total resistance.

The attenuation length is given by $2Z_0/R_l$, where Z_0 is the characteristic impedance of the tube and R_l is the sum of the anode and the cathode resistance per unit length. The attenuation length of a 4 mm tube with an aluminum cathode (0.3 Ω/square) and a 25.4 μm tungsten wire anode is calculated to be 3.8 m. This agrees with the measured attenuation shown in Fig. III.1. This agreement gives us confidence that we can predict the attenuation length of the copper coated tube with a 38 μm wire. An attenuation length of 7.5 m is expected, which leads to a 41% attenuation for a pulse traveling the full 4 m length of a tube. This is an acceptable amount of attenuation. At this time copper coated tubes are on order. When they arrive, in the near future, the attenuation length will be measured.

III.4. WIRE SUPPORTS AND TERMINATIONS

The anode wire stretched along the axis of a tube with a given electric field in the region between them becomes unstable if the voltage is raised beyond a point which is determined by the tension and the unsupported length of the wire. There is a maximum amount of tension which the wire can withstand and also a limit to the tension that a given support structure can hold. In the present design the wire tension is limited to 50 g to keep the supports from becoming awkward even though the maximum tension that the wire can withstand is more than this. An analysis of this situation shows that the electric fields required for gas amplification near the wire lead to a maximum unsupported length which is much less than the full tube length of 4 m.[23] The wire will have to be supported every 0.8 m along its length. This section describes the features which are necessary for a good wire support and the design that has emerged to embody them.

The wire support should satisfy the following requirements:

1) It should be low in density to minimize the amount of material.
2) It should be short to minimize the dead area in the tube due to the wire supports.
3) It should not induce breakdown.

4) It should allow the wire to be removed and replaced if necessary.

5) It should hold the wire centered to ±25 μm.

6) It should be rigid so that it does not deform when close packed into an array.

The design which has been developed for prototype testing is shown in Fig. III.2. It has two opposed vee openings with the apex of each vee at the point where the wire is supposed to be held. The wire tension holds the wire straight between one apex and the next. This device, known as the double vee, is molded in two identical halves and then snapped together. The material is a very strong thermosetting plastic known as Vectra. It does not induce breakdown up to 1.4 times the usual operating voltage. It is possible to thread the wire through several double vees positioned regularly along the straw. First a thread is blown through on a current of air. Then the wire is attached to the thread and pulled through. The accuracy of positioning with no applied voltage is about ±30 μm. An improved version of the wire positioner is planned which will be a little longer, more open and more streamlined.

A terminator is required at the far end of the tube from the amplifier to terminate the tube transmission line in a resistor equal to the characteristic impedance of the line and a capacitor for blocking the DC voltage and for compensating for the lossy nature of the transmission line. The characteristic impedance of a transmission line formed by a 38 μm diameter inner conductor and a 4 mm diameter outer conductor is 279 Ω. The optimum capacitor size for a tungsten wire and a 0.15 μm copper cathode is about 90 pf. Neither of these values needs to be more precise than ±20%. A possible approach is to mold something similar to a double vee out of resistive plastic and coat it with Mylar to form a capacitor. The length of the terminator would be about 8 mm to achieve the required amount of capacitance.

III.5. OPERATING CHARACTERISTICS OF STRAW TUBES

III.5.1. Gas Gain

Some of the conditions of operation have been mentioned already in connection with questions of radiation damage and survivability of the straw tubes in the SSC environment. The gain must be as low as possible consistent with obtaining good resolution so that the current draw is minimized. A gain of 2×10^4 has been used in the

section on aging. One effect of the high counting rate which might be considered a problem, namely ion space charge from a previous track altering the the drift properties for the next track, has been studied.[24] There is no problem of this type in any conceivable SSC radiation environment.

III.5.2. Drift Properties of the Gas

The gain as a function of voltage has been measured for CF_4-20% isobutane in 4 mm straw tubes. The shape is more accurately known than the scale. The error on the scale is probably about 15%. The gain curve with a 25.4 μm wire in Fig. III.3 continues from less than 10^3 to more than 2×10^5 without showing any evidence of a transition to limited streamer mode. The gain can even be raised beyond this to about 4×10^5. In contrast to argon-based gases, CF_4 is a good insulator, better than air, and does find some use as an insulating gas in electrical equipment.

The drift velocity for pure CF_4 can be found in the literature.[25] The velocity has been measured up to electric field strengths of 70 kV/cm although there is some disagreement between measurements made at these high electric fields. Measurements in the mixture CF_4-20% isobutane have been made up to about 5 kV.cm[26] but measurements made at higher field strength in other mixtures, such as CF_4-methane[27], show what happens as the concentration of the secondary component increases. The drift velocity decreases quite uniformly over the range of electric field strength values and the position of the peak in the velocity shifts to lower electric field.

The drift velocity in CF_4-20% isobutane is shown in Fig. III.4. Unfortunately the measurements do not agree on the scale, although the shape of the curves is about the same. A choice has been made to treat the most recent measurement as correct in scale and let the others help determine the shape. The peak drift velocity is about 120 μm/ns at about E=5 kV/cm. In the 4 mm straw tube, the electric field strength at the cathode is already as high as 2.3 kV/cm, at an applied voltage of 2 kV, and increases to about 45 kV/cm at a point 100 μm from the wire where the avalanche starts. The mean value is 10 kV/cm. There are no measurements over most of this range. The curve drawn in Fig. III.4 continues beyond the measured points at a constant ratio to the measurements made of the drift velocity in pure CF_4. The drift velocity is about 105±15 μm/ns except above 30 kV/cm where it gets somewhat higher. This value for the drift velocity agrees with the

value that is used to best fit tracks in the prototype modules. It is clear that more measurements of the drift velocity are necessary.

III.5.3. Resolution

The resolution is related to the gain and the gas properties. The resolution has been measured to be about 100 μm in a short section of a straw tube assembly where only the performance of the gas and electronics is tested and not the mechanical stability and precision of the structure. These studies are being extended to larger modules and better electronics.

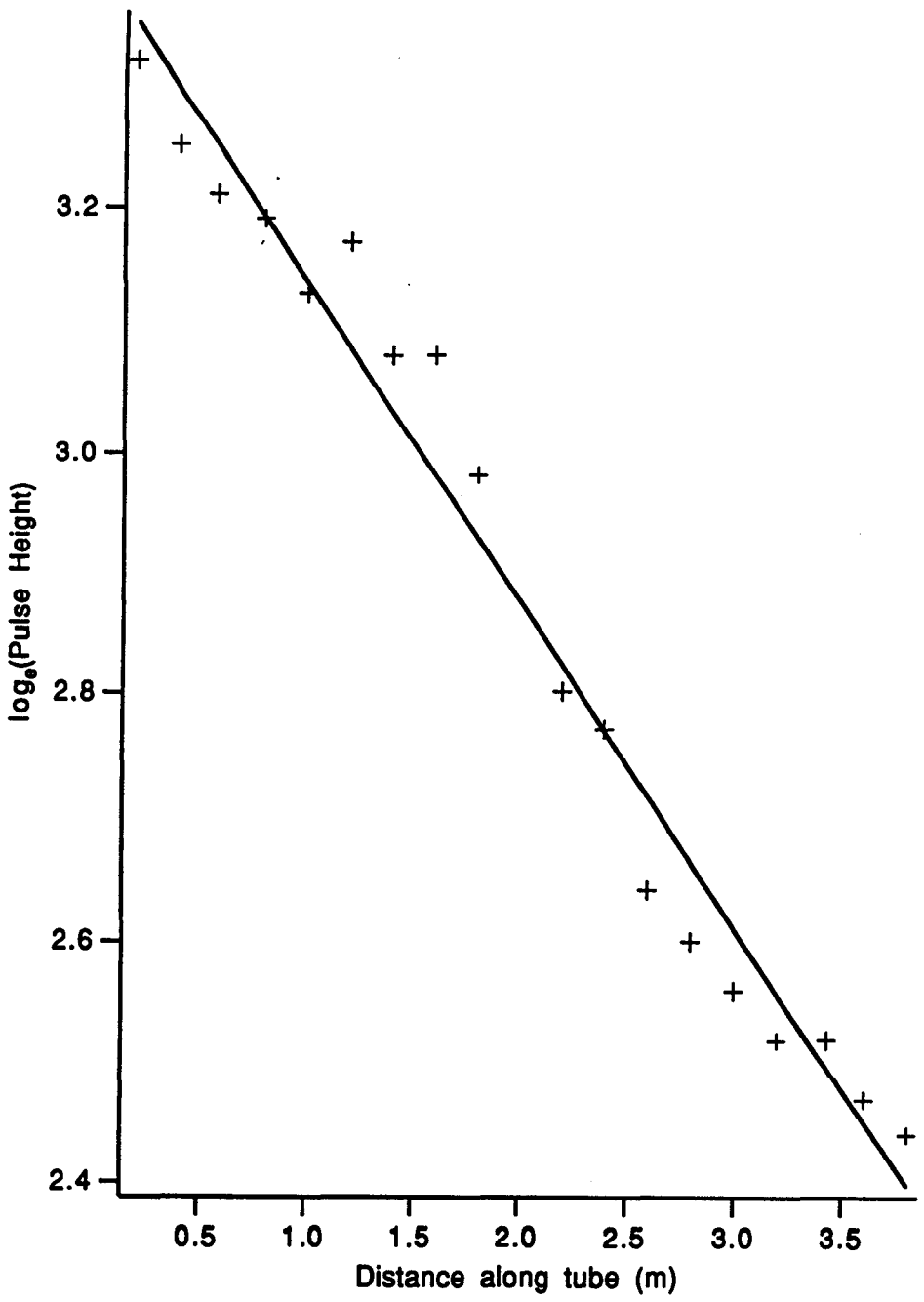

Fig. III.1. The pulse height of signals from an Fe^{55} source in a 2 m unterminated 4 mm straw tube. Both the direct signals and the reflected signals are plotted. The error on each point is about ±15% reading error.The attenuation length is 3.8 m.

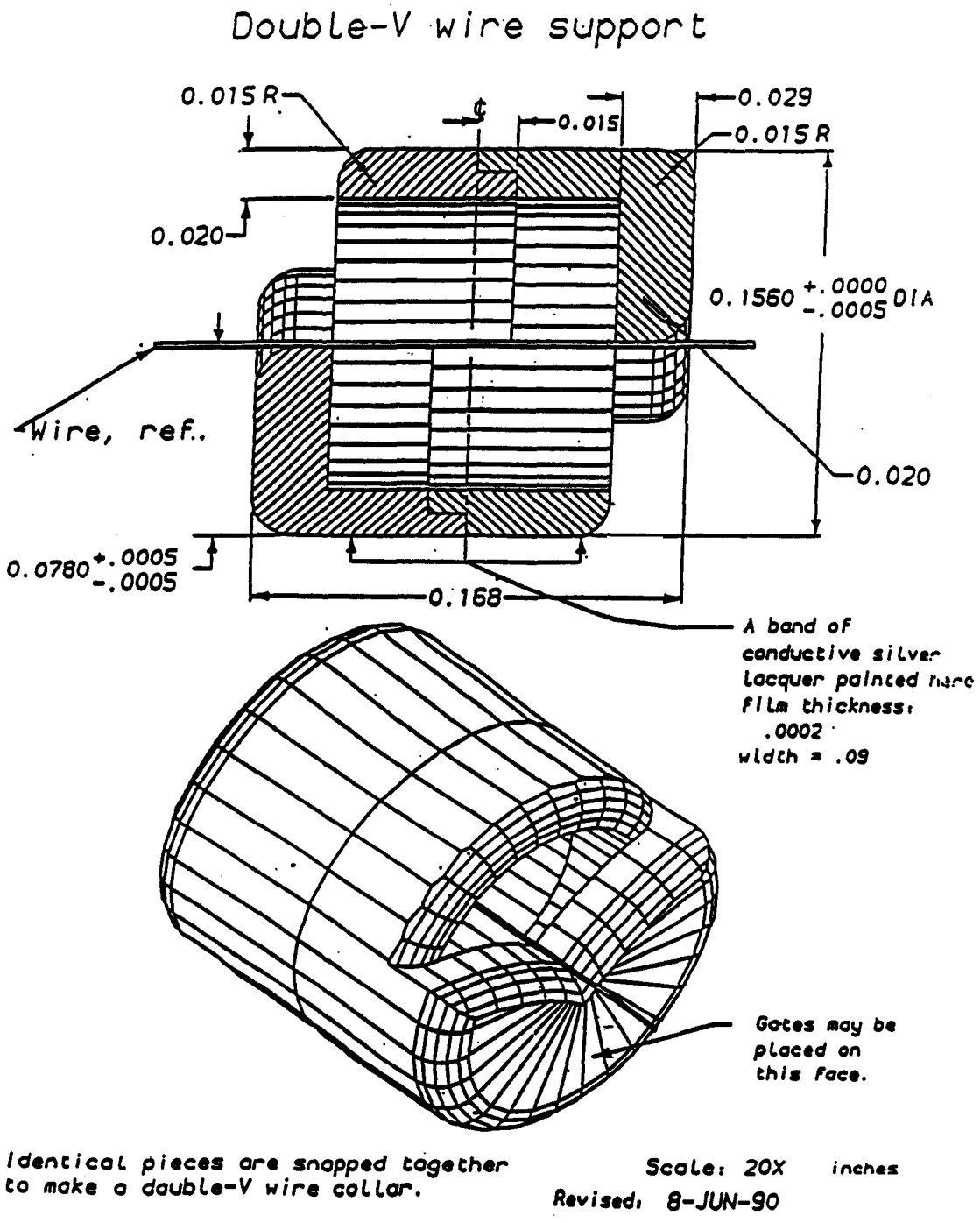

Fig. III.2. A detailed drawing of the double-V wire support.

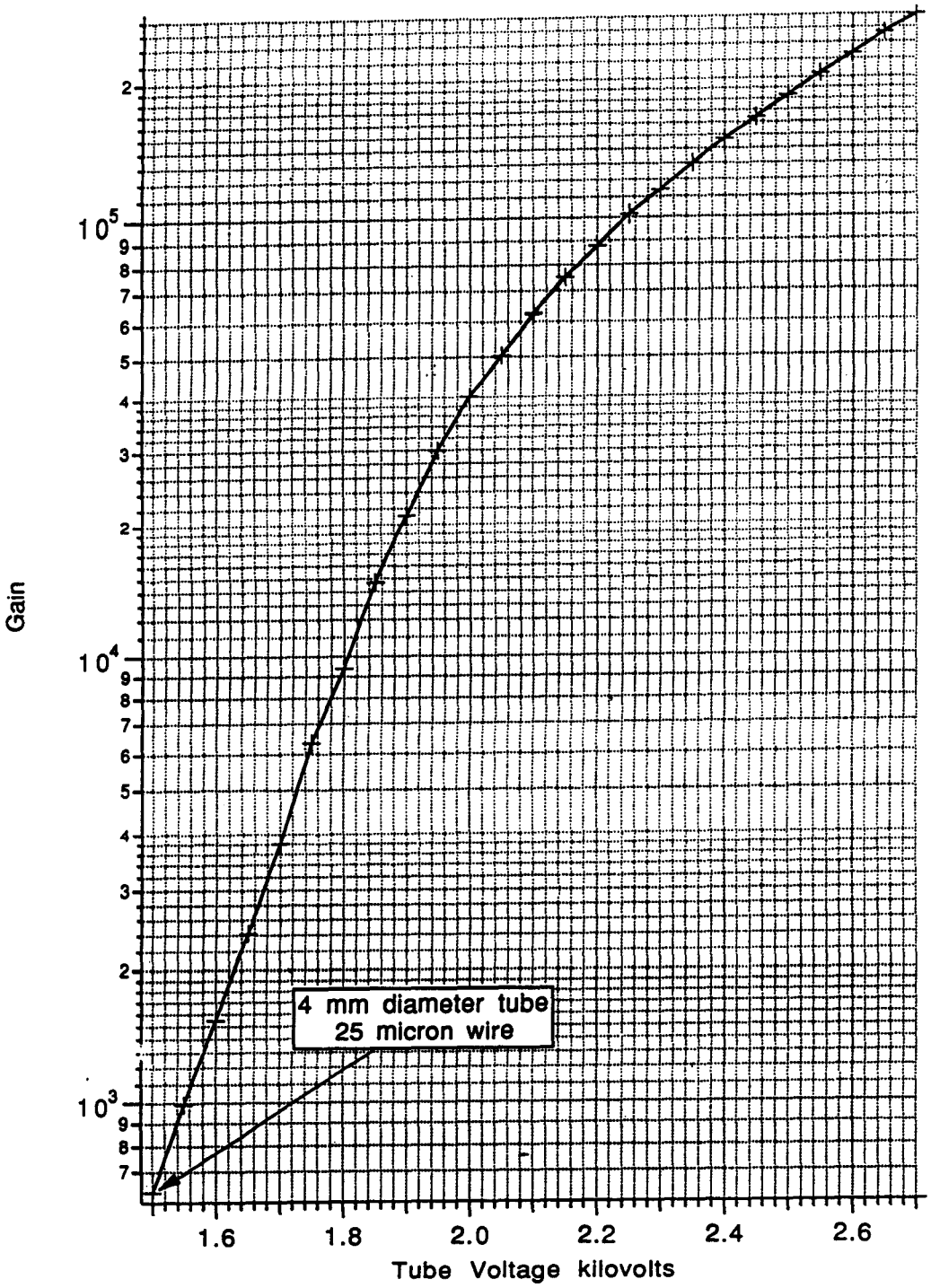

Fig. III.3. The gain curve of a 4 mm straw drift tube with CF_4 -isobutane 80:20 gas. The absolute calibration of the curve is accurate to about 15% but the shape of the curve reflects the true dependence of the gain on voltage.

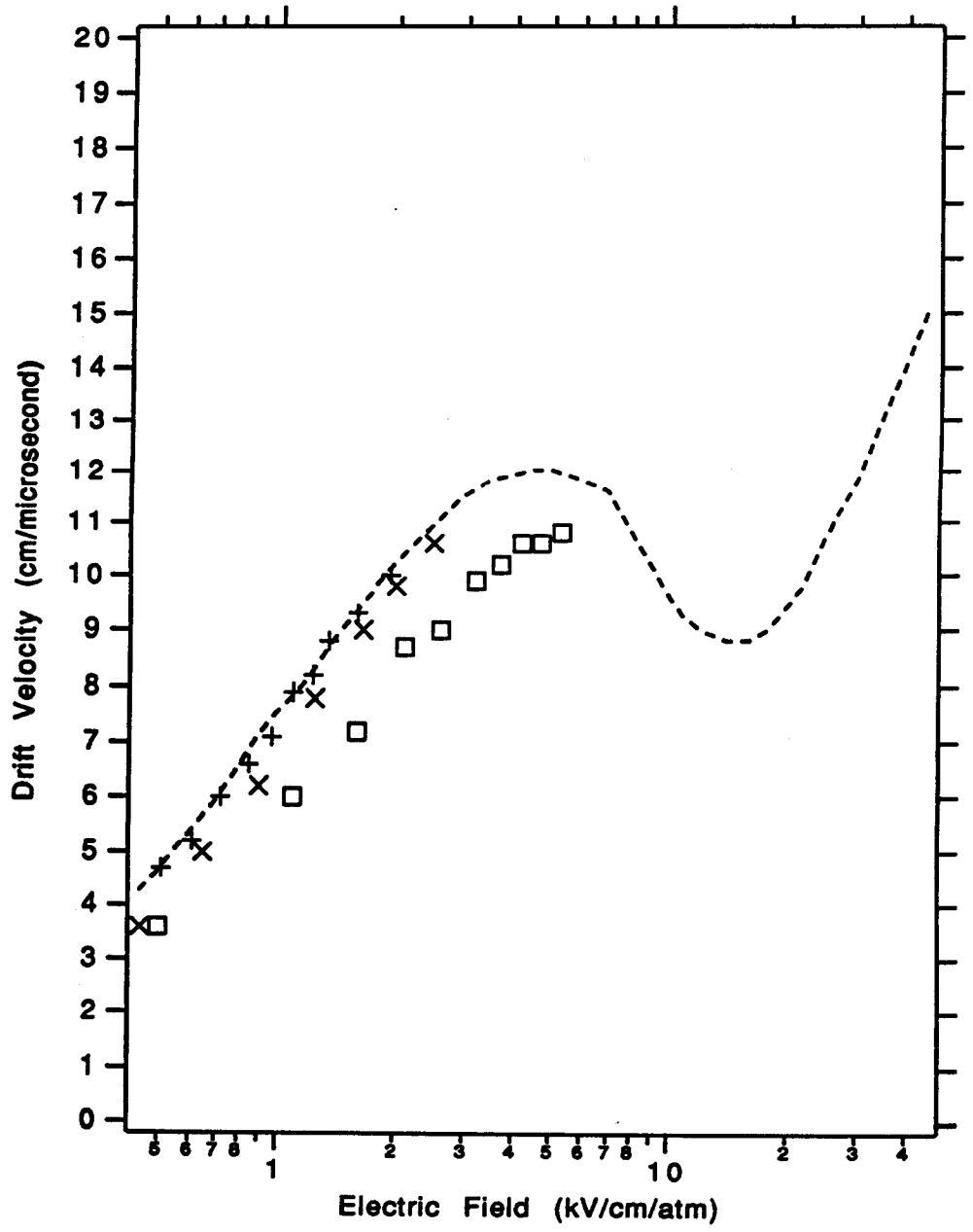

Fig. III.4. Measurements of the drift velocity in CF_4-isobutane 80:20 as a function of electric field strength. The squares are from R. Openshaw,*et al.*, the + are from T. Yamashita, *et al.* and the × are from J. Va'vra, *et al.* See the references. The curve is drawn through the points of Va'vra and continued according to the shape of the pure CF_4 and CF_4 - CH_4 mixture curves.

IV. MODULES

IV.1. INTRODUCTION

We have carried out a detailed study of a modular straw drift cell tracking system for the central tracking region of the SDC detector. The tracking system consists of a series of concentric superlayers coaxial with the beam direction. The superlayer design is shown in Fig. IV.1. The superlayers are made up of close packed trapezoidal modules, each of which contains about two hundred 4-meter-long drift cells. The cell cathodes are formed from light weight plastic straws. A number of prototype modules have been constructed. Although more work needs to be done, these tests and prototypes all indicate that a viable tracking system for the SDC detector can be built using straw tubes in modules.

IV.2. MODULE CONCEPT

The module concept evolved as a method of assembling several hundred thousand drift chamber cells into a tracking system. This requires mass production techniques, quality control, and repairability, as well as low cost. In the module concept the straws are grouped into six or eight layer packages with a strong outer cover. The basic module design is shown in Fig. IV.2. This manner of construction allows the chambers to be mass produced and tested before they become part of the superlayer system.

There are two aspects of the design that are critical. One is the outer shell of the module and the other is the endplate. The outer shell holds the straws rigidly in a close-packed position, maintains the alignment along the length of the module, and takes the compressional load of the wire tension, which is about 12 kg force. Since the straws have an internal support every 80 cm, they can be forced into a rigid close-packed array at these points and bonded before insertion into the shell. The unsupported 4 meter external shell does not have to be straight to 50 microns, since it is only between the 80 cm attachment points that it will be a free span. An independent alignment method will be used to attach the module to the cylindrical support structure and provide the overall straightness. Also the trapezoidal cross section must be maintained between 80 cm support points by the shell. The endplate structure and the bonded straw positions maintain this shape at the support

points. The endplate serves as the hold down point for the wires, the gas manifold for flowing gas through the straws, and the interface for the HV and electronics.

A total of six small prototype chambers have been built to test out details of this design. The basic prototype design is shown in Fig. IV.3. This 25 cm long module contains 64 straws. The modules are presently in use at Indiana University, University of Colorado, University of Michigan, University of Pennsylvania, and KEK.

IV.3. CARBON FIBER SHELL

The straw cathodes are not naturally straight. They have an average bowing of 2-4 cm over a 4 meter length. They also have a very weak bowing resistance and will not support the wire tensional loads by themselves, even if glued in larger arrays. All methods of assembling straw structures must confront these properties of the straws. That is, the straws must be held straight in some manner, must be formed into regular arrays by some means, and the wire tension must be transferred to some external support structure. It is the external carbon fiber shell that accomplishes this purpose.

A design of the graphite/epoxy straw module shell has been completed. Detailed design calculations on the module have been performed, and specifications and detail drawings produced to define completely the module for fabrication. The design is shown in Fig. IV.4. During this design work it was found that the major loads on the shell were the thermal loads that develop as it cools back to room temperature from the maximum curing temperature. The stress-free temperature of a cured composite is close to the maximum cure temperature at which most of the cross-linking occurs in the polymer used for the matrix. Because of the high coefficient of thermal expansion (CTE) of the epoxy which is about $21\times10^{-6}/°F$, and the negative CTE of the graphite which is about $-1.38\times10^{-6}/°F$, compressive buckling stresses can be induced in the thin graphite laminates. The induced compressive stresses in the thin laminates would cause warping and waviness of the modules. Such warping and waviness are unacceptable in the module; consequently a design was found which involves laying up the thin laminates on a polyimid foam. This enormously increases the flexural modulus and buckling strength of the laminate while imposing very little weight penalty on the module. In fact, the design using the foam core saves weight over that of the solid laminate for the case of designing to prevent buckling due to the wire tensioning forces; i.e., only 0.009-in. thickness of

graphite are required to prevent wire-force buckling, whereas six plies of 0.0025 in. per ply (0.015-in of graphite) would have been required in a solid laminate.

The one meter long shell that has been constructed, and the four meter long shell now being built were both designed at Indiana University, Oak Ridge National Laboratory, and Composites Horizons, Inc., of Covina, California. This company has had extensive experience in manufacturing carbon fiber and Rohacell foam structures. The design utilizes a light weight Rohacell foam, IG-31, in the lid and base structure to increase transverse strength and eliminate buckling. The side walls contain about 1 mm of Rohacell foam. This was included for both buckling strength and for additional strength against straw pressure from the inside.

Each side of the foam panel is covered with a 3 ply carbon fiber layer. In initial tests a carbon fiber prepreg material with a thickness of 0.002 in. was used. This fiber has a modulus of 59 M lb/in^2 and a resin curing temperature of 250°C. The lid and base of the shell are formed separately using matched graphite molds, which were machined by Coast Composites, Irvine, California. The mold machining is held to straightness and flatness tolerances of ± 25 microns. Measurements of the straightness of the 1 meter prototype indicate it is well within the ± 50 micron straightness tolerance we require.

The total material in the shell has been calculated in Section VI.4. For 0.006 in. laminate on a shell built with IG51 foam the total average thickness of a shell is 0.5% X_0. For the final shell we will use 0.0015 in fiber and IG31 foam for a total thickness of 0.36% X_0.

IV.4. STRAW ALIGNMENT

IV.4.1. Straw Stability

The construction of a long straw drift chamber requires that the sense wire be positioned accurately along the axis of the cylindrical cathode. We have investigated the electrostatic stability requirements for this geometry.[23] The result of this study shows that with a 50 gram tension a 25 micron diameter sense wire should be electrostatically stable in a 4 mm diameter straw at 2500 V if the support points are about 1 meter apart. This is quite critically dependent on the alignment of the wire in the straw. We will need to keep the

straw and wire coaxial to better than 100 microns. We have designed several wire support systems.[28] The wire support system which has been used in building the prototype modules is referred to as the "double V," shown in Fig. III.2. It is assembled by snapping together two identical plastic extrusions. Each half consists of a thin cylinder and an end cap with a V shaped passage for the wire and drift chamber gas. The vertex of the V is positioned at the axis of the cylinder. These can be produced cheaply and with sufficient precision by RTI Plastics in Minneapolis, Minnesota.

IV.4.2. Straw Centering

The basic drift cell is constructed with a plastic based cylindrical cathode structure and a 25 micron diameter wire along the axis. The tubes are 4 mm in diameter with a 37 micron wall thickness. The weight of a straw is 0.5 grams/meter. The straws are very light weight and not very strong. The module concept requires that these straws be bonded into bundles and enclosed in a carbon fiber shell. The bonding is done by clamping the straws at 80 centimeter intervals. At each clamp point it is the internal wire support (the "double V") that supports the clamping load. Due to the clamping load the cylindrical wire supports "self center" and align in a regular array. Measurements of this alignment have been made both directly with an optical comparator and by an X-ray of the wire positions of the assembled chamber.[29] See the reference for details.

IV.4.3. Centering Tests

Two types of tests were performed on the double V's.[30] First, the straws and wire spacers were clamped without gluing. This array was measured while still inside the clamp. The positions of the double V's were determined by using a Nikon optical comparator with a measuring accuracy of about 50 microns (0.002"). However, it is estimated that the location of the vertex of the double V could be found to about 25 microns (0.001").

The second measurement was made on an array of straw sections that had been glued with Eccobond 45 epoxy. This particular array was formed layer by layer with a bead of glue applied on the surface of each layer before the next was laid down. The bottom, top and sides (in contact with the clamp) were not glued. After the array had cured it was removed from the clamp and measured in the same manner as the first array.

The determination of the self centering errors of the double V's was made by fitting the measurements to an ideal close packed cylindrical array. This was done using MINUIT and using the x, y centroid, the rotation angle, and the close-packed diameter as fitting parameters in a chi-squared minimization procedure.

The resulting fits gave the following results:

Clamped array (no glue) fitted diameter= 4.044 ± 0.00025 mm (0.15921")
Sigma= 35 microns (0.0013")

The deviations of the fit in both x and y are shown in Fig. IV.5 a, b.

Unclamped glued array Fitted diameter 4.046 ± 0.001 mm (0.15930")
Sigma 30 microns (0.0012")

The deviation of the fit in both X and Y is shown in Fig. 4-7 a, b

The more important result is the self-centering error we have determined. We conclude that the unclamped array can be modeled by a perfect array with an error at each wire position of less than 0.030 mm (1.2 mils). (We believe that much of this error is measurement error due to a lack of precision in determining the vertex of the double V.) This error is well within the requirements set for the tracking precision in the SDC. We intend to use this modeling technique for the final modules, so that a rather restricted number of parameters will be used to determine the wire positions of the module.

In a second test of one of the short 64-straw modules the wire positions (not the V's) were determined by direct measurement of an X-ray photo of the chamber. This measurement is reported in Ref. 29. The direct measurement of the variation in the wire position will take into account both the misalignment of the wire spacers in each end of the module as well as a misplacement of the wire in the double V. These measurements showed that the deviation of the wire position in a plane was less than 25 microns. This again confirms that we can easily meet the 50 micron tolerance requirement.

IV.4.4. Shell Straightness

We have tested several 1-meter shells. These were produced for us by Composites Horizons, Inc. The final configuration of the shells is still being worked out, but the initial measurements look very encouraging. The thickness of the lid and the base components of the module are within ± 0.0025 in. for several different layup configurations. This is presently at the level of our requirements. The individual flatness of the components before bonding was also measured. It was also appears to be within the ± 0.0025 limit.

The more critical measurement of the unconstrained straightness of the shells has also been measured for the first prototype module. This was done by resting the shell on its edge as shown in Fig. IV.6. The module was constrained in the vertical at only one point in order to allow the module to take its natural shape. The position of a cross hair fiducial at various positions along the length of the shell was measured optically. In Fig. IV.6 the results of one of these measurements is shown. It indicates that the maximum deviations from a straight line are of the order of 0.004 to 0.005 inches. This is somewhat larger, but very close to our required tolerance. We believe we have identified the cause of the variations: the trimming of the lid and shell to the final dimensions was not done with the required precision. This is being addressed by Composites Horizons and is not expected to be difficult to correct. We will be producing several more one meter modules and measuring them. The four meter module of the same design is scheduled to be ready in December, 1991.

IV.5. ENDPLATES

The end plate has multiple functions: it serves as a hold down point for the wires; it is the gas manifold for distribution of gas to the many straws in a module; and it is the interface for the high voltage and signal electronics, according to the present design. The details may evolve somewhat at a later date.

Figure IV.7 shows a detail of the end of a module. In the present design the straws and wire supports will be premounted in the shell. The wire supports will be attached inside the straws and near each end of the straw. The shell will clamp the straws and wire supports in a closed-packed geometry. The endplate will be inserted into the shell but will not touch the straws or wire supports. The sense wires will be tensioned by clips

in the endplate. The endplate acts as one side of a gas manifold. The drift chamber gas enters each straw through the same hole that holds the solder clip. The other side of the gas manifold is a plate that contains feed throughs for the signals. These extend through the gas manifold and make contact with the solder clips. The printed circuit board for the electronics is attached to the feed through plate. This construction results in a very short end section on each module and a very low mass connection. Our goal is to keep this material to a few percent of a radiation length.

IV.6. HIGH VOLTAGE CONNECTIONS

The high voltage connection and the signal processing will be done on only one end of the module. In the present design the inside cathode structures are at ground and the signal wires are at positive high voltage. The cathode connections to ground are made by an application of conducting epoxy on the ends of the straws. The conducting epoxy connects the inner surface of each straw with its neighbor all the way out to the inner surface of the module shell. This connection is then carried out by a thin copper foil to the outside of the end plate. The high voltage connection is made to each wire through a 10 MΩ isolating resistor. The signal is capacitively coupled to the output. The a high voltage distribution is shown in Fig. IV.8. This is a prototype board under construction, using in-line capacitors. We are also considering a design with high voltage on the cathodes which might simplify this distribution system.

IV.7. GAS CONNECTIONS

Each module will be flushed with a CF_4-Isobutane(80%-20%) gas mixture. The gas enters the module through a gas connection on the end plate as shown in Fig. IV.7. The total gas flow in the module is set by changing the volume of the straws every few hours. See Section VII.2.4. A special feature of the modular design is that the shell also functions as the gas envelope. There is essentially no pressure on the straw wall, so that gas connections to the individual straws is not necessary. The only gas connection is that between the endplate and the shell, where an epoxy bond can be cleanly made. The endplate manifold is formed with a more conventional rubberized gasket.

In the prototype designs the gas flows through the length of the module and exits at the far end. It would be returned to the distribution system via a light weight gas line attached to the top of the module. We are also working on a design for a gas system that circulates the gas down one half of the module and returns it through the other half to the gas exit on the same end of the module. This will tried out in the near future.

IV.8. ELECTRONICS CONNECTIONS

The signal electronics connection is made directly on the endplate. This is shown in Fig. IV.9. Each of the solder clips is contacted by an extension on the outer cap plate. This signal lead is directly attached to a a multi-layer printed circuit board which contains the HV distribution and the blocking capacitors, as well as the preamplifier, shaper and discriminator. The front end electronics is discussed in Section V.

One of the design features which will be incorporated into this board is the provision of isolation traces and ground planes to reduce cross talk between lines leading from the chamber to the preamplifier. Once the signal emerges from the amplifier discriminator chip it is virtually immune from crosstalking to its neighbors but the board must be designed to keep the output signals from influencing the inputs and inducing oscillations. All this is, however, within the technology that is available.

Each tube will be terminated at its far end with a complex impedance designed to absorb the pulses from the lossy transmission line formed by the anode and the cathode of the straw drift tube. The preamplifiers also have an input impedance which is fairly well matched to the impedance of the straw tubes, which is about 300 Ω. The terminations eliminate reflections which would increase the occupancy by almost a factor of two.

IV.9. MODULE LAYOUT

IV.9.1. Axial and Trigger Superlayers

In addition to the detailed module design, the layout of the modules has been optimized for the five superlayer tracker. This involved developing a program to optimize the size, position and separation of each module in a superlayer. In particular the study

investigated ways that the modules could be positioned so that high momentum particles have a minimum number of lost hits in the boundary regions of modules. One way that this can be accomplished is to stagger alternate modules in the radial direction. The unequal radial spacing between modules reduces the required spacing between modules while maintaining a maximum number of hit straws. Configurations have been found that should allow high momentum tracks to have the full complement of hits. A typical layout is shown in Fig. IV.10.

IV.9.2. Stereo Superlayers

The present tracker design will incorporate stereo modules in at least two of the superlayers of the tracking system. The stereo superlayer utilizes the same six layer trapezoidal modules that are used in the nontrigger axial superlayers. The modules are held straight by a machined surface on the support cylinder. Each one is positioned at about a 3° angle with respect to the cylinder axis. The separation of the adjacent modules thus changes as a function of the distance from the center of the cylinder. These modules are also positioned at two different average radial distances, so that there is complete coverage of all tracks in the the overlap region of adjacent modules. The position of the modules in this stereo configuration has been worked out in detail and is given in (ref Westinghouse). This is shown in Fig. IV.11 for adjacent modules, and in Fig. IV.12 for the entire superlayer.

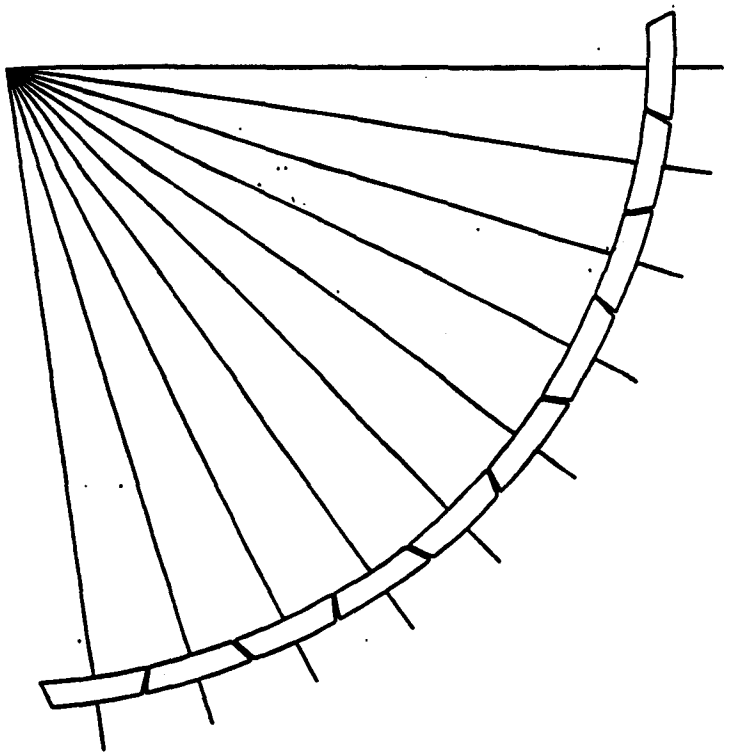

Fig. IV.1. The formation of the superlayers from trapezoidal shaped modules. The radius of the superlayer is chosen to match a fixed size module.

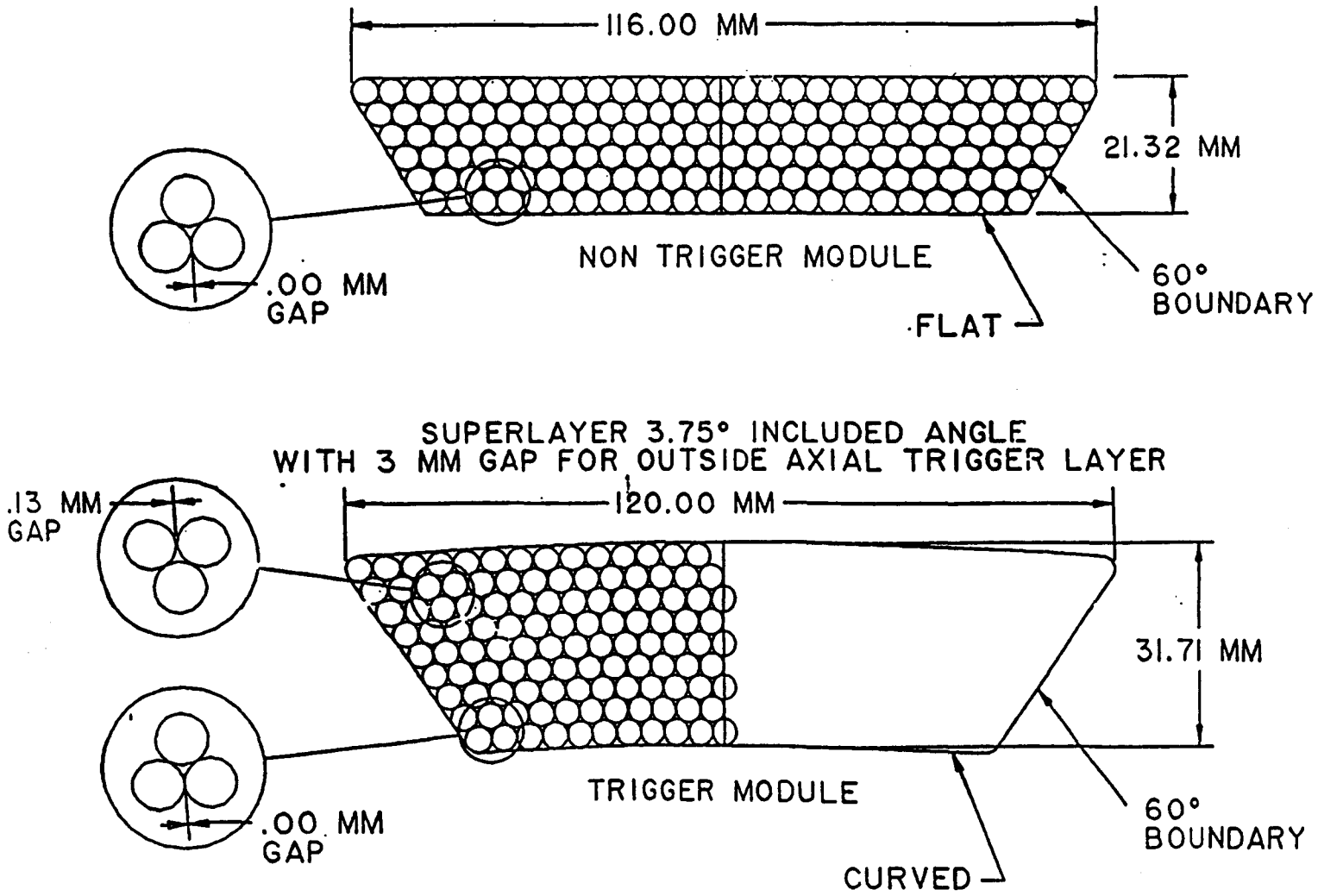

Fig. IV.2. The basic module design is shown here schematically. The two basic designs are shown; a 6 layer module for non-trigger layers and stereo layers, and a 9 layer trigger module that has all straws on a radial line. The present design will probably use an 8 layer trigger module.

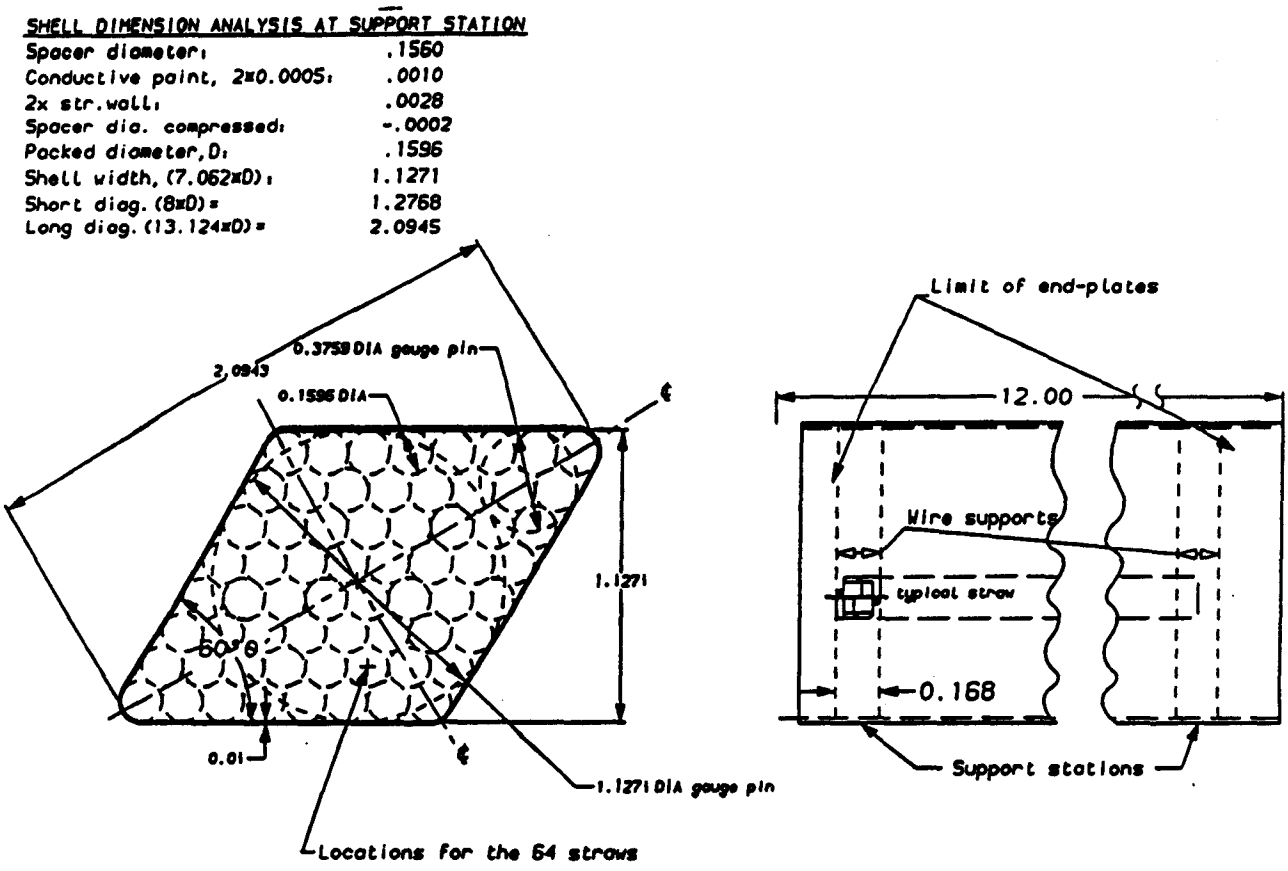

Fig. IV.3. A 64 straw test module with a length of 30 cm.

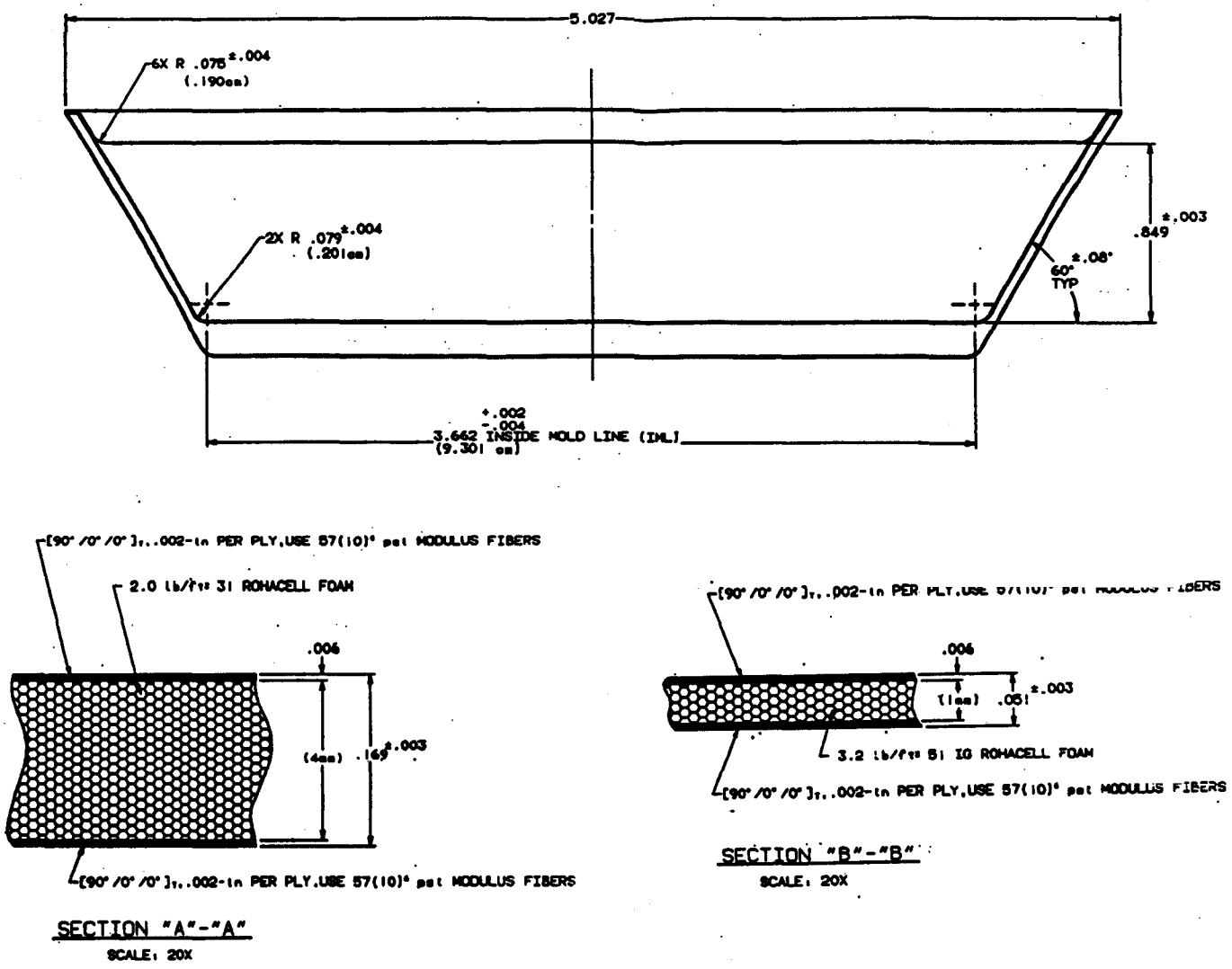

Fig. IV.4. The cross section details for the full size prototype module, showing the Rohacell foam sandwich construction. A detail of foam construction is shown in the insert.

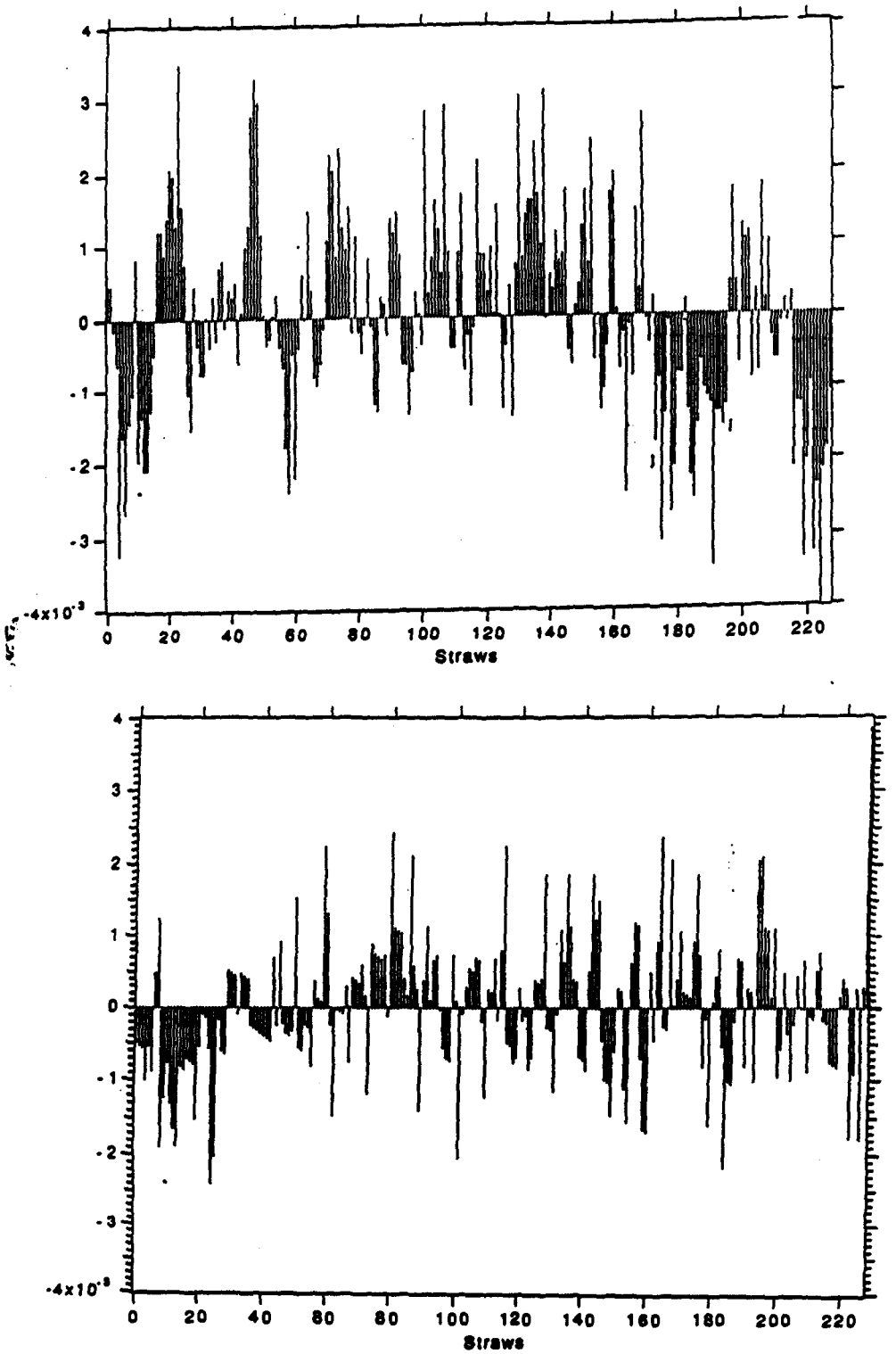

Fig. IV.5. The deviation of the theoretical close packed fit in x position (a) and y position (b) for an 8 layer trapezoid.

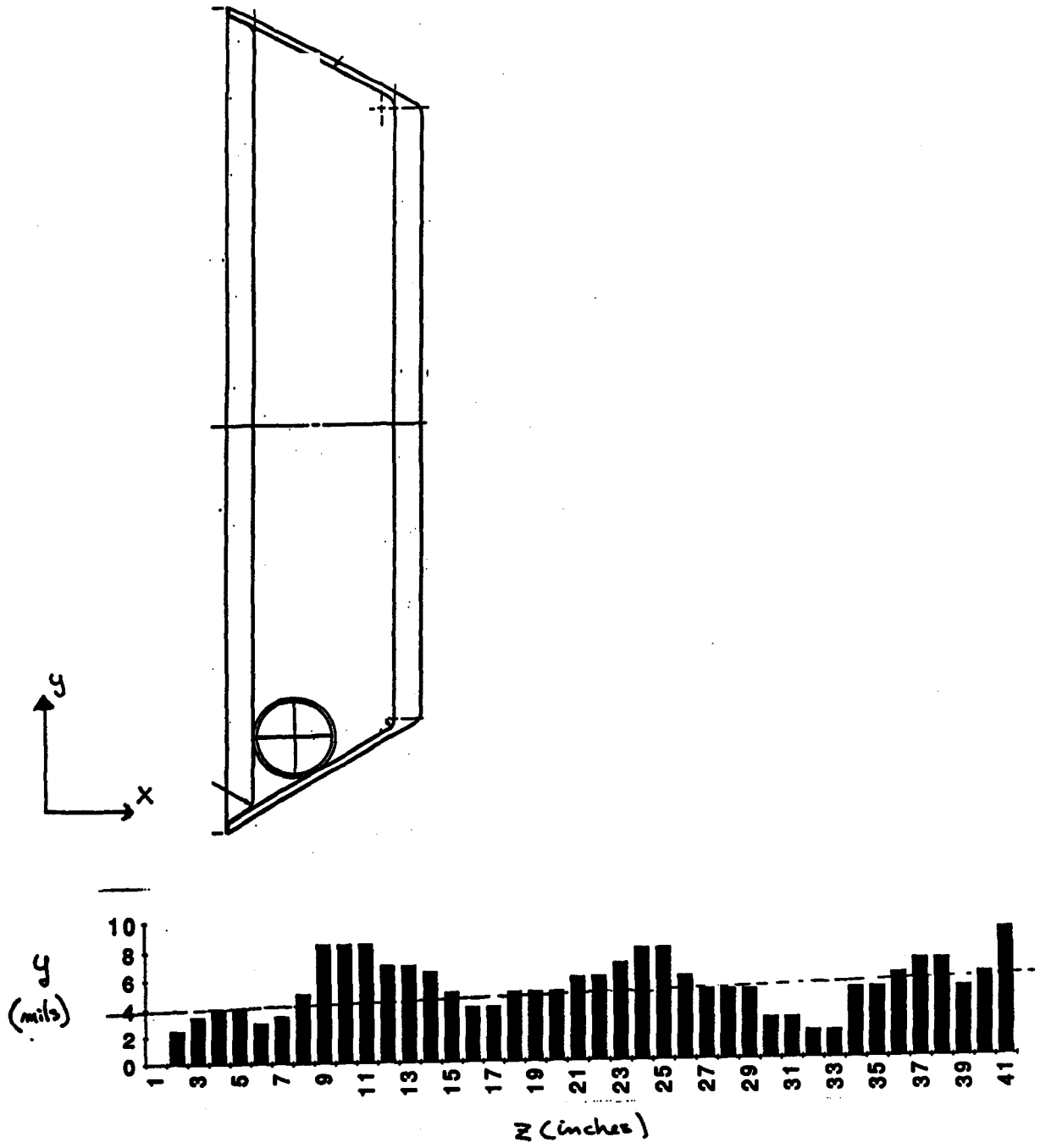

Fig. IV.6. The vertical displacement of the inside shell corner as measured in the first prototype one meter shell.

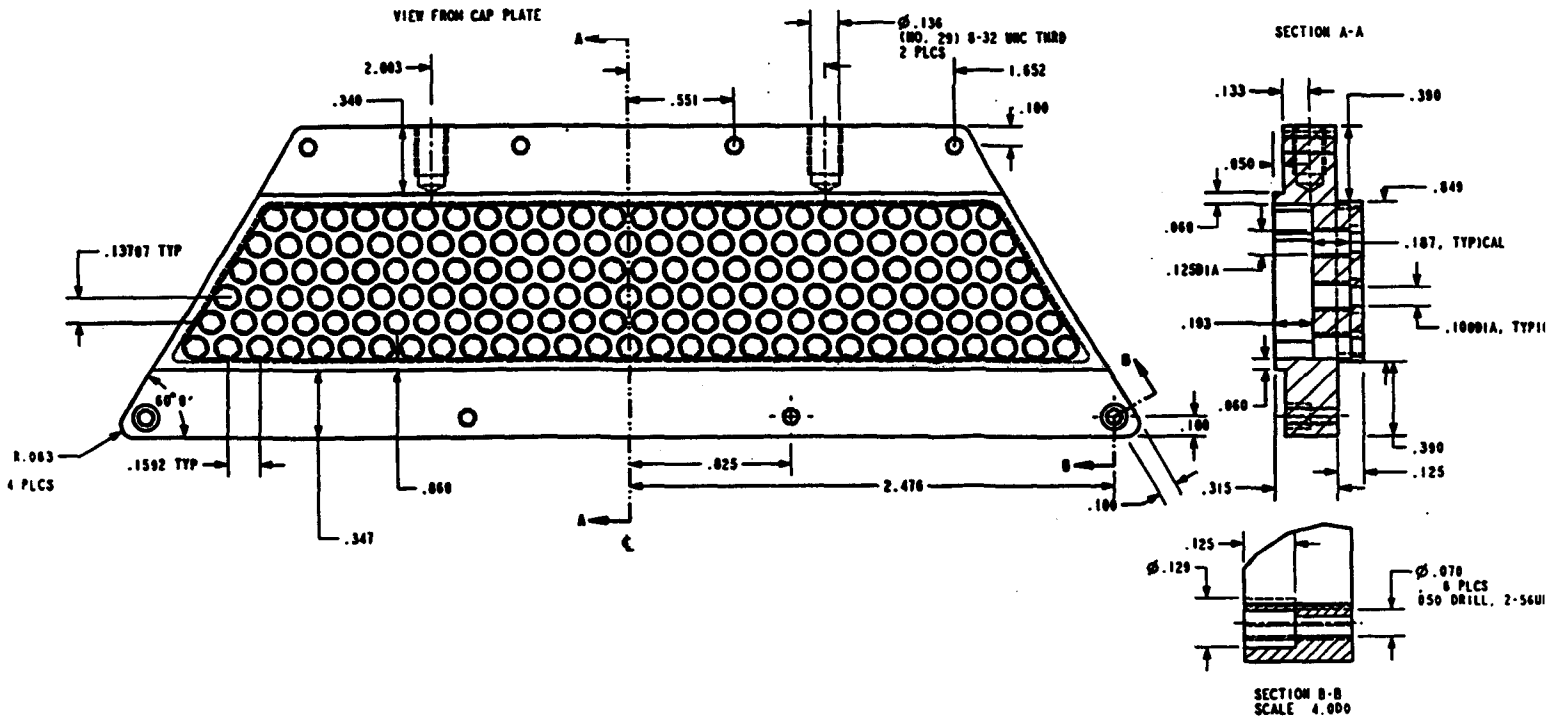

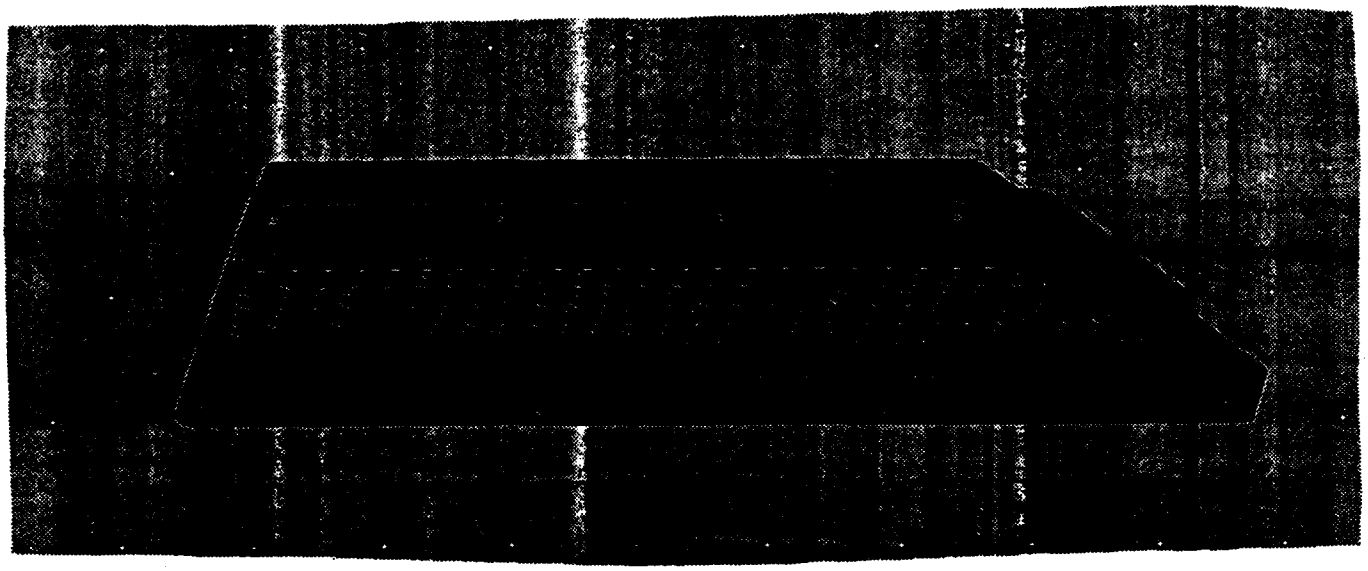

Fig. IV.7. a) Details of the end of a module. The end of the straws stops short of the end plate. The End plate holds the wire tension clips, provides the gas manifold, and hold the cap plate which carries the electronics. b) An isometric view of the end tension plate that is bonded to the shell.

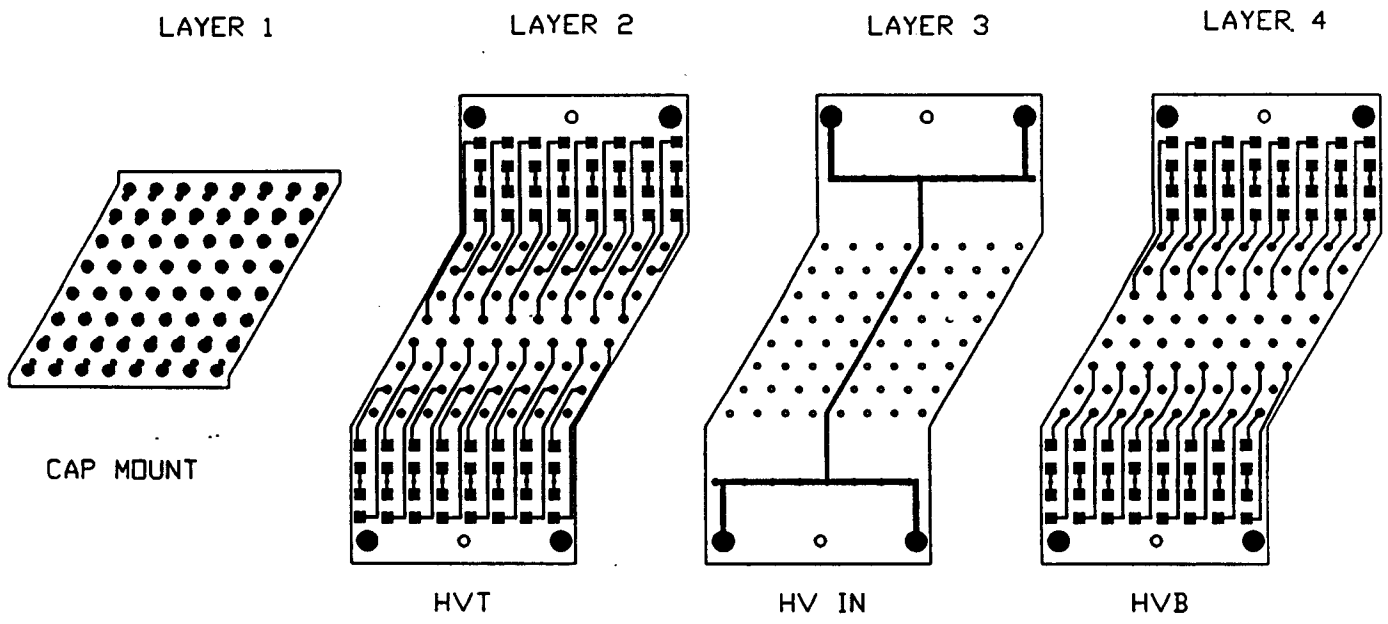

Fig. IV.8. A schematic view of the High voltage distribution board that mounts on the cap plate. Blocking capacitors are connected at the 6 4 wire locations.

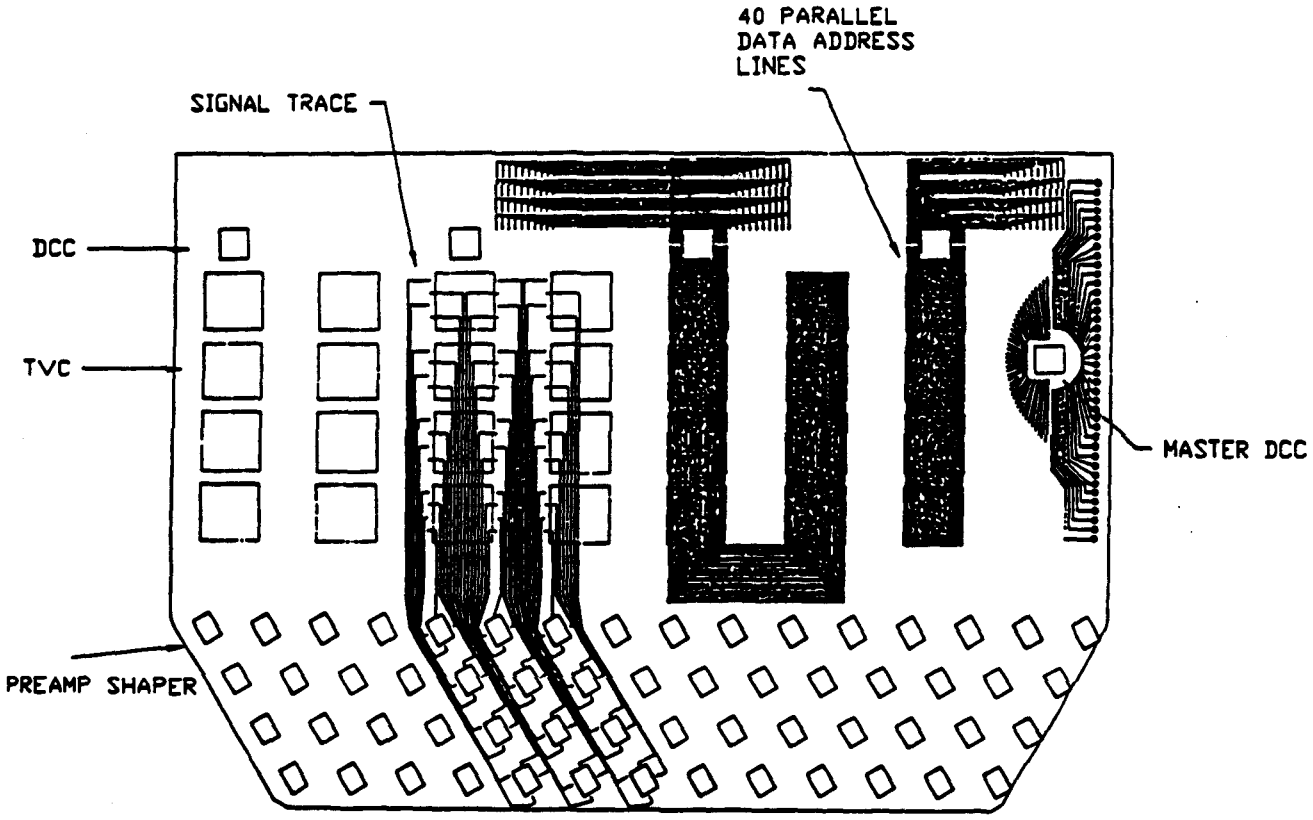

Fig. IV.9. A view of the connection of the front end printed circuit board that connects to the cap plate.

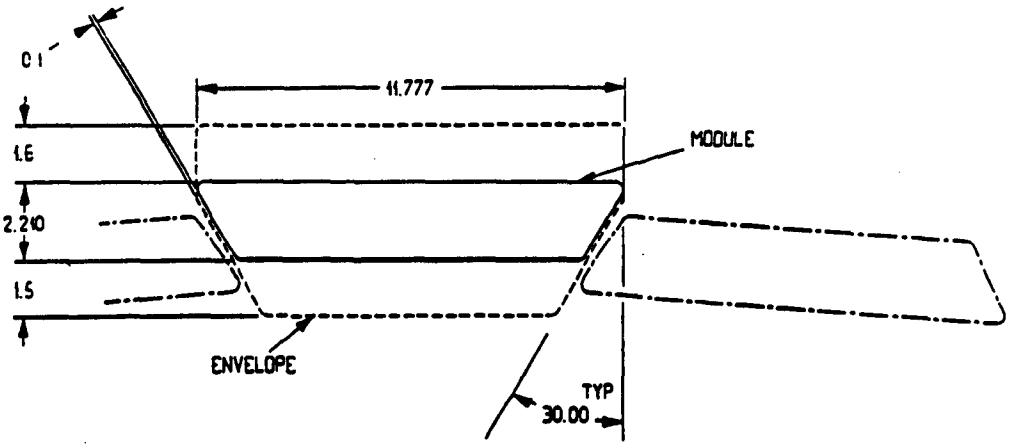

Fig. IV.10. A typical layout of modules in a nontrigger superlayer, showing the vertical stagger needed to get full coverage of all tracks.

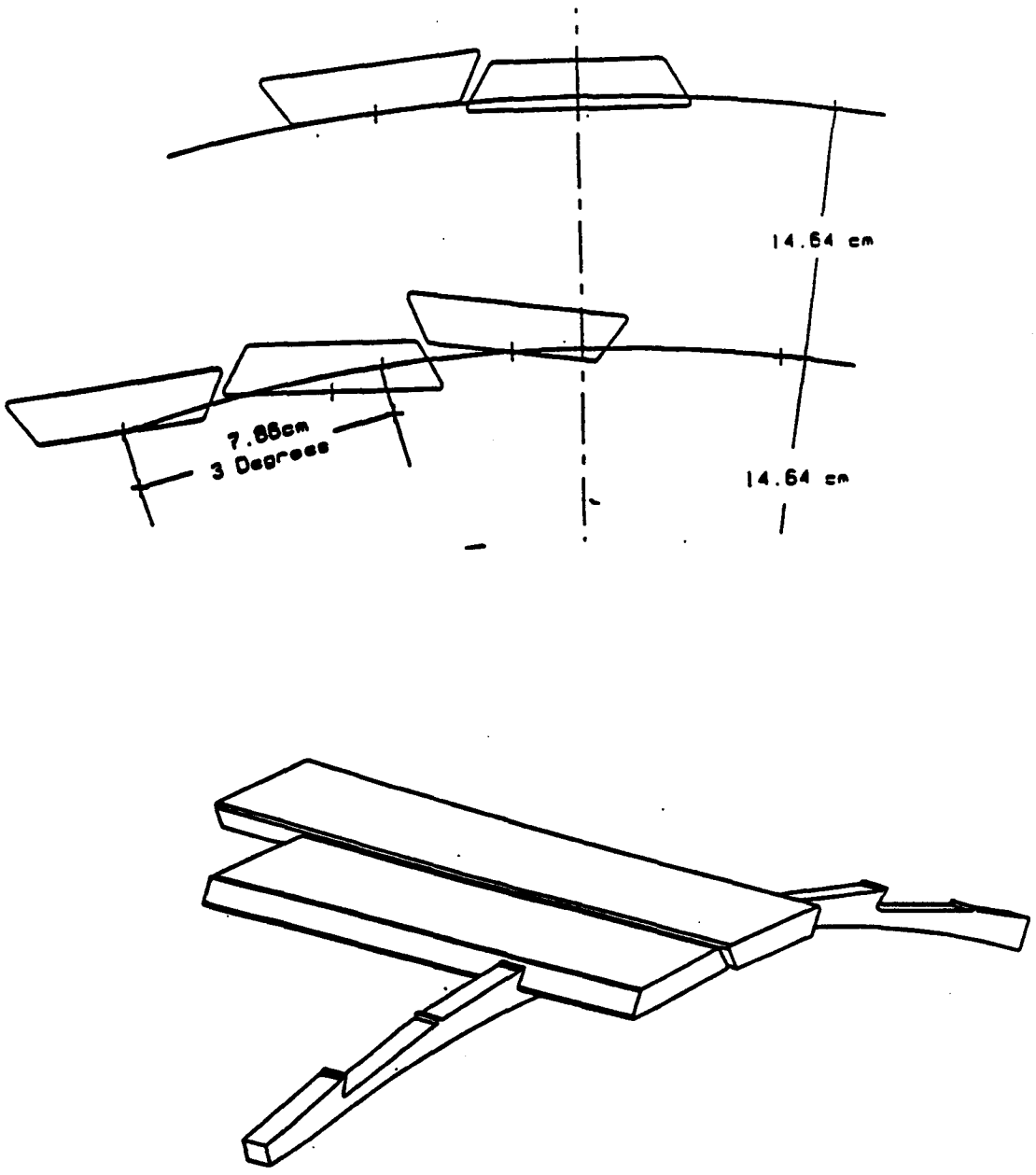

Fig. IV.11. a)A typical layout of stereo modules, showing the vertical stagger and the offset at the end planes. b) The mounting of the stereo modules on the shim rings.

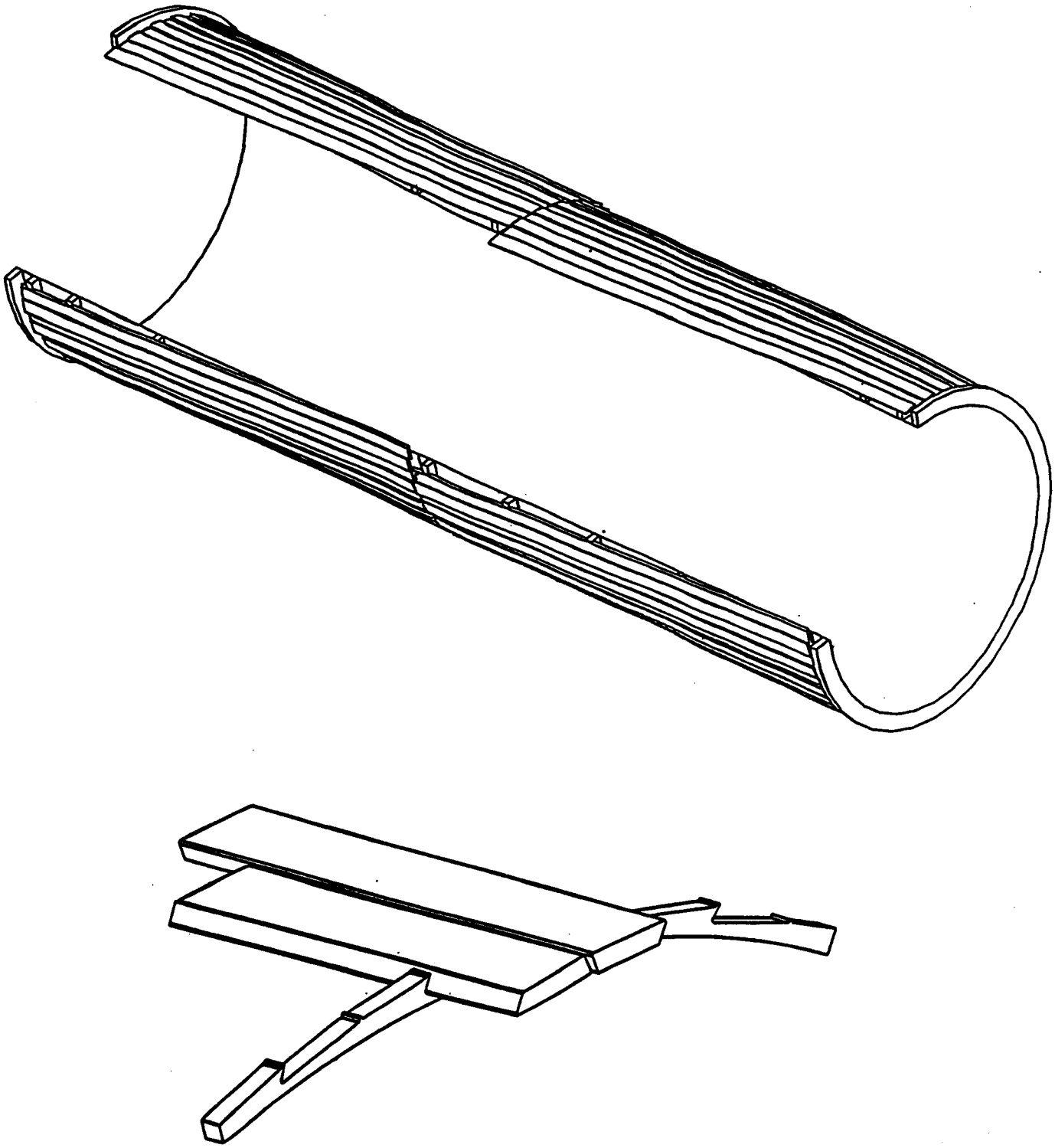

Fig. IV. 12 a) the stereo superlayer as seen in an isometric view. b) Detail of a stereo layer at the midpoint of the cylinder.

V. FRONT END AND TRIGGERING ELECTRONICS

V.1. INTRODUCTION

This is a preliminary DRAFT description of the Front End and Triggering Electronics system for the Straw Tracker. The system described below is an amalgamation of the KEK and Penn systems and has not yet been thoroughly reviewed and revised and is subject to change without notice. We are describing a system that goes from a contact at the straw anode and cathode (see Section IV.8) and contains all of the DAQ and trigger interface and trigger generation functionality necessary for full SSC operation up to but not including the *SDC Standard* DAQ and Trigger boards and fiber optic transmission cable(s) going to the off-detector DAQ and Trigger systems (Fig. V.3). Some features of interface design and geometric or physical constraints are speculation at this time. In general we will try to note all such assumptions.

We begin with a general discussion of the technical and performance requirements demanded by the application and then describe a particular possible logical implementation based upon work done both at KEK (the TMC) and at Pennsylvania (preamplifier, shaper, and discriminator) including details of design, simulation, and test. The necessary electrical connections and passive components and a detailed description of a possible scheme to actually implement the physical interconnections and support required are included in the full Straw Electronics Preliminary Conceptual Design Report.[31] In all of the following, we are assuming a *module* or Front End Board (FEB) of about 200 (140 to 256) active straws per readout assembly. A module (as in Fig. V.1) is defined as an independent subsystem that may be bench tested and verified independent of detector and central DAQ and Trigger connections.

A group of about 64-128 *modules* connect to a standard SDC crate via a Crate Interface Card (four to eight modules per card). The Crate Interface Card is Straw System specific. Four or eight such Crates will be located at each end of the detector in the Electronics/Access area outside of the calorimeter as indicated in Fig. V.2. Each crate is also independently testable with or without Crate Interface Cards using the standard DAQ/Trigger interfaces. High Voltage is supplied, on a module by module basis, to the Crate Interface Cards (and thence via the module cable to the module itself) either directly from the High Voltage Supplies (wherever they are) or indirectly via a Straw System Specific connection within the SDC standard Crate.

V.2. OVERVIEW OF ELECTRONICS SYSTEM AND SYSTEMS REQUIREMENTS

The Straw Electronics can be divided into logical blocks, data flow paths, and physical objects. Not all of these different views wind up with the same objects, but they are all valid and useful ways of describing the system. The logical blocks, arising from the basic design requirements, are:

- High Voltage Connection and Distribution System - the means of providing power to the detectors and providing the interface between the Anode and Cathode and the active electronics section.

- Preamplification, Shaping, and Tail Cancellation - the initial analog processing steps serving to maximize the signal to noise (S/N) ratio and minimize the double pulse resolution time.

- Discrimination - the conversion from the leading edge of a analog pulse to a digital signal.

- Time measurement - the conversion from the leading edge of a discriminator pulse to a digitized time of occurrence.

- Level 1 Storage - the temporary storage of time data while the Global Trigger System calculates whether or not a given crossing had possibly interesting data (about 3-4 μs).

- Level 2 Storage - the temporary storage of time data satisfying the L1 Trigger while the Global Trigger System completes a more exhaustive calculation (from 10 to 50 or more μs).

- Trigger Generation - the *local* generation of track segments from *local* discriminator signals, found track segments are passed on *to* the Global Trigger System in time for use in the L1 Trigger.

- Trigger Interface - receivers and buffers to distribute the minimum set of signals from the Global Trigger System - Clock, L1 Accept, L2 Accept, and L2 Strobe.

- Data Readout - buffers, drivers, and interfaces to the Data Acquisition System (DAQ).

The data flows of interest are:

- Data to DAQ.

- Trigger Data to the Global Trigger.

- Slow Controls to and from the experiment control.

The data flow will be discussed in some detail in section V.3.1.

The probable physical partitioning and detailed implementation are discussed in the SDC Straw Tracking Electronics Preliminary Conceptual Design Report - Draft Version 2.0, Arai, Ikeda, Newcomer, Van Berg, Watase, and Williams.

V.2.1. Design Requirements

For a high precision drift tube or straw tracking system, it is necessary to accurately measure the time of arrival of the first electron (or cluster of electrons) at the anode. This, combined with the desire to operate with as low a gas gain as possible, implies the use of a low noise preamplifier with rise time sufficiently fast to provide the desired time resolution, but sufficiently slow to provide acceptable signal-to-noise.

In addition, because of the high rate of pulses on individual wires - for the inner wires at a luminosity ~ 10^{33} the rate will approach 5 - 6 MHz - excellent double pulse resolution is very important.

The basic design goals which seem reasonable are:

- < 0.75 ns time accuracy in order to ensure spatial precision of < 150 μm .

- Double pulse resolution of 20 - 30 ns. We have adopted the specific goal of having the return to baseline for a single cluster be less than 15 ns.

- Semi-gaussian shaping to minimize baseline shifts and noise from parallel current sources.

- On-chip Level 1 storage for 3 - 4 μs and Level 2 storage for a latency interval of order 50 μs.

- Ability to simultaneously acquire new data, store data, and read out interesting data without self interference or causing interference to other systems.

- Ability to withstand ~ MRad and $> 10^{13} n/cm^2$ over the life of the experiment.

V.3. SYSTEM OVERVIEW

Figure V.3 shows a simplified interconnection of the key elements in the Straw Tracker - from detector through to the Trigger and DAQ systems. WBS (Work Breakdown Structure) numbers for each of the major blocks are indicated to aid the reader. (Note that the WBS structure indicated comes from the predecessor document *SDC Straw Tracking Electronics Preliminary Conceptual Design Report, Draft Version 1.1, August 16, 1991, Newcomer, Van Berg, and Williams* and has not yet been reconciled to the present combined KEK-Penn design.) To date, it is the very front end blocks (analog signal processing and time measurement) shown in Fig. V.4 which have been given the most attention, and rightfully so, since they are repeated for every straw tube and since they define the performance of the system as a whole. We also will discuss briefly the nature of the signal from the straws as this is important for optimizing the electronics.

V.3.1. Data Flows

Data to DAQ. Figure V.5 shows a data flow diagram of the proposed straw-tube detector readout system. Modules or Front-end boards (FEB) of 140 to 256 straws each are mounted directly on the detectors, and Local Straw Crates are placed outside of the barrel calorimeter ,as shown in Fig. V.2. Approximate Data Formats and Rates at the Module, Crate, and System level are indicated in Table V.1.

Trigger Path. Signals from the outer one or two superlayers are used to form track trigger signals. These trigger signals will be used for matching with calorimeter, muon, and silicon tracker signals. Since the straw-tubes are arranged in radial *towers* pointing to the beam interaction point and half-cell staggered, two different types of trigger algorithm, time difference and time sum (mean timer), are possible. The method of measuring the time difference within cells on a track is shown in Fig. V.7. The time difference is inversely proportion to the transverse momentum p_T for properly arranged straws. By changing the clipping time T_C, the p_T threshold value is adjustable over a range of a few GeV/c. The mean timer circuit for staggered cells is shown in Fig. V.8. Since the sum of straw signal timing is constant and equal to the maximum drift time, the mean timer circuit creates a pulse at fixed time after the passage of the track. Although the signal has a timing ambiguity that depends on the z-position of the track (dependent upon signal propagation delay down the straw and partially compensated for by η dependent particle propagation delays), the ambiguity is $< \pm 3$ ns, and thus the mean timer can be used for identifying the bunch crossing. There are several schemes to use combinations of this information and extract a high p_T track segment trigger signal. Jay Chapman (Michigan) is studying various 9 cell and 8 cell track trigger circuits (see Section V.9 and Trigger Conceptual Design Report). The muon chambers and shower maximum detectors will have 1024 ϕ bins, while the outermost straw superlayer has about 2600 ϕ bins. Thus track trigger signals will be combined at the module or FEB in order to reduce the number of cables. (Note that the required trigger bandwidth from the module, even with a limited number of ϕ bins, completely dominates all the other required bandwidths.) Further study is required to optimize the trigger generation logic to be as effective, reliable, flexible, and inexpensive as possible . Figure V.6 shows the trigger-information flow from the straw-tube detector and indicates the return path of Clock, L1 and L2 signals from the Trigger System to the detector.

A key element in both the time difference and mean timer circuits is a delay line. The TMC itself is a combination of delay lines and memories, and has precise delay elements. It may be natural to include the trigger circuits in the TMC, but it is also possible to implement the circuits in a separate chip. This is a complex question which involves the relative quantization of TMC and Trigger signal paths and basic packaging technologies.

Module Level Data Packet		
Header + Flags	6 bits (?)	
Physical Address	1 Byte	
L1 Trigger I.D.	1 Byte	
Bunch Counter	2 bits	
Fine Time	7 bits	
Total per hit	4 Bytes	1.4×10^6 **Bytes per second**
Crate Level Data Packet		
Header + Flags	8 bits (?)	
Module Address	6 bits	
Physical Address	1 Byte	
L1 Trigger I.D.	1 Byte	
Bunch Counter	2 bits	
Fine Time	7 bits	
Total per hit	5 Bytes	7.7×10^7 **Bytes per second**
Straw System Level Data Packet		
Header + Flags	10 bits (?)	
Crate Address	4 bits (?)	
Module Address	6 bits	
Physical Address	1 Byte	
L1 Trigger I.D.	1 Byte	
Bunch Counter	2 bits	
Fine Time	7 bits	
Total per hit	6 Bytes	1.5×10^9 **Bytes per second**

Table V.1. Data Formats and Rates for the Straw Tracker System. These estimates are based upon a 60 MHz crossing rate, a very conservative 10% occupancy per crossing with a three crossing overlap and a 10,000:1 $L1 \times L2$ rejection. The system has 135,000 straws with 200 per module, about 42 modules per Crate, and 16 Crates (8 each end) for the entire system.

It is possible that stiff track trigger signals with different p_T thresholds would be desired. To control the number of cables used, while keeping the several p_T thresholds, it is possible that multi-value logic with two or three different levels could be used. More detailed p_T and track position information could be available for the Level 2 trigger, but this would involve additional trigger data paths. For instance, it would be possible to send 500 bits of information to the Global Level 2 Processor in 5 μs by using a 100 Mbps serial line.

A more detailed description of the circuits planned for trigger formation appears in Section V.9 and in the Trigger System Conceptual Design Report.

Control Path. Figure V.9 shows a diagram of the control path for the front end electronics. Each module or FEB has a serial network interface which is used for slow control of the system. All the monitoring, calibration, diagnostics are done through the serial network. The serial networks in each module or FEB are linked via the Crate DAQ interface to the SDC Control Network. Supervisory and diagnostic control is then available to any legitimate processor in the network. The FEB includes test pulse circuits for the preamp and the TMC and the module or FEB can be independently bench tested by any system capable of connecting to the serial network interface. This serial network may be a standard network (such as JTAG/IEEE 1149.1) or may be SDC specific.

V.4. FRONT END ELECTRONICS AND ANALOG SIGNAL PROCESSING

Each straw sensor will require a preamplifier, shaper, discriminator, time converter, Level 1 and Level 2 storage arrays, and a data sparsification unit. Bipolar technology offers optimal performance for the preamplifier, shaper and discriminator. Bipolar's high gain-bandwidth at low power is unmatched by any other commercially available technology, it demonstrates the best noise performance for shaping times of less than 20 ns, and the matching of the control voltage between transistors. CMOS, because of its high density and potentially low power dissipation, is clearly the technology of choice for the time measurement block, which must include memory for the Level 1 and 2 storage, and must include much of the overall control logic.

Due to the high occupancy and low operating gain in the straw tube system, it is necessary to carefully consider the characteristics of the straw tube as part of the readout system.

V.4.1. Properties of the Straw Signal

The drift velocity for ionized electrons in CF_4, the *fast* gas being explored for use in straw tubes, is about 100 μm/ns. A position accuracy of 100μm,therefore requires sub-nanosecond timing accuracy from the electronics. Since there is no plan to store charge information for offline analysis, it will be important to trigger on the avalanche from the initial drift electrons to get the most accurate timing information. This condition severely restricts the amount of charge available to trigger the electronics. Most of the signal from the straw is induced by the motion of positive ions towards the cathode, a process that takes about two hundred microseconds to complete; much of this signal must be truncated. The equation below gives the ratio of the total charge collected at the anode as a function of time for a straw tube of wire radius a and cathode radius b.

$$\frac{Q}{Q_m} = \frac{\ln(1 + t/t_0)}{2ln\,(b/a)} \qquad (1)$$

For a typical straw tube t_0 is 2 ns or less and $2ln(b/a)$ is about 10. After three t_0, about 6 ns, only 14% of the induced charge has been collected. Adding 2% for the electron contribution, only about 16% total charge for a single avalanche cluster has been collected. It becomes quickly apparent that the t_0 for a chamber directly affects the timing resolution when the gas gain must be limited. Extending the measurement time decreases the timing accuracy for signals of different amplitude due to time slewing. Decreasing the measurement time reduces the available signal and, in gain limited applications, may severely affect the signal to noise.

To estimate the timing resolution for a given charge collection, or shaping time, the input signal is convoluted with a preamplifier and shaper transfer function. Figure V.10 shows a simulation result of the effects of intrinsic noise from the straw and preamplifier with multipole shaping on the timing resolution. These studies have led to the conclusion that a five to seven nanosecond shaping time gives reasonable signal to noise, without compromise to the goal of a locally determined sub-nanosecond timing accuracy. This

gives an approximate available signal of 0.64 fC (4000 *e*) per drift electron for a terminated straw tube operated at a total gain of 5×10^4.

We have developed and tested a lumped sum model of the straw tube as a lossy transmission line. Signal to noise for a straw tube with a transmission line termination requires careful analysis. The complex impedance of the lossy straw tube requires a complex rather than purely resistive termination. A suitable passive circuit is formed by adding a small capacitor in series with the termination resistor. The signal, of course, is absorbed at the termination end and therefore only half of the total charge is available to the readout amplifier. In addition, when formed with only passive components, the intrinsic noise in a measurement is dominated by the termination (assuming a well designed preamplifier). In this situation, the choice of symmetric shaping may help reduce the noise. In Fig. V.11 the shaping time is assumed to be 5 ns and the straw is assumed to be terminated with a 300 Ω resistor. The RMS equivalent noise in electrons is plotted as a function of detector capacitance, (length of the straw tube) for different numbers of equivalent pole shaping stages. It can be seen that a considerable reduction in noise is achieved as the number of shaping stages is increased.

While simulations show that significant additional noise reduction is possible by replacing the passive components at the termination end with an active load, at a power cost of about 3 mW per channel, the additional cost and detector design complexity probably argues against this possibility.

V.5. BIPOLAR PREAMP AND SHAPER

Several different designs for bipolar preamplifiers and shapers have been pursued both at KEK using an advanced NTT process and at Pennsylvania using both a complimentary AT&T process and a high speed Tektronix process. The discussion below concentrates on the AT&T preamplifier design, but similar performance is obtainable from the NTT design, and the full multi channel Preamp / Shaper / Tail Cancellation / Discriminator chain will first be realized in the Tektronix process. It is important to note that the circuit design is, to first order, independent of technology and any of the above technologies could be used to fabricate the production devices.

Circuit Design. For the preamplifier design, we have chosen a cascoded common emitter configuration with a dominant pole primarily determined by the feedback network (Fig. V.12). This self-biasing circuit allows the input transistor to be large and operate near it's noise optimum, while requiring only a modest supply voltage of 3 to 4 volts. The power dissipation is therefore relatively low and the circuit may be easily implemented in advanced, high speed technologies that characteristically have low breakdown voltages. As shown in the figure the common emitter structure is duplicated and forms a pseudo-differential input for the fully differential shaper.

A differential structure has been implemented in the shaper to help eliminate sensitivity to external sources of noise conducted in through power supply lines or radiated into the chip itself. In the original prototype version of the amplifier, fabricated in the AT&T ALA200 linear array, the "dummy" side of the preamplifier had a bandwidth limit of 3 MHz. This helped to reduce the thermal noise, improving the S/N by about 15% in a realistic system with a 10 pF detector capacitance. In a new version fabricated at AT&T in December 1990, the bandwidth of the balance side amplifier is matched to the input amplifier to provide fully differential inputs (other than the inherent asymmetry in the straw tube itself). While this increases slightly the thermal noise, it was felt that it would aid significantly in noise rejection (such as from RF pickup in connections to the straw tube) and would provide a more robust system, at least for initial field tests.

The shaper has one zero matched to cancel the dominant pole of the preamplifier and three equivalent integrations that limit the bandwidth and maintain pulse symmetry (Fig. V.13). Good matching is achieved in the pole-zero cancellation by choosing components of the same types to dominate the pole and the zero. The integration poles are formed in the collector nodes of each differential pair. The collector resistor times the stray capacitance at each node sets a time constant of about 1.7 ns for each stage. These time constants match to within a few percent between stages, but are expected to vary more chip to chip. Manufacturers four sigma guarantees are about ±25%, but quoted *typical* numbers are less than ±15%, and our experience over a small number of wafers is that the variation has always been less than ±10%. Nevertheless, we are investigating methods to *program* this shaping time, so that preamplifiers may be matched to each other and perhaps tuned for the best system S/N.

The semi-gaussian pulse symmetry realized by use of multiple pole shaping is demonstrated in Fig. V.14 which shows the shaper response for a 1 fC input pulse formed

by injecting a 1 mV signal into a 1 pF capacitor. The amplitude of this pulse is within 15% of the value predicted by SPICE simulation and is well within range of uncertainty in the measurement.

The intrinsic amplifier noise is primarily determined by the size of the input transistor and it's quiescent current. In the design stage, the noise performance was optimized for an amplifier with a pure detector capacitance of 5 to 10 pF. The quiescent current was set to about 0.5 mA and an input transistor of 75 μm emitter length was used to achieve a base resistance of about 15 Ω. Noise performance in the prototypes was checked using a method suggested by Jarron where the threshold required for a discriminator efficiency of 12, 50 and 88 percent is recorded for a input pulse of known charge. The 12 and 88 percent points give the noise FWHM in terms of threshold voltage and the 50 percent point calibrates the threshold voltage in terms of input charge. A comparison of the measured results and SPICE calculations using transistor models provided by AT&T for several values of detector capacitance is shown in Fig. V.15. The agreement between measurements and model based calculations encourages our reliance on SPICE based modeling to predict the performance of system blocks.

V.6. BIPOLAR DISCRIMINATOR

We are presently exploring the design of very low power timing discriminators intended for use with the preamp and shaper. The present design goals are:

Power	5 - 10 mW
Minimum Threshold	10 mV
Hysteresis	2 mV
Time Slewing	1 ns (3-300 mV overdrive)
Output Drive	150 mV diff. into 5 pF

Our designs attempt to take full advantage of the benefits of advanced bipolar technology. Since base emitter matching between transistors is about 1 mV, it is possible to design for a reliable minimum input signal of 10 mV or less without input trimming. High unity gain bandwidth transistors allow for the use of cascaded gain blocks with feedback to implement hysteresis and reduce time slewing. Drawing on previous experience in the design of differential discriminators, we have developed several possible

configurations suited to particular bipolar technologies and are planning to implement a design in our next bipolar run. An example of the near threshold performance of one design, modeled using Tektronix SHPi technology is shown in Fig. V.16. The top part of the figure shows the response of the discriminator to inputs just below and just above threshold; the bottom half shows the change in the output timing as a function of the overdrive. From 3 mV to 12 mV, the largest overdrive used, the output delay shortens by about 1 ns. From about 500 μV to 3 mV the output delay changes by nearly 2 ns. With a power requirement of 7 mW this circuit should easily satisfy our design goals.

V.6.1. New Prototypes

As noted above, a multi-channel (8 channels per chip) preamp/shaper/discriminator with detector tail cancellation has been designed and will be fabricated in the Tektronix SHPi process (layout of the preamplifier and first shaper section is shown in Fig. V.17. The low stray capacitance of this process allows a much lower power dissipation that in previous designs, 7 mW in the preamp and shaper and 7 mW in the discriminator. Revision of the preamplifier by increasing the open loop gain has reduced its sensitivity to the size of the detector capacitance. It is no longer necessary to optimize the preamp power supply voltage for input capacitance in the range of 0 - 20 pF.

To satisfy impedance matching criteria for the muon group, the input impedance has been tuned to be approximately 120 Ω over the useful bandwidth of the preamplifier, with a smooth roll off at high frequency. The tail cancellation circuit is based on a design by John Oliver (Harvard).

This second generation prototyping amplifier will have current programmable analog outputs, before and after the detector tail cancellation, as well as current programmable differential discriminator outputs capable of driving 100 Ω lines. To make it easier to use in a variety of designs, only two power supplies are required.

V.6.2. Radiation Hardness of Complete Amplifier

Six channels of the AT&T preamplifier have been exposed to Co^{60} radiation at BNL. Three channels were exposed to 1 MRad and three to 2 MRad. A small gain loss of approximately 5% was measured for those channels exposed to 2 MRad and there was essentially no change in the noise (the measurements actually indicated a small decrease,

but this is probably due to systematic uncertainties in the measurements). Rise time measurements indicate an increase of approximately 0.6 ns for all channels and only one channel out of six had more than a 1 mV shift in the DC output voltages.

V.7. DRIFT TIME MEASUREMENT

The Time Measurement block takes randomly occurring discriminator signals and provides a digital output that accurately defines the time for the front edge of each discriminator pulse associated with an event accepted by the Level 1 and Level 2 triggers. Two different devices have been under development to satisfy these functions - the TMC (Time Memory Cell) developed at KEK and the TVC/AMU (Time to Voltage Converter and Analog Memory Unit) developed at Pennsylvania. Both devices have demonstrated multiple hit time resolutions better than one nanosecond. At the moment the TMC, which contains the Level 1 but not the Level 2 storage is in a more nearly final form and is used as the basis for this conceptual design. However, it is necessary to develop a chip to store the results of the TMC output during the Level 2 processing and to provide an interface to the Data Collection Chip. The Level 2 Buffer chip (L2B) is an all digital device and is regarded as being relatively straightforward to develop. Possible interference from the high speed digital signals from the L2B to the preamp inputs is a significant issue that must be addressed. It will also be necessary to increase the radiation hardness of the chip set. Some work on the TVC/AMU will continue and it should be available as an alternative device if some unforeseen problem should arise with the TMC.

V.7.1. TMC

Time Memory Cell (TMC) chip is a low-power time-to-digital converter chip which includes the first level buffer inside the chip. The TMC records the history of the input signal in a memory array using a fully digital method. The input signal is fed to the data line of each CMOS memory cell, and each "write" signal to the memory cell is delayed column by column with a variable delay element which is controlled by a feedback circuit. Thus in the present chip a 31.25 MHz write signal is delayed about one ns per column across the 32 bits of column width and then the write pointer is advanced to the next row in the 32 row array. This yields a nanosecond by nanosecond history of the input signal across a 1,024 nanosecond memory (32 rows by 32 columns). Table V.2 summarizes the specifications of the present chip (TMC1004).

	TMC1004	TMC-SSC
No. of Channels	4 channel	4 channel
Least Time Count	1 ns / bit	2 ns / bit
Time Range	1.024 μs (4 ch), 2.048 μs (2 ch) or 4.096 μs (1 ch)	4 μs
Clock Frequency	31.25 MHz	31.25 MHz
Time Resolution	σ = 0.52 ns	σ = 0.75 ns
Number of Rows	32	128
Number of Columns	32	16
Data Encoding	32 bit to 5+1 bit	16 bit to 4+1 bit
No. of Pins	I/O pins = 54 Power / Gnd pins = 34	I/O Pins ~ 50
Supply Voltage	3.0 V	3.0 V
Power Consumption	7 mW / ch	~ 8 mW / ch
Chip size	5.0 x 5.6 = 28 mm^2	6 x 7 = 42 mm^2

Table V.2. TMC1004 and TMC-SSC Specifications

The time resolution of the present chip is $\sigma = 0.52$ ns. This can be explained with a combination of the digitization error ($\sigma_{dig} = 1/\sqrt{12} = 0.29$ ns) and the TMC inherent error ($\sigma_{TMC} = 0.43$ ns). To increase the buffer length while keeping the silicon area within an acceptable level, we propose to increase the least count to 2 ns/bit instead of 1 ns/bit of the present chip. If the σ_{TMC} of new chip is the same as the present one, the time resolution will be

$$0.75ns = \sqrt{(2ns/\sqrt{12})^2 + (0.43ns)^2}.$$

This resolution is expected to be within the requirement of the wire chamber readout. For the TMC-SSC we would then have 16 columns (at 2 ns each) with 128 rows (to give a 4 μs Level 1 delay time) driven by the same 31.25 MHz clock. The increase in silicon area is only 50% even with the quadrupled buffer length, because the control logic and interconnection pads occupy about 70% of area in the present chip. Table V.2 also shows

the specification of the proposed TMC-SSC chip. Figure V.18 shows a block diagram of the TMC-SSC. In the TMC-SSC, we propose to encode 16 bit data to 4 data bits plus one carry bit, and use the system clock of 31.25 MHz (32 ns period). As described in the next section, it is still possible to extract data synchronized with 16 ns trigger signal. The encoding scheme reduces required output pins and data size, and the lower clock frequency eases the chip design and reduces the power consumption.

V.7.2. Level 2 Buffer

Figure V.19 shows a block diagram of the Level 2 Buffer (L2B). The L2B consists of encoder logic and a buffer memory, a buffer controller, a bus interface, TMC control logic, and trigger control logic. The buffer controller has two pointers and the buffer works like a ring buffer. This chip is a fully digital chip using ASICs such as gate arrays or standard cells. In the L2B, the data from the TMC is reconstructed to drift time as shown in Fig. V.20. Since the maximum drift time of a straw is around 30 ns, several rows of data have to be read out from the TMC for each trigger (to allow for the uncertainty in beam crossing). The L2B reconstructs the drift time from this data. Referring to the phase synchronization of the Level 1 trigger signal, the L2B recognizes the starting point of the data and then calculate the drift time. Although the figure shows only one data point, it is possible to process multi-hit data.

V.8. ELECTRICAL INTERFERENCE

One of the most difficult problems to model accurately is the potential interference (cross talk) from one part of this system to either another part of the straw system or to some other detector system. It must be remembered that the basic sensitivity of the front end electronics is about 1 fC for a signal with a pass band centered at about 50 MHz (~ 5 ns t_r, t_f) and that each electronics channel is connected to a detector that is 3 to 4 meters in length. Thus, in the time domain, a single 5 V transition with at $t_r < 5$ ns and a signal to preamp (or straw) capacitive coupling of about 200 aF (2×10^{-16} F) is sufficient to cause a discriminator firing, and, in the frequency domain, the 3 to 4 meter straw detectors act as dipole antennas tuned to a $1/4\lambda$ frequency of about 75 MHz - distressingly close to the ~60 MHz beam clock. The most likely result of assembling all of the pieces (mechanical and electronic) of the straw tracker is the production of 130,000 locked oscillators.

Since the actual calculation of most of these interactions is beyond the present state of the art, it will be necessary to be as conservative as possible in designing the electronics to avoid oscillatory behavior. In addition, it will be necessary to fabricate relatively large scale test detectors that would simulate many of the final relationships just to check for unfortunate interactive behavior.

There are a variety of strategies available to implement *conservative* designs, but they are variations of two basic themes - avoid causing problems by keeping signals small, slow, and differential, and avoid seeing problems by keeping inputs shielded, using differential structures to subtract common mode noise, and keep the potential signal paths short (avoiding *ground loops*). These strategies are all fairly obvious and straightforward, but only large scale tests will give us confidence that whatever measures we adopt are sufficient.

The arguments for the various strategies are:

- Small signal size - since the energy transferred via capacitive coupling is proportional to the ΔV, using low level (perhaps a few hundred mV) signals can reduce the capacitive coupling effects by nearly a factor of 25.

- Slow signals - since the amplifier bandwidth is limited on the low side and since inductive coupling depends upon di/dt, a slow edge (t_r, t_f >> 100 ns) will couple very inefficiently and a reduction of cross talk of one or two orders of magnitude is possible.

- Differential Signals - even fast, large edges, if they are generated and transmitted differentially, will be less likely to cause cross talk. The amount of cross talk reduction varies with the exact means of driving and transporting signals, but is acknowledged to be generally in the region of a factor of ten.

- Shielding - obviously by reducing capacitive and inductive linking of circuits, it is possible to control cross talk. Very good industrial strength shielding can provide 60 to 90 db of rejection over frequencies from tens of Hz to GHz - unfortunately, this involves unacceptable amounts of copper and steel (for the magnetic component of the field, $\vec{B}$. Nevertheless, the straw cathodes

(uniformity, electrical depth, and termination) can have a strong effect on the ability of the system to avoid oscillation.

- Differential Structures - at the amplifier input can, if properly connected to the detectors, subtract out a great deal of the system wide *common mode* noise. The prototype preamplifiers are designed with this in mind.

- Short Signal Paths - (and matched differential signal paths) tend to make inputs less effective antennas, and also make outputs less effective radiators of signal.

Some of these strategies will affect how we partition and package the various functions of the straw electronics system. For example, the prototype TMC involves a relatively large number (16) of single-ended 5 V output lines with potential transitions every 30 ns. These signals go directly into the L2B. While it would be possible to go to fully differential low level signals (as we will probably have to do for the connections from P / S / D to TMC), it may be more efficient and effective to repartition the functionality and include the L2B functions within the TMC chip (perhaps two channels per die). This would eliminate many fast single-ended signals, and it would cut down on the total number of pads needed on the die, but it would force the redesign of a complex and tightly packed system.

In any event, a series of tests using the eight channel P / S / D at full density (i.e., about 200 channels on a few hundred square cm) on various prototype chambers will be done in 1992 to try to understand the severity of the problem and to provide some partially quantitative levels. The results of these tests will have to be fed back into both the electrical and physical design of the system.

V.9. TRIGGER

V.9.1. Introduction

The design characteristics of a straw tube trigger are described, the single superlayer simulation results are presented, and the initial test of the mean timer circuits proposed for the trigger are displayed and discussed. An eight tube axial superlayer is proposed as the basic detector element for an SDC straw tube trigger input. Trigger circuits

based on mean timers are proposed for the processing element that generate stiff track signals from these superlayers of straws. The use of three such superlayers for Level 1 and Level 2 trigger input would provide a robust and extensible trigger that could be implemented simply in low luminosity data taking and be enhanced for high luminosity periods. However, after descoping, the current design has only two outer axial superlayers, so some compromise must be made to achieve suitably low false trigger rates at higher than design luminosity.

The proposed trigger design is based on superlayers of eight straws. The processing of signals from these straws for triggering will be integrated into the front-end cards with the trigger signals extracted from the discriminator outputs as they pass between the bipolar preamplifier/discriminator chips and the CMOS level 1 storage chips. The trigger will be formed in chips specifically designed for trigger processing. Output from the trigger chips, stiff track signals, will pass to the global trigger logic through an information path independent of the data acquisition path.[32,33] If one chooses to process 4 trigger groups in each trigger chip, then each trigger chip inputs 20 straw signals. Of these signals 4 are copies of the cells input to the adjacent trigger chip so that the number of unique inputs to each trigger chip is 16. This is to be compared to the 4 channels/chip of the preamplifier/discriminator and of the level 1 storage. In chip count the trigger is 1 of 8 (1 trigger circuit for every 4 preamplifier/discriminator circuits plus 4 level 1 storage circuits). This 12.5% increase in the electronic component count will be reflected as a cost increment for the trigger. A better estimate might be 15% since there will clearly be additional development costs. Higher channel count is possible in the trigger chips but connection complications work against their use.

The robustness of the trigger depends on the level of redundancy of the trigger information. A single 8 deep superlayer of straws provides triggering with an efficiency and false triggering rate that is quite sufficient at low luminosities and backgrounds. Multiple trigger layers offer increased efficiency and greater rejection of false triggers. Since the trigger chips are completely integrated within the chamber electronics, it is prudent to include these trigger chips on more than one superlayer of straws. The optimal choice of trigger layers is three. These trigger layers must be axial and function most efficiently if placed at large radii. This choice permits a Level 1 trigger composed of 2 of 3 coincidences of wedges in ϕ. The overall trigger design assumes that the trigger primitives used in the Level 2 trigger decision are generated and issued as part of the Level 1 information flow. The choice of three trigger superlayers would provide for significantly

enhanced processing and momentum resolution in triggers formed at Level 2. This offers precise strip, calorimeter, and muon matching at Level 2 if and when such processing is found to be necessary or desirable. With only two axial trigger layers, possibilities are available for reducing the false trigger rate using an OR of the two superlayers. It may also be possible to use a segment in the outer stereo superlayer, although the p_T is less well defined, in coincidence with a high-p_T segment in one of the two outer axial superlayers. An added advantage would be z information at Level 2.

V.9.2. The Single Superlayer Trigger

Stiff tracks are sensed in the superlayer of straws by demanding that the arrival times of hits from the wires be consistent with the patterns possible for high momentum tracks. The drift times in radially aligned tubes change linearly as the track diverges or converges from the radial line connecting the wires. The amount of this change is a measure of the transverse momentum of the track. These times can be quickly processed to select tracks that are sufficiently radial to be higher than a preselected cutoff in momentum. In addition, the time variations in signal arrivals can be eliminated so that a unique crossing number can be assigned to each stiff track sensed. With the correct choice of signal handling, the residual time jitter can be reduced to that from variations in the arrival times from the distribution of track z positions. This 8 ns jitter is well within the 16 ns crossing time and should not lead to any incorrect crossing tags. A simulation of this distribution of output times is displayed in Fig. V.21. The simulation includes minimum bias events from several previous crossings. As a result, the outputs for times other than the desired peak are also seen.

The circuit that provides both momentum selection and crossing number is a digital mean timer.[34] The characteristics of a digital mean timer are that it accepts two digital pulse inputs and outputs a single pulse at the average time of the two inputs offset by a fixed delay if and only if the time difference of the two inputs is less than a preset number. Fig. V.22 displays one of 8 proposed connections of these mean timer circuits to an 8-straw-deep superlayer. Two pairs of radially aligned wires one from each side of the 1/2 cell staggered pattern are separately averaged to a common radial position. These two averages are again averaged in a third mean timer that makes use of the fact that the sum of the distances from the track to the left and right staggered patterns is a constant. This second mean timer eliminates the variation in pulse times due to differing drift distances. Several patterns meeting these conditions are processed in parallel in separate circuits. This

parallel processing is possible since mean timer circuits are very small as measured in silicon area. A single mean timer is much less than 1% of the area of a modest CMOS chip. The outputs from the 8 individual pattern circuits are combined as 2 of 8 coincidences into a single output that flags a stiff track. A programmable transverse momentum threshold is provided.

V.9.3. Simulation of the Superlayer Trigger

Extensive simulation of this triggering algorithm has been performed. This simulation was carried out for the outermost superlayer of the proposed straw tube tracker at the design luminosity of 10^{33} cm^{-2} s^{-1}. The results of these simulations are summarized in Fig. V.23. In this figure the turn-on behavior of the trigger is shown for a 10 GeV setting of the threshold. The sufficiency of this threshold behavior has been demonstrated recently for electrons by Sullivan.[34] Table V.3 gives the triggering efficiency as a function of transverse momentum from the turn-on curve of Fig. V.23. The table also gives the false triggering rate of the design as a function of the hit occupancy within the trigger group. False triggers are defined as triggers not accompanied by a track with p_T greater than 3 GeV. According to the work of Sullivan[34] this false rate has little effect on the quality or rate of the electron triggers. The results displayed in Fig. V.23 indicate that the trigger efficiency rises steeply from threshold to around 94% and that the false triggering rate due to occupancy of overlapping soft tracks is well under one per crossing at SSC design luminosity. In addition, the effect of a non-uniform B field at the 6% level[35] as expected in the central tracker softens the turn-on threshold slightly. Changing E × B effects in the end regions of the central tracker are of the same order and contribute a similar softening to the threshold. The trigger momentum resolution of 10% at 10 GeV is not expected to degrade beyond 15% due to these B-field related variations.

V.9.4. Chip Performance

Trigger chip development for SSC gas tracking detectors began[36] with the fabrication of an analog implementation of a circuit called a synchronizer. This circuit is essentially a dual analog mean timer. It has been superseded by the digital implementation already introduced above. The digital circuit requires no calibration and no special effort to avoid cross coupling of analog and digital sections of the chip. All future work will be with the digital chip.

Trigger Threshold	
p_T	Fraction Accepted
1.0	0.0080
2.0	0.0192
3.0	0.0272
4.0	0.0420
5.0	0.0516
6.0	0.0541
7.0	0.0621
8.0	0.1232
9.0	0.3396
10.0	0.6109
11.0	0.7940
12.0	0.8656
13.0	0.9005
14.0	0.9093
15.0	0.9162
16.0	0.9194
17.0	0.9284
18.0	0.9366
19.0	0.9441
20.0	0.9409
21.0	0.9486
22.0	0.9425
23.0	0.9467
24.0	0.9597
25.0	0.9600

False Rate	
Occupancy	Fraction Accepted
0.30	0.0000
0.35	0.0005
0.40	0.0011
0.50	0.0044
0.60	0.0247
0.70	0.0535
0.80	0.1111
0.90	0.2206
1.00	0.2447
1.10	0.3125
1.20	0.4495
1.30	0.4763
1.40	0.6209
1.50	0.6756
1.60	0.6984
1.70	0.8086
1.80	0.8333
1.90	0.8429
2.00	0.9735

Table V.3. The trigger efficiency versus p_T and the false triggering rate versus local occupancy. Local occupancy is defined as the average number of hits per trigger unit tube.

The digital circuit is based on 2 ns digital delay elements. It contains 15 delay elements in the momentum (angle) selection portion of the circuit and 30 delay elements in the total drift time section. This gives it a range of up to 30 ns in the timing difference of radial wires and up to 60 ns of maximum drift time. Values less than these extremes are programmable within the chip. The circuitry for locking of the delay element timing to an external clock is provided within the chip as are numerous diagnostic points. We have tested the delay cell and locking circuits and have found them to function over the range of 1.3 ns to 4.0 ns, consistent with the CAD simulations. The mean timers have been observed to function including the drift time and momentum restriction circuitry. No design errors have so far been found.

Figure V.24 illustrates the overall performance of the chip. In this plot the relationship of the aligned wire inputs is demonstrated. Since the LV511 IC tester used in this work samples outputs rather than measures times, the relationship between the input timing is evaluated and displayed for a predetermined fixed output time. This is equivalent to measuring the relationship that exists between two numbers that have a constant average. The correct relationship is linear with a falling 45° slope. In addition, the IC imposes a maximum allowed time difference between its inputs. The region of signal output seen in Fig. V.24 illustrates both of these characteristics. A falling 45° line with a cutoff at large coordinate differences is evident. Plots have been generated (not shown) for more restrictive time differences and observed to behave as designed.

V.9.5. Trigger Modularity and Data Flow

The stiff track signals from the individual superlayers are designed to flow to a global trigger processor located at ground level. The exact modularity of this data collection is still being debated. The trigger data multiplexing depends on whether the choice is made to send the trigger primitives (stiff tracks with trigger group locations) synchronously or asynchronously. This also remains under debate. The modularity and information flow for the straw trigger outlined below must therefore be considered preliminary since the precise details of the information flow must await firm decisions about the general data flow of trigger information.

A natural choice for the trigger grouping is into 64 regions of ϕ. This leads to about 80 trigger units from 20 trigger chips distributed over 16 cm of circumference. If one

wishes to accept only one stiff track signal from each of these 64 ϕ regions while restricting the bandwidth from each region to one GHz fiber channel, then the data from each stiff track must be compressed into 16 bits. If three bits are allocated to momentum information, then the position information can be easily represented in the remaining bits. Even with this restricted choice of one stiff track for each of the 64 regions, the bandwidth of the data flow is seriously underutilized. With less than one in five of the crossings yielding a single stiff track signal, the 64 trigger data fibers contain data a small fraction of 1% of the time. A scheme where each region presents any second stiff track to both its neighbor regions for transmission should that region not contain a stiff track, is a possible way to use the distributed bandwidth to overcome the local congestion. Asynchronous transmission schemes take this shared bandwidth to it logical conclusion.

Whatever the transmission scheme for the trigger data, the stiff track finder must issue its track primitives in the form of trigger unit ϕ locations and track momenta. In synchronous transmission the arrival time designates the crossing. In asynchronous (buffered) transmission the crossing number must be included with the data so that resynchronization can be accomplished by the central trigger processor.

V.9.6. Summary

The preferred design for the trigger of the straw tube central tracker would consist of integrated stiff track sensing on three superlayers of axial straws. However, only two outer axial superlayers are available for the trigger. The trigger primitives, the stiff tracks found, are to be collected for regions of ϕ and transmitted via fibers to the global trigger electronics on the surface. This trigger data can be sent synchronously each 16 ns or asynchronously with crossing number tags. The number of such trigger fibers is of the order of 128 or less with a rather low duty cycle. The trigger primitives will be stored in the global trigger crates for processing by the first and second triggers.

Both trigger levels are expected to make use of these trigger primitives in a manner that evolves as the luminosity of the collider increases. Initially, the first level trigger will likely use an OR of the two outer axial superlayers in crude ϕ bins. Sophisticated first level triggers might do combinatorial logic on the pattern of hits including the actual trigger unit ϕ locations. This could provide improved momentum resolution up to the constraints imposed by the non-uniform field effects.

The second level trigger will likely process all of the superlayer primitive information in conjunction with the calorimeter and muon data. Since these other systems offer z information, the matching to them includes the option to correct the momentum of the central tracker with the known z position. For this correction to improve the momentum, individual superlayer trigger ϕ locations will be needed. At second level, we may be able to use trigger primitives from the outer stereo superlayer, which would give z information from the tracker.

The instrumentation of trigger chips on three superlayers of straws (the outer two axial superlayers, plus the outer stereo superlayer) appears completely justified since it:

1. Permits a natural enhancement of the trigger as the luminosity increases. Without this data few options will exist and changes in the on-chamber electronics will be very difficult.

2. Eases the integration of the front end and trigger electronics by making all axial layers identical.

3. Represents a modest increase in cost.

4. Provides handles to overcome unanticipated problems.

Fig. V.1. Approximate layout of the electronics module or Front End Board and attached cable.

Fig. V.2. Module and Crate physical placement on the detector. This view assumes a granularity of 8 modules per Crate Interface Card - implies 8 dedicated Tracking Crates for a 130,000 straw detector - 4 Crates per each end of the barrel calorimeter.

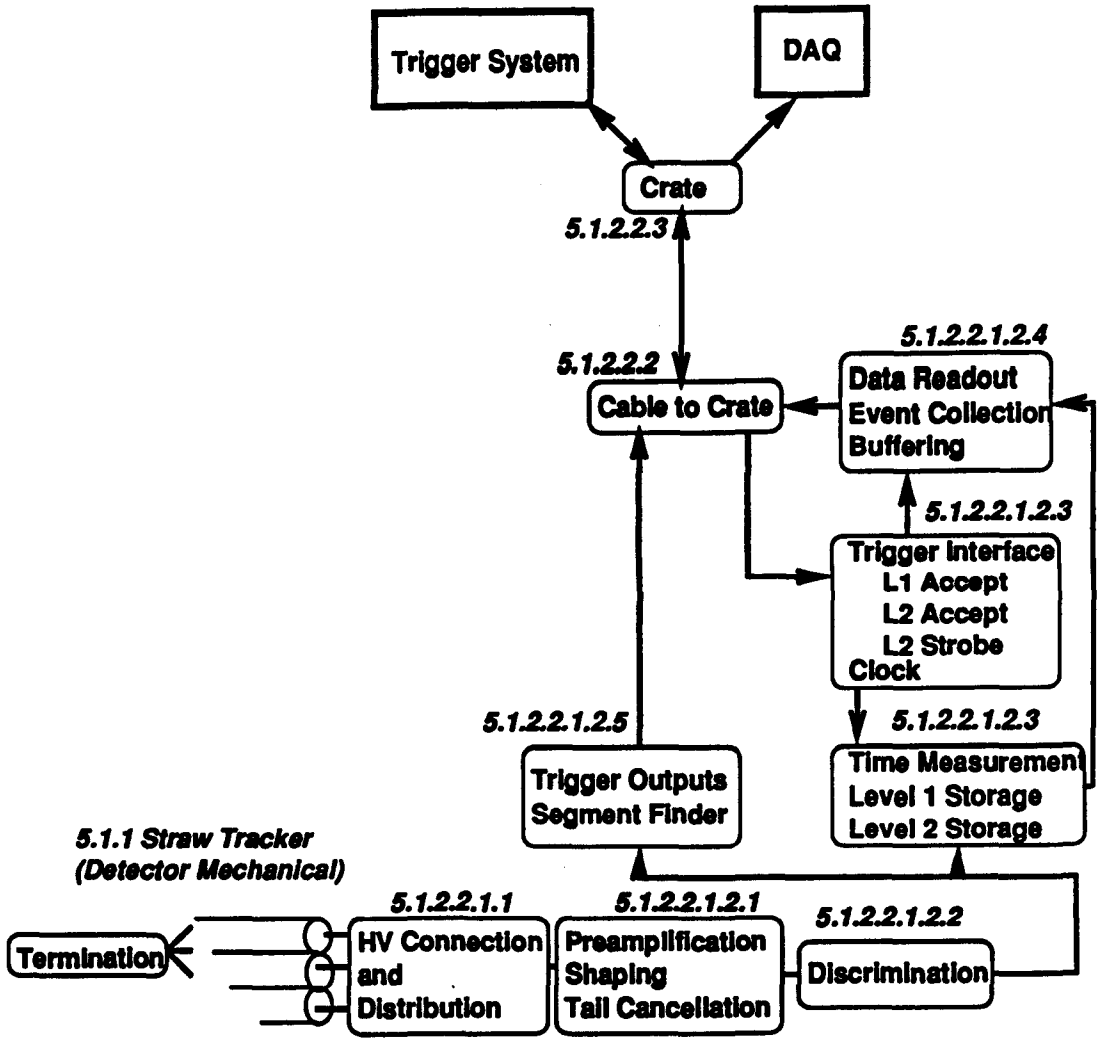

Fig. V.3. Block diagram of the straw readout system with WBS numbers indicated. Note that this particular WBS numbering scheme is outdated and incomplete.

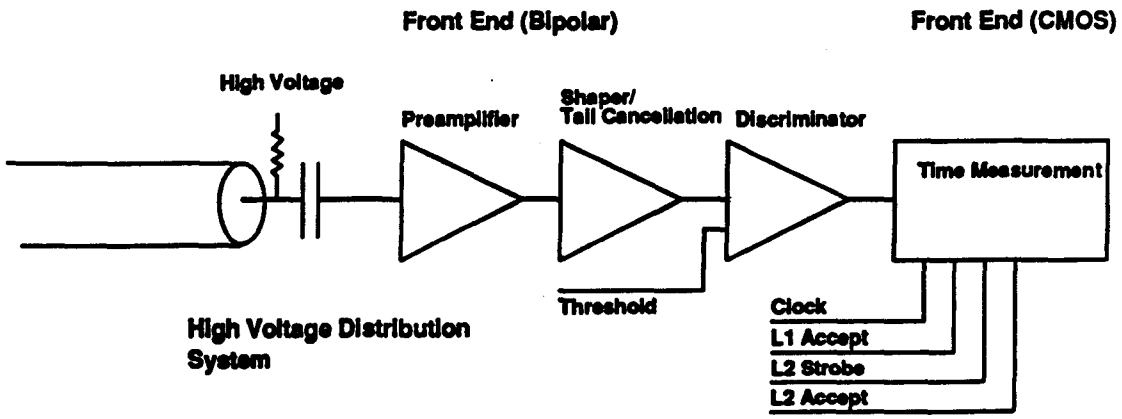

Fig. V.4. Block diagram of the straw front end.

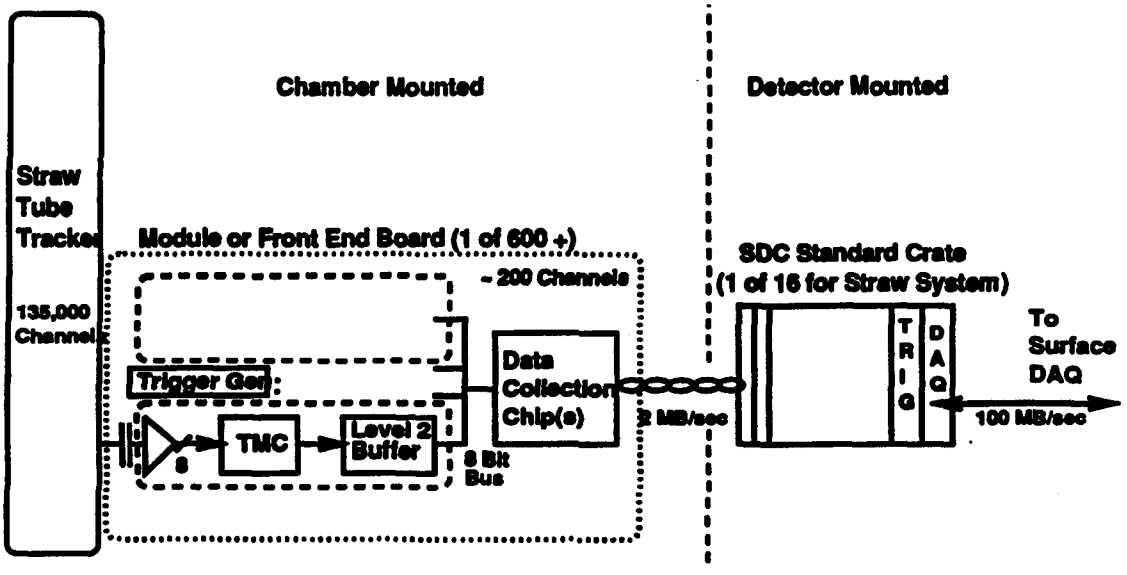

Fig. V.5. Data flow - from the straw to DAQ.

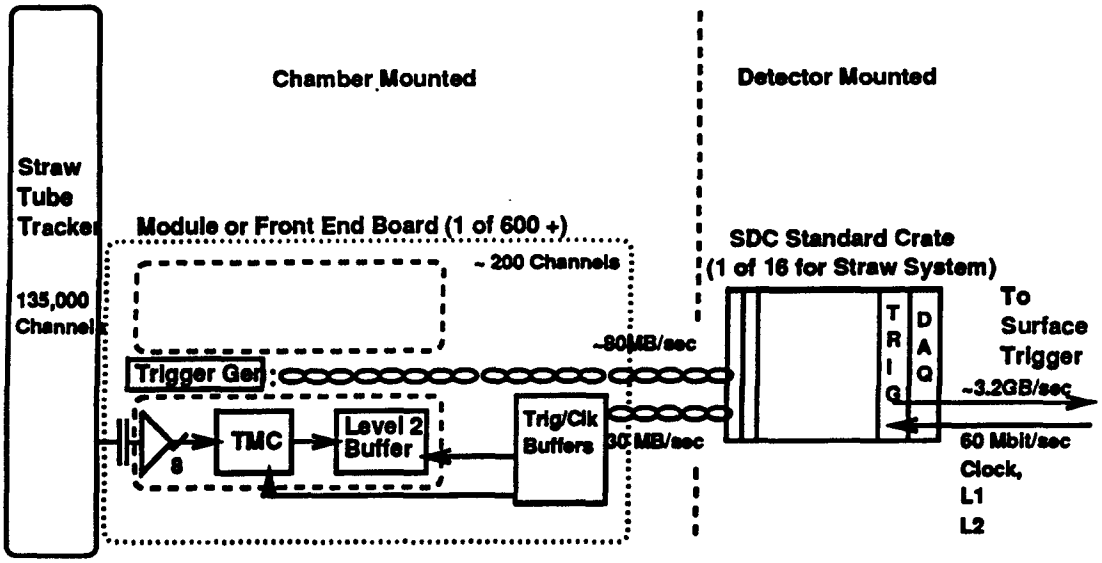

Fig. V.6. Trigger paths for Level 1 segment finding in the straw electronics.

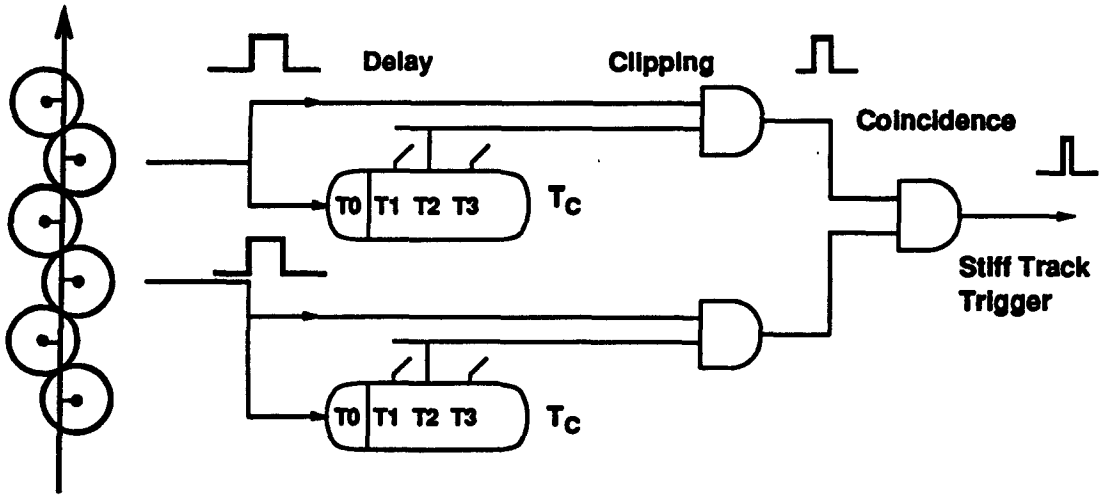

Fig. V.7. Time difference method of segment finding.

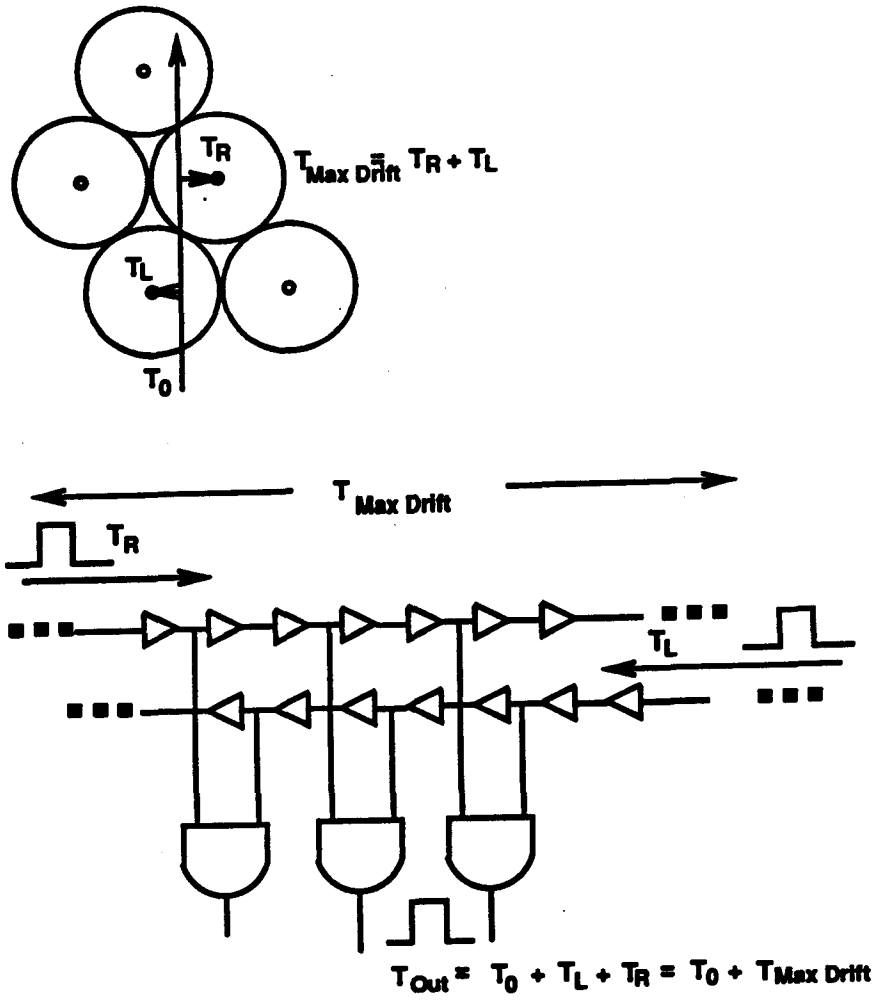

Fig. V.8. Mean time method of segment finding.

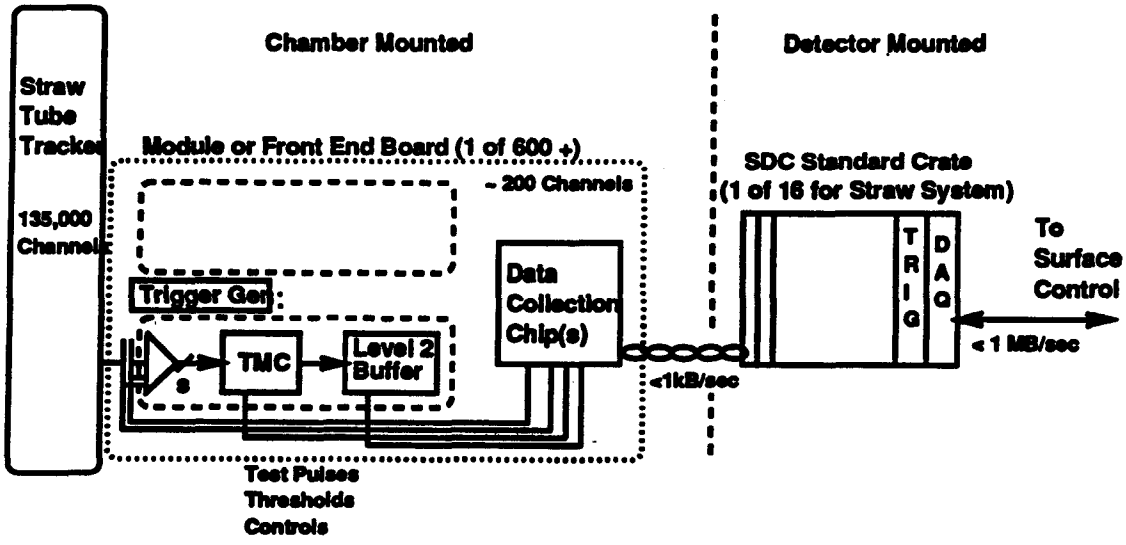

Fig. V.9. Control path to the straw electronics.

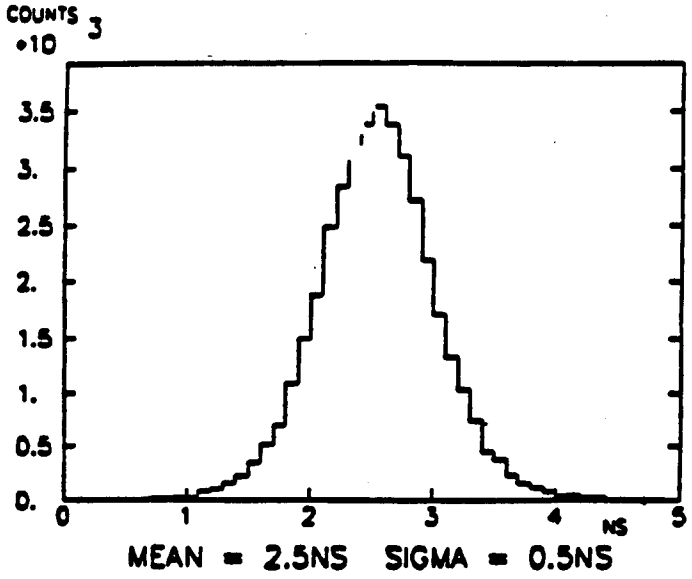

Fig. V.10. Simulated timing resolution showing of the effects of intrinsic noise from the straw, amplifier and shaper. The straw t_0, and electronic t_m, 5 ns, S/N is 6:1 and the effective threshold is 3 times the RMS noise.

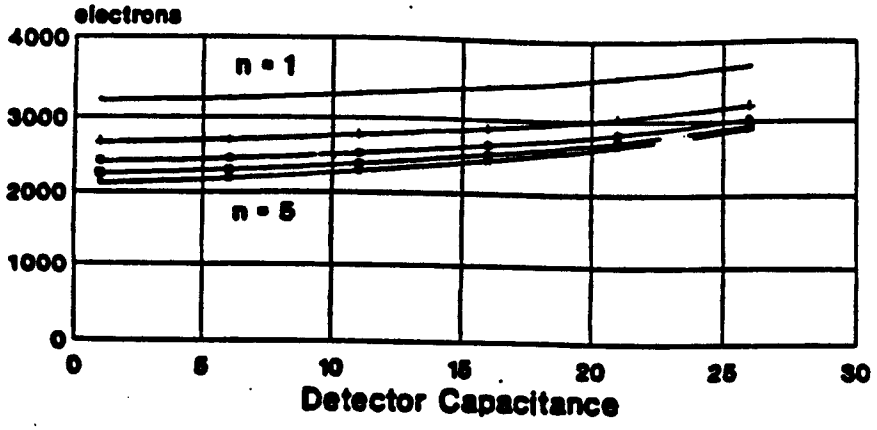

Fig. V.11. Calculated ENC_t for our prototype preamplifier as a function of detector capacitance for different numbers of shaping stages. The noise contribution due to a 300 Ω termination resistor has been included.

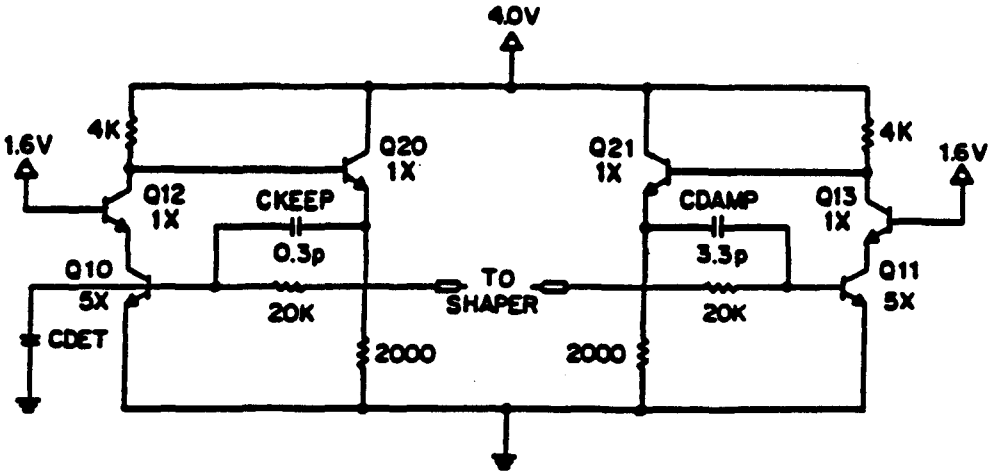

Fig. V.12. Schematic for prototype preamplifier.

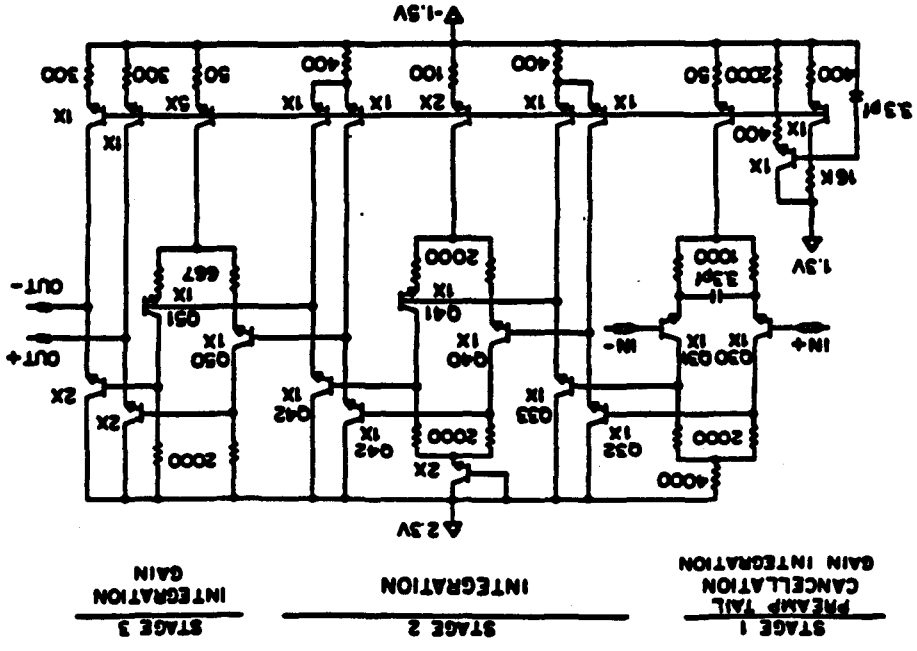

Fig. V.13. Schematic for prototype shaper.

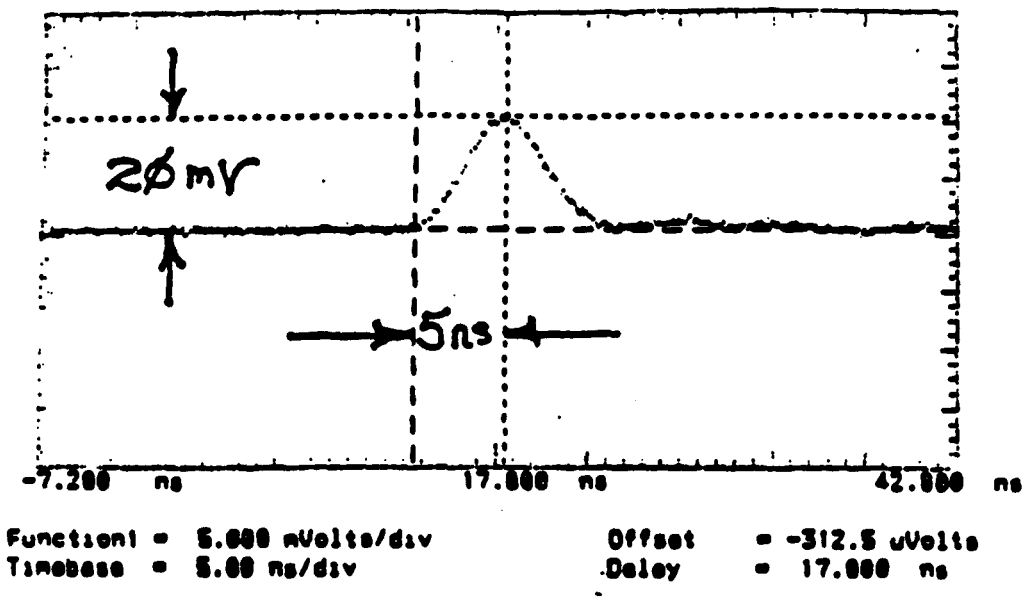

Fig. V.14. Shaper response for a 1 fC impulse input, averaged over 40 pulses.

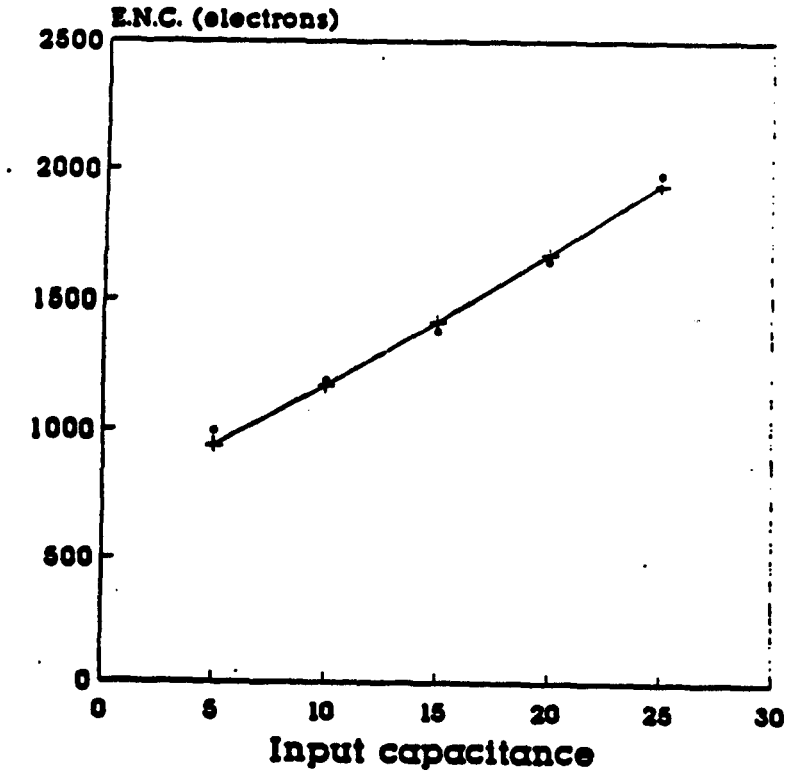

Fig. V.15. Comparison of simulated and measure noise.

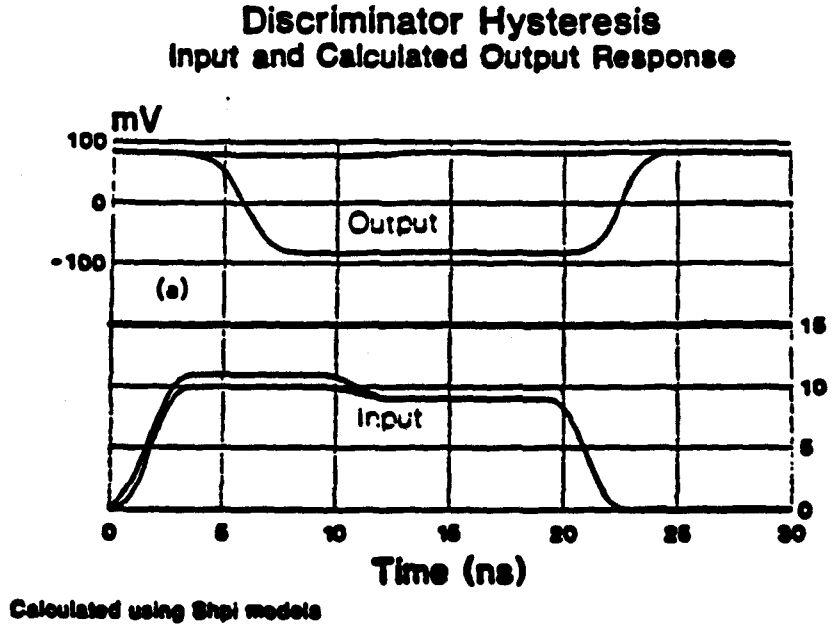

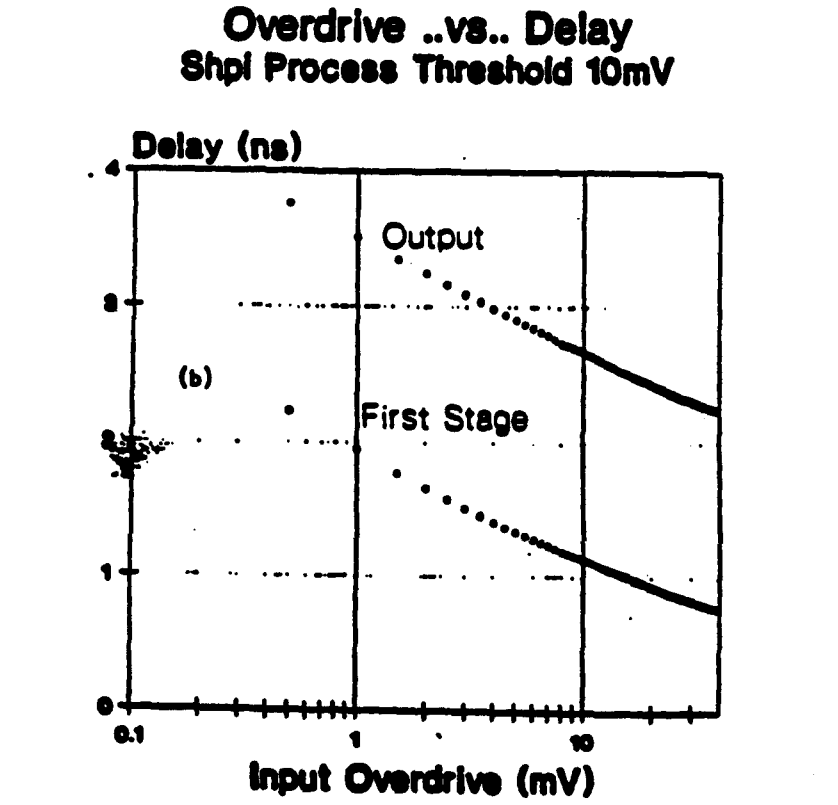

Fig. V.16. Low power discriminator (8 mW) output wave forms for input pulses just above and below threshold (SPICE modeling result).

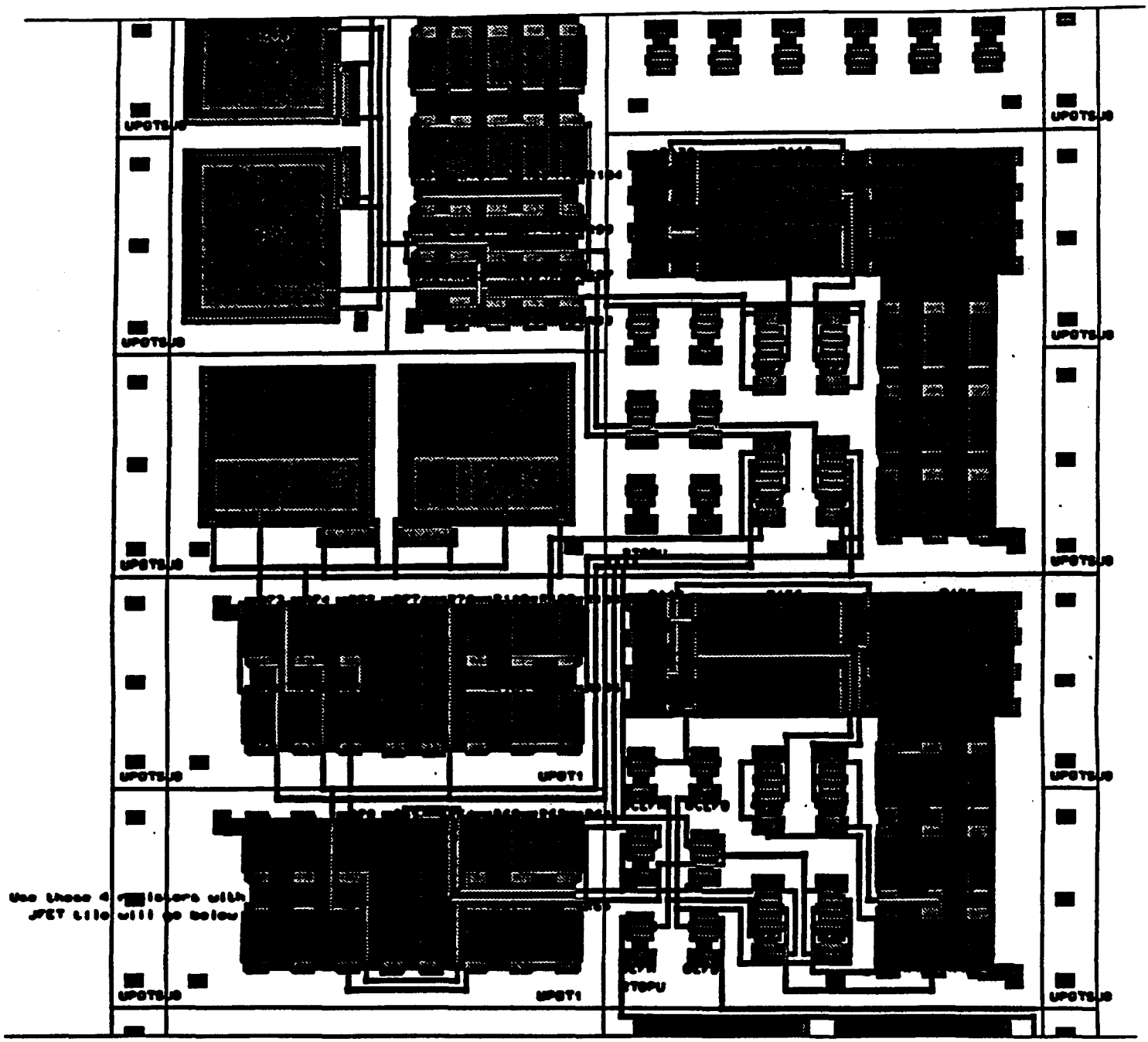

Fig. V.17. Layout of the preamplifier and first stage of shaping amplifier in the Tektronix SHPi Quick Tile process. Note the isolating substrate contracts along both sides of the amplifier chain.

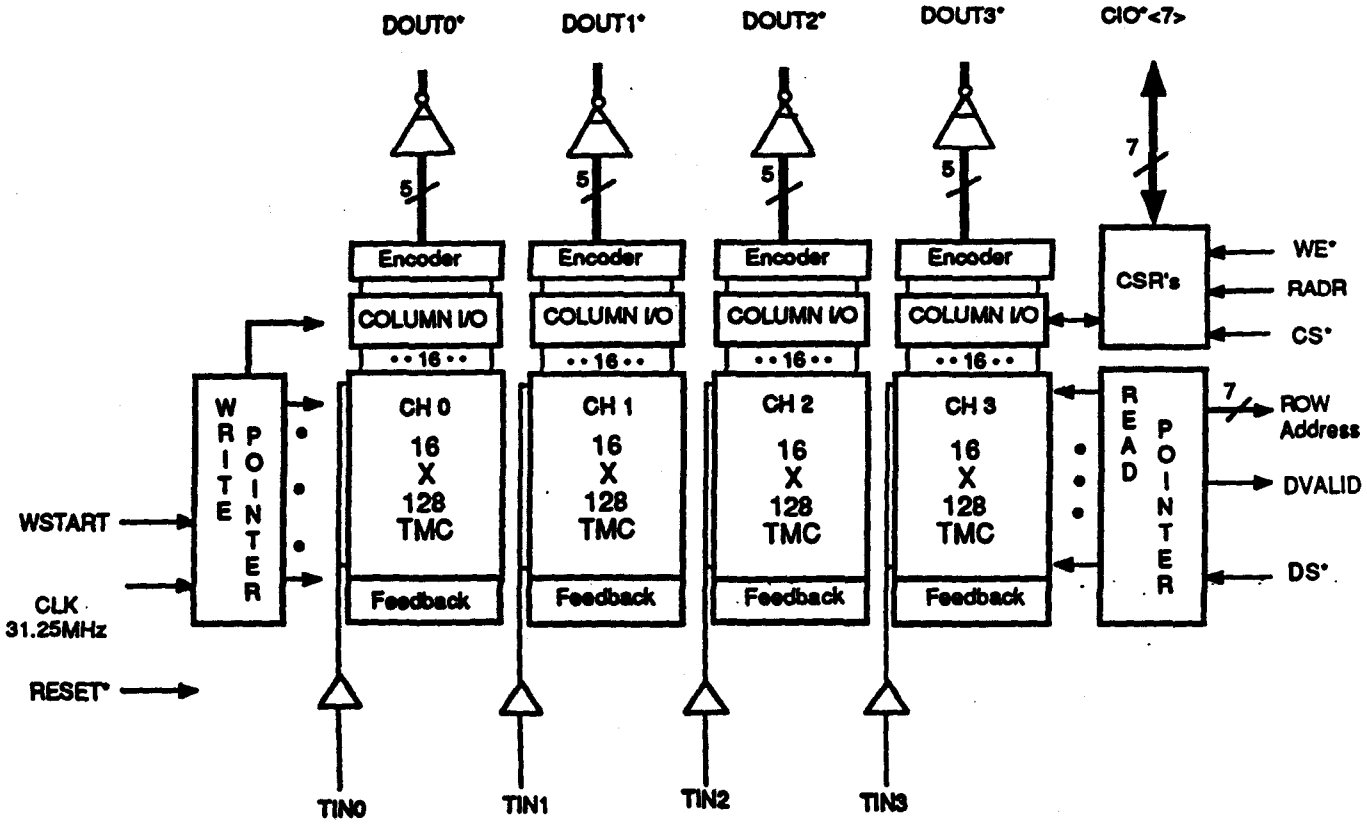

Fig. V.18. TMC-SSC block diagram.

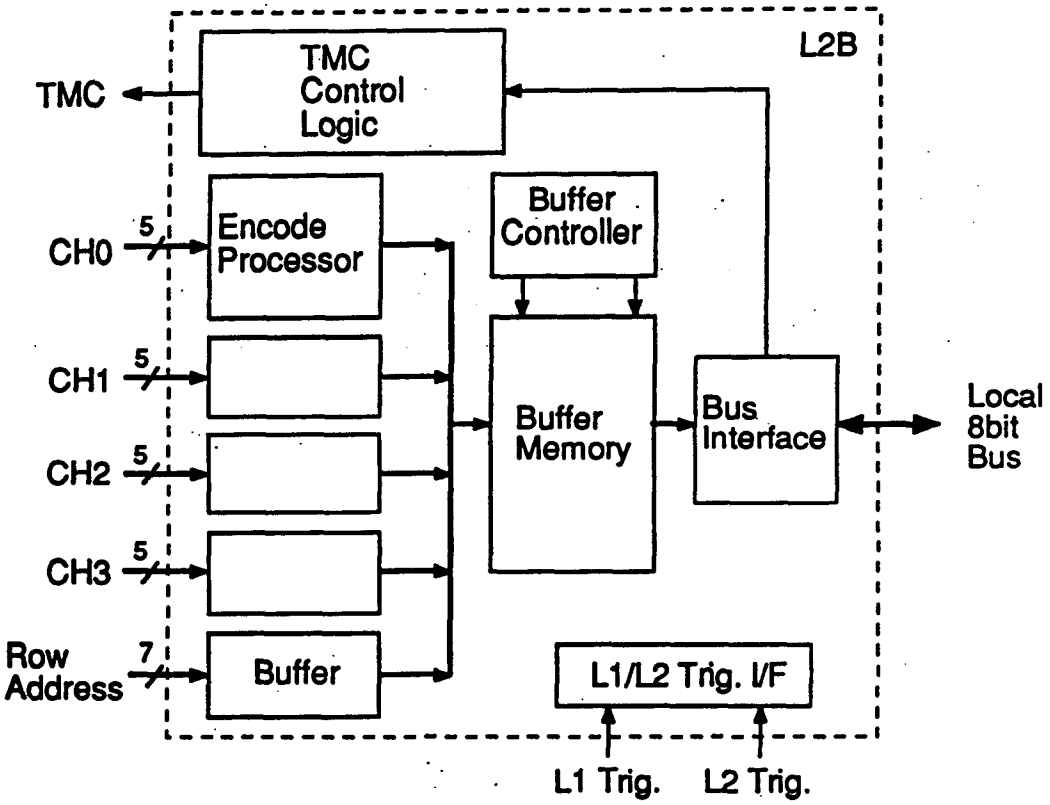

Fig. V.19. Level 2 buffer - block diagram.

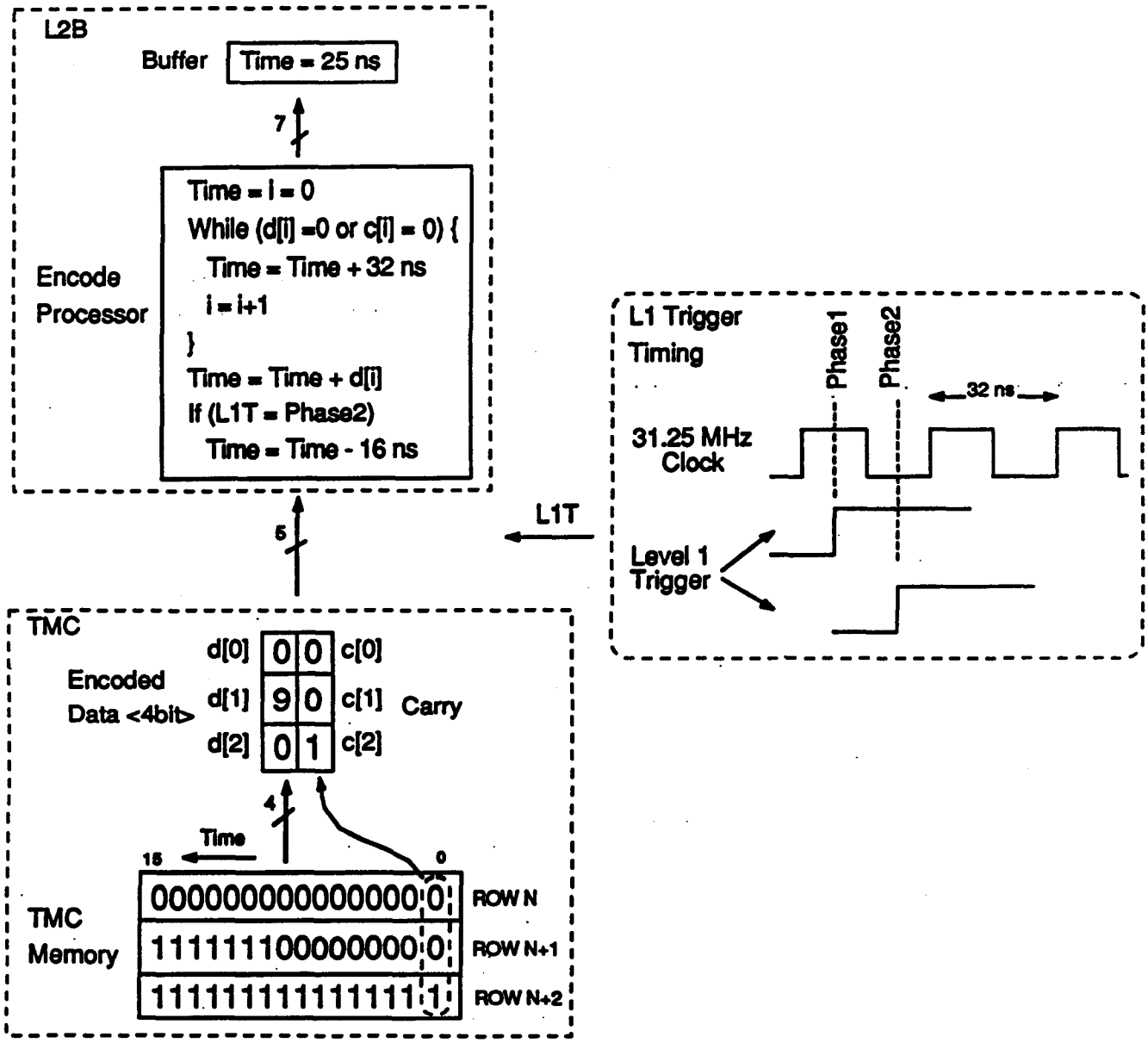

Fig. V.20. TMC-SSC and L2B data encoding scheme.

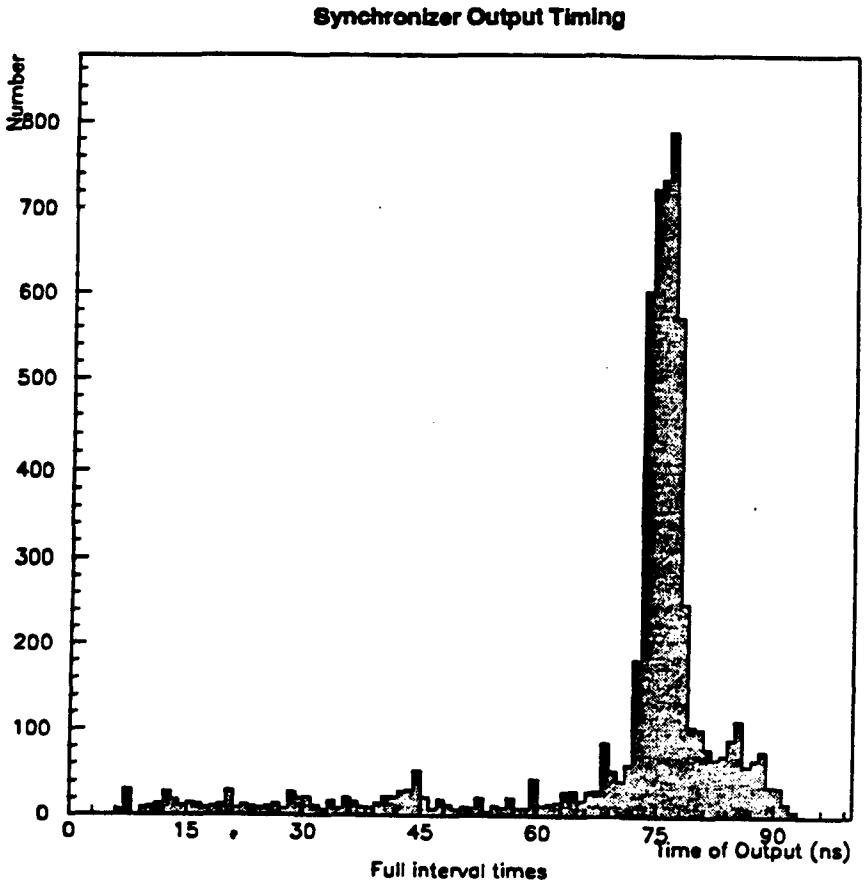

Fig. V.21. Pulse timing for the GEANT simulation of tracks in the outer layer of the SDC detector instrumented with mean timer circuits that produce an output time displaced from the particle passing time by a fixed value, ~45 ns. An additional 30 ns delay is seen in the plot due to the particle flight time to the superlayer and the propagation time of the signal to the end of the straw. This particle and signal flight time varies over a range of about 8 ns and is therefore the major contributor to the spread in the arrival times.

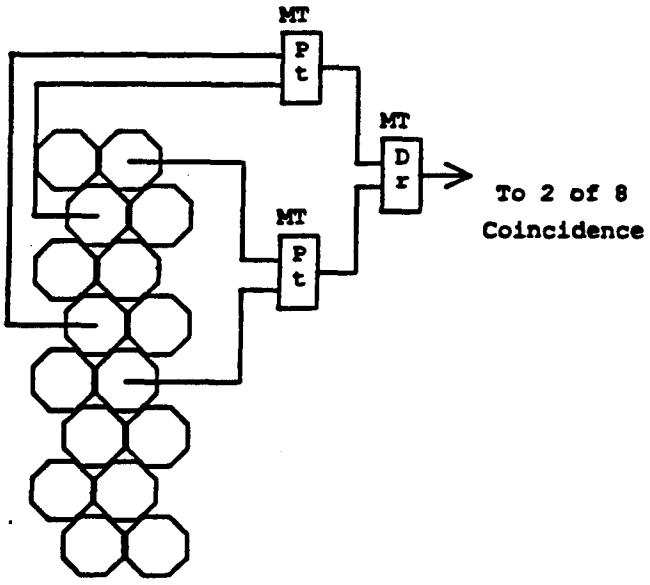

Fig. V.22. A representative mean timer connection for an 8 tube superlayer. The connection shows two mean timers each requiring hits to be consistent with a preset momentum lower limit and output pulses averaged in time to a common radial position. The third mean timer averages these output pulses to arrive at a final pulse whose timing is fixed relative to the particle passage time plus the signal propagation time from its z position to the end of the straws. The pattern shown is one of 8 used in a two-fold coincidence to produce a stiff track trigger.

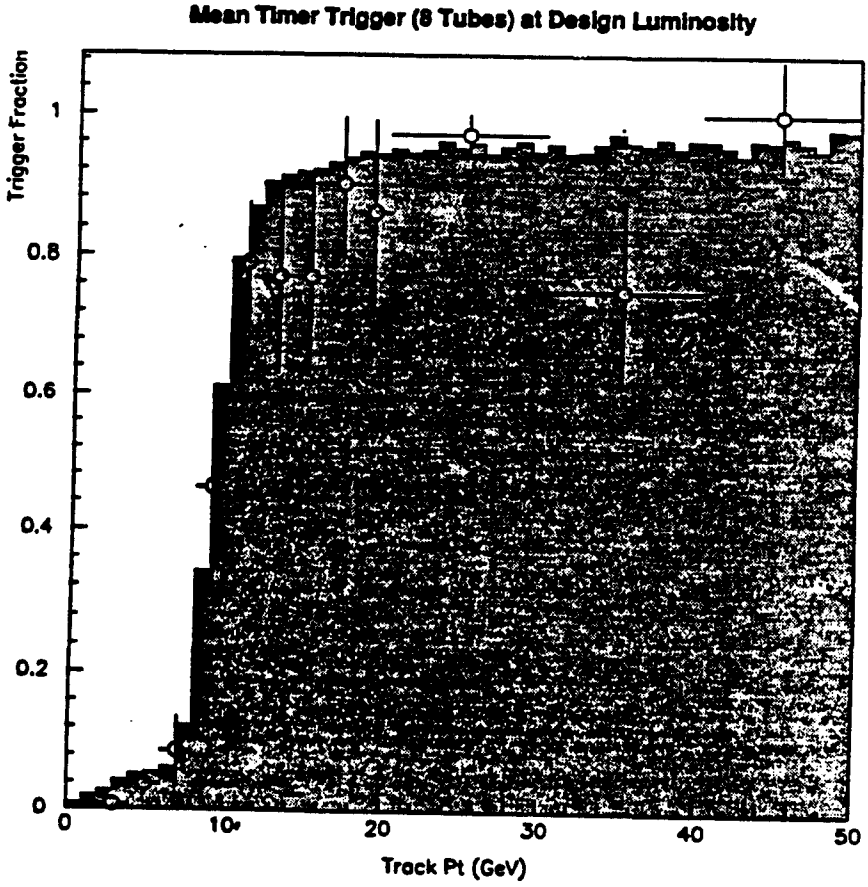

Fig. V.23. The efficiency as a function of p_T for a digital mean timer based trigger operating on signals from an 8 tube deep superlayer of packed straw cells. The points are from a GEANT simulation of Higgs $\rightarrow Z\,Z$ events at 10^{33} cm^{-2} s^{-1} luminosity, and the shaded histogram is for a fast parametrized simulation tuned to match the GEANT points.

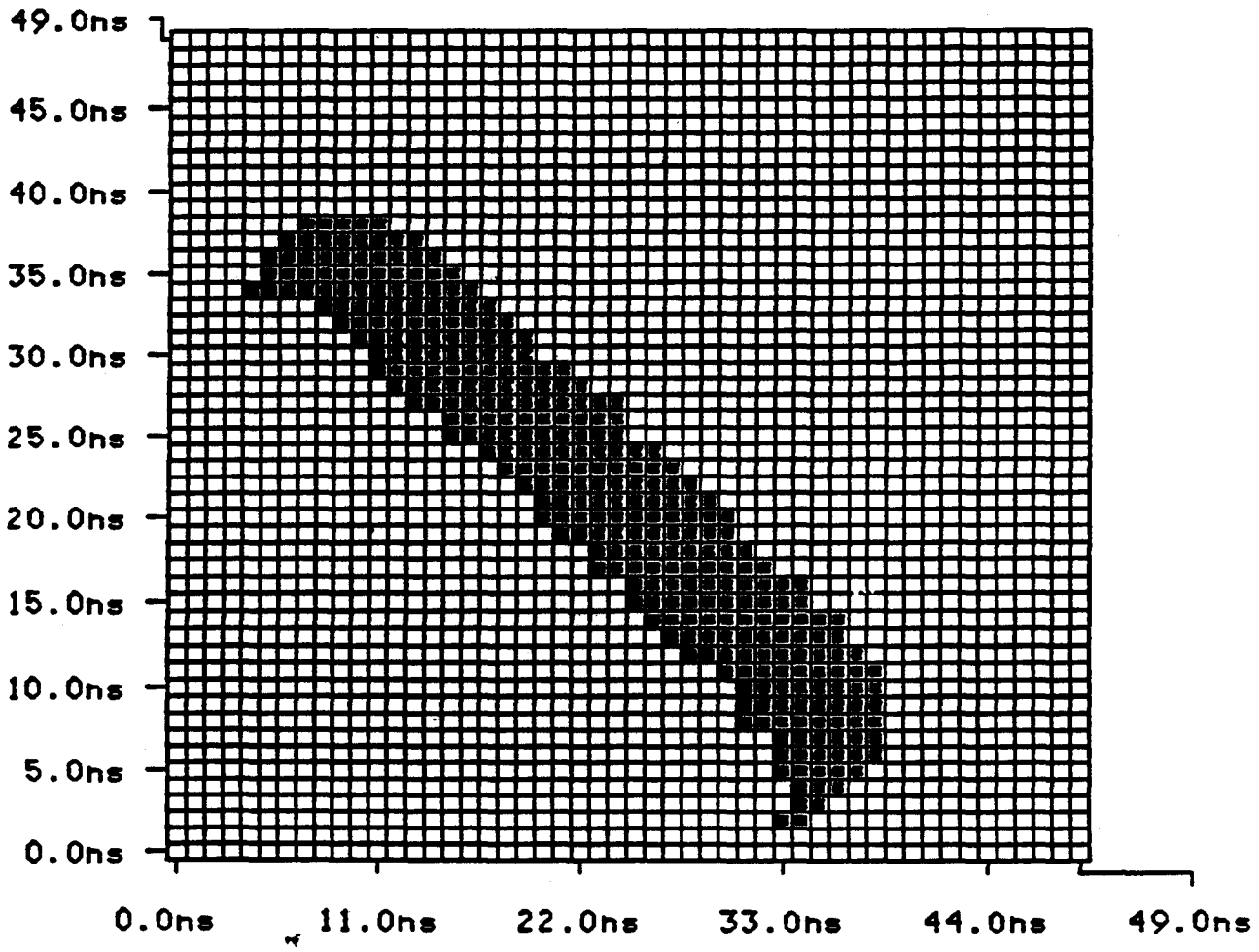

Fig. V.24. A test plot of the p_T cut portion of the mean timer IC. The axes are the times of the aligned wire inputs and the plotted points are those values of the axis coordinates for which an output was generated at a predetermined value. A falling 45° is expected for correct averaging of the input times. The cutoff of the line at large coordinate differences is due to the time difference restriction (momentum cut).

VI. TRACKING SYSTEM SUPPORT AND ASSEMBLY

VI.1. INTRODUCTION

The central tracker requires a support system that is extremely rigid and light weight. The design of this support system is described in the following sections of this report. This includes a careful study of support materials, a design of a support structure, and an analysis of the assembly sequence. The resulting design has been studied with a finite element analysis.

VI.2. MATERIALS REQUIREMENTS

From the structural engineering stand point, the material requirements of the central tracker are very restrictive. The support structure must be fabricated with minimum quantities of material but the final structure must have maximum rigidity or stiffness. These requirements of infinitely thin, but also infinitely stiff are conflicting and a compromise is required. Additionally, stability, minimum creep, and resistance to deterioration from radiation are required.

VI.2.1. Candidate Materials

Beryllium is the best known material that satisfies the requirements outlined above, but it is costly and difficult to work with. Other candidate materials are available and have been listed in Table VI.1. Aluminum is listed in the table mainly as a reference material. However, aluminum, which does have a reasonably long radiation length, can be used as a structural material on a limited basis.

VI.2.2. Selected Composites

Graphite fiber resin matrix composite has been selected as the leading candidate for the basic structural material for a variety of reasons. This radiation hard material exhibits a high stiffness to weight ratio with an effective radiation length of 25 centimeters. The basic fabrication technology exists for the proposed construction of large cylinders utilizing foam cores and large single unit spaceframes. Structural stability is insured because the

large components result in a minimum number of mechanical joints and thus susceptibility to mechanical creep is reduced.

Rohacell foam is the leading candidate foam to be used in the foam core constructions. Composite layups in the form of a large ultra thin shell must develop stiffness and strength in the skin without flexing and buckling. To prevent buckling and out of plane bending, foam cores are used. The core in these composite fabrications acts as a simple spacer between the face sheets and thus is subjected to very little stress. A simple adhesive bond is formed between the face sheets and the core as a result of controlled "bleeding" of the resin as the composite cures. Because of the very low stresses, core structural strength is not a requirement. Stability in a radiation environment and low radiation length are required. Based on these needs the lowest density and the longest radiation length Rohacell foam 31Ig listed in Table VI.1 should be used. A sightly more dense Rohacell may be necessary based on the required composite cure temperature. Rohacell WF will withstand higher temperatures than IG.

VI.2.3. Selected Layups and Constructions

A quasi-isotropic layup of [0 +/-60]symmetry has been chosen as the prime construction for all carbon graphite composite components. Table VI.4 lists the mean and variance properties expected for this composite. This construction is a balanced and symmetrical layup. Using the same layup for both the struts and the composite cylinders has advantages and some disadvantages. The advantages seem to outweigh the disadvantages at this point.

The quasi-isotropic layup of [0 +/-60]symmetry was first chosen as the prime construction layup for the cylinders because of several reasons including the one that shear stiffness or substantial shear modulus is mandatory. Most of the deflection in the case of gravity loading is cylinder shear deflection. A finite element model with and without substantial shear modulus (G) produced huge deflections as described in Section VI.4. Again, the results of the analysis demand a layup design for the cylinder with generous shear modulus. The [0+60-60]sym layup meets all the requirements.

For the spaceframe struts, this layup results in a lower axial modulus than what can be achieved by placing more fiber in the axial direction. At first glance a stiffer axial strut would seem to be very desirable. It is not! There is a high price to pay for the stiffer strut. This higher modulus would be achieved at the expense of a lower strut shear modulus and

an unbalanced thermal expansion coefficient between the cylinder and strut. The unbalanced thermal expansion condition is judged to be unacceptable. During temperature changes the cylinder would expand in the radial direction. The struts or spaceframe would shrink with its slightly negative coefficient of expansion and pull away from the cylinders. The finite element model has shown that the lower axial modulus in the struts appears to be acceptable. A 50 percent decrease in strut modulus increased the total deflection of the tracker by only 17 percent. The spaceframe and cylinders act like two mechanical springs in series. Most of the deflection is in cylinder shear deflection. Classical spring calculations calibrated by the finite element model predict that it would require a four fold decrease in the strut or spaceframe axial modulus to increase the overall tracker deflections by 50 percent. This preliminary investigation indicates that, based on the need to control thermal expansion and similarly, but to lesser extent, moisture expansion, a layup design of [0+60-60]sym best meets the requirements of the tracker support structure.

VI.2.4. Background on Material Selection

The graphite composites being considered for this construction are commercially available materials. There are several matrix and fiber systems being considered and further testing and evaluation will be required to determine their final suitability. Factors such as manufacture and environmental stability must be considered. Technology advances should be monitored in this rapidly developing industry to identify the most suitable material available at the time of actual construction.

Background on Graphite Fibers. Two types of graphite fibers were considered for this material. They are the Amoco P75 pitch precursor fiber and the Hercules UHM pan based precursor fiber. Table VI.2 lists several mechanical and thermal properties for the fiber materials. The P75 fiber is the higher modulus fiber but has lower elongation to failure. The UHM as a pan fiber is usually easier to handle during manufacture.

Background on Resin Matrix. The resins systems being investigated include the epoxies and cyanate esters. Cyanate esters are presently the leading candidate resin material because of low moisture absorption and thus smaller elongation for a given humidity level. Table VI.3 is a list of properties for several matrix systems including the more mature industrial resins for comparison.

Discussions of Composite Layups. A quasi-isotropic layup of [0 +/- 60]symmetry is being recommended as the prime construction for all graphite composite components. Table VI.4 lists the mean and variance properties expected for this composite. This construction is a balanced and symmetrical layup. The advantages of this construction includes:

1) The symmetrical wrap is stable against warping during curing process.
2) The symmetrical wrap will produce a lower coefficient of thermal expansion and moisture expansion than non-quasi-isotropic layups.
3) A 6 layer construction is the thinnest quasi-isotropic layup.
4) The 60 degree symmetrical wrap yields a respectable shear modulus.

The P75 fiber composite was found to have the most complete data base from which to project composite variabilities during actual construction. This information was used to do the sensitivity analysis to predict actual composite and component projected behavior. See Section VI.4.2 for more information including results of the analysis. Expected variability in the composite is due to the following conditions:

1) Variance from the material and lamina properties.
2) Variance on lamina of base line 60% fiber volume.
3) Variance expected in fiber volume from basic lamina construction and layup construction.
4) Variance in wrap angles.
5) Variance due to hygroscopic behavior.

The Table VI.4 lists the mean and variance properties expected for this construction. The modulus values listed in this table are lower than the usual reported modulus properties. The explanation for this lower modulus is as follows: The modulus of a carbon/graphite lamina is not linear, but behaves more like a quadratic material. The usual reported modulus is for a higher strain rate. This structure will be loaded to a lower strain rate than the usual reported modulus (E secant). To accommodate this fact the modulus in the table reflects the expected in service strain rate .

The design of this structure is intended to incorporate the requirements of a stable system in an environment of changing temperature and humidity. The quasi-isotropic construction can be designed for an extremely low coefficient of thermal expansion. Table VI.5 gives two comparisons of the thermal expansions of composites . The moisture elongation data is given in table VI.6. Less data is available for this latter condition. The design of the composite will require a balance of all requirements.

VI.2.5. Radiation Lengths Calculated

The minimizing of material in the tracking volume is a requirement that is discussed at length in Section II.1.3,. A material budget of less than 0.8% of a radiation length for each superlayer is presented as the goal. This requirement is very restrictive and can only be satisfied by an exhaustive effort at minimal use and optimum placement of structural material in each superlayer.

To better understand the available options and to insure the optimum placement of the structural material within a superlayer, a radiation length calculation for a superlayer was performed. The module material was included in this calculation. These modules are fully described in this report in Section IV.1.and Section IV.2.

A summary of the results are presented in Table VI.7. Examination of this summary table indicates that compliance to the maximum allowable total radiation length per superlayer results in a .25% allowable radiation length for each support cylinders.

A similar calculation was performed to determine the impact of structural material in the end region caused by the spaceframe cylinder support structure. This spaceframe is described in this report in Section VI.3.1.

A summary of the results are presented in Table VI.8. Examination of this summary table confirms that the spaceframe, because of its optimized structural strut geometrical design, has little impact on radiation length. The total radiation length when spread over the entire end area is equivalent to a disk of aluminum only 200 microns thick. Strut size and wall thickness can be freely tuned to produce optimum mechanical performance.

VI.3. SUPPORT STRUCTURE COMPONENTS DESCRIPTION

The detector elements that do the actual particle tracking require a support structure to support or fix them at the proper location inside the overall detector. These detector elements or modules described in this report in Section IV.1 are somewhat robust in and of themselves, but they still require a relatively substantial support structure to assure alignment over their four meter length.

Developing a sound conceptual methodology for this support structure is not a trivial matter considering the huge size to weight ratio of the tracker. The 3.6 meter diameter and 8.0 meter length generates a 90.0 cubic meter volume which is estimated to weigh approximately 1000 kilograms. This results in a very light average density of 15 kilograms per cubic meter. As described in the Section VI.2. of this report, this support system must be constructed using minimum quantities of radiation hard low radiation length material but must maintain maximum rigidity and stability. With these goals and restrictions in mind, a conceptual methodology has been developed for a central tracker support structure for the straw tube modules. This support structure concept will be referred to as the "spaceframe support system" in this report. Figure VI.1 shows a view of the completely assembled central tracker including modules and Fig. VI.2 a completed spaceframe support. A considerable amount of physics evaluation and engineer analysis has been performed on this maturing concept. The methodology dictates that to achieve 10 micron long term alignment the following is required:

1) Structural stability is achieved by using an absolute minimum number of mechanical joints between graphite composite components,
2) Minimizing the tolerance buildup by using only a small number of large components with simple geometry which are thus relatively easy to manufacture to high tolerances, and
3) Performing final alignment testing on the assembled support structure in its fully simulated, in service and gravity loaded support environment.

This strategy is not only needed, but it reduces costs by requiring precision fits only at the major component interfaces and the module-structure interface. Using the spaceframe support system allows module and structure component fabrication to occur in parallel. This is a major advantage because of its potential to reduce fabrication cycle time and shorten the schedule. There are only two basic types of large components used in the spaceframe support system. They are large graphite composite cylinders and spaceframes.

The spaceframe is shown in Fig. VI.2 a basic support cylinder is shown in Fig. VI.3, and the assembly of the two can be seen in Fig. VI.1. In the following, Sections VI.3.1 through VI.3.4, the details of major component fabrications and designs are developed in more detail.

VI.3.1. Spaceframes

The heart of the support system is the two spaceframes. A three dimensional view of the composite spaceframe is shown in Fig. VI.2. The composite spaceframes perform three basic functions:

1) Furnish four load points that support the tracker to the surrounding detector at the outside diameter.
2) Support the silicon detector at the inside diameter.
3) Registers the five superlayer composite cylinders and thus the detector elements themselves.

This is a state-of-the-art, mechanically tuned, monolithic composite structure that will perform all these tasks well. Kaiser Aerotech, San Leandro, California 94577, a world class supplier of composite materials and fabrications similar to these spaceframes, has been assisting Westinghouse in the concept and cost estimating of these spaceframes. They are an interested potential spaceframe vendor.

The material selection process for the spaceframe components is discussed in Section VI.2.2 of this report. The specific recommended layup construction for the spaceframe is documented in Section VI.2.3 and is defined to be matched to the composite cylinders with a balanced and symmetric [0+60-60]sym layup. In Section VI.2.3, the theory is developed that the spaceframe and the composite cylinder should be matched and moreover have identical composite layup constructions. Thus, the response of the two components to gravity, thermal, and moisture loads would be designed to be identical, at least in the ideal case.

Each spaceframe is fabricated from three basic high stiffness graphite components. These components are struts, joints and rings. The struts are thin walled tube shaped structures made by the heat curing of wrapped B-Staged graphite cloth. Examples of the proposed shapes that are presently being studied are shown in Fig. VI.4. The cross

sectional size of these struts or tubes is a remarkably small 2 by 4 or 4 by 4 centimeters in cross section with a 0.2 centimeter wall. These tube sizes which were selected on a first cut basis have been analytically shown to be of a functional size in Section VI.4. No actual analytical evidences has been found to eliminate round tubing from consideration and in fact it may be the preferred shape. The joints are also fabricated thin walled hollow shaped structures made by the heat curing of wrapped B-Staged graphite cloth. A conceptual drawing of a joint that connects round tubing is shown in Fig. VI.5. More engineering will be required before actual drawings and specifications can be made. Rings are the third component required for spaceframe fabrication. The composite rings are shown in Fig. VI.6 . The two sets of five rings would be fabricated by hand layups of autoclave heat cured B-Staged graphite cloth. The rings are manufactured with oversized thickness either by specifying a thicker cross section or by incorporating pads into their thickness. Small gussets may be required to reinforce the ring to strut interface. They are shown in Fig. VI.7.

Each spaceframe is assembled by adhesively joining the three components struts, joints and rings into an assembly on a large fabrication tool. This tool is not required to be a precision tool. The tool must be very stiff and fit snugly while rigidly holding the assembled spaceframe. Once assembled the tool with the spaceframe is transferred to a large simple three axis boring mill. On the mill each of the five oversized rings is ground to a predetermined cylinder matching diameter. Since grinding generates only small tool forces and the total operation consists of a single setup with a simple two axes move, 75 micron diameter tolerance including a 50 micron concentricity should be achievable.

VI.3.2. Support Cylinders

These fabricated, foam filled, ultra thin double wall composite cylinders are used as structural members, but the cylinders equally important purpose is to furnish a stable base for the modules. The sequence of figures numbered VI.8 through VI.12. are intended to display the pertinent features and needs of the cylinder manufacturing process. Hercules Aerospace Company, Magna, Utah, a world class supplier of composite materials and fabrications similar to these cylinders, has been assisting Westinghouse in the concept and cost estimating process. They are an interested potential cylinder vendor.

Design of Support Cylinders. The design features of the five cylinders can be viewed in Fig. VI.9. Note that the construction concept uses two composite face sheets with a foam filled core. The factors surrounding the selection of the core material and the use of graphite composites are discussed in this report in Section VI.2.2. The most restrictive design requirement for the cylinders is the need to use minimum quantities of material and thus achieve the lowest possible radiation length. The specific recommended layup construction is documented in Section VI.2.3. and is defined to be matched to the spaceframe struts with a balanced and symmetric [0+60-60] layup.

The composite layups design was also selected based on the thinnest available high modulus graphite fiber. A balanced and symmetrical layup with the needed in-plane shear modulus requires 6 plies. Thus, each of two face sheets is 0.127 millimeter or 0.009 inch thick of 6 ply B-Staged tape lamina construction. This is considered to be near the minimum. Hercules Ultra High Modulus fiber may be able to be used to achieve 0.006 inch thick composite layups.

The cylinders have a very large radius of curvature. A foam core is needed to give these cylinders some out of plane bending stiffness. The core acts as a space between the composite face sheets. Since increasing the cylinder stiffness is a goal, the maximum allowed core thickness of 6 millimeter is used. This thickness limit is set by the total radiation length limit per superlayer which is defined and discussed in this report in Section VI.2.5 .

The end closeout design features of the cylinders can be viewed in Fig. VI.9. This area forms the mechanical connection with the spaceframe. A dense core material will be required to withstand the forces that the mechanical connections will apply. This dense core material can range from a denser 300 grade Rohacell foam to graphite composite layups. If a layup is used, the coefficient of thermal expansion will be matched to the cylinder hoop expansion. Although more engineering is needed, none of the issues appear difficult to solve.

The graphite hardware fasteners are shown in the Fig. VI.9. They are commercially available from Kaiser Aerospace, San Leandro, California. The Table VI.9 lists the properties of the hardware. Preliminary evaluation indicates that this hardware satisfies the requirements imposed upon it by the interface connection. Other than thermal expansion, aluminum hardware might also satisfy the requirements.

Fabrication of Support Cylinders. The cylinders are to be formed on individual mandrels. Figure VI.8 shows the type of mandrel that would be used to form the cylinders. These mandrels would be placed in a simple taping machine similar to the concept shown in Fig. VI.10 and 6 layers of the B- Staged lamina would be applied. The foam core which was previously thermally formed to the correct radius would be placed on the mandrel and filament applied to hold it in place. After the end closeouts are installed the last 6 layers of the B-Staged lamina would be applied. Vacuum bag technology would most probably be applied to consolidate the composite. The number of cure cycles required or whether a oven or heater strips will be used has not been determined. There are advantages to keep the cure temperature lower but this must be weighed against other factors such as stability of the composite. Additional detailed engineering work is needed in this area.

VI.3.3. Shim Ring Module Supports

Predictable composite cylinder diameters are impossible to obtain without making several parts of each size and by iteratively sizing the tooling. For this tracker program, trial and error sizing would be prohibitively expensive. The part size is unpredictable after it has gone through the composite thermal curing cycle. The unmatched high coefficient of expansion of the steel mandrel versus the near zero coefficients of the composite and associated expansion stress cycle produces an unpredictable diameter. A quality cylinder can be produced on the first attempt by rotating the mandrel and part during the cure cycle but it will be of an unknown diameter. A slight taper on the mandrel is being considered to assist in part removal.

Cylinder shim rings solve this problem of unpredictable diameter as well as other problems. The concept of shim rings is very simple. Fabricate the composite cylinders in the normal way. Then prior to removing the cylinder from the mandrel, coat the outer surface with a material that can be machined to size. When the coating takes the form of relatively thick strips or bands of a material like Rohacell foam bonded to the composite cylinder, a fabrication such as the one shown in Fig. VI.11 can be made. These shim rings can be machined or ground to a precision diameter.

A conceptual machine tool drawing is presented as Fig. VI.12 that will do the shim ring machining. This two axis machine is equipped with a precision laser type encoder that allows 2 to 3 arc second type indexing of the mandrel. This accuracy translates

mathematically into 23 micron and 10 micron radial positioning accuracy for the largest and smallest cylinders respectively. Linear way systems are commercially available that will carry the spindle and will be straight to within 25 microns. It is a simple matter to align optically the mandrel axis to the spindle way system axis to a high tolerance. A 50 micron parallel placement should be achievable. Thus, shim rings can furnish a surface that can be machined or ground to a predetermined diameter. They also make stereo or axial position measurement possible in that they furnish a surface into which a stepped "hour glass" shape can be machined. The detailed view of the stereo and axial shim rings are shown in Fig. VI.13. This same view is again shown in detail with the modules in place in Fig. VI.14. Axial or trigger modules require simple facets to be machined into the shim rings. This operation requires the spindle way system and the mandrel axis to be parallel and the mandrel to be indexed. Stereo modules require steps or shelves to be machined into the shim rings at approximately 3 degrees. Stereo preparation of the shim rings simply requires an adjustment in the machine tool such that the spindle way system and the mandrel axis are parallel in the vertical plane but skewed in the horizontal plane by 3 degrees. The accuracy of the 3 degree specification is not a requirement but consistency from module to module is. This consistency is automatically obtained because all 360 degrees of modules are done in a single setup.

VI.3.4. Mandrels For Large Precision Cylinders

The concept of machining or grinding composite parts while on a mandrel has been conceptually investigated. Some special concerns were developed which are addressed here. First, can a set of mandrels be obtained that meet the concentricity requirements that are required? Concentricity is required if the shim ring diameters are to be machined accurately. No difficulty was found in obtaining a quote for concentricity of 125 micron. Chromium Industries, Inc., Chicago, Illinois, quoted that tolerance for Group 1 from Fig. VI.8. See Section VIII.2. for a copy of the quotation. Closer tolerances of 50 microns are achievable if deemed necessary but are more costly.

The second concern that needs to be addressed is longitudinal bending of the mandrel. Mandrels are traditionally viewed as beams supported between two points deflecting from bending and shear forces. This is because this type of mandrel depends upon its surface with its large diameter and thus huge area moment of inertia to limit the bending deflections to within reasonable limits. Typically, the sag is on the order of 500 microns. This deflection is much too large for a shim ring machining application.

A large straight mandrel without bending can be built. The design of the mandrel can be altered to eliminate bending almost entirely, minimize shear deflection, and result in a mandrel which, when placed in its bearings, remains almost perfectly straight. A slightly oversized shaft should be specified but the bearings can be standard size. The design of the mandrel is such that the shell is not bending but is simply supported at its quarter points along its length by disks. The disks are relatively thin so that no bending loads are transmitted between the shell and the shaft. The shaft supports all the bending loads. The mandrel is conceptually shown is Fig. VI.8. An analysis of this mandrel is documented in the appendix of this report. The finite element model used to do the analysis together with a deflection plot is included in this section as Fig. VI.15 Fig. VI.16. On the deflection plot, Fig. VI.16, note the lack of bending in the shell and that all the deflection is in the shaft. This result is further documented in Table VI.10. The Stress levels are acceptable in the case of the 12 inch shaft and the 1 inch thick disk. The total shell bending deflection from end to center to end is .60027 minus .59948 or 0.00079 inches. The mandrel shell bending of 20 microns is well within desirable limits.

It is not a foregone conclusion that it is an absolute necessity that the cylinder shim ring machining be done on the mandrels. End plug tooling could be built that would substitute for the mandrels. Tooling forces would be very low from machining a material like Rohacell foam. It is of value to know that mandrel deflections can be understood through design efforts .

VI.3.5. Module Attachments

Considerable discussion has surrounded the subject of module attachment. The engineering effort on module attachments is not complete and hopefully will be reconvened in the near future. Module attachment, in general, refers to the method by which the module is attached to the support cylinder via the shim rings. A good view of shim rings and support cylinders is shown in Fig. VI.13 without modules and Fig. VI.14 with modules. Module location will be discussed first, followed by module attachment.

The modules will be located at approximately 80 centimeters intervals along their length. The shim rings will have fiducials placed in them during the machining operation that was discussed in Section VI.3.3. These shim ring fiducials will mate with matching module fiducials placed in the module shells during shell fabrication. The conceptual

drawing of module and shim ring fiducials are shown in Fig. VI.17. This method of module location through matching fiducials should produce acceptable tolerances. The module fiducial placement since it is located by shell tooling should be perfectly repeatable from module to module. The Shim ring locations should also be very good since each cylinder will be done on a single setup and within the accuracy of the machine tool which is discussed in Section VI.3.4 For purposes of repair and maintenance, the modules should be removable and replaceable from a fully assembled support structure. This issue effects the complexity of the attachment. From the point of view of what the support structure will accommodate conceptually , a wide range of options are available. The spaceframe support system can be assembled in any of the following ways:

1) The modules can be attached permanently to the shim ring cylinders before the cylinders are assembled to the spaceframes.
2) The modules can be installed with removability features to the shim ring cylinders before the cylinders are assembled to the spaceframes.
3) The modules can be installed with removability features to the shim ring cylinders after the spaceframe support structure is assembled.

The modules will also be attached at the same approximate 80 centimeters intervals along their length. Option 3 is the preferred assembly method that is advocated. This option is the most user friendly in that it allows for maintenance, repair and replacement options. In this option provisions for locating an attachment will be placed in the shim rings during the machining operation which locates the shim ring fiducials. These shim ring attachments will mate with a matching module attachment placed in the module shells during shell fabrication. In Fig. VI.18 the schematic drawing of module and shim ring attachment are shown. The goal is to develop a tool that can reach into the inner part of the detector and disconnect or connect the series of attachments that hold a particular module so that it can be removed or replaced.

This removable module attachment concept will produce an acceptable connection. This engineering effort on module attachments is not yet complete.

VI.4. ASSEMBLY OF THE SUPPORT STRUCTURE

It is proposed that the support structure be assembled while in the horizontal and not in the vertical position. Horizontal assembly should reduce the risk of damage to the tracker components and should be less costly.

A three dimensional view of the assembled spaceframe support system is shown in Fig. VI.2, and the completed central tracker with the modules installed is shown in Fig. VI.1.

Assembly will be carried out using a cantilever beam that is fixed to the floor at the inboard end and has two removable and adjustable supports at the midpoint and outboard end. A spaceframe is first installed on the inboard end by simply shuttling it into position by sequentially removing and replacing the two supports. Each of the five cylinders and finally the outboard spaceframe are moved into their final position in the same manner. Figs. VI.19 through VI.25 show the assembly sequence which is described below to build the modular central tracker utilizing the spaceframe support system. Tracker components are moved to and onto the assembly fixture with a specially designed hay wagon type carriage fitted with a simple, manually operated, four point and independent hydraulic elevating and leveling system that positions the different diameter cylinders and the spaceframes. During the sequential cylinder assembly, the free ends of the cylinders are held in position with simple adjustable bladder jacks placed between the adjacent outboard cylinder ends.

VI.4.1. Tooling Requirements

Cantilever Beam. This beam is fixed to the floor at one end and has removable inboard and outboard supports at the other end. The beam has a free length of more than twice the length of the completed tracker, and has surfaces that provide for alignment and positioning of the spaceframe support tooling.

Spaceframe Positioning and Alignment Tooling. This tooling is constructed from welded square or rectangular thin wall mechanical steel tubing. These fixtures are stress relieved, machined and fitted with adjustable positioning hardware.

Carriage. The carriage has a hay wagon like configuration. The bed is designed to be a rigid structure supported from three points, two at the back axle and one centered on the front axle. The front support forms a pivot so that no floor induced bending or torsion is transmitted to the load. Each front wheel turns on casters independently of the front main axle to promote turning and minimize torsional tipping effects. The hay wagon carriage is fitted with a simple, manually operated, four point and independent hydraulic elevating and leveling system that positions the different diameter cylinders and spaceframes.

Cylinder #1, #2, and #3 Support Tooling. An internal support structure is required on the outboard end of each cylinder during the assembly process to support the free end cylinder weight. The basic design is the same for all cylinders except that larger cylinders require larger radii tooling. The tooling must be removable after the tracker assembly is completed.

An external support cradle is used to support the cylinders at the quarter points and move the cylinders from the shipping container onto the assembly beam. The external cradle system is the same for all except for changes to accommodate the larger radii and longer length of the outer cylinders.

Cylinder #4 and #5 Support Tooling. The external support cradle is again the same as the tooling used for cylinders #1, #2, and #3 except for required provisions to accommodate the larger size of the cylinders. Bladder jacks placed between cylinders #3 and #4 are proposed for use to support the free outboard end of cylinder #4. These cylinders are all the same length so that access is limited. Therefore, these fluid operated inflatable supports or jacks appear to offer a good workable solution. They are adjustable and easy to remove. Cylinder #5 does not require an internal support since the cradle will be used for support of the free end until attachments are completed.

VI.4.2. Assembly of Cylinders to Spaceframes

A required sequence of steps or operations is listed that will accomplish the assembly of the major support components into a completed central tracking support structure.

1. Set up and level the cantilever assembly beam and supports.
2. Install alignment tooling in the spaceframes.
3. Instal and align the inboard spaceframe and the outboard spaceframe.
    A. Remove the outboard assembly beam support.
    B. Place both spaceframe assemblies on the assembly beam in their proper orientation.
    C. Replace the outboard assembly beam support.
    D. Place both spaceframe assemblies in their proper locations and replace the inboard assembly beam support.
    E. Position and align both spaceframes to each other and fix the inboard spaceframe in place.
    F. Lock the adjustments of the outboard spaceframe and remove it by removing the inboard assembly beam support.
    G. Move the outboard spaceframe out.
    H. Replace the inboard assembly beam support.
    I. Remove the outboard assembly beam support.
    J. Remove the outboard spaceframe and place it in the shipping container until step 6.A.

4. Installation of Cylinder #1, #2, #3, and #4.
    A. Place cylinder #1 on the external positioning carriage.
    B. Slide the cylinder over the support beam.
    C. Replace the outboard assembly beam support.
    D. Remove the inboard assembly beam support.
    E. Move the cylinder into near final position.
    F. Replace the inboard assembly beam support.
    G. Position and align the cylinder to the spaceframe.
    H. Install the internal cylinder support on the outboard end.
    I. Fit the cylinder to spaceframe connecting hardware.

J. Lower the external cylinder support system and remove the carriage.

K. Remove the outboard assembly beam support.

L. Repeat steps A through K for cylinder #2 through #4.

5. Installation of Cylinder # 5.

A. Place cylinder #5 on the external positioning carriage

B. Slide the cylinder over the support beam.

C. Replace outboard assembly beam support.

D. Remove the inboard assembly beam support.

E. Move the cylinder into near final position.

F. Replace the inboard assembly beam support.

G. Position and align the cylinder to the spaceframe using the external cylinder support system.

H. Fit the cylinder to spaceframe connecting hardware.

I. Remove the outboard assembly beam support.

6. Installation of the outboard spaceframe.

A. Remove the outboard spaceframe and alignment fixture from the shipping container and place on the assembly beam.

B. Replace assembly bean outboard support.

C. Remove inboard assembly beam support.

D. Slide outboard spaceframe assembly into place.

E. Replace inboard assembly beam support.

F. Position and align the outboard spaceframe to the cylinders.

G. Fit the outboard spaceframe connecting hardware.

7. Final assembly and alignment testing.

A. Optically check the alignment of all cylinders.

B. Tighten all hardware cylinders to spaceframes.

C. Remove the external support tooling for cylinder #5.

D. Install the external support tooling to carry the Central Tracker by the four support load points.

E. Support the central tracker from the four load points while releasing it from the assembly beam and the spaceframe

support tooling.

F. Remove all internal support tooling.

G. Recheck alignment optically with the central tracker supported on the four support load points.

H. Remove the inboard assembly beam support.

I. Roll the carriage and tracker to the outboard beam support.

J. Replace the inboard support.

K. Remove the outboard support.

L. Roll the carriage and central tracker support structure away from the assembly beam.

VI.4.3. Modules onto Support Structure

The detector elements or modules which are fully described in this report in Section IV.2. are sufficiently robust due to their graphite shell that they can be handled by hand. The modules will arrive on site in shipping containers. It is assumed that the modules can be handled by two people manually. The modules will be installed through the open areas between the spaceframe struts as can be seen in Fig. VI.25. Tooling and supports will be required to support the module as it is being slid into position, registered on the fiducials, and locked into place. This tooling has not been engineered as of the writing of this report. In Section VI.3.5 there is a description of the attachment and fiducial design being proposed for module attachment.

VI.5. SUPPORT STRUCTURE ANALYSIS

The deflections resulting from loads applied to a five cylinder all modular straw tube central tracker were calculated using the ANSYS finite element analysis package. The deflections induced by gravity, thermal expansion, and moisture expansion were studied. Several sets of high and low material property values were used in the analysis to evaluate the variations that can occur in actual fabrications. Deflections were studied with each cylinder supporting one superlayer of straw tube modules. Two different ways of supporting the gravity load of the silicon inner tracking system were tried: one with the load applied to the ends of the innermost superlayer and one with the load applied to the inboard sides of each spaceframe.

VI.5.1. The Tracker Description

The deflections of the central tracker under its own weight have been estimated for the design shown in Fig. VI.26. This design is composed of five concentric structural cylinders which are attached together at the ends by a spaceframe of hollow struts shown in Fig. VI.27. The six cylinders, each of which supports one superlayer of detectors, are made of identical symmetrical sandwiches of foam core with outer skin layers of graphite laminate. The entire structure is supported at the four corner points as indicated in Fig. VI.28. The vertices of the outer ring of the space frame lie in a horizontal plane through the axis of the structure. Each cylinder is attached at each end to an angle-section ring which is connected to the spaceframe.

Figure VI.4-7 shows some details of the spaceframe portion of the structure. Dimensions are given both for the angle section used to attach the cylinders and for the hollow box section used for all the struts making up the frame itself. Dimensions are given for the support cylinders and for the cross section and some conceptual features of the end closeout attachment to the spaceframe.

The straw detector module design is shown in Fig. VI.29. The modules consist of trapezoidal shells whose interior space is filled with straw detectors 4.0 millimeter in diameter and weighing 0.5 grams per meter. The walls of a shell are made of sandwiches of graphite-epoxy skins encapsulating a thin foam core, similar to the structure of the support cylinders. Each module superlayer is attached to its supporting cylinder by shim rings which are indicated in Fig. VI.14. The modules are more or less loosely attached to these rings. Since the modules are not connected to each other and are not firmly attached to the cylinders, they contribute negligible stiffness to the cylinders. They can therefore be treated initially as non-structural mass whose dead weight constitutes much of the load on the structure. This assumption is to be validated and studied by further analysis. The module design shown in Fig. VI.14 is estimated to exert a force of 0.2167 kilograms per meter (non-trigger module) and 0.2503 kilograms per meter (trigger module).

VI.5.2. The Finite Element Model

To assess the deflections of this structure due to gravity, thermal, and moisture loading, a finite-element model was constructed using the ANSYS package. This model, drawn in Fig. VI.30, shows that the structure has two vertical planes of mirror symmetry

dividing it end-to- end and side-to-side. Because of this symmetry, only a quarter of the structure needed to be modeled. This complete model was run to get a good detailed pictures of the displacement patterns of the tracker structure.

The space frame is modeled with the ANSYS STIF4 3-dimensional beam element, using the two cross-sections indicated in Fig. VI.30, the rectangular box section for the frame proper, and the angle section for the rings to which the cylinders attach.

The cylinder elements shown in Table VI.12 are the ANSYS "Layered Shell Element" STIF91, which models a sandwich of various materials all with different thickness and material properties. The sandwich for the cylinder element, with a superlayer "cladding" on the outside, is shown in Fig. VI.31. It contains a sequence of five materials. The center (no. 4) layer is the structural foam core of the cylinder, a relatively thick layer of Rohacell 31. The center line of this layer corresponds to the nominal radius assigned to the shell element. Attached to the surface of the foam (i.e., material layers 3 and 5) are the graphite-epoxy skins of the cylinders, incorporating the combined elastic properties of a multi-ply layup.

Each superlayer of modules is modeled by a layer of nonstructural (very compliant) material, just outboard of the cylinder's outer skin. This module layer (material layer 1) is given a nominal density of 2044 kilograms per cubic meter; non-trigger module layers have a nominal thickness of 1.00 millimeters while the heavier trigger module layer is assigned 1.159 millimeters thickness.

The symmetry of the structure is enforced in this partial model by applying appropriate constraints to the nodes lying in the two vertical symmetry planes. As the figure indicates, the model has been constructed with the origin of global coordinates at the end rather than at the geometrical center of the structure, so that the end-to end symmetry plane is not the global X-Y plane, although the lateral symmetry plane is the global Y-Z plane.

The single-point support indicated in Fig. VI.30 appears as a vertical constraint applied to one node at an outer vertex of the frame. The model mesh is relatively coarse because only displacements are being sought, and not stresses. Similarly, the application of the dead weight of the modules at the discrete locations of the shim rings has not been

considered. Each superlayer has been incorporated into the model of its support cylinder as a sort of nonstructural (but heavy) "cladding."

VI.5.3. The Material Variation Sensitivity Analysis

Graphite fiber resin matrix composite has been selected as the leading candidate for the basic structural material for a variety of reasons. The material selection process for the cylinders is fully discussed in Section VI.2.2. and the specific recommended layup construction is documented in Section VI.2.3. Table VI.4 in Section VI.2.3 lists the mean and variance properties expected for a actual composites component. This table makes an attempt to scientifically estimate what the "High", "Mean", and "Low" versus theoretical material properties of a real component would be. Actual versus theoretical material property variances will occur in a manufacturing environments. This spread is generated by several variables including environmental conditions like shop humidity and temperatures changes, "workmen dependent" manufacturing items like slight deviations in layup composite angles, and spread on incoming raw materials such as allowed variabilities in fiber modulus. These "High", "Low", and "Mean" values were used as input in various combinations to the finite element model. Table VI.11 lists the combinations that were used and gives the resulting deflection in microns. The column number from Table VI.4 is referenced to the set of material properties used in the particular case number.

This sensitivity analysis has been an intensive effort and considerable data was generated, some of which remains to be analyzed as of the writing of this report. No surprises are expected, and it is felt that all potential issues can be dealt with by utilizing the suggested methods listed in the conclusion to this section.

Discussion of Results. The quasi-isotropic layup of [0 +/-60]symmetrical was first chosen as the prime construction layup for the cylinders for several reasons including the shear stiffness or substantial shear modulus that is needed in the cylinders. Most of the deflection in the cylinders in the case of gravity loading is shear deflection. A finite element model with and without substantial shear modulus (G) produced huge deflections. Previous finite element analyses, which are included in the appendix of this report, also indicate that the cylinders, except for local effects near the supports, remain round, assuming that adequate support is provided. In the spaceframe, the struts function as beams and can be analytically approached as beams. Beam deflection or the beam reaction to load is from bending or axial compression. The beam stiffness or deflection resistance

to load is controlled by the beam material modulus, length, and cross sectional area. In the case of the spaceframe, the strut modulus is set by the cylinder modulus, the length for practical purposes is fixed, but the cross sectional area is not fixed. By increasing cross sectional size, the allowed spaceframe bending can be adjusted. In a like manner but with limited independence, strut axial compression deflections can be controlled by increasing the wall thickness.

Unlike cylinder composite skin or the total cylinder thickness, as shown in Section VI.2.3, changes in strut size have minimum impact on tracker radiation length. As further analytical work toward minimization of tracker deflection is undertaken through further finite element studies, which are required, the option of changing strut size should be used to assist in optimization.

The finite element model shown in Fig. VI.32 indicates that the axial stiffness in the struts appears to be acceptable. A 50 percent decrease in strut modulus only increased the total deflection of the tracker by 17 percent. The spaceframe and cylinders act like two mechanical springs in series. Most of the deflection is in cylinder shear deflection. Classical spring calculations calibrated by the finite element model predict that it would require a four fold decrease in the strut or spaceframe axial modulus to increase the overall tracker deflections by 50 percent. These preliminary results indicate that, based on the need to control thermal expansion and similarly but to lesser extent moisture expansion, a layup design of [0+60-60]sym best meets the requirements of all tracker support components.

The cylinders with very large diameters have a shallow radius of curvature. A foam core is needed to give these cylinders some out of plane bending stiffness. The core acts as a spacer between the composite face sheets. Since increasing the cylinder stiffness against this type of loading was judged as desirable, the maximum allowed core thickness of 6 millimeter is used. This thickness limit is set by the total radiation length limit per superlayer which is defined and discussed in this report in Section VI.2.5.

The end closeout design features of the cylinders can be viewed in Fig. VI.9. This area forms the mechanical connection with the spaceframe. A more dense core material will be required to withstand the forces that the mechanical connections will apply. This dense core material can range from a denser 300 grade Rohacell foam to graphite composite layups. If a layups is used the coefficient of thermal expansion must be matched to the

cylinder hoop expansion. Although more engineering is needed, none of the issues appear difficult to solve.

Analysis Recommendations. The tube or strut sizes for the spaceframe which were selected on a first cut basis have been analytically shown to be of functional size. In order to increase the bending or axial stiffness of this item so as to reduce overall tracker deflection, the cross sectional size or wall thickness of these struts should be increased. Changing the layup construction is deemed to be counter productive since this creates a mismatched expansion coefficient between the spaceframe and the cylinders. This subject is discussed in Section VI.2.3.

Using a higher stiffness or modulus fiber is a potential method of both reducing cylinder and spaceframe deflection. This could conceivably be accomplished without any size or thickness increases. Ultra thin fiber with very high modulus tends to be expensive and also is brittle but remains a potential course of action.

The spread in the variance properties for expected constructions as displayed in Table VI.4 can be reduced. This spread is generated by several variables including potentially controllable environmental conditions like shop humidity and temperature changes. Other items sometimes refereed to as "workmen dependent" manufacturing items like tighter control on layup composite angles could be exercised. Finally the allowed spread on the fiber modulus of the incoming raw materials could be more tightly controlled. All or some of these items can be studied and potentially used to achieve a more closely specified more predicable final product.

VI.6. TOLERANCES DURING ASSEMBLY

The tolerance on final dimensions for a large structure such as this central tracker is a function of the design specified as well as the processes by which the components are manufactured, assembled, and controlled. During the design process it is very important to specify achievable requirements that are truly manufacturable and measurable. An attempt has been made to satisfy all these requirements.

VI.6.1. Quality of Fabrication

The design concept is to manufacture a few large simple components, accurately machine them, and assemble them to obtain a precision structure. The components are preassembled into low tolerance assemblies. These preassembled units are in turn machined to high tolerance with single setup, simple move, two axis linear or single axis rotary move machine tools. It is a requirement that all machine tools used be in good condition. Their good condition should be confirmed by laser alignment testing just prior to performing machining operations on primary components. The assembly concept consists of final assembly of a minimum number of simple measurable shapes. Machining of the cylinder shim rings involves a linear spindle move that should be straight with in 0.001 inches, parallel to the mandrel axes to within 0.002 inches, and a azimuthal indexing that should be with in .001 inches.

Machining of the spaceframe rings that locate the cylinders radially is done on a three axis boring mill that should produce parts concentric to within 0.003 inches. When assembled to the spaceframes, the cylinders are adjustable in the azimuthal direction with respect to each other (within measurement accuracy of 0.001 inches) to align superlayer modules.

In a simple way, the above should sum to:

Azimuthal locations indexing linear	0.001
Straight linear	0.001
Total	0.002

Radial Locations	Straight Linear	0.002
	Parallel Axes	0.002
	Concentricity	0.003
	Total	0.007

VI.6.2. Stability of the Fabrication

The final structure should be stable. Graphite composite structures are stable materials when properly fabricated and fully cured. Graphite composite and Rohacell foam as structural materials have been determined to be radiation hard to the levels of radiation expected in the central tracking region of the detector.

Thermal expansion is not perceived to be a problem since the graphite composite layup being specified for this construction has a near zero coefficient of expansion. See Section VI.2. for the actual values of the layups that are being considered for use. Thermal expansion can be further controlled by accurately regulating the temperature in the detector by careful heat removal.

Moisture expansion is reversible. If the composite structure does experience swelling from spending time in a humid environment, the swelling can be reversed and completely recovered by simply placing the structure in a controlled environment. The plans indicate that there will be humidity control within the detector.

VI.7. FINAL ASSEMBLY AND TESTING

VI.7.1. Modules

There are three types of modules. Each of the trigger layers is formed from radial trapezoidal modules constructed to match the radius of the super layer. A third type of module with trapezoidal cross section is used for the stereo modules and the inner axial superlayer. The number that need to be produced is 192 outer trigger modules, 160 inner trigger modules, and 384 non-trigger modules. These modules will be build in a number of locations. It is anticipated that this could be done in three locations.

Once the modules are completed they will be tested on site. This test will include x-ray measurements to determine the wire positions at each hold down point and the relative positions of the hold down fiducials at this point. They will also be tested with high voltage and gas flow to record cosmic rays and to verify the resolution specifications.

Once tested the modules will be packaged and sent to the tracking assembly point at the SSCL.

VI.7.2. Cylinders and Spaceframe

When the cylinders have been constructed, they will be shipped to the tracker assembly point at the SSCL. The assembly sequence has been described in Section VI.4.

After assembly, the fiducial points on all cylinder ends will be mapped and the entire tracker coordinate system established.

VI.7.3. Superlayers

Once the cylinders are in place and their alignment is complete, the process of attaching the modules will take place. The details of the hold down fixture were discussed in Section VI.4. Each module must be lifted into position on the cylinder. This will be done with the aid of an cantilevered holding arm which positions a module above the attachment points and then inserts it in the lock down pins. The endpoint hold down points determine the orientation of the module and the overall alignment precision. The attachment of the modules will be done in a symmetric order so as to load the cylinder uniformly. The attachment of modules for the stereo is done in the same manner. The cantilevered arm will be positioned at the 3° stereo position for module insertion. Some of the modules are positioned in line with the space frame struts, however this can be handled by having a section on the cantilever that can make a transverse shift of up to 20 cm.

Once the modules are in place the visible fiducial points will be mapped to check the the position of each end point with respect to the cylinder axis. This can be done optically from each end.

VI.7.4. Insertion in Magnet

When the modules are attached, and the utilities are in place, the entire tracking cylinder (8 meters in length) will be lowered down to the interaction point. The tracking system will be supported on the four attachment points (two on each end) in a frame which can be slipped along the length of the magnet, positioned radially, and then stabilized while the attachment to the calorimeter is made. The support for the tracker is shown in Fig. VI.28.

MATERIAL		Elastic Modulus E-Msi	Density ρ (lb/in^3)	CTE α ppm/F	Tensile Ultimate Strength Ksi	Compressing Strength Ksi	Volume Change 50% Humidity Percent	Effective Radiation Length L-cm
MATERIAL CANDIDATES								
Graphite & Resin**	X(Zero)	14.70	0.0600	-0.16	49.7	22.7	0.006***	25.7
	Y(90 Deg)	14.70			73.0	33.8		
	Shear	5.57			20.0			
Carbon-Carbon**		16.00	0.0600	-0.11	40.0	40.0	0.0	18.8
Al-MMC sub f*		53.07	0.0907	0.60	100.0	40.0	0.0	11.8
Al-MMC sub p****		15.07	0.1000	5.00	75.0	75.0	0.0	9.0
Rohacell 31 lg		0.005	0.0012	2.05	0.142	0.057	0.2	936.6
51 WF		0.011	0.0019	1.83	0.232	0.116	0.2	576.4
300 WF		0.052	0.0109	?	1.450	2.320	0.2	99.9
REFERENCE MATERIALS								
Aluminum		10.40	0.1012	12.89	75.0	40.0	0.0	8.9
Beryllium		42.05	0.0665	6.44	40.0	27.0	0.0	35.4
Copper		16.99	0.3219	9.39	10.0	10.0	0.0	0.0

*Graphite Fiber (P-110) MMC-Metal Matrix Composite, uni-directional properties

**[0 +/-60]sym Composite Properties

***CME of 0.397 in/in/%R.H.@R.T.

****Particle Reinforced MMC-Metal Matrix Composite, machineable, brazable

Table VI.1. Candidate materials for tracker construction.

Material Source	P75 - Pitch Amoco	UHM - PAN Hercules
E1, Msi	75	64
CTE1, in/in/F	-7.70e-07	-5.72e-07
Tensile Strain, %	0.4	0.8
Density, lb/in^3	0.072	0.068

Westinghouse
Science & Technology Center

Table VI.2. Mechanical and thermal properties of materials.

Resin	ERL-1962	ERL-1939-3	HX 1553	954 - 3	934	3501-6	R500
Source	Amoco	Amoco	Hexcel	Fiberite	Fiberite	Hercules	3M
TYPE	Epoxy	?	Epoxy Cyanate	Cyanate Ester	Epoxy	Epoxy	Epoxy
Tensile Stress, Ksi	10	11	12	9.4	7.10	10	8.3
Tensile Modulus, Ksi	0.540	0.480		0.44	0.6	0.643	0.507
Tensile Strain, %	2.1	3		2.5	1	1.7	1.9
Water Absorption, %	3.4	2	2	0.95	4.6	1.2	1.56
Conditions	a	a		b	b	c	d
Density, lbm/in^3	0.046	0.045	0.046	0.043	0.047	0.046	0.045
CTE, in/in/F	3.6e-05		3.58e-05			2.43e-05	
Cure Temperature	350	350	350	350	350		350

CONDITIONS

a. 2 weeks soak @ 160°F
b. 48 hrs @ boil
c. 24 hrs @ boil
d. 100% RH/88°C to equilibrium

Table VI.3. Properties of resin matrix systems from supply sources.

Modulus	Low Material				High Material				Mean Material	
Wrap Angles	[0 +/-55]		[0 +/-65]		[0 +/-55]		[0 +/-65]		[0 +/-60]	
Moisture****	0%	0.2%	0%	0.2%	0%	0.2%	0%	0.2%	0%	0.2%
Column Number	1	2	3	4	5	6	7	8	9	10
EX, MSI	11.900	11.800	11.700	11.600	16.900	16.800	16.600	16.500	14.700	14.600
EY, MSI	9.020	8.970	14.600	14.500	12.800	12.700	20.800	20.700	14.700	14.600
EZ, MSI	0.924	0.900	0.897	0.874	1.060	1.030	1.030	1.000	0.982	0.957
GXY, MSI	5.170	5.140	3.620	3.590	7.320	7.270	5.100	5.060	5.570	5.530
GYZ, MSI	0.421	0.421	0.444	0.423	0.513	0.513	0.546	0.546	0.498	0.498
GXZ, MSI	0.446	0.446	0.423	0.409	0.548	0.548	0.515	0.515	0.499	0.499
MUXY	0.451	0.451	0.211	0.211	0.461	0.461	0.216	0.216	0.318	0.318
MUYX	0.342	0.342	0.263	0.263	0.348	0.349	0.271	0.271	0.318	0.318
MUYZ	0.201	0.201	0.221	0.221	0.266	0.266	0.328	0.328	0.232	0.231
MUZY	0.021	0.020	0.014	0.013	0.022	0.022	0.016	0.016	0.016	0.015
MUXZ	0.163	0.163	0.241	0.241	0.249	0.249	0.326	0.326	0.232	0.231
MUZX	0.013	0.012	0.018	0.018	0.016	0.015	0.020	0.020	0.016	0.015
ALPHA-X*	-0.182	-0.189	0.149	0.135	-0.337	-0.343	-0.100	-0.111	-0.155	-0.164
ALPHA-Y	0.234	0.219	-0.115	-0.123	-0.039	-0.051	-0.286	-0.296	-0.155	-0.164
ALPHA-Z	22.900	22.900	22.900	22.900	20.000	20.100	20.100	20.100	20.50	20.600
CME*** E-6/% Moisture Absorbed										118.000
CME** E-6/% Relative Humidity										0.397

* E-6/oF **Calculated (118E-6*0.185/55)
*** For P75/ 954-3 , 0.185% Moisture Absorpted @ 55% R.H.@RmTemp/Fiberite
**** Moisture - Hygrothermal Effect Estimate

Viewgraph 3
RLS
10.31.91

Westinghouse
Science & Technology Center

Table VI.4. The mean and variance properties of the materials.

Material	P75/954-3	P75/ERL 1939-3
Source	Fiberite	Amoco
Resin Content	38%	
Fiber Volume		59%
CTE1, in/in/°F	0.007	-0.27 for 1.5 mil ply -0.17 for 2.5 mil ply
CTE2, in/in/°F		-0.23 for 1.5 mil ply -0.19 for 2.5 mil ply
Thermal History		-275°F to 212°F 1st cycle average

Westinghouse
Science & Technology Center

Table VI.5. Comparisons of thermal expansion properties.

Material	P75/954-3	P75/934
Resin Content	30%	30%
Water Absorption, %	0.185 55% R.H./RT/EQ	0.51 50% R.H./150 F/EQ
CME, 10^{-6} in/in/%	118	155

Viewgraph 5
RLS
10.31.91

Westinghouse
Science & Technology Center

Table VI.6. Thermal and moisture expansion properties.

SUMMARY TABLE OF RADIATION LENGTH CALCULATIONS

TABLE #	SUPPORT CYLINDER GRAPHITE TK/LAYER INCHES	SUPPORT CYLINDER FOAM TYPE	SUPPORT CYLINDER FOAM TK INCHES	SHIM RING EFFECTS	MODULES GRAPHITE TK/LAYER INCHES	MODULES FOAM TYPE	MODULES FOAM TK INCHES	MODULE EDGE EFFECTS	PERCENT RADITION LEN/LAYR CM
2	0.0045	31IG	1	NO	0.006	51WF	0.14	NO	0.87
2	0.0045	51WF	1	NO	0.006	51WF	0.14	NO	1.04
4	0.0045	31IG	1	NO	0.0045	51WF	0.14	NO	0.93
5	0.0045	31IG	1	NO	0.0045	31IG	0.14	NO	0.88
6	0.0045	31IG	0.59	NO	0.0045	51WF	0.14	NO	0.83
7	0.0045	31IG	0.59	NO	0.0045	31IG	0.14	NO	0.78
3	0.006	31IG	0.23	NO	0.0045	31IG	0.14	NO	0.71
12	0.006	31IG	0.47	NO	0.0045	31IG	0.14	NO	0.77
11	0.009	31IG	0.23	NO	0.0045	31IG	0.14	NO	0.77
8	0.009	31IG	0.23	NO	0.0045	31IG	0.14	YES	0.79
9	0.009	31IG	0.23	YES	0.0045	31IG	0.14	YES	0.80
9 (SAME AS ABOVE EXCEPT EDA = 1.63)									2.11
10 (SPACEFRAME END DISK SPREAD RADIATION LENGTH CALCULATION)									0.21
0.21 RAD LG IS EQUIVALANT TO 0.007 Inch Thick Aluminum Sheet)									
0.021 Inch Thick Graphite Sheet)									

Table VI.7. Summary of radiation length calculations.

SUPERLAY NUMBER	COMPONEN	QUANITY #	AZMUTHA WIDTH INCHES	RADIAL LENGTH INCHES	DISK AREA TOTAL SQ IN	COMPONE TOTAL SQ IN	PERCENT COMPONE COVERS
5 TO 4	STRUTS	16	0.79	5.51	2126.98	69.62	3.273
	JOINTS	16	1.57	1.57	2126.98	39.68	1.866
	RINGS	1	N/A	0.59	2126.98	238.12	11.195
4 TO 3	STRUTS	16	0.79	5.51	1936.10	69.62	3.596
	JOINTS	16	1.57	1.57	1936.10	39.68	2.049
	RINGS	1	N/A	0.59	1936.10	217.66	11.242
3 TO 2	STRUTS	16	0.79	11.02	3299.55	139.23	4.220
	JOINTS	16	1.57	1.57	3299.55	39.68	1.203
	RINGS	1	N/A	0.59	3299.55	197.21	5.977
2 TO 1	STRUTS	16	0.79	14.17	3120.35	179.01	5.737
	JOINTS	16	1.57	1.57	3120.35	39.68	1.272
	RINGS	1	N/A	0.59	3120.35	156.31	5.009
	AVERAGE PERCENT OF AREA STRUT COVERS						4.21
	AVERAGE PERCENT OF AREA JOINT COVERS						1.60
	AVERAGE PERCENT OF AREA RING/(CYLINDER END) COVERS						8.36

Table VI.8a. Summary of spaceframe dimensions and constants.

ITEM	PERCENT LOCAL RAD LG	PERCENT AREA COVERED	PERCENT SPREAD RAD LG
Strut	1.944	4.21	0.082
Joint	2.955	1.60	0.047
Ring	0.972	8.36	0.081
Average Per End			0.21

Or Equal To

0.007 Inch Thick Aluminum Sheet

0.021 Inch Thick Graphite Sheet

Table VI.8b. Summary of average radiation length for spaceframe.

K-KARB[R] CARBON-CARBON AND GRAPHITE EPOXY BOLTS BY KAISER AEROTECH

Fabricated Bolt Material Properties:

Bolt	Size	Tap Drill Inches	Thread Shear Psi SS Ult	Thread Shear Pounds @ 1.5 o.d.
A) Alum	1/4-20	0.204	36000	7060
B) Steel	1/4-20	0.204	32000	6276
C) K-Karb	1/4-20	0.204	3640	714
D) K-Karb	3/8-16	0.316	2640	1242
E) K-Karb	1/2-13	0.422	1970	1653

Table VI.9. Fabricated bolt properties.

Shaft Dia in.	Dsk Tk in.	Disk Nom. kips -in.	Disk Slope	Disk σ_θ ksi	Disk σ_r ksi	Displacement Inches					
						Place	Cyl End	Disk	Cyl Midpt	Local Max.	Local Min.
8.0	1.0	179.	0.0186	74.5	83.7	T/B	2.32452	2.32413	2.32464	2.3259	2.3226
						Side	2.32448	2.32441	2.32463		
						Shaft		2.32377			
8.0	2.0	642.	0.0092	67.0	75.1	T/B	1.61647	1.61655	1.61710	1.6196	1.6137
						Side	1.61642	1.61672	1.61715		
						Shaft		1.61634			
10.	1.0	93.	0.0091	34.1	38.2	T/B	1.11005	1.10961	1.11011	1.1107	1.088
						Side	1.11001	1.10988	1.11009		
						Shaft		1.10928			
10.	2.0	494.	0.0062	41.4	46.5	T/B	0.89374	0.89371	0.89422	0.8960	0.8916
						Side	0.89369	0.89388	0.89425		
						Shaft		0.89352			
12.0	1.0	63.	0.0051	17.8	19.9	T/B	0.60024	0.59978	0.60027	0.6005	0.5994
						Side	0.60020	0.60005	0.60024		
						Shaft		0.59948			

Table VI.10. Mandrel stresses and displacements.

Case #	Type	Material Properties * Spaceframe	* Cylinders	Deflections Microns Radial	Microns Axial	Forces Lb./In. Radial	Lb./In. Axial
	Gravity						
1	Vertical	5 High-Modulus	5 High-Modulus	98.7	N/A	N/A	+/-2.6
2	Vertical	4 Low-Modulus	4 Low-Modulus	151.8	N/A	N/A	+/-2.6
3	Vertical	10 Mean-Modulus	10 Mean-Modulus	116.5	N/A	N/A	+/-2.6
4	With Silicon	10 Mean-Modulus	10 Mean-Modulus	145.5	N/A	N/A	+/-3.2
	Thermal						
5	Radial	3 High-CTE	8 Low-CTE	-15.2	+14.4	+2.2	0.0
6	Axial	3 High-CTE	6 Low-CTE	-3.2	+41.4	-0.3	-0.5
7	Radial	6 Low-CTE	1 High-CTE	+11.1	+21.4	-1.0	0.0
8	Axial	6 Low-CTE	3 High-CTE	-5.9	-17.5	+0.7	0.0
	Humidity						
9	50%	10 Mean-Modulus	10 Mean-Modulus	+33.5	-81.9	-3.8	+0.9
10	25%	10 Mean-Modulus	10 Mean-Modulus	+16.8	-40.9	-1.9	+0.5

VI.4

* Column Number From Table Number ~~VI-1-D~~ titled" Composite Variation" Refers to the Set of Material Properties Used in the Particular Case #

Table VI.11. Finite element analysis of variance of materials.

***** CENTROID, MASS, AND MASS MOMENTS OF INERTIA *****

CALCULATIONS ASSUME ELEMENT MASS AT ELEMENT CENTROID

CENTROID		MOM. OF INERTIA ABOUT ORIGIN		MOM. OF INERTIA ABOUT CENTROID	
XC =	838.69	IXX =	0.1460E+10	IXX =	0.5750E+09
YC =	-0.58137E-02	IYY =	0.1460E+10	IYY =	0.4032E+09
ZC =	1903.7	IZZ =	0.4412E+09	IZZ =	0.2694E+09
		IXY =	-118.3	IXY =	-1309.
		IYZ =	3622.	IYZ =	917.8
		IZX =	-0.3847E+09	IZX =	0.5380E+07

*** MASS SUMMARY BY ELEMENT TYPE ***

TYPE	MASS	(kg)
1	18.712	struts
2	6.186	rings
3	151.984	shim-rings w/ modules
9	67.408	cylinders
TOTAL	244.290	quarter-model

Table VI.12. Cylinder elements used in ANSYS analysis.

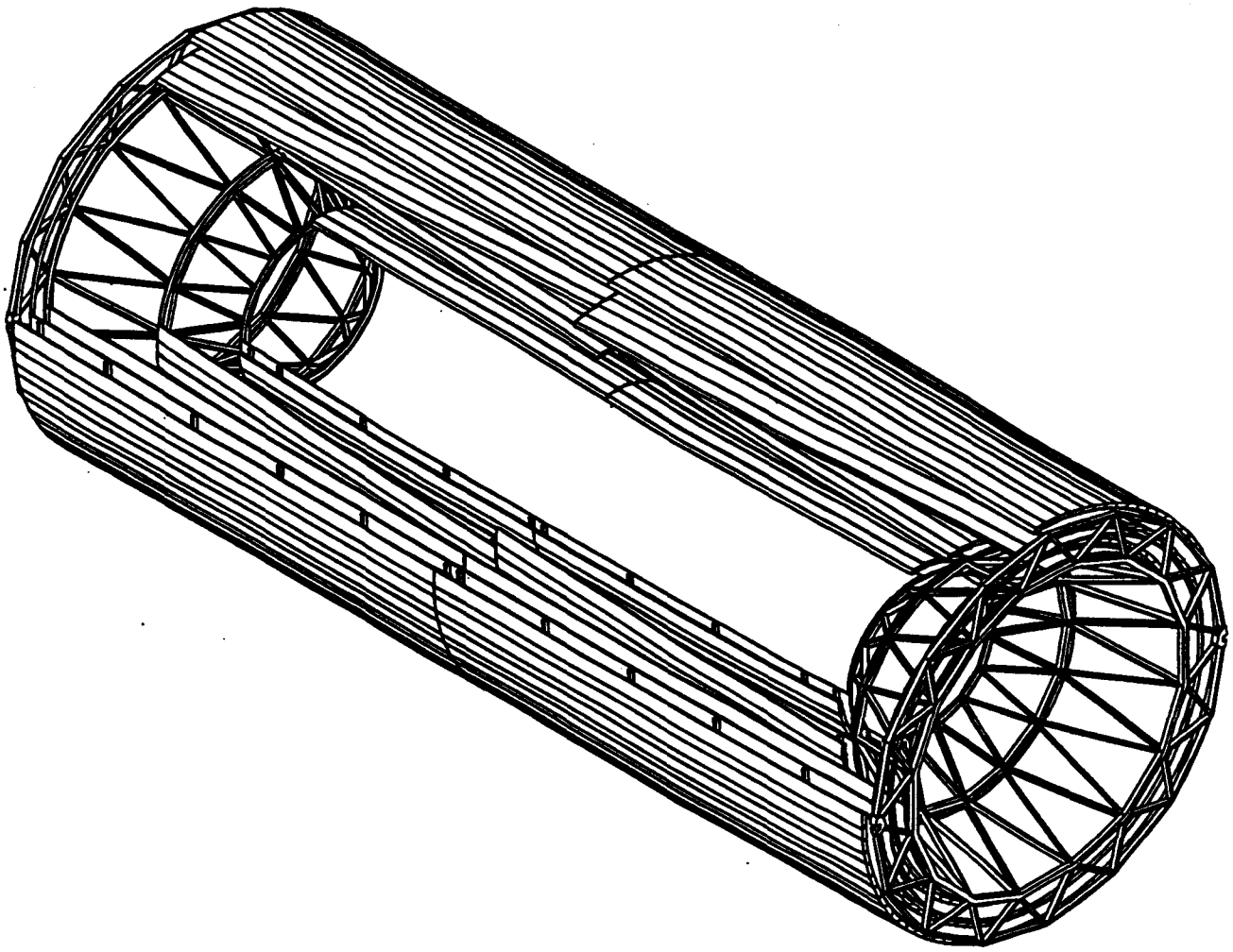

Fig. VI.1. Completely assembled central tracker.

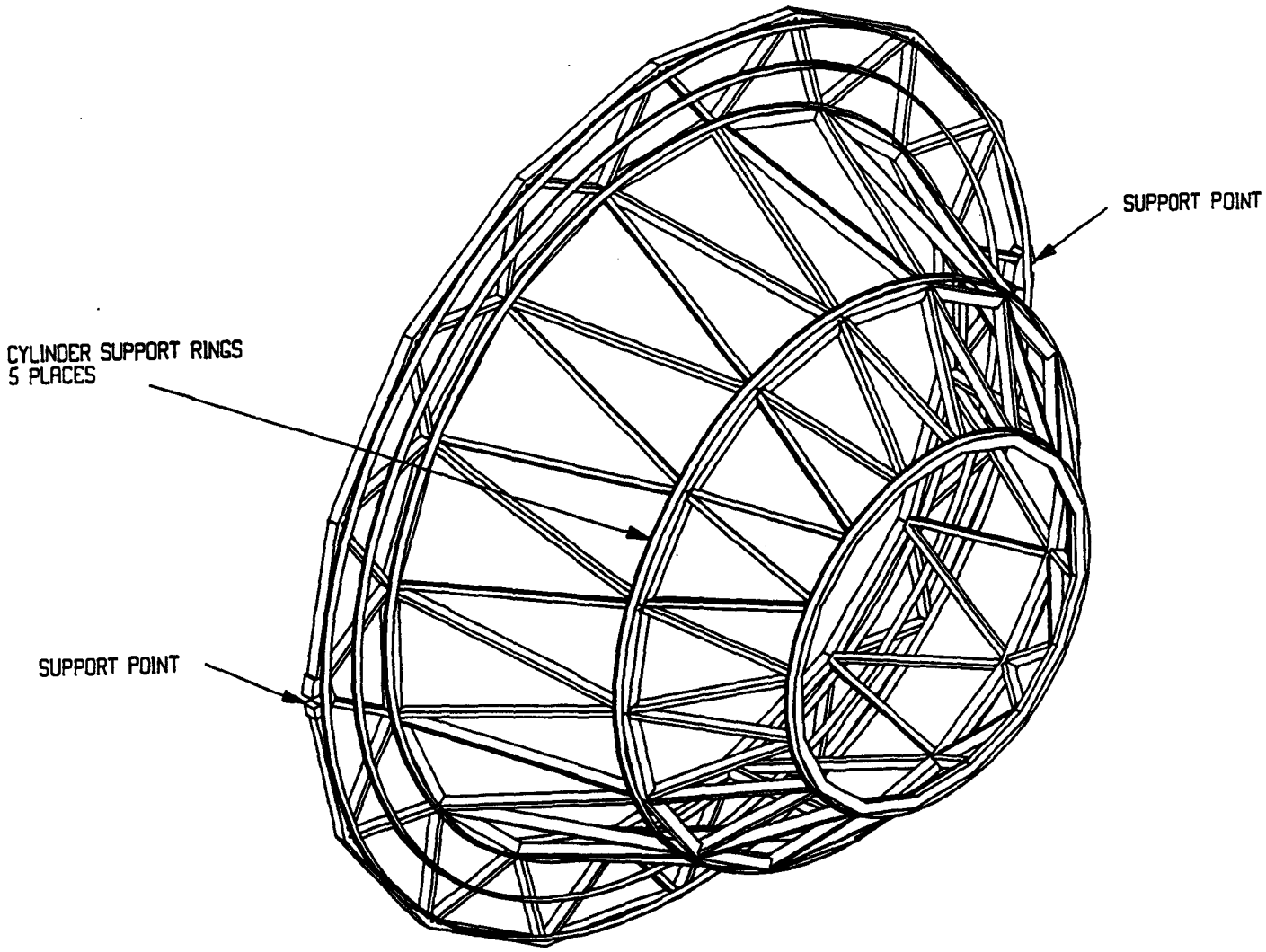

Fig. VI.2. Completed spaceframe support system.

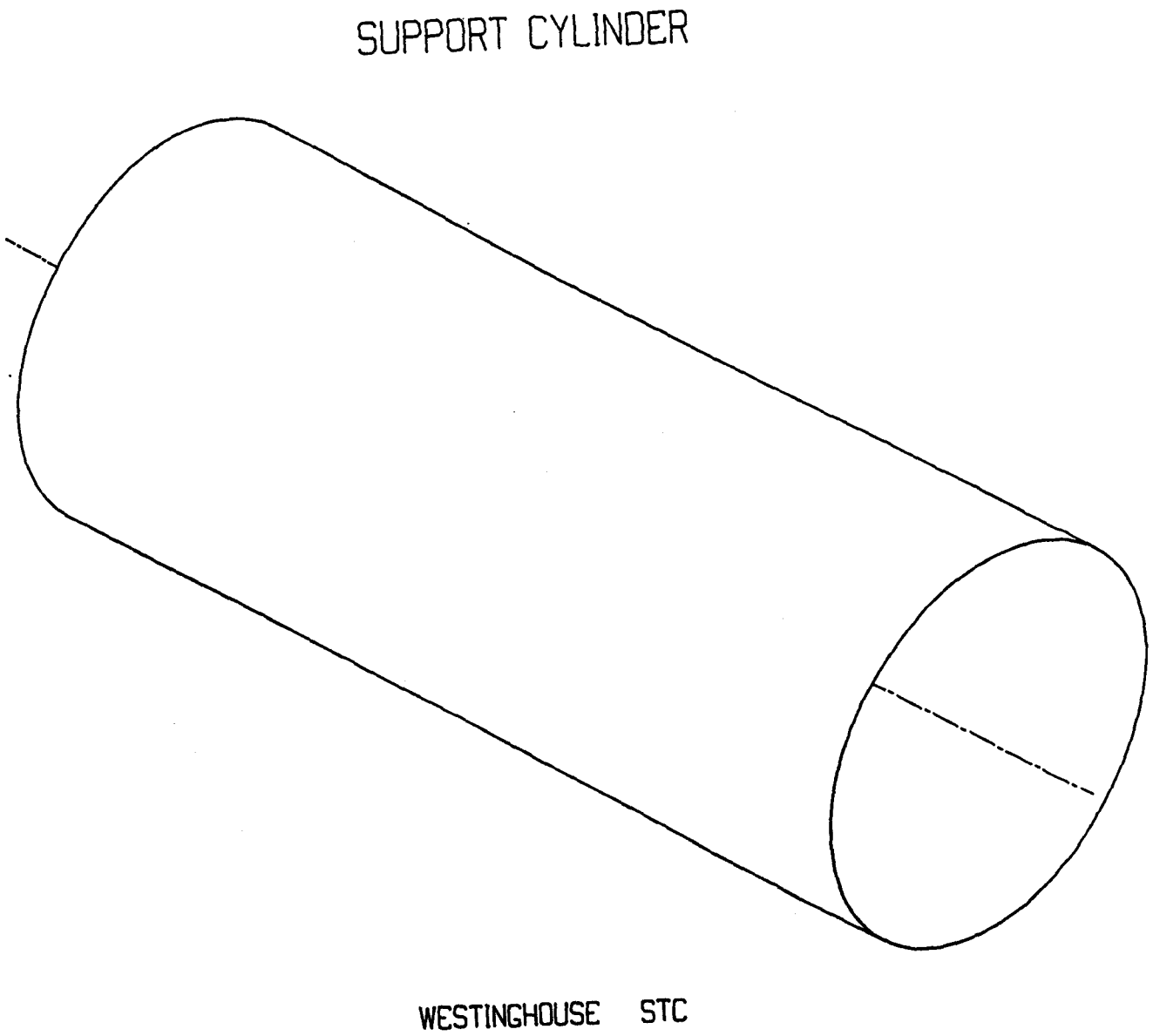

Fig. VI.3. The basic support cylinder for the modular tracker.

STRUCTURAL TUBING,QUANITIES FOR TWO SPACE FRAMES

ALL DIMENSIONS IN CM

ITEM	H X W X T	L	QUAN
A	4 X 4 X .25	25.7	32
B	2 X 4 X .25	52.2	62
C	4 X 4 X .25	37.9	32
D	2 X 4 X .25	85.4	64
E	4 X 4 X .25	49.8	32
F	2 X 4 X .25	43.6	56
G	2 X 4 X .25	63.2	24
H	2 X 4 X .25	34.9	4
I	2 X 4 X .25	55.9	4
J	2 X 4 X .25	54.1	4
K	2 X 4 X .25	41.5	4

MATERIAL - GRAPHITE COMPOSITE

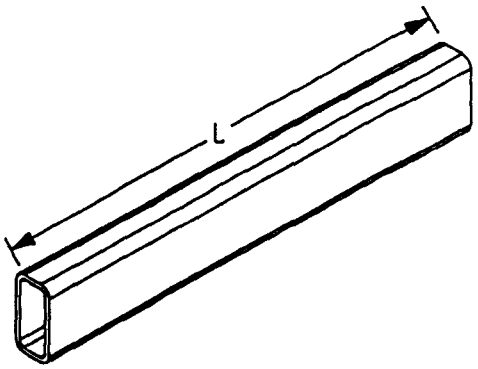

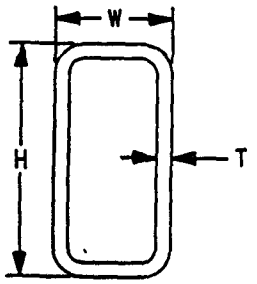

Fig. VI.4. Examples of the strut shapes under study.

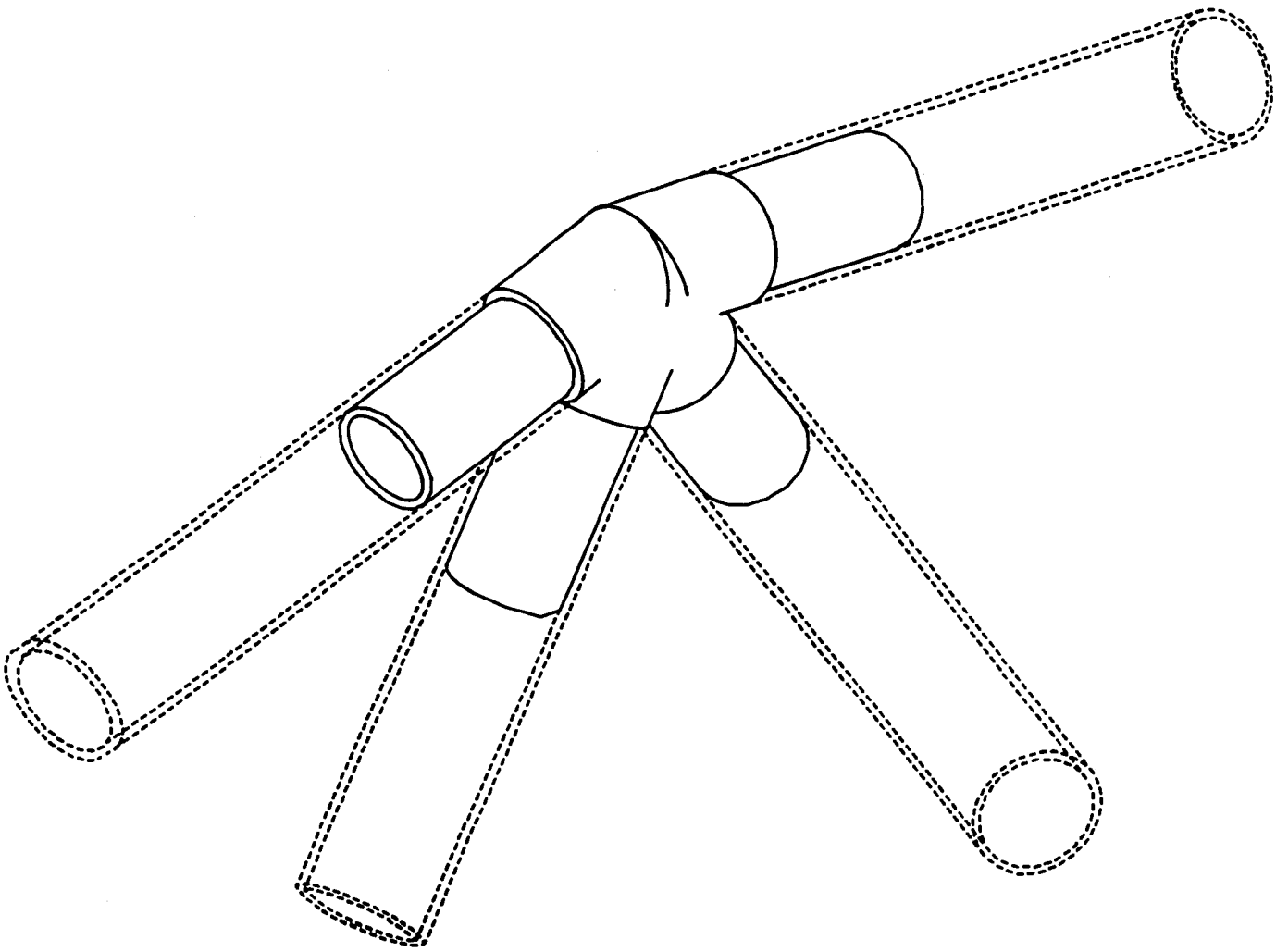

Fig. VI.5. The proposed strut connector for the spaceframe.

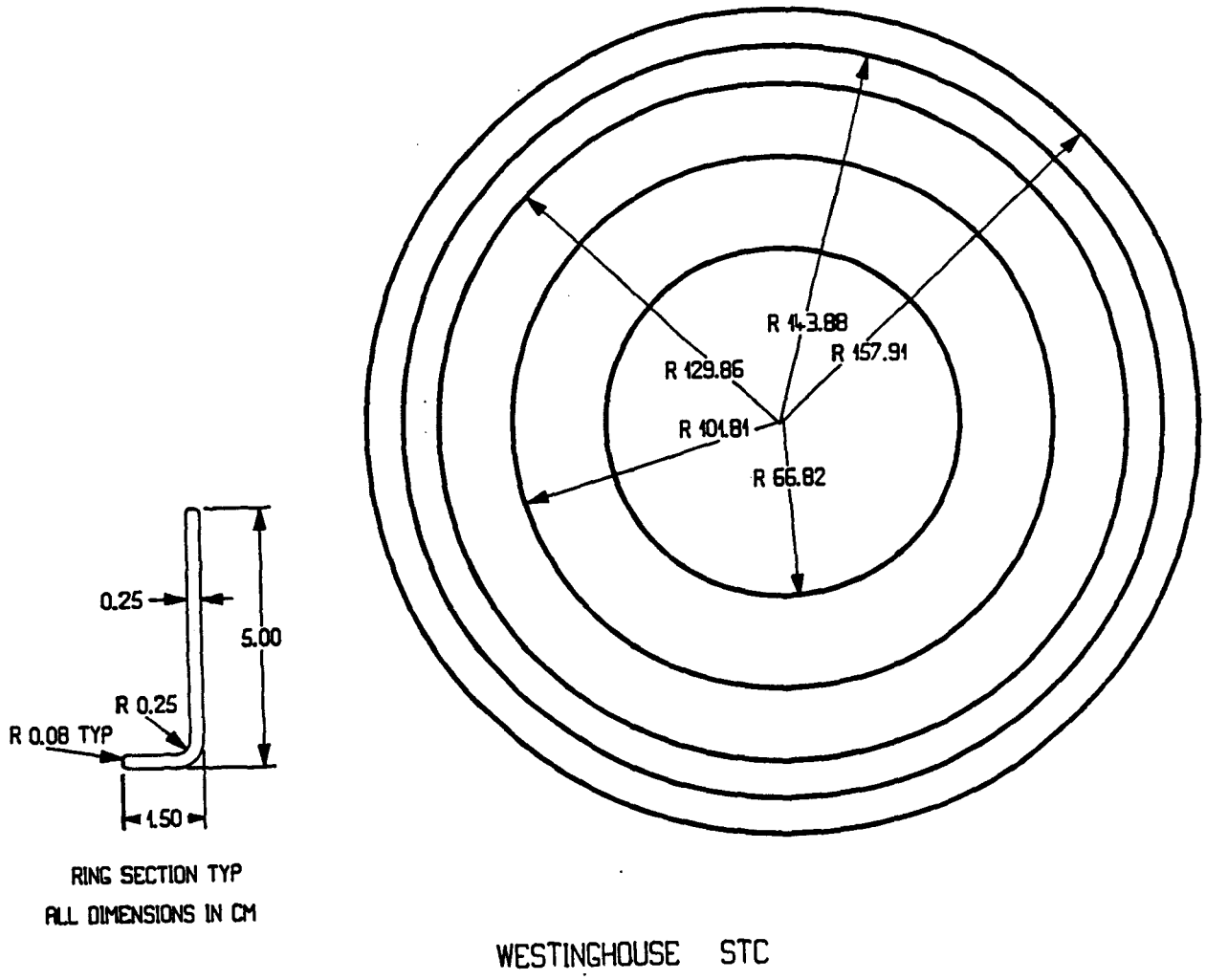

Fig. VI.6. The support ring component of the spaceframe.

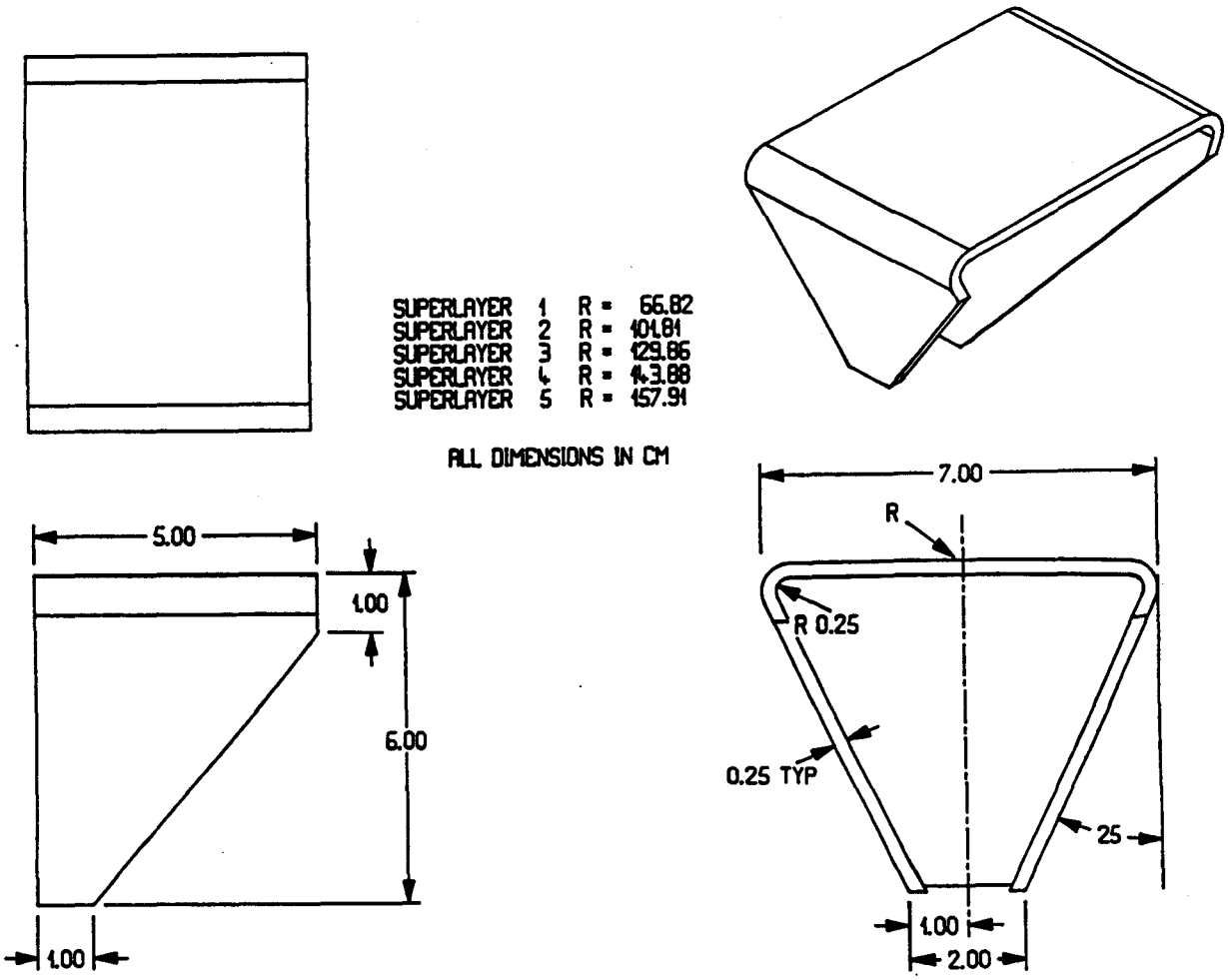

Fig. VI.7. Attachment gussets for the ring to strut connection on the spaceframe.

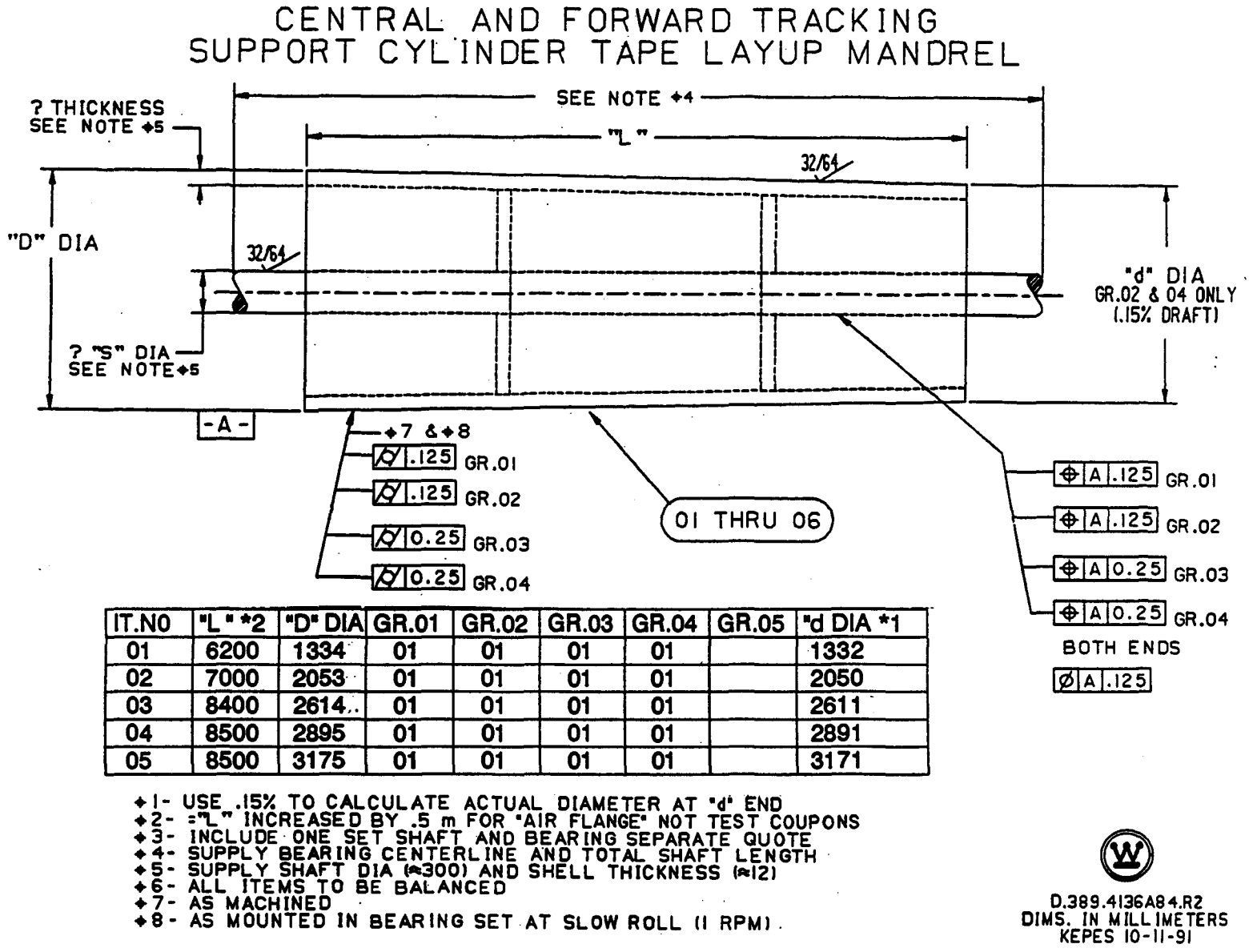

IT.NO	"L" *2	"D" DIA	GR.01	GR.02	GR.03	GR.04	GR.05	"d DIA *1
01	6200	1334	01	01	01	01		1332
02	7000	2053	01	01	01	01		2050
03	8400	2614	01	01	01	01		2611
04	8500	2895	01	01	01	01		2891
05	8500	3175	01	01	01	01		3171

✦1- USE .15% TO CALCULATE ACTUAL DIAMETER AT "d" END
✦2- ="L" INCREASED BY .5 m FOR "AIR FLANGE" NOT TEST COUPONS
✦3- INCLUDE ONE SET SHAFT AND BEARING SEPARATE QUOTE
✦4- SUPPLY BEARING CENTERLINE AND TOTAL SHAFT LENGTH
✦5- SUPPLY SHAFT DIA (≈300) AND SHELL THICKNESS (≈12)
✦6- ALL ITEMS TO BE BALANCED
✦7- AS MACHINED
✦8- AS MOUNTED IN BEARING SET AT SLOW ROLL (1 RPM).

D.389.4136A84.R2
DIMS. IN MILLIMETERS
KEPES 10-11-91

Fig. VI.8. The support cylinder mandrels.

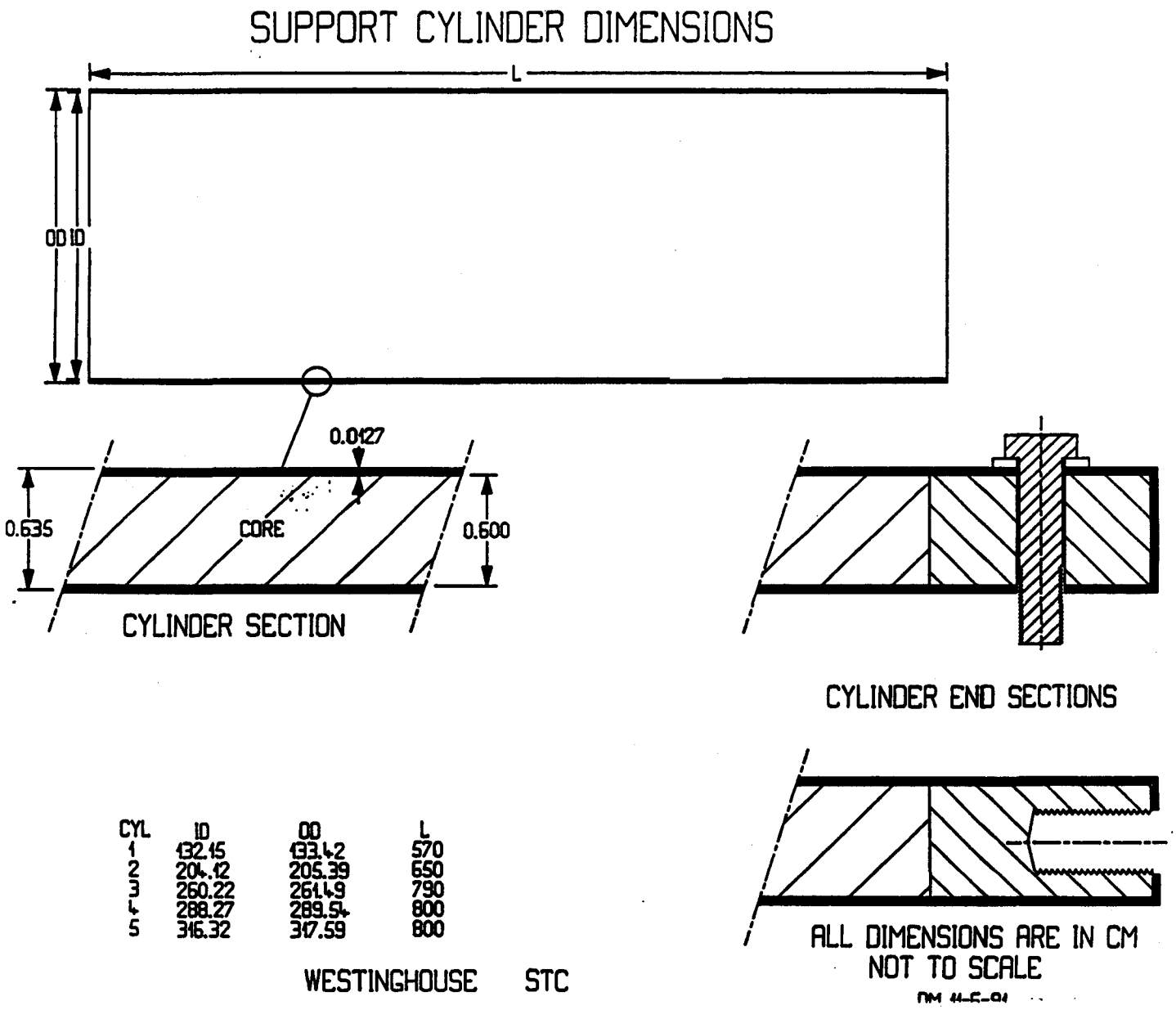

Fig. VI.9. The basic design of the cylinders.

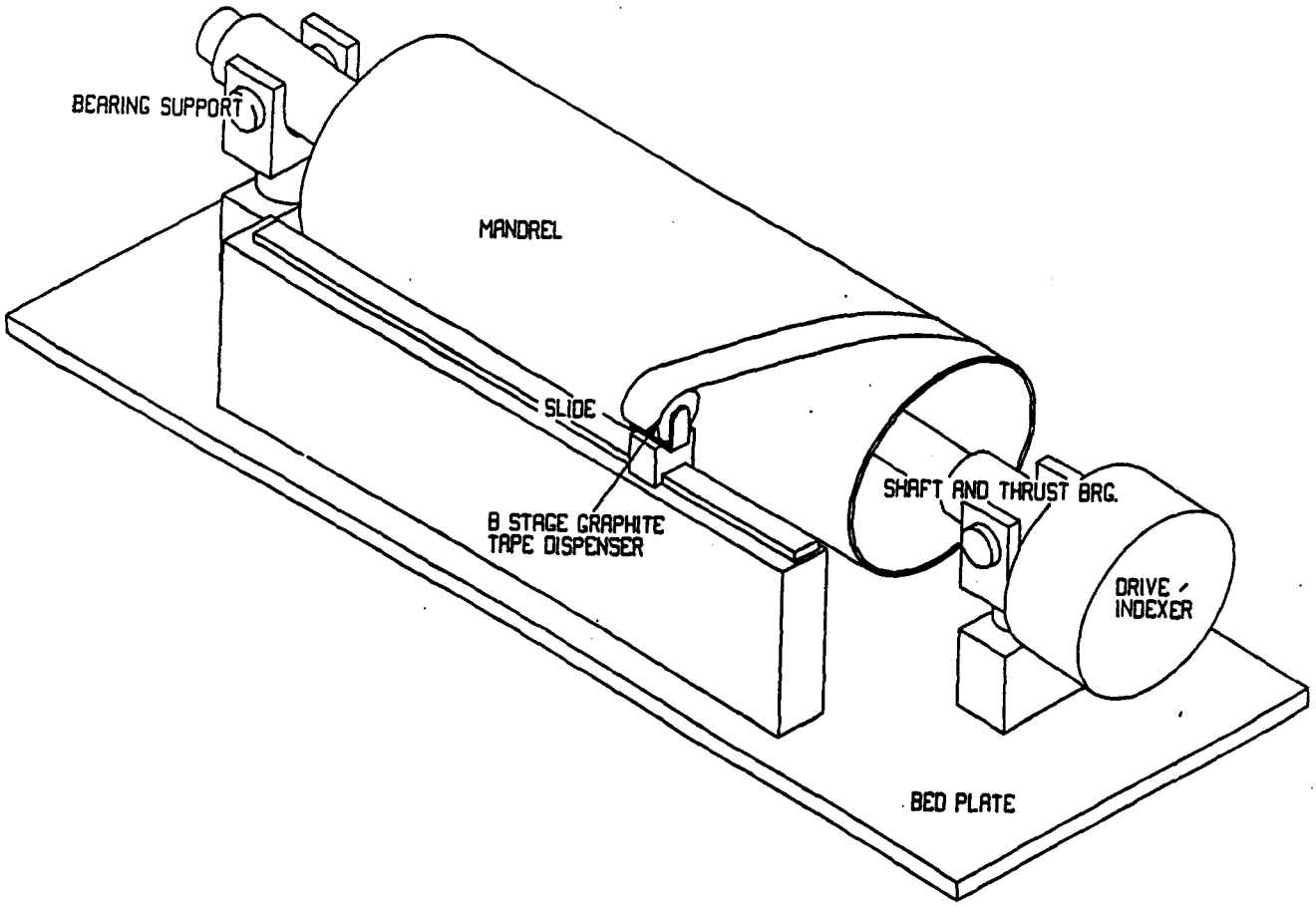

Fig. VI.10. The mandrel used for construction of the cylinders, showing the taping operation.

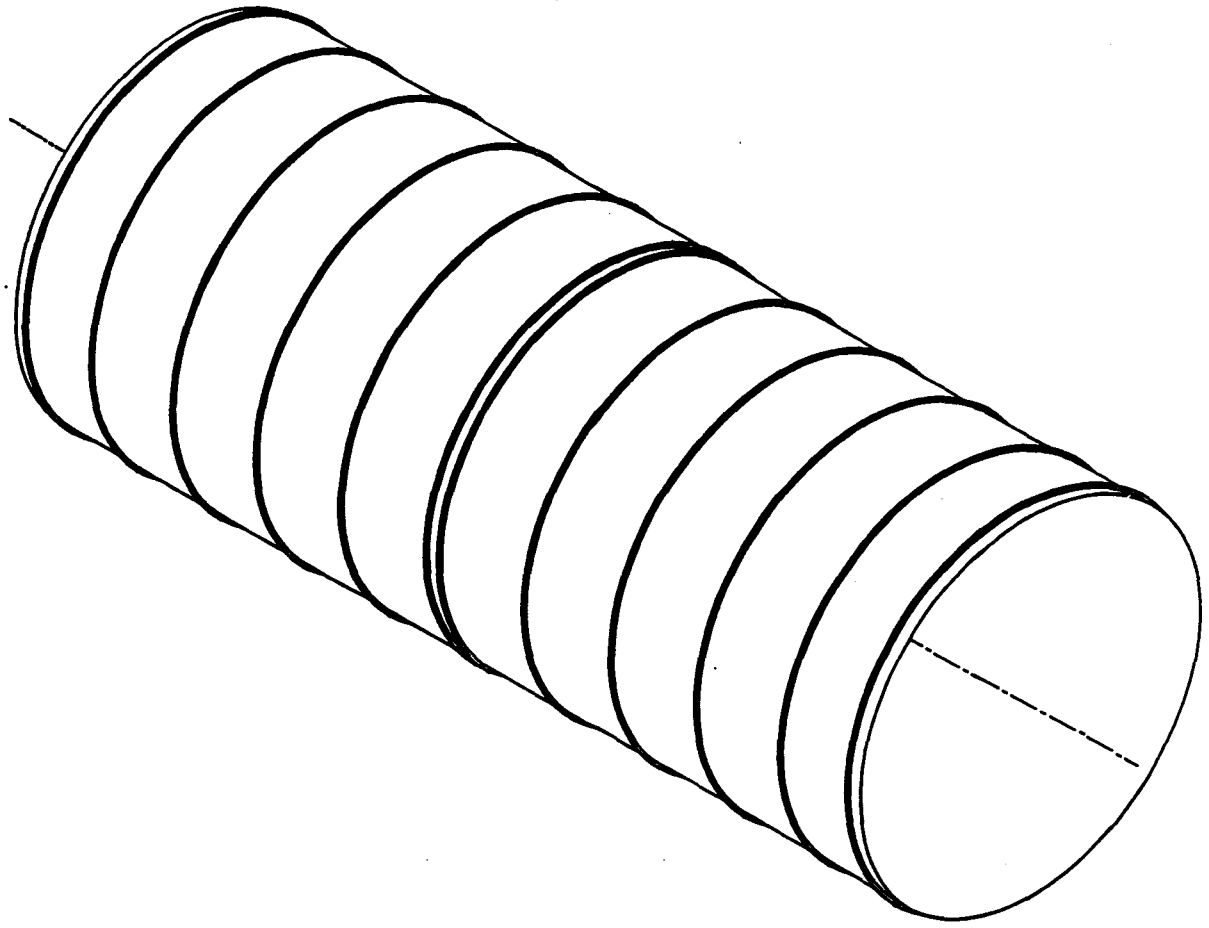

Fig. VI.11. A completed cylinder with shim rings attached.

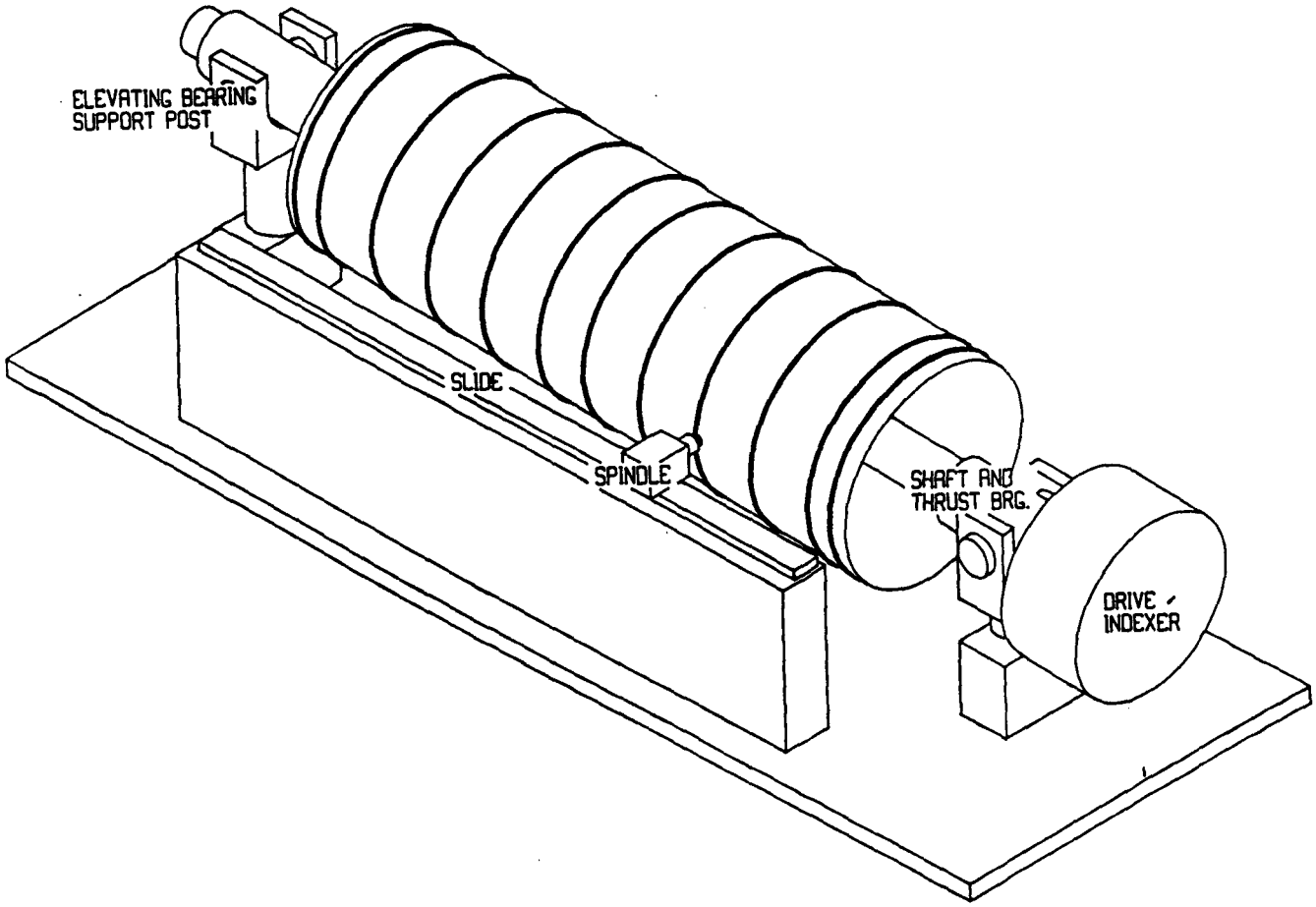

Fig. VI.12. Machining of the shim rings on a completed cylinder.

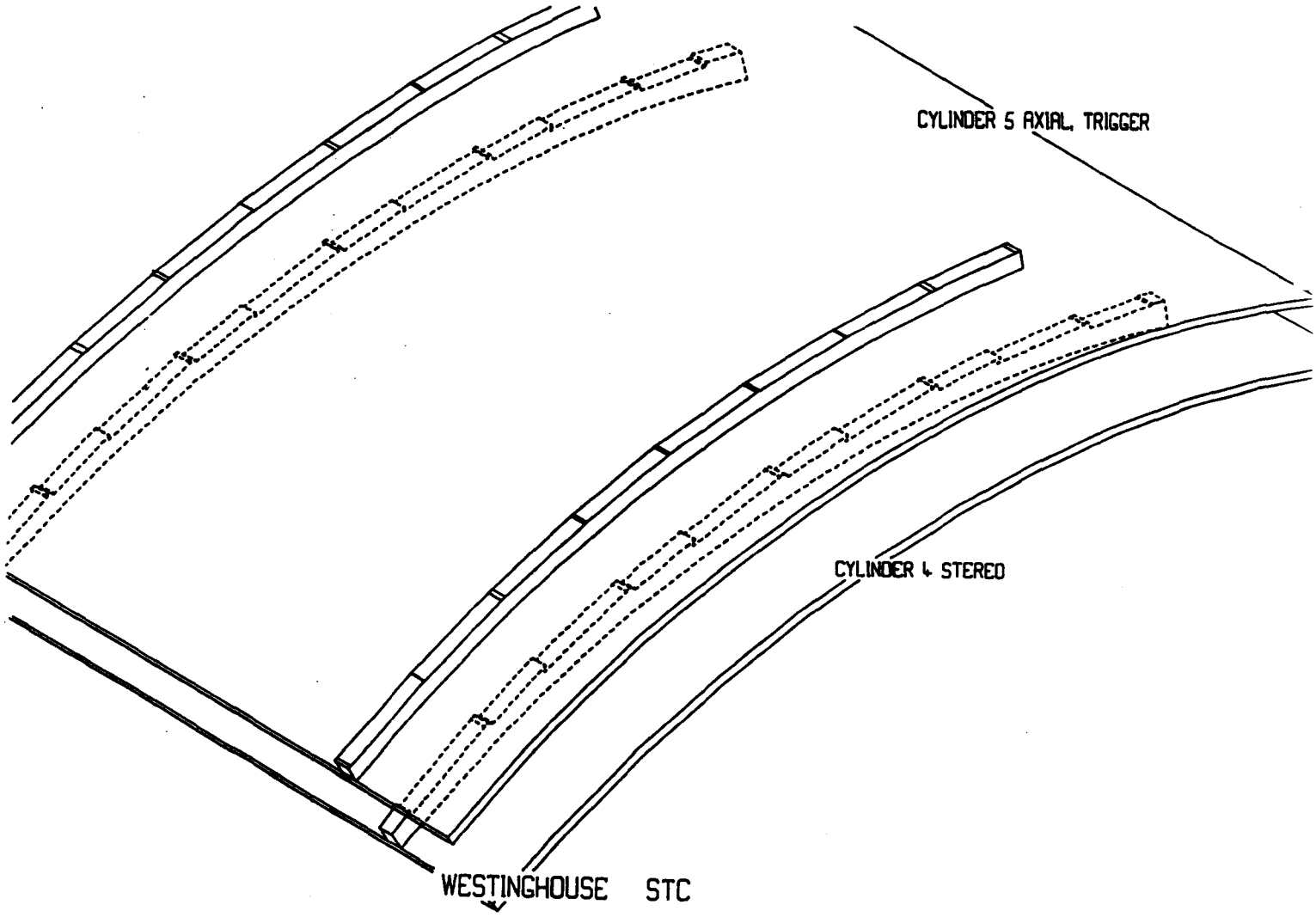

Fig. VI.13. Detail of the stereo and axial shim rings.

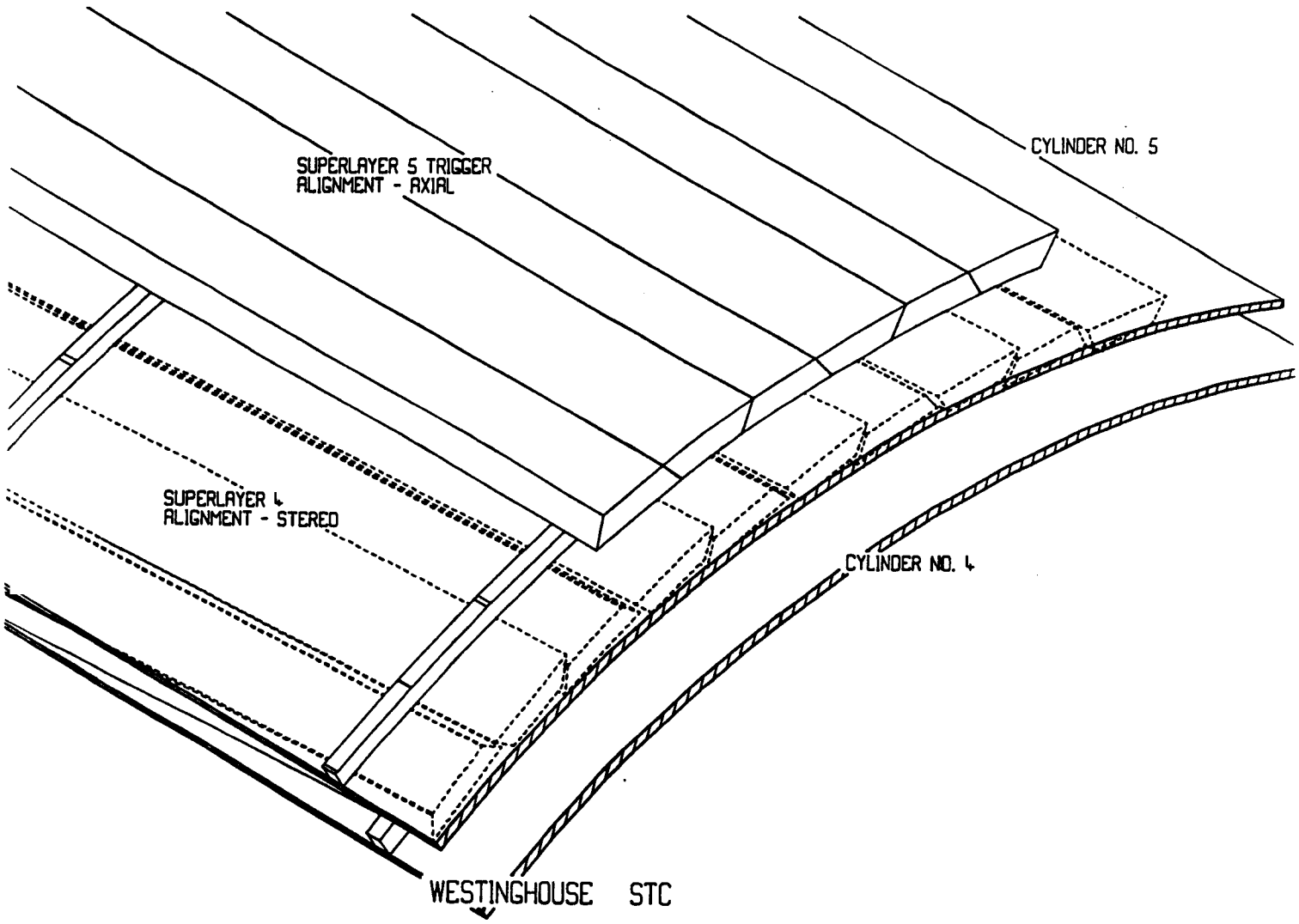

Fig. VI.14. Detail of shim rings with modules installed.

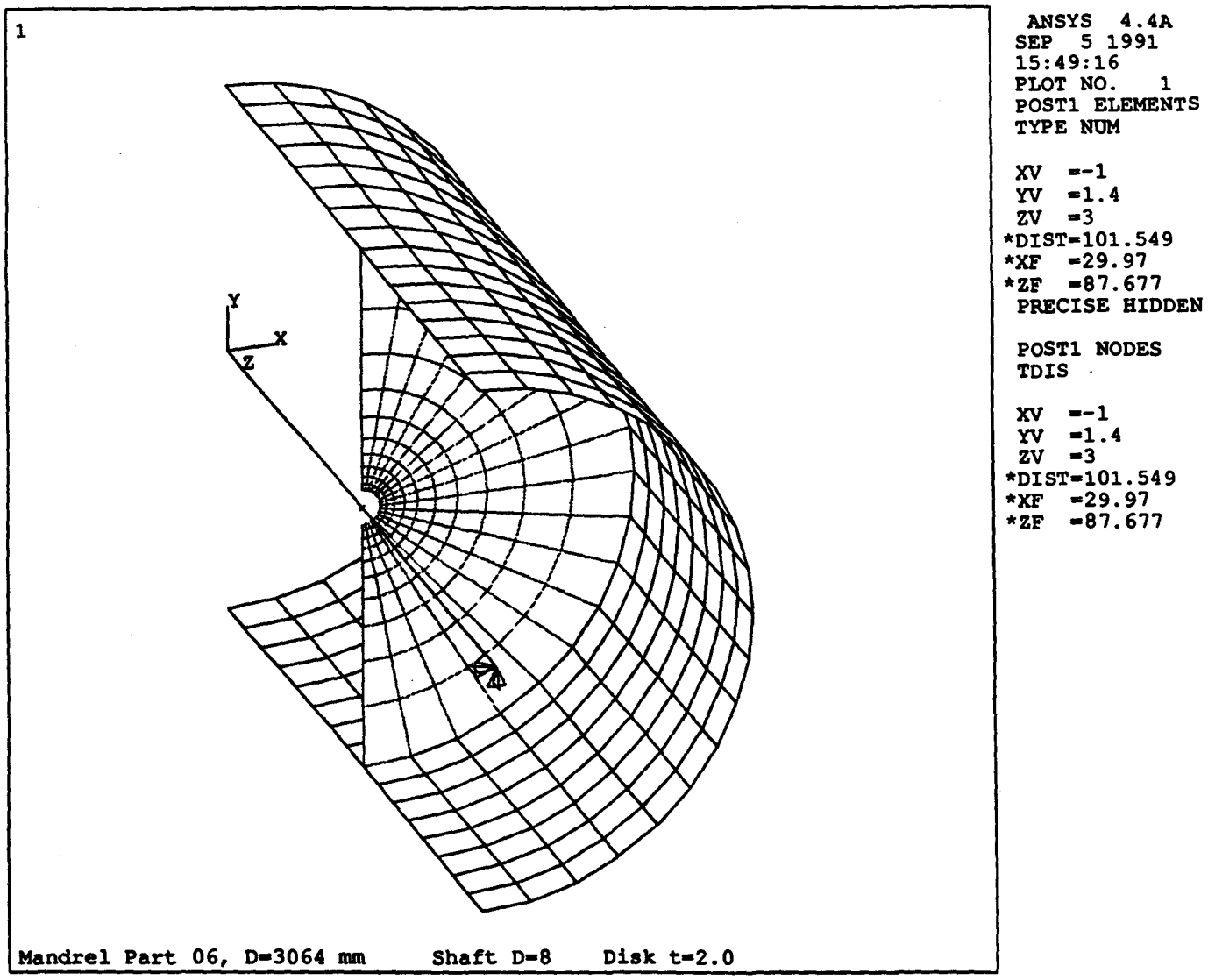

Fig. VI.15. Finite element analysis model.

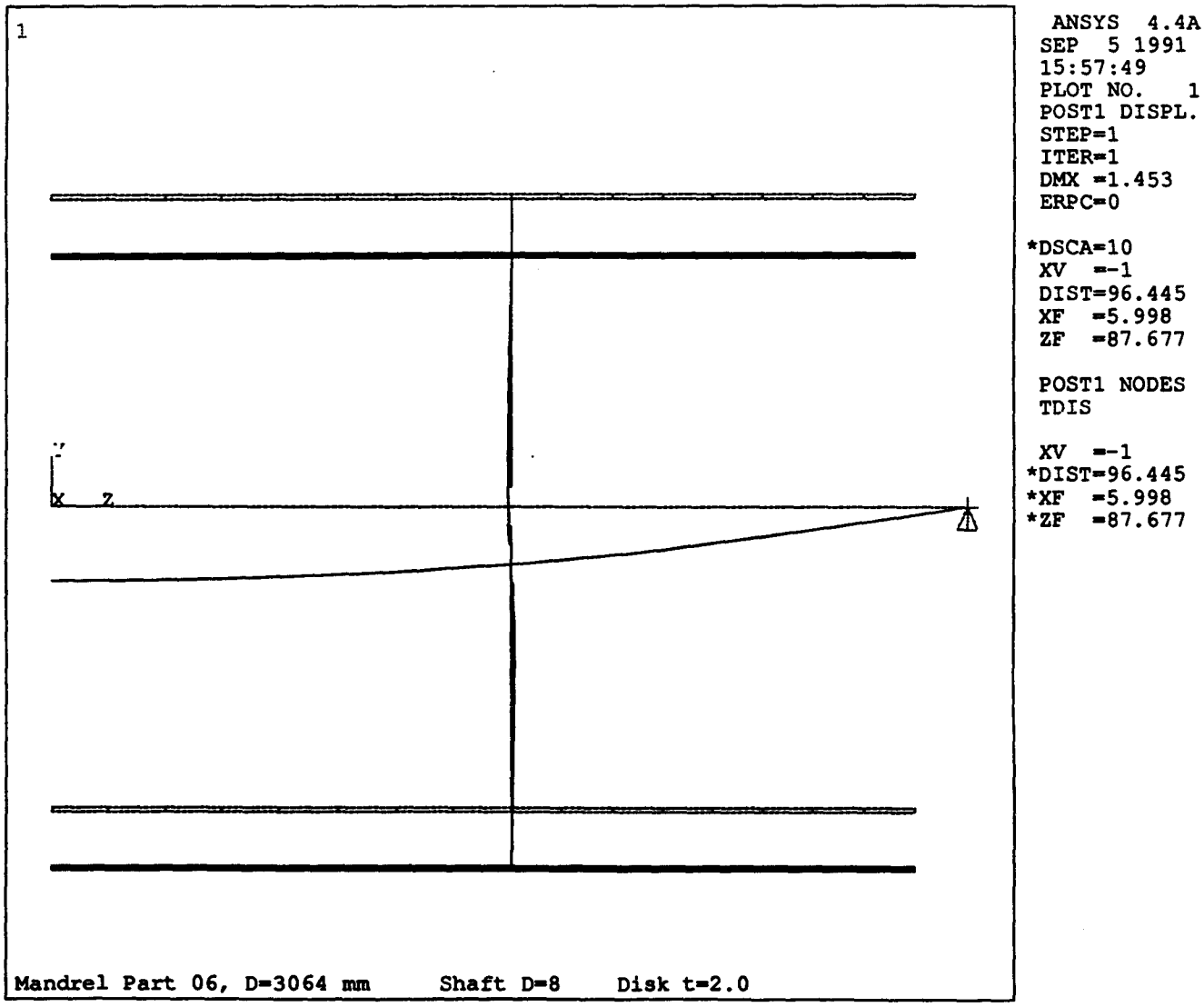

Fig. VI.16. Deflection plot for finite element analysis.

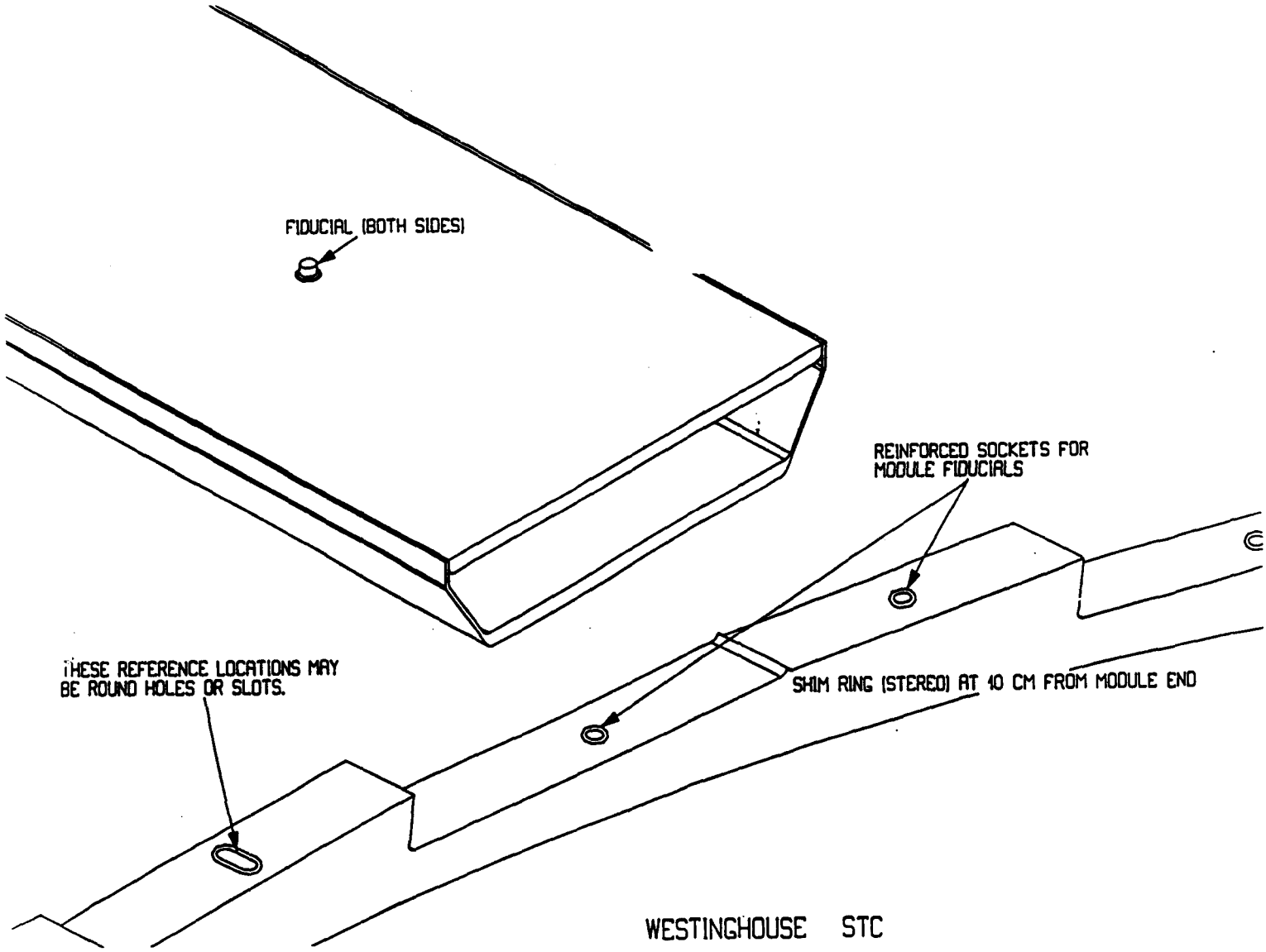

Fig. VI.17. Conceptual drawing of module and shim ring fiducials.

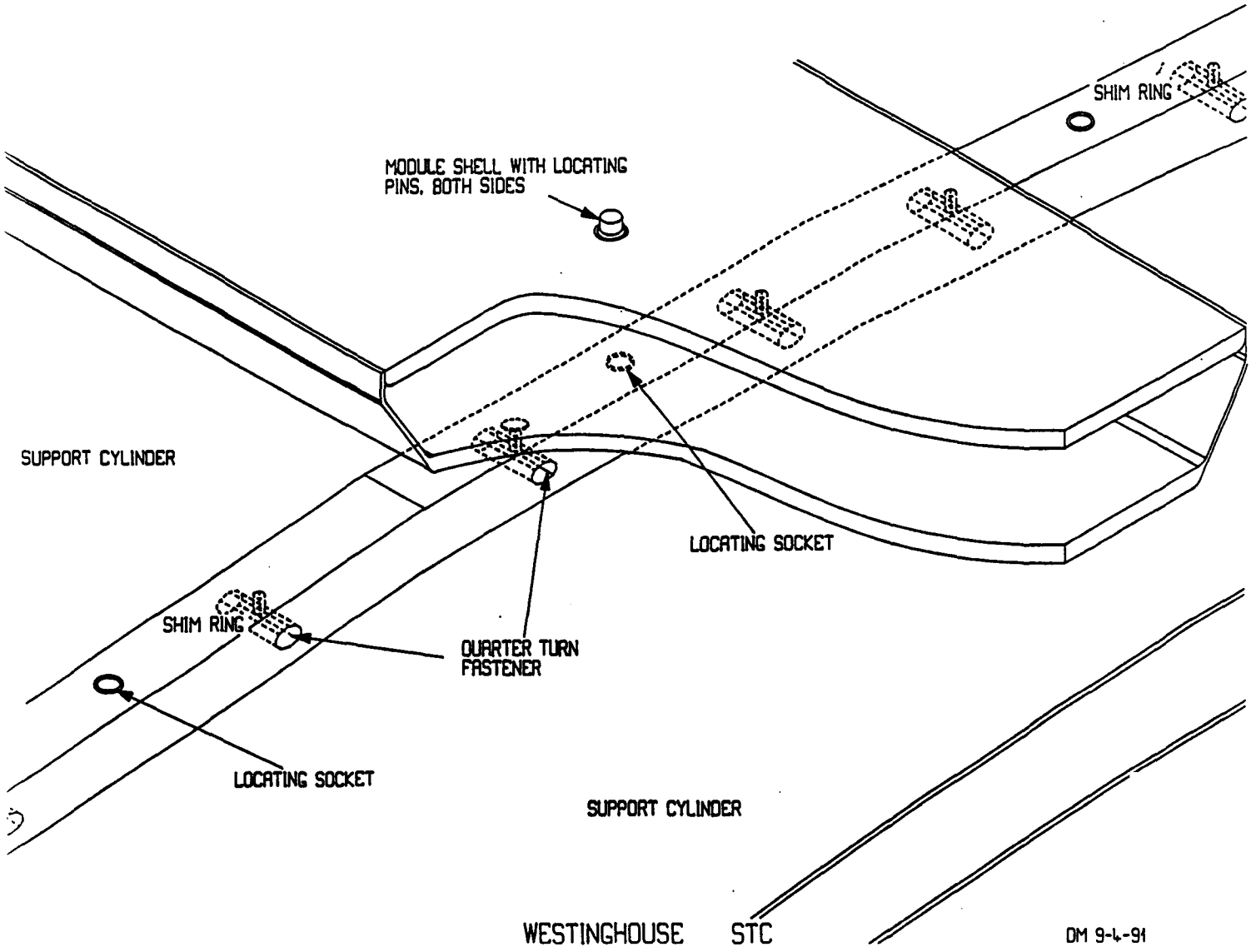

Fig. VI.18. Conceptual design of module and shim ring attachment.

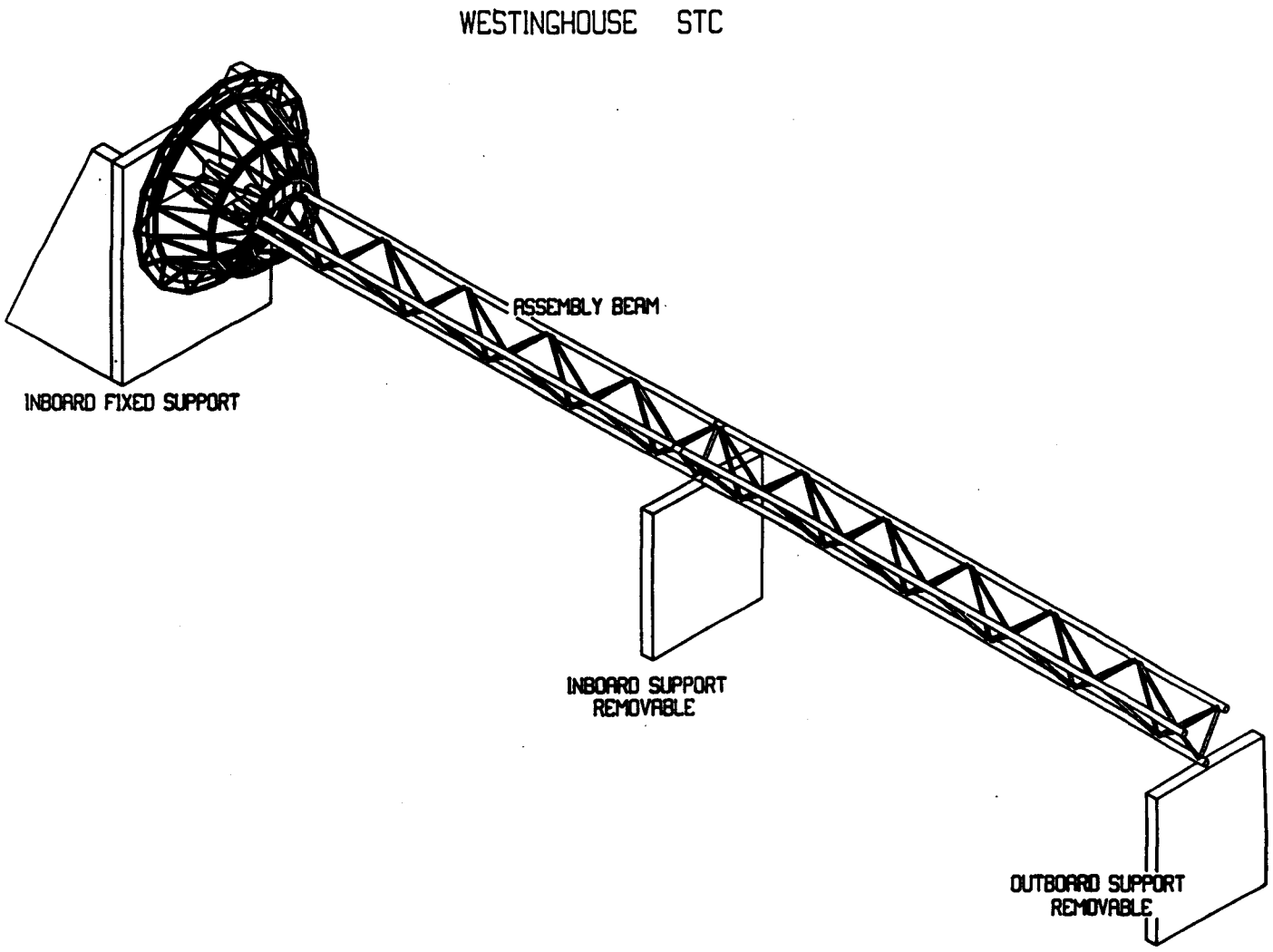

Fig. VI.19. Spaceframe on assembly fixture.

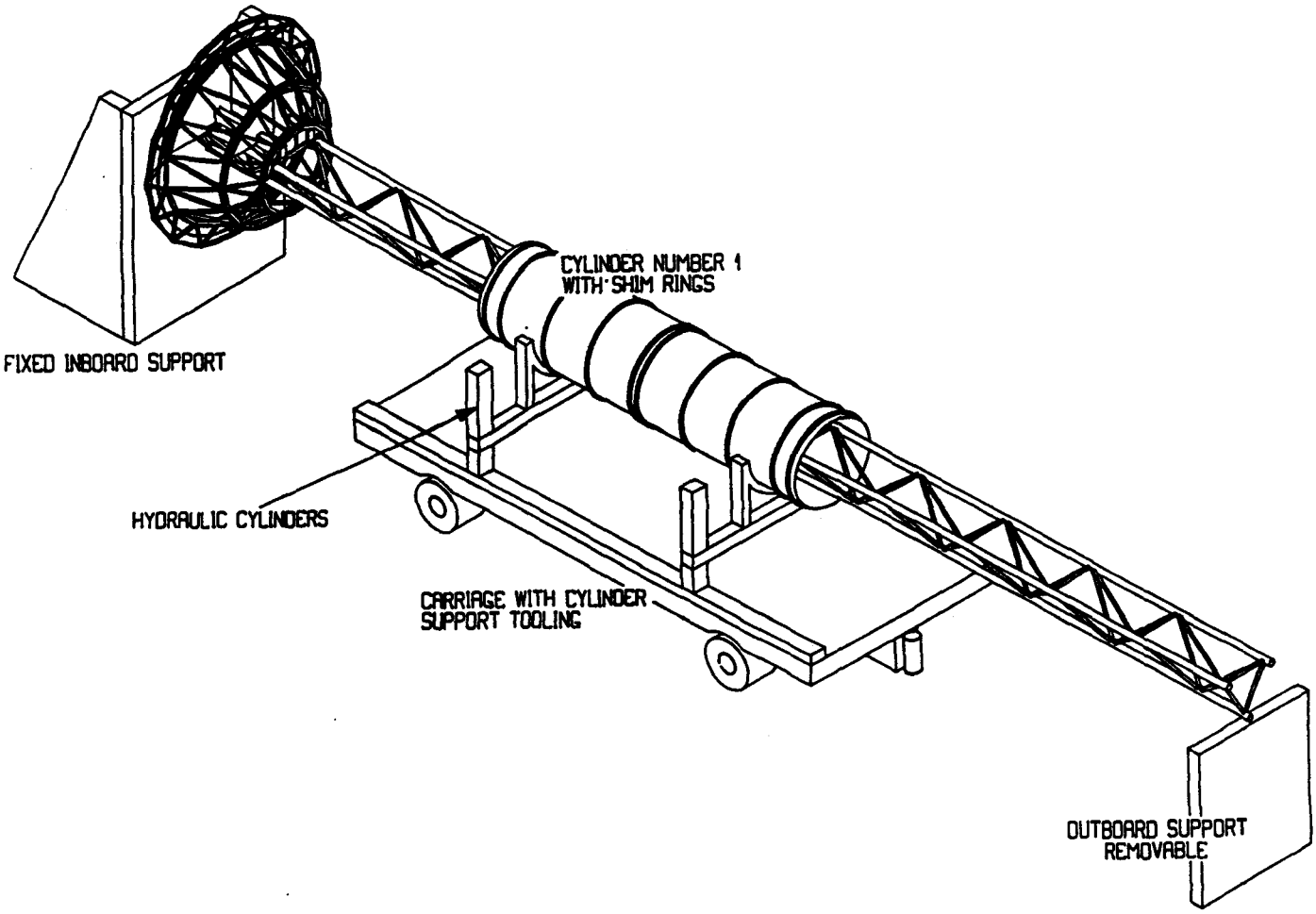

Fig. VI.20. Installing support cylinder #1 on the spaceframe.

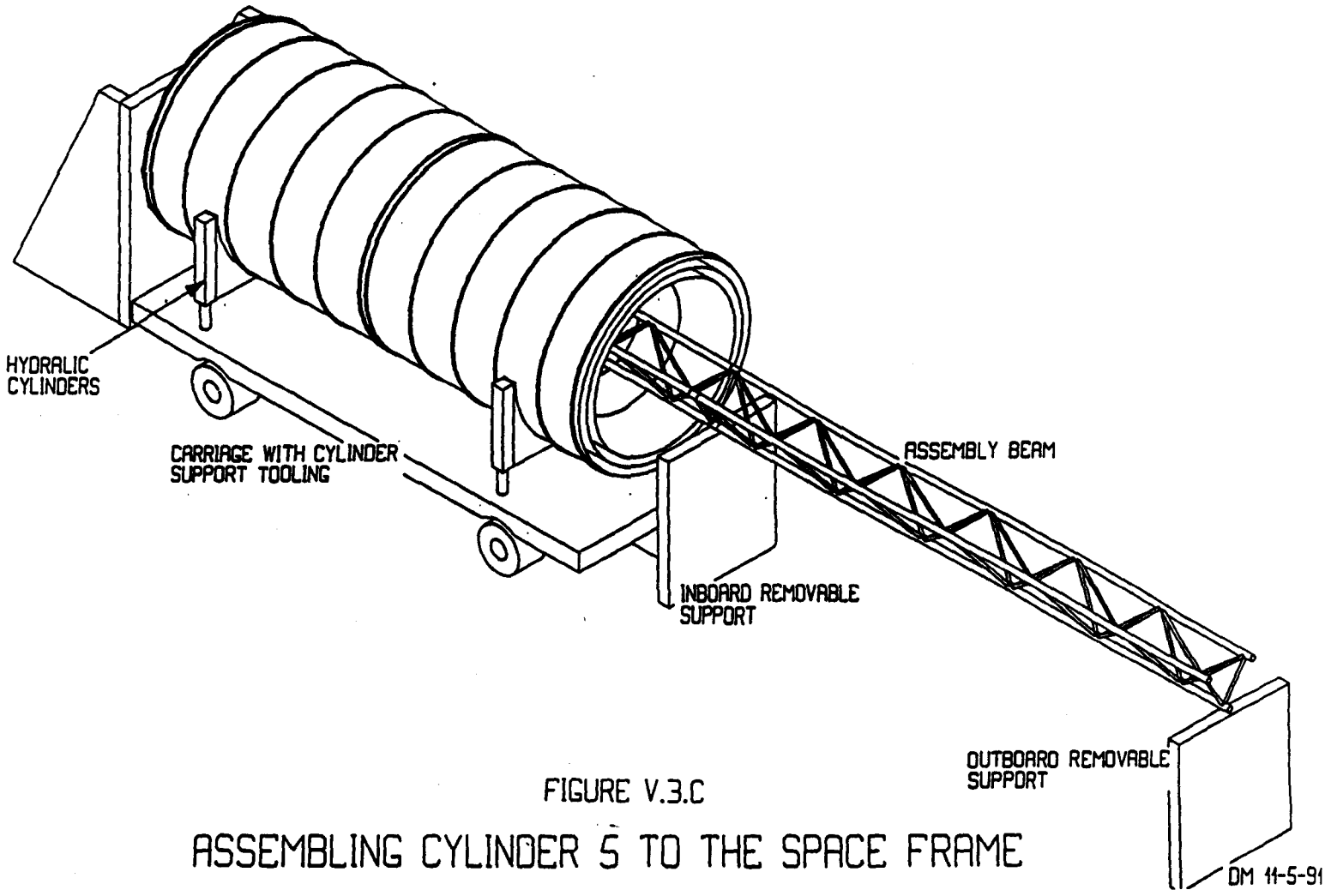

FIGURE V.3.C

ASSEMBLING CYLINDER 5 TO THE SPACE FRAME

Fig. VI.21. Installing cylinder #5 on the space frame.

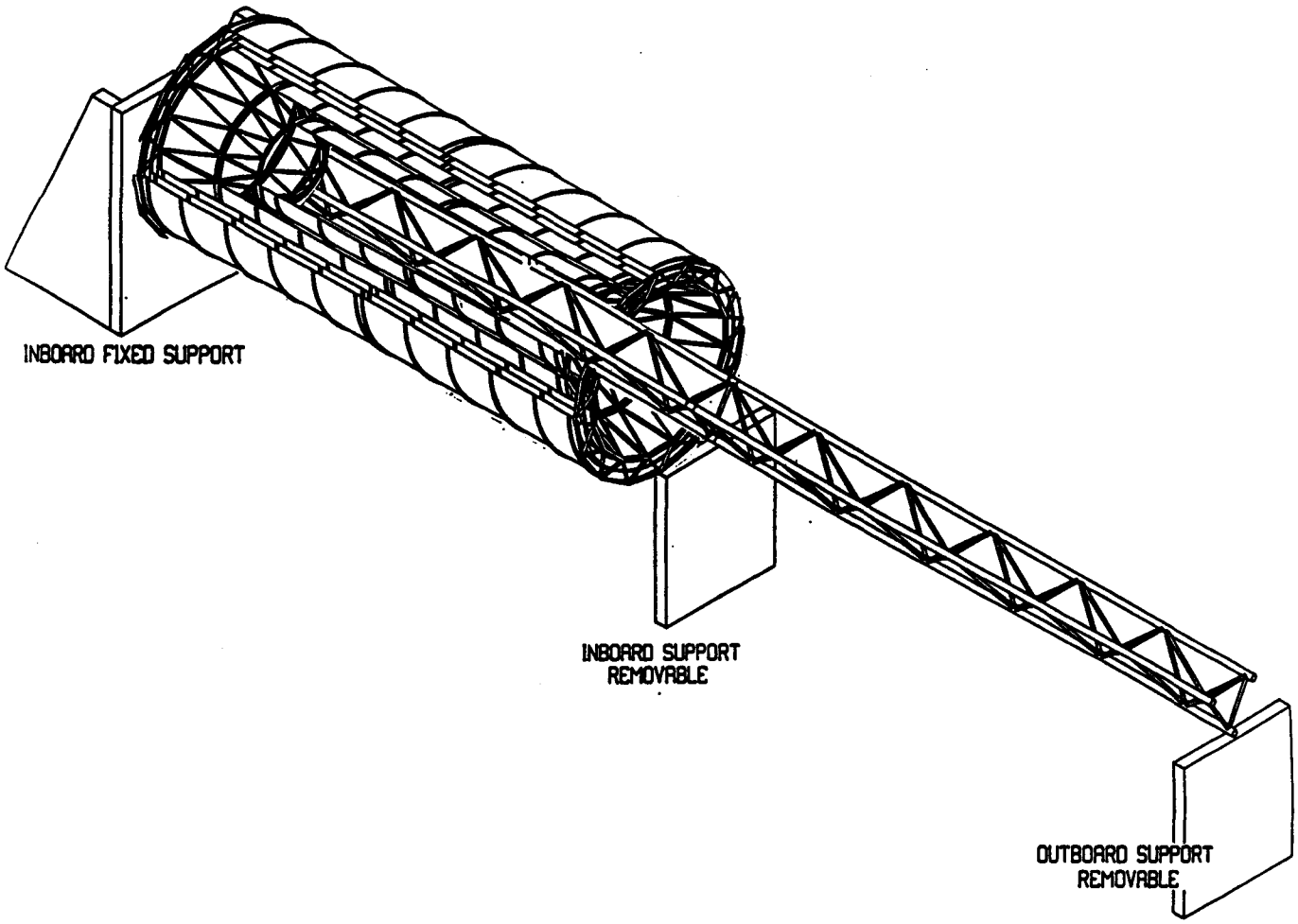

Fig. VI.22. Completed tracking cylinders on assembly fixture.

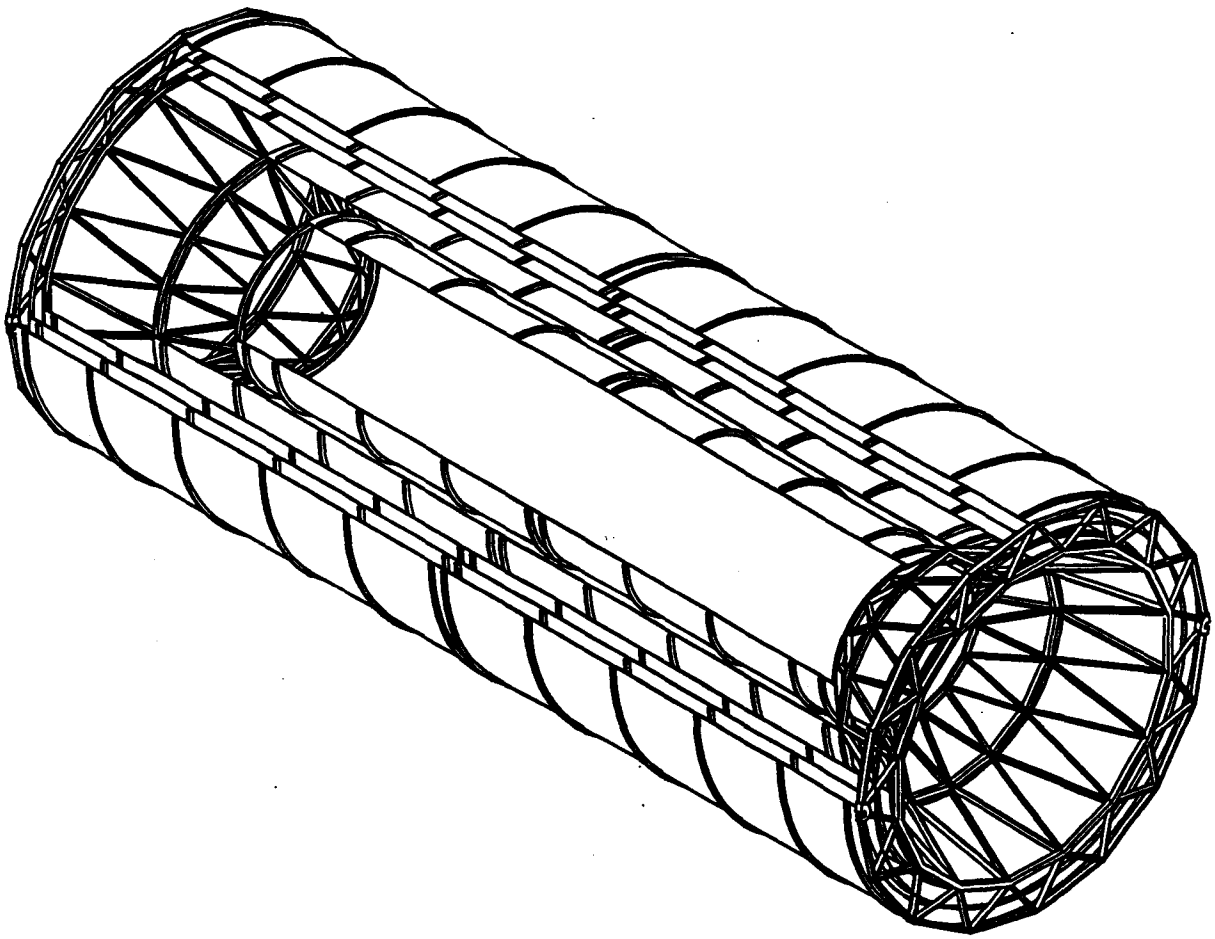

Fig. VI.23. The complete spaceframe support.

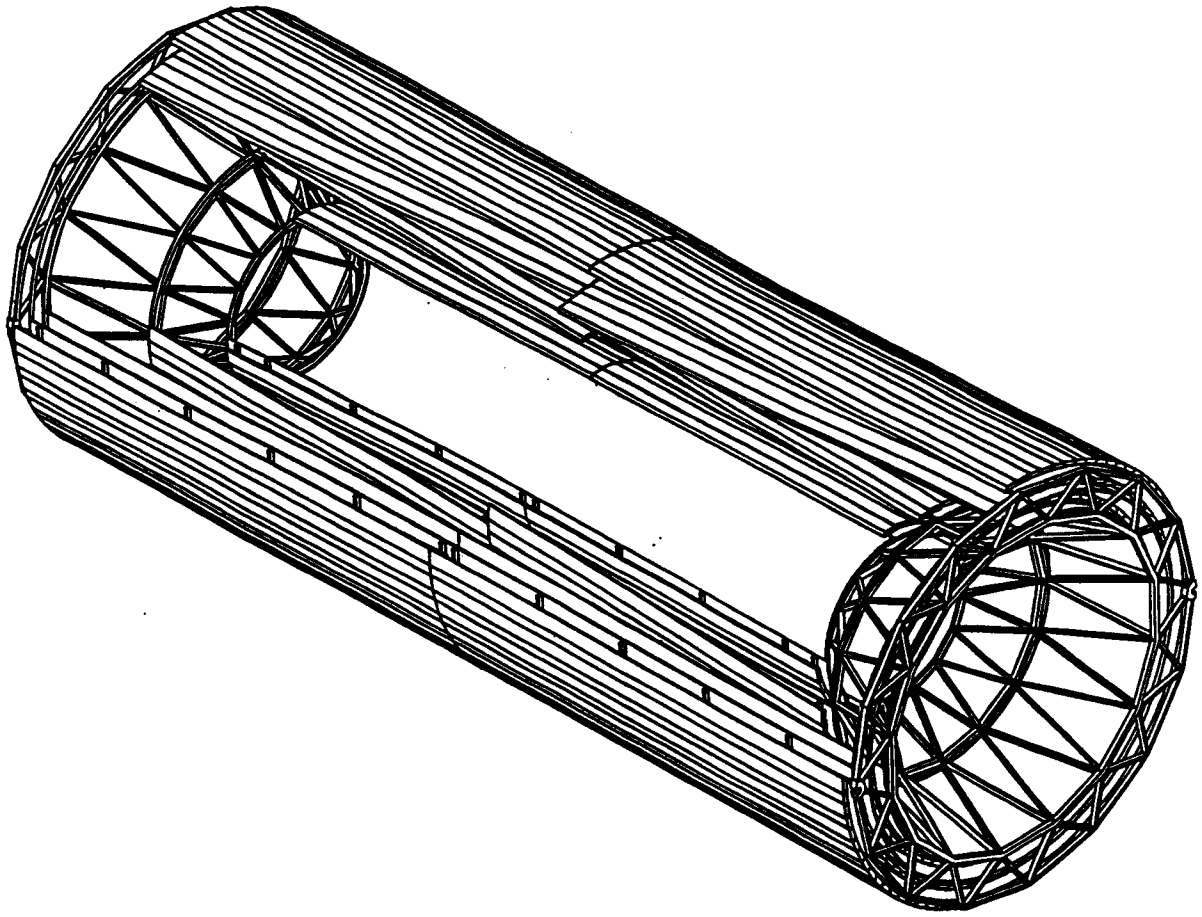

Fig. VI.24. The completed tracker with modules attached.

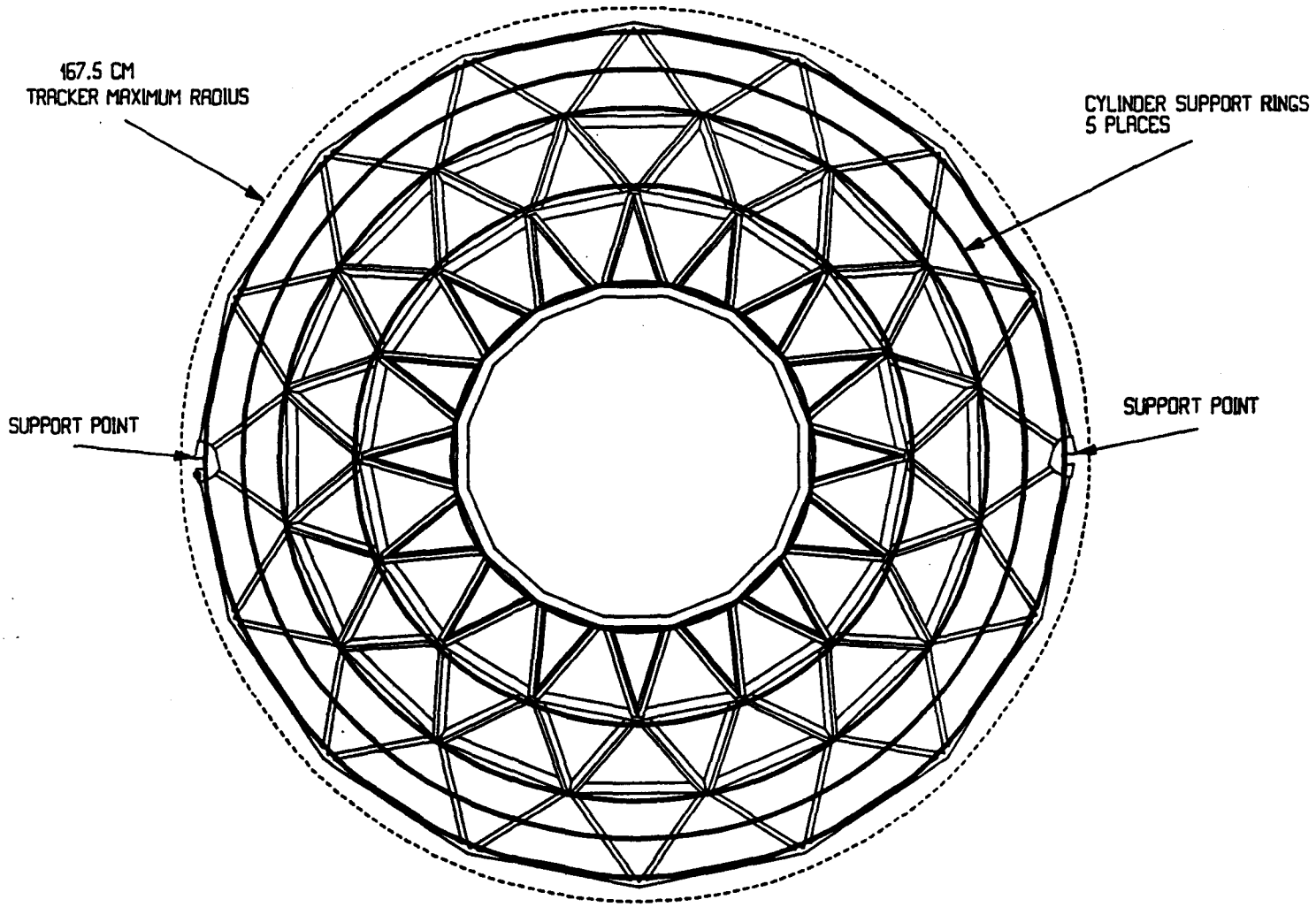

Fig. VI.25. Spaceframe end view.

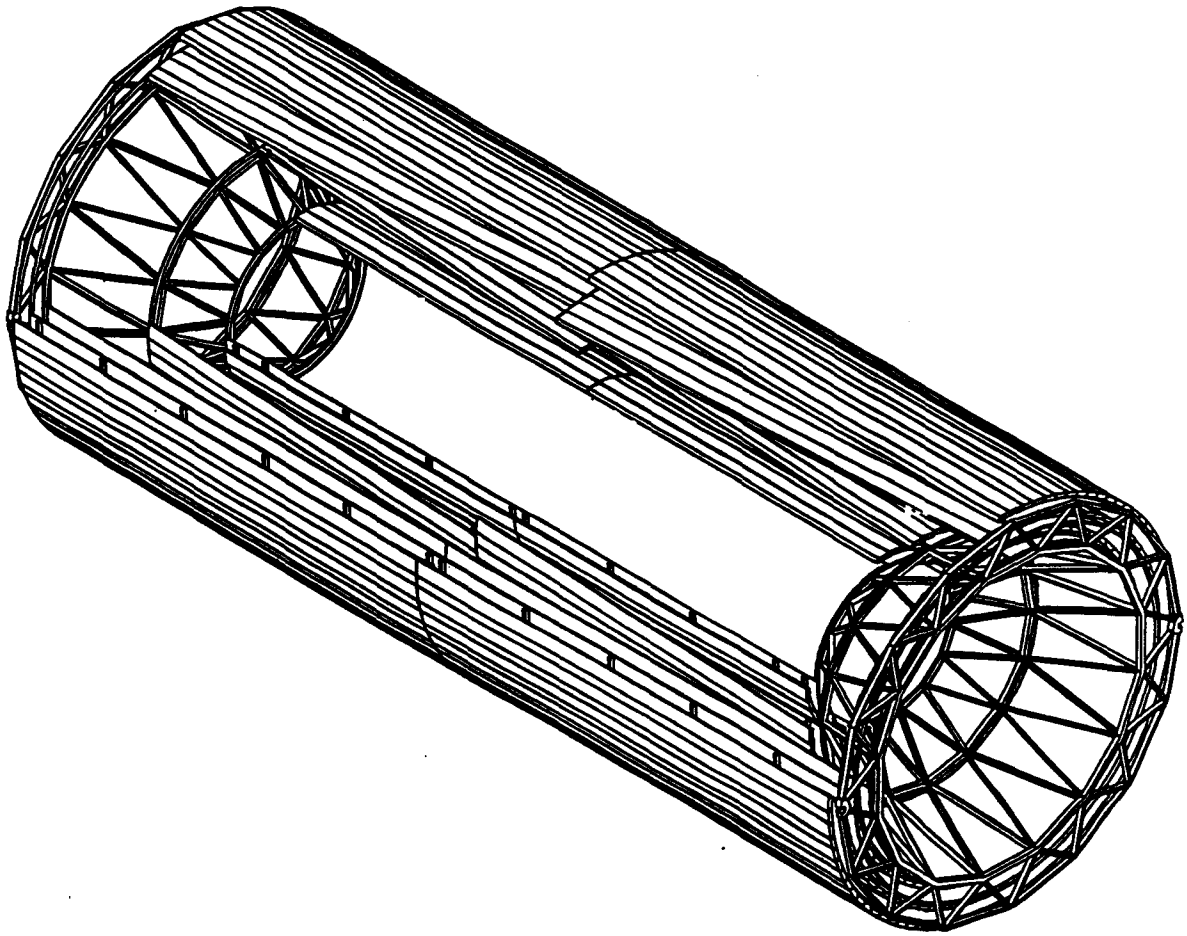

Fig. VI.26. Model of tracker showing the five concentric cylinders.

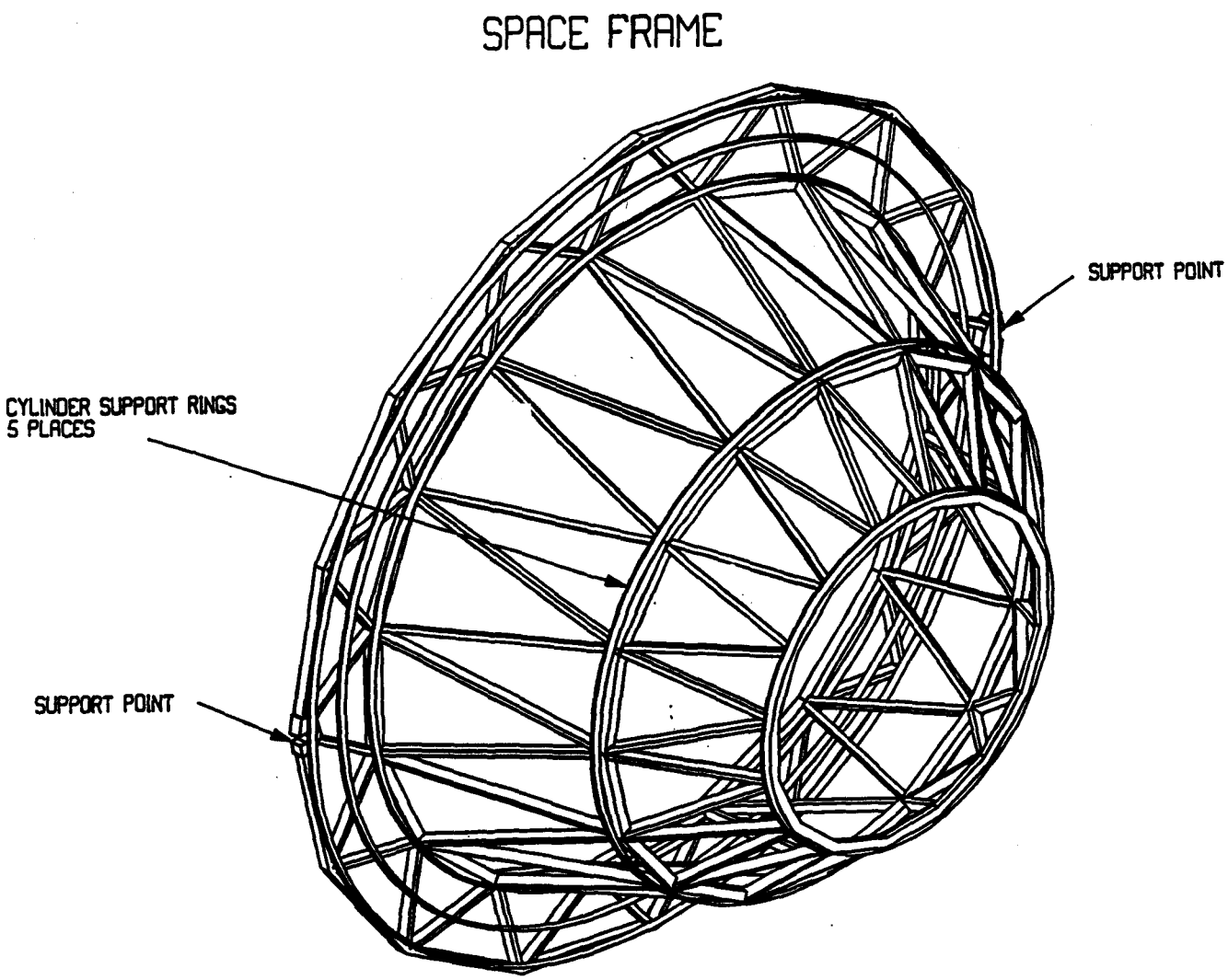

Fig. VI.27. Detail of the spaceframe support.

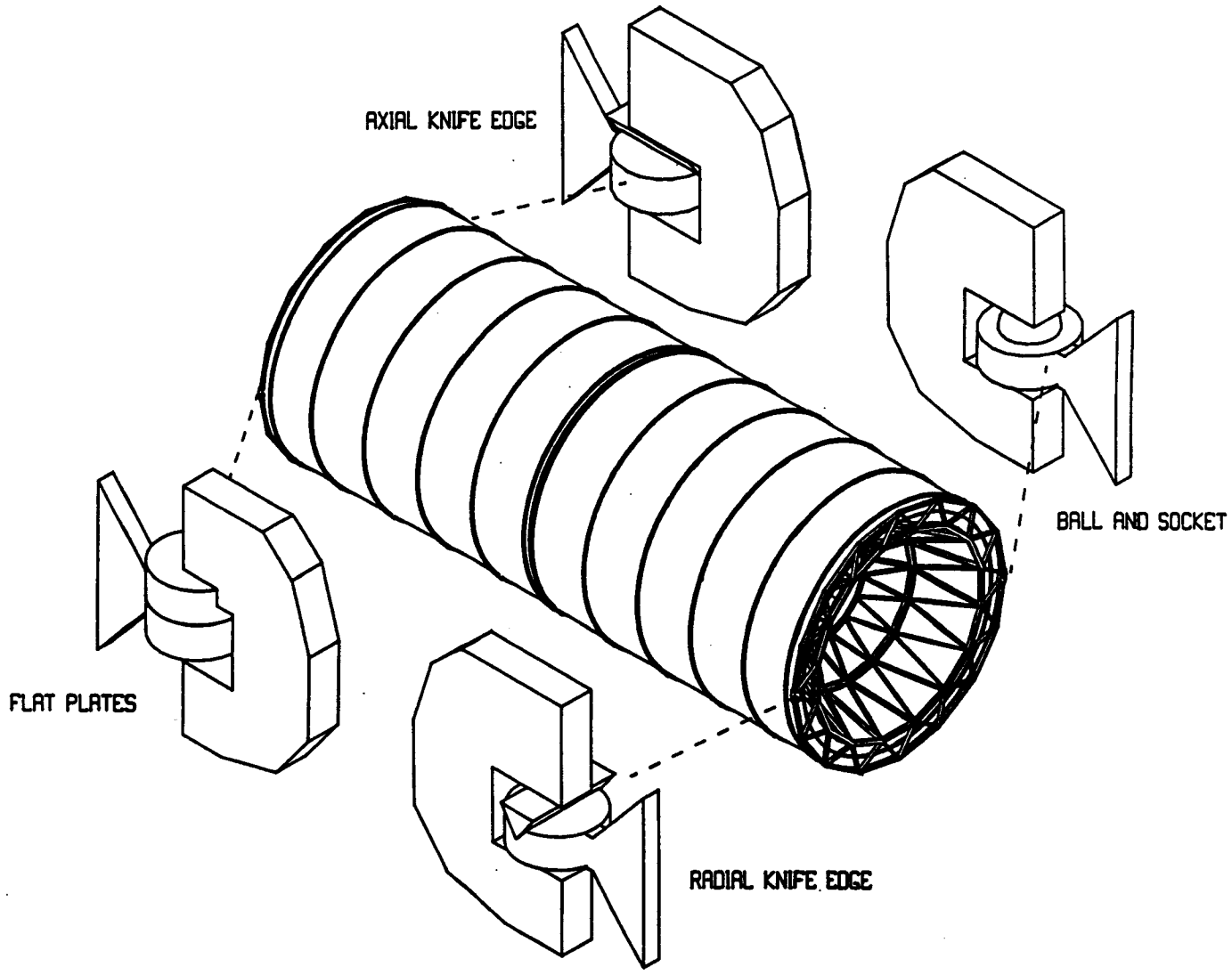

Fig. VI.28. A schematic of the central tracking mounting.

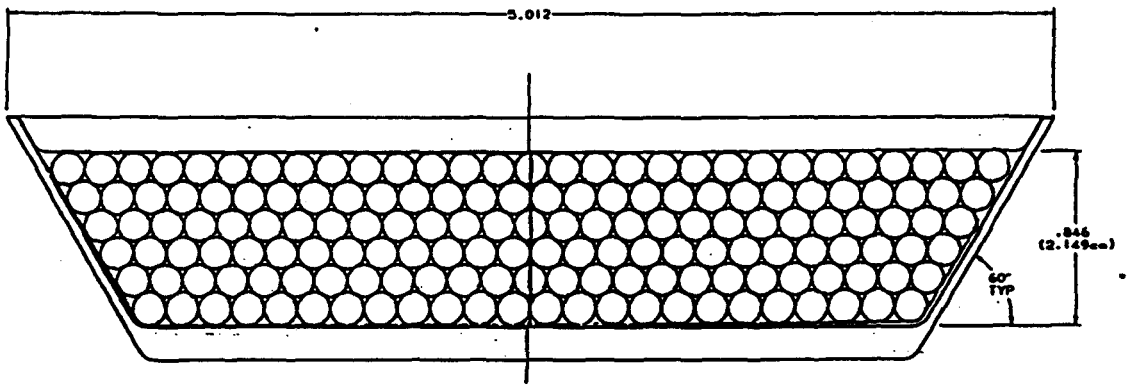

DIMENSIONS IN INCHES

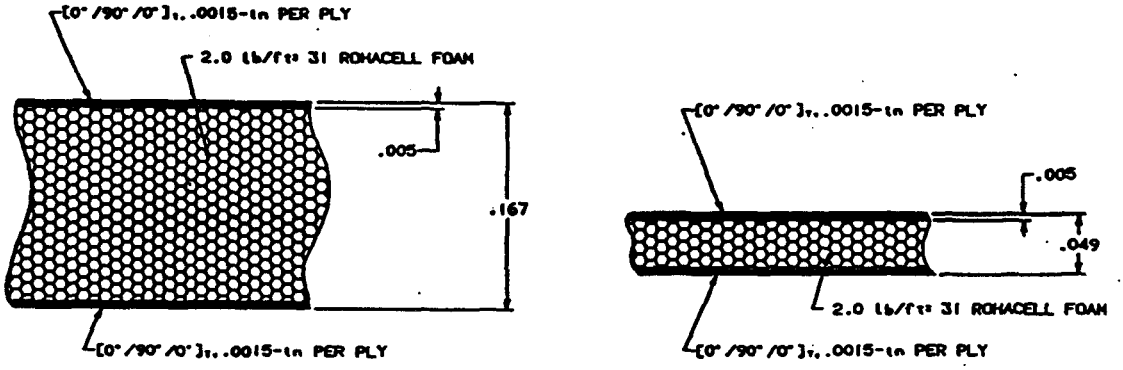

Fig. VI.29. Details of the cross-sectional view of the non-trigger module.

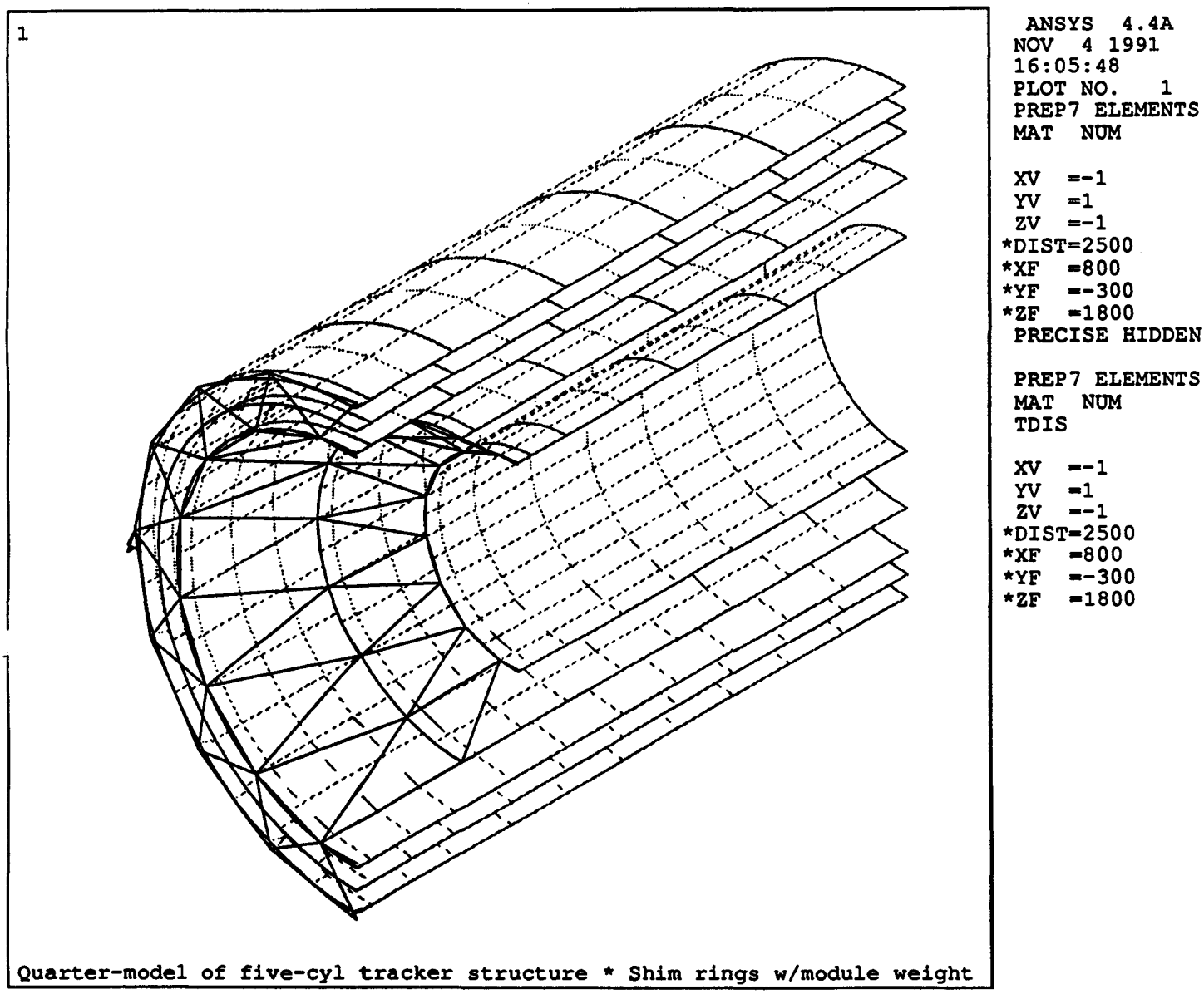

Fig. VI.30. ANSYS model of the tracker.

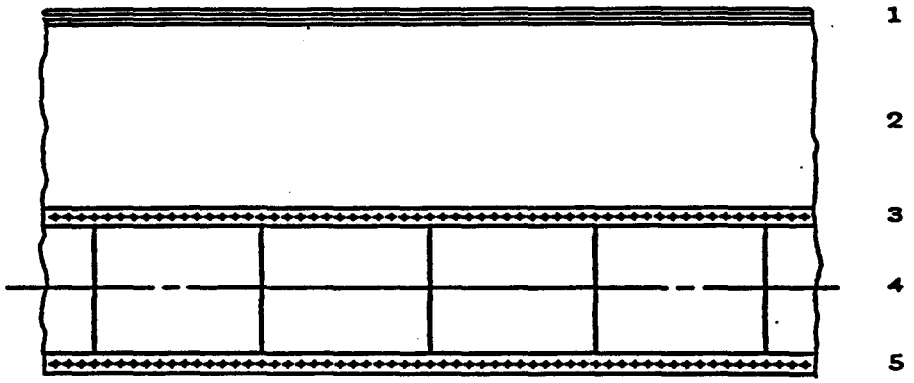

Fig. VI.31. Cylinder elements specified in the ANSYS model.
1) Non-structural superlayer of modules with mass included.
2)Dummy non-structural standoff layer.
3 and 5) Six-ply filament-wound epoxy-graphite skin.
4) Rohacell-31 foam core.

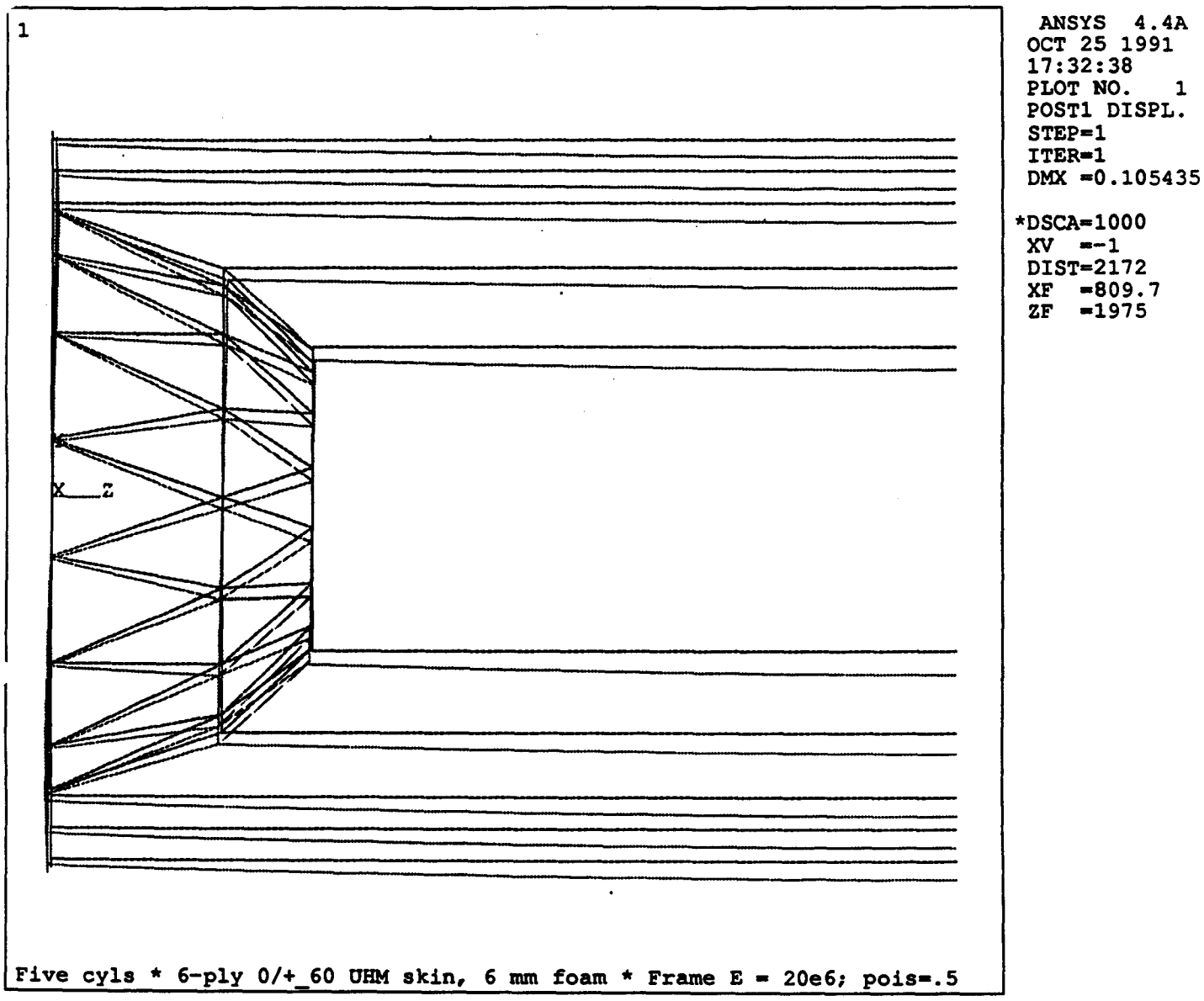

Fig. VI.32. A deflection analysis of the support structure with ANSYS.

VII. INTEGRATION

VII.1. MATERIAL

The basic straw material represents a total thickness of $\pi \times$ wall thickness for each straw. For a six layer system this is 697 microns of mylar. We take into account the internal wire supports by increasing this by 10% giving a total of 0.32% of a radiation length for each straw layer. In the modular version the carbon shell thickness will be 0.23% of a radiation length at 90° incidence. The support cylinder will have about 0.25% of a radiation at 90°. There may also be a small amount of extra material in the support structure for attaching modules on the cylinder. We estimate that each superlayer will have about 0.8% of a radiation length at 90 degree. The end plates can be quite thin. The end plates for the prototype 64 straw module have an effective thickness of less than about 0.5 cm of plastic. This would contribute a thickness of about 2% of a radiation length normal to the ends. To this must be added the printed circuit board, electronics, cooling, cabling, and cylinder support struts. Figure VII.1 shows the effect of these items as a function of η.

VII.2. UTILITIES

VII.2.1. Low Voltage Power

The low voltage power will be distributed to the on-board electronics on the same ribbon cable that is used for the signals. The total current to each module is estimated to be 1 amp. The voltage of the supplies is 5 volts. The supplies will be housed on the external surface of the barrel calorimeter.

Each cable from a module will be a strip 5 cm wide with a copper thickness of 0.5 mm. There will be one strip cable for each module. The cables will be routed to the outer radius on the space frame struts. This is shown in Fig. VII.2. It is anticipated that there will be a total cross section of 40 cm^2 for each super layer. At the outer radius they will penetrate the gap between the two calorimeters and connect to electronics located on the outside of the barrel calorimeter.

VII.2.2. High Voltage

The modules will be individually connected to a high voltage supply. This supply will operate at about 2000 V. The maximum current draw expected for each wire is about 1 microamp, so each module can draw up to about 200 microamps. The supplies will be located on the outer surface of the calorimeter barrel with an independent distribution to each module. The high voltage cables will be supported on the spaceframe structure. The maximum cable length is estimated to be 8 meters.

VII.2.3. Instrumentation

There will instrumentation for monitoring the chamber that must be considered in the total utilities.

Leak Detection. At four points on each superlayer there will be a miniature leak detector. These will monitor the dry nitrogen atmosphere to determine is there is the presence of oxygen and/or isobutane. The positions of these will be determined by the flow pattern of the inerting gas.

Temperature monitors. At four locations on each superlayer there will be temperature monitors to verify the temperature stability of the system. These will supplement a temperature monitor in the inerting system which sets the ambient temperature. These will be useful for determining excessive electronics temperatures or other anomalies.

Position sensors. The extreme conditions on the relative rotation of the superlayers will probably require that we monitor the relative positions of each, perhaps at several points.

Voltage sensors. The high voltage and low voltage systems will require a monitor at the front end electronics. The number and location will depend on the specific distribution system for both low voltage power and drift chamber high voltage.

VII.2.4. Drift Cell Gas

The gas that will be used in the modular chambers is CF_4-Isobutane (80%-20%). It will be supplied to each chamber via a gas manifold on the inboard side of the superlayer. This is shown schematically in Fig. VII.3. The requirement of the gas flow for normal operation is about 2 cm^3/sec for each module. This flow rate corresponds to about 200 cm3/sec for each superlayer. The exhaust flow baffle is adjacent to the input gas. Both gas plumbing systems will be supported by the space frame out to the largest radius. Each superlayer's supply and return line will be about 25 mm in diameter. At this point they will exit the tracking volume via the split between the two calorimeter halves. The cross sectional area of the supply and the return is anticipated to be less that 20 cm^2 for each end of the tracker.

The gas plumbing will exit the detector and pass through one of the access shafts to the surface. At the surface there will be a gas recovery system. The purity specifications for the drift gas are:

1) < 50 ppm O_2
2) <500 ppm H_2O
3) <500 ppm N_2
4) <10 ppm F_2+Cl_2+Br_2
5) <10 ppm HCL, HF
6) <50 ppm CO_2+CO
7) <500 ppm Ar

The above ground facilities have not yet been designed in detail, but will include:

1) a gas purification station for removing isobutane and contaminants.
2) a remixing station to establish the correct CF4-isobutane ratio
3) gas monitoring instrumentation for verifying the gas mix
4) pumps for return flow to the experiment.

VII.2.4. Electronics Cooling Gas

The front end electronics will require cooling. The estimated power dissipation is about 5 watts/module. The cooling gas requirements have been worked out. They are shown in Table VII.1..There will be up to four cooling supplies and returns per superlayer. Each will be about 1 cm in diameter and have a flow rate of 0.7 liter/sec. This is shown in Figure VII.4.. At present it is anticipated that the cool gas can be dry air.

VII.2.5. Inerting Gas

The entire tracking system will be sealed from the outside during operation. There will be a continuous flow of dry nitrogen passing axially through the tracker. This will keep the oxygen fraction low and provide a low humidity environment for the tracking detectors and the onboard electronics. The total flow required is not yet determined. This gas will be piped from the surface, and will enter the tracking volume via the split between the calorimeters. The gas will be exhausted externally.

VII.3. ACCESS AND MAINTENANCE

The access required for repair and maintenance of the modular tracker will be at two basic levels. Work on the power supplies, signal distribution and gas distribution system can be done by entering the region just outside of the barrel calorimeter. Since this is all easily accessible the time for quick repairs such as card replacement, check of high voltage system can be done in a few hours.

Access to the front end could be a much more time consuming task. The inner radius cylinders might be accessible by entering along the beam pipe area. However , for the outer superlayers the front end of the detector will need to be open. It will require the following operations:

1) Move the forward calorimeter
2) Retract the forward toroids
3) Retract the endcap calorimeter
4) Retract the intermediate tracking
5) Repair the components

6) Reposition the intermediate tracking
7) Reposition the endcap calorimeter
8) Reposition the forward toroids
9) Reposition the forward calorimeter

An estimate of the required time is 11.5 days. The replacement of a module, if required, will also depend on the super layer. In the opened position it may be possible to replace a module on the inner super layers. However on the outer superlayers there is not the axial space required to pull out a module. For this operation the removal of the endcap calorimeter may be necessary. We feel that this is not unreasonable, since this major change will probably only be considered during an extended shutdown period.

VII.3.1. Electronics

The most likely access reason is for the replacement of an electronic card. There will need to be extensive burn-in time prior to close up in order to keep the failure rate low.

VII.3.2. High Voltage

There may need to be access to repair a high voltage short if a wire breaks. This would be isolated to one module, so the initial access would be to the high voltage supplies to simply remove the high voltage. Access to the region of the front end electronics would be required to remove the broken wire or to isolate it from the high voltage. We are investigating the possibility of using remote fusing to remove individual wires from the high voltage.

VII. 3.3. Gas

Access to the gas system should be straight forward in the gas mixing areas and in the region of the barrel calorimeter. If a leak were detected in the tracking region, it would be necessary to access the front end electronics area, determine the point of the leak and either repair it or remove one module from the gas system.

VII.4. SAFETY

VII.4.1. High Voltage

The high voltage system is one source of safety hazard. The principle area of concern is on the chamber at the front end electronics. The high voltage distribution system is presently handled on a printed circuit board attached to the module endcap. This will be covered and protected from contact. The actual distribution is done inside the chamber. The carbon fiber shell and the outside mylar shell of the straws will maintain a barrier to the high voltage which is on the signal wires. In the case of a broken wire there is sufficient insulation to maintain a stand off.

VII.4.2. Drift Chamber Gas

The drift chamber gas is a potential safety hazard. In addition to the danger of suffocation hazard, there is a potential for fire due to the isobutane. We have not yet establish the exact flammability for the gas, but there are indications that the mixture of CF_4-isobutane is basically not flammable, but the exact isobutane fraction is not yet decided. There is a hazard for fire, of course, in the gas mixing room.

VII.4.3. Inerting Gas

Since the entire tracking system will be flushed with dry nitrogen, there is a hazard of suffocation. The gas monitoring system will track the oxygen content and indicate the the extent of diffusion into the system. Access to the front end electronics will then require that the inerting gases are cut off, and a flushing system enabled to bring air into the area.

ELEMENT NAME	TOTAL PER SUP. LAYER (BOTH ENDS)	DIAM cm	FLOW l/sec	MEDIUM	PRESSURE MPa	PRESSURE DROP MPa	TEMP RISE C	NO. OF SUPER LAYERS	TOTAL SYSTEM MASS FLOW scc/sec
COOLING ASSEMBLY									
Electronics Cooling Suppl	4	1	0.7	Air	0.1	0.0017	_	4	11200
Electronics Cooling Retur	4	1	0.7	Air	0.1	0.0017	18.5	4	11200
Straw Cooling Supply	1	1	TBD	Air	TBD	TBD	TBD	4	TBD
Straw Cooling Return	1	1	TBD	Air	TBD	TBD	TBD	4	TBD
DRIFT GAS									
Drift Gas Supply	4	1	0.086	CF4/ISO	0.1	TBD	TBD	4	1380
Drift Gas Return	4	1	0.088	CF4/ISO	0.1	TBD	TBD	4	1380

Table VII.1. The specification of the gas flow rates, pressure drops and mass flow for the drift gas (CF_4- Isobutane) and the cooling gas (N_2)

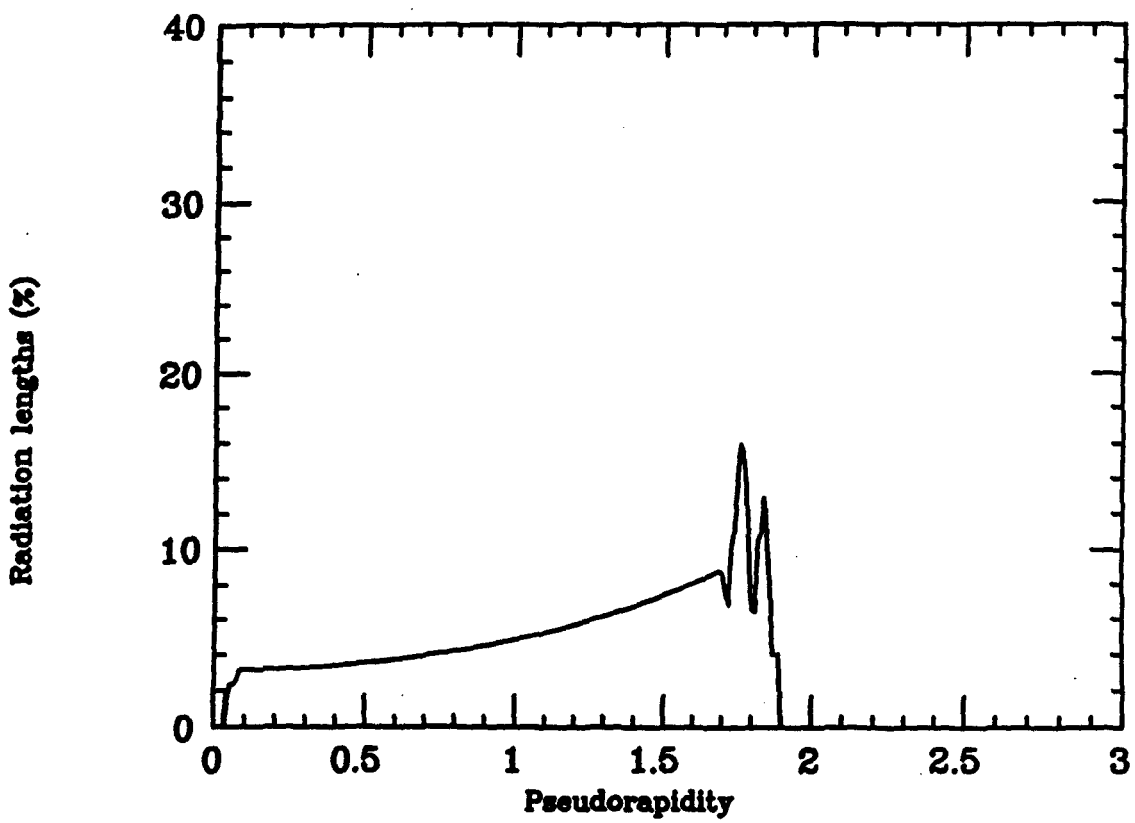

Fig. VII.1. The plot of material (radiation lengths) as a function of η for the five super layer straw tracking system.

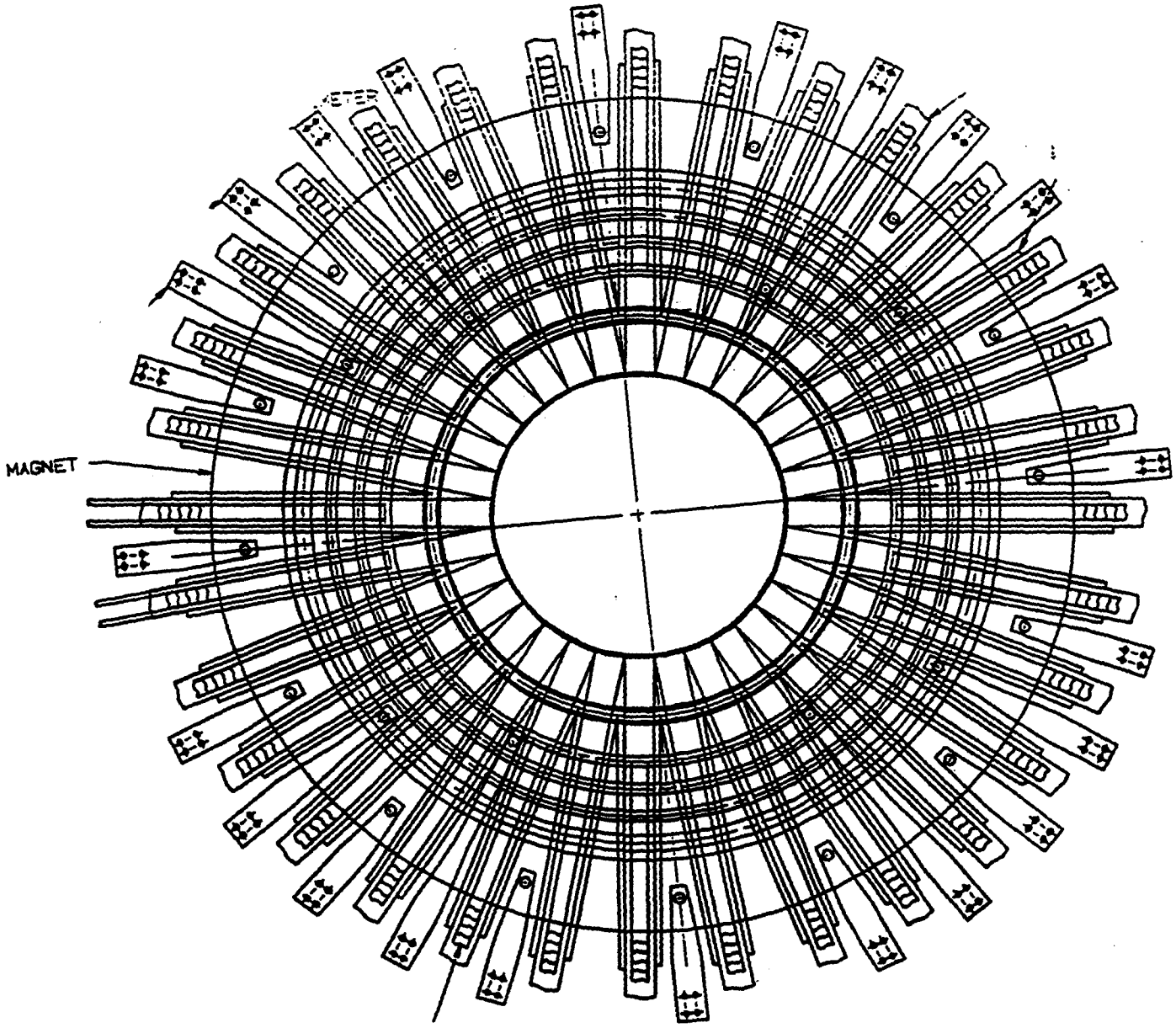

Fig. VII.2. A schematic of the signal cable routing from the front face of the modular tracking system.

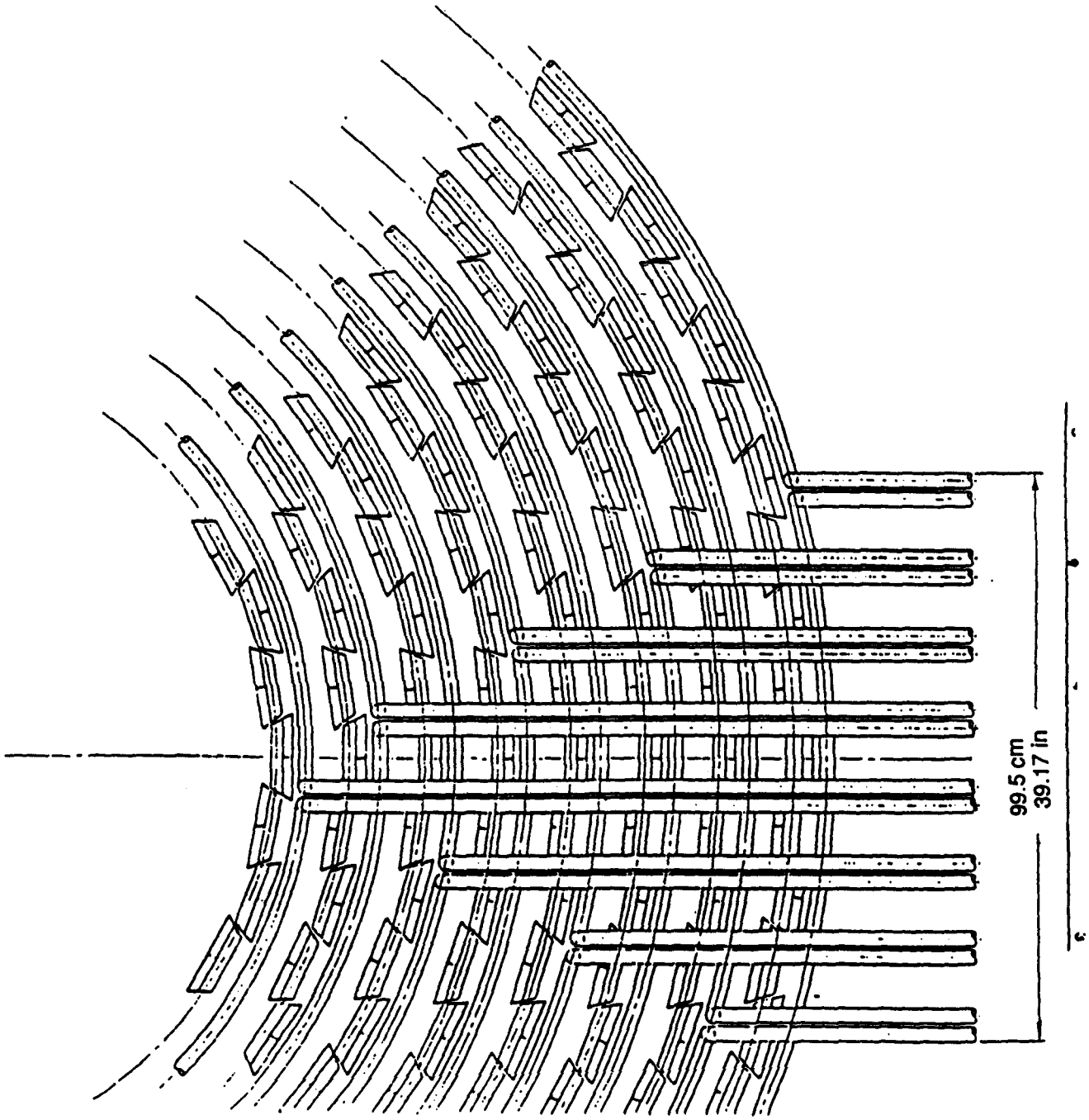

Fig. VII.3. The drift gas utility system on the front face of the detector. The support frame is a generic support, not the space frame detailed in this report.

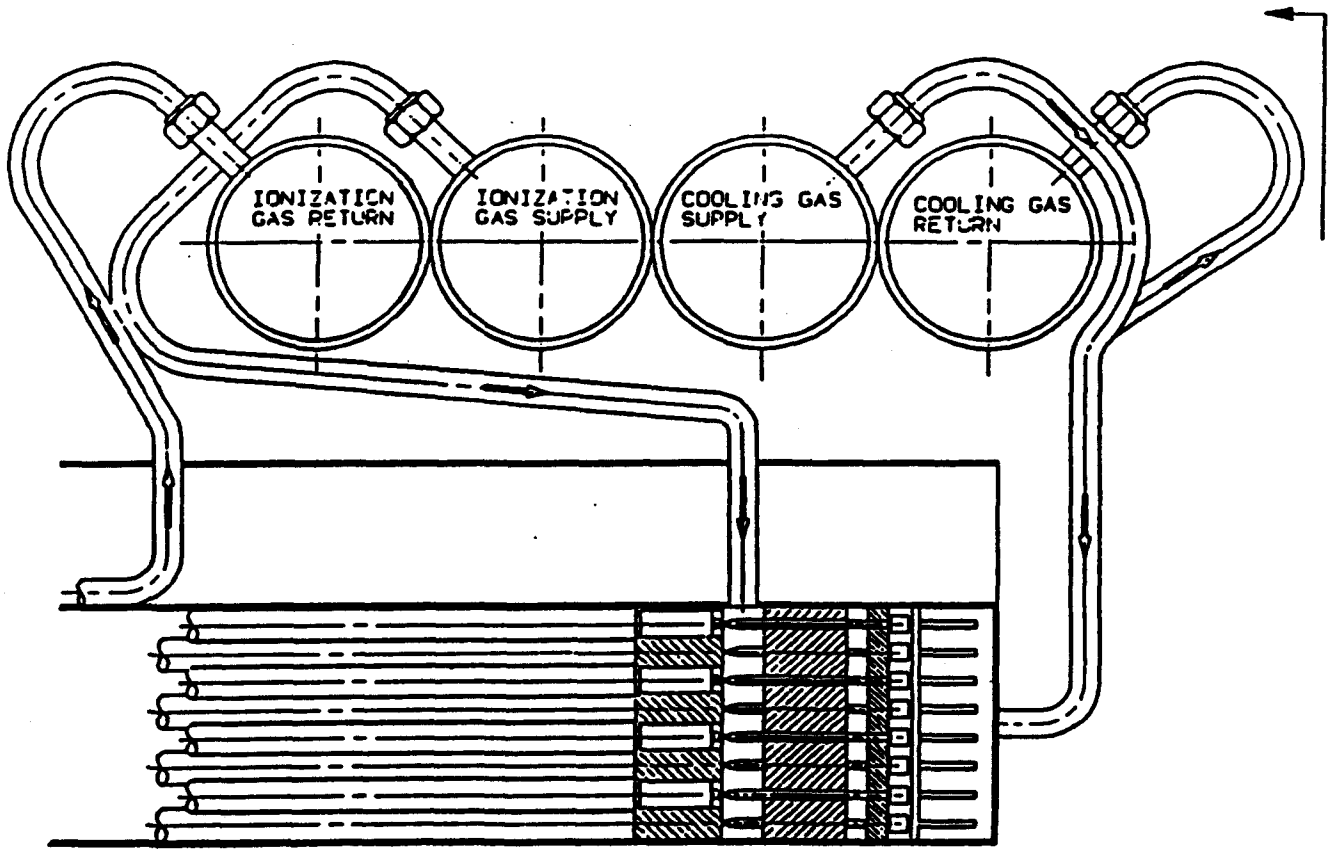

Fig. VII.4. A conceptual design of the electronics cooling gas utility system on support frame of the tracker.

VIII. COST AND SCHEDULE

VIII.1. COST

TABLE NUMBER 2
FUNCTIONAL COST BREAKDOWN FOR MODULAR STRAW CENTRAL TRACKER 11-06-91

			K$ w/cont	K$ wo/cont
A1	SHELLS			
		DESIGN	322	241
		PROCURE	2511	1874
		FABRICATE	526	393
		TOOLING	1079	863
B1	CYLINDERS			
		DESIGN	226	184
		PROCURE	5474	4450
		FABRICATE	85	69
		TOOLING	2602	1923
		ALIGNMENT	312	254
C1	STRAWS			
		DESIGN	185	161
		PROCURE	1912	1670
		FABRICATE	598	519
		TOOLING	525	423
D1	SUPPORT STRUCTURE			
		DESIGN	178	267
		PROCURE	2609	2108
		FABRICATE	340	267
		TOOLING	70	55
E1	ASMB MODULES			
		DESIGN	774	680
		PROCURE	104	89
		FABRICATE	1504	1315
		TOOLING	792	635
E2	FACILITIES MODULES			
		DESIGN	21	17
		PROCURE	384	315
		FABRICATE	839	688
		TOOLING	0	0
F1	INSTALL MODULES			
		DESIGN	151	120
		PROCURE	11	10
		FABRICATE	497	395
		TOOLING	136	112

			K$ w/cont	K$ wo/cont
G1	ASSEMBLE STRUCTURE			
		DESIGN	173	142
		PROCURE	59	45
		FABRICATE	278	228
		TOOLING	691	540
G2	FACILITIES STRUCTURE			
		DESIGN	78	71
		PROCURE	59	54
		FABRICATE	0	0
		TOOLING	0	0
H1	SHIP AND TEST			
		DESIGN	23	16
		PROCURE	25	18
		FABRICATE	19	13
		TOOLING	1224	967
I1	INSTALLATION			
		DESIGN	133	90
		PROCURE	703	475
		FABRICATE	42	28
		TOOLING	794	597
J1	PROGRAM MANAGEMENT			
		DESIGN	2306	1994
		PROCURE	981	795
		FABRICATE	441	371
		TOOLING	0	0
K1	R & D EFFORTS			
		DESIGN	85	64
		PROCURE	88	68
		FABRICATE	201	156
		TOOLING	0	0
L1	DRIFT GAS SYSTEM			
		DESIGN	14	12
		PROCURE	372	315
		FABRICATE	811	688
		TOOLING	0	0
	TOTAL		34	28

TABLE NUMBER 1 11-06-91

DATA SHEET FOR FUNCTIONAL COST BREAKDOWN FOR MODULAR STRAW TRACKER

TITLE	OBS · OD	EN	ENM	EA	EAM	DR	DRM	TE	TEM	LA	LAM	EXP	K$ MINOR	K$ MAJOR	EDIA$	EDIA+C$	MFAL$	MFAL+C$	TMAT$	TMAT+C$	BASE$	BAS+C$
TRIGGER STRAW TOTALS		131	0	0	0	60	0	0	740	0	0	0	282	394	79891	92178	216153	249603	675500	774445	971544	1116226
TRIGGER SHELL TOTALS		124	0	68	0	120	0	0	609	0	0	0	114	840	118264	158474	177828	238290	953750	1278025	1249842	1674790
TRIGGER ASSEMBLY TOTALS		20	0	388	0	20	0	0	2268	0	0	0	49	0	141820	162149	662258	760123	49000	59185	853076	981456
AXIAL & STEREO STRAWS TOTAL		110	0	47	0	45	0	0	1037	0	0	0	170	350	80610	92999	302668	348274	994367	1137197	1377646	1578472
AXIAL & STEREO SHELLS TOTAL		96	0	150	0	90	0	0	736	0	0	0	70	850	122256	163823	214912	287982	920000	1232800	1257168	1684603
AXIAL & STEREO ASSEMBLIES TOTAL		350	0	1140	0	20	0	0	2231	0	0	0	40	0	538350	811853	653222	743731	39867	44881	1231440	1400266
CYLINDERS		166	60	28	0	302	38	50	50	0	0	0	0	4450	183776	226044	89210	85128	4450000	5473500	4702988	5784873
SHIM RINGS		29	54	50	0	30	5	98	161	0	0	0	8	0	39369	48818	102147	128662	8000	9920	149518	185403
SPACEFRAME		8	14	20	0	10	1	10	45	0	0	0	0	1900	13438	16529	22889	28092	1900000	2337000	1936277	2381821
ASSEMBLY & MACHINING		134	116	1	0	50	25	60	206	0	0	0	5	0	78349	90101	140195	161224	5000	5750	223544	257074
MODULE INSTALATION		175	123	1	0	120	30	298	826	0	0	0	10	0	120000	150521	394661	497383	10000	10900	524661	658802
MOUNTS		87	23	7	0	60	21	8	71	0	0	0	125	0	68382	87529	40496	51835	125000	160000	233878	299365
FINAL ASSEMBLY		63	49	5	0	100	25	37	160	0	0	0	40	0	63168	83382	88238	116474	40000	52800	191408	252859
STRAW TOOLING		224	24	24	24	400	52	8	16	0	0	0	20	120	241064	298919	42188	52313	140000	173600	423252	524830
SHELL TOOLING		283	52	64	38	420	56	42	70	0	0	0	353	135	287763	358095	87228	108971	488000	611840	862989	1078902
MODULE ASSEMBLY TOOLING		88	38	5	23	100	17	90	45	0	0	0	92	398	74893	93183	69936	87013	490000	611840	834631	791834
MANDRELS		40	15	5	0	5	0	25	0	0	0	5	50	1506	21690	29498	14215	19332	1561000	2122960	1596905	2171790
TAPING MACHINE		34	11	12	0	45	6	23	23	0	0	0	10	261	34199	45143	20453	26998	271000	357720	325652	429881
SUPPORT STRONGBACK		12	0	2	0	24	4	2	0	0	0	0	25	0	13962	18701	1864	2212	25000	29800	40868	48714
SUPPORT ALIGN TOOL		28	5	5	7	0	0	38	23	0	0	0	16	175	14533	17440	22392	26870	193000	231600	229925	275908
MACHINING STATION		38	12	12	0	48	8	24	24	0	0	0	10	297	36096	46203	21498	27517	307000	392960	384594	466680
S/L ASMB TOOLING		14	0	1	0	28	4	0	0	0	0	0	45	50	15879	20325	1300	1864	95000	121600	112179	136062
FINAL ASMB TOOLING		15	0	0	30	3	0	0	0	0	0	0	37	0	7890	10099	9750	12480	37000	47360	54640	69938
TRANSPORT TOOLING		30	0	3	0	60	9	10	0	0	0	0	35	100	34305	43910	5845	7481.6	135000	172800	175150	224193
ERECTION TOOLING		45	0	2	0	90	11	10	0	0	0	0	45	100	50645	87296	6495	8870.8	145000	187800	202140	263767
TEST EQUIPMENT		72	27	0	30	0	0	0	56	0	0	0	62	375	33192	42965	38549	50373.8	437000	576400	508741	669738
TRACKER UTILITIES		309	0	14	7	485	56	10	545	0	0	0	237	0	304624	383692	182535	230257	237000	297780	724159	911717
TESTING FUNCTION		28	5	0	0	20	3	0	338	0	0	0	0	75	18486	24864	101392	132988	75000	102000	194678	259853
FINAL ALIGNMENT WORK		17	5	2	4	24	4	10	18	0	0	3	15	0	16287	22936	13081	18778.1	18000	25020	47368	66734
TRACKER TRANSPORTATION SYSTEM TOT.		15	0	0	0	20	3	0	0	0	0	0	10	0	13415	19854	975	1443	10000	14800	24390	36097
ERECTION SSCL		81	41	0	0	33	10	5	90	0	0	0	0	0	38646	54364	49891	69847.4	0	0	88737	124231
DRIFT GAS SYSTEM		104	10	50	0	79	19	5	55	0	0	0	115	360	89869	133006	28305	41891.4	475000	703000	593174	877899
MODULE FACILITIES		9	750	8	0	18	378	0	750	0	0	0	40	275	11949	14100	687600	811368	315000	371700	1014549	1197187
SUPPORT FACILITIES		13	750	8	0	26	379	0	750	0	0	0	0	315	17043	20792	687925	839269	315000	384300	1019968	1244361
COST & SCHEDULE		154	0	0	0	0	0	0	0	0	0	54	0	0	70994	78093	0	0	54000	59400	124994	137488
TECHNICAL MGR		2300	500	875	0	830	0	0	0	0	0	325	0	0	2E+06	2E+06	230500	255855	325000	360750	2104925	2336466
R & D EFFORTS		400	0	0	0	600	0	480	0	0	0	40	80	350	444400	586608	140160	185011	470000	620400	1054560	1392020
INSTALLATION & TEST		87	119	2	5	71	32	89	206	0	25	67.5	0	0	83832	84795	156024	201396	67500	88325	287358	374510
																					27713706	34366170

MODULAR STRAW CENTRAL TRACKER

CONTINGENCY TABLE REV.C

	ACTIVITY	RISK FACTOR			WTG FACTOR			CONTIN.
		TR	CR	SR	TR	CR	SR	%
1.2	CENTRAL TRACKER (Ave Rating)	4.5	3.8	4.4	2.9	1.7	1.0	24
1.2.1	MODULES							
1.2.1.1	TRIGGER MODULES							
1.2.1.1.1	STRAW ASSEMBLIES	4	1	4	2	2	1	14
1.2.1.1.2	END PLATE SUB ASSEMBLY	4	2	4	2	2	1	16
1.2.1.1.3	POGO PLATE SUB ASSEMBLY	4	2	4	2	2	1	16
1.2.1.1.4	SHELLS ASSEMBLIES	6	3	4	4	2	1	34
1.2.1.1.5	MODULE ASSEMBLY	3	4	2	1	2	1	13
1.2.1.1.6	TEST MODULES	4	3	4	2	1	1	15
1.2.1.1.7	SHIP MODULE ASSY'S	2	4	8	4	2	1	24
1.2.1.2	AXIAL/STEREO MODULES							
1.2.1.2.1	STRAW ASSEMBLIES	4	1	4	2	2	1	14
1.2.1.2.2	END PLATE SUB ASSEMBLY	4	2	4	2	2	1	16
1.2.1.2.3	POGO PLATE SUB ASSEMBLY	4	2	4	2	2	1	16
1.2.1.2.4	SHELLS ASSEMBLIES	6	3	4	4	2	1	34
1.2.1.2.5	MODULE ASSEMBLY	3	4	2	1	2	1	13
1.2.1.2.6	TEST MODULES	4	3	4	2	1	1	15
1.2.1.2.7	SHIP MODULE ASSEMBLES	2	4	2	1	2	1	12
1.2.2	SUPPORT STRUCTURE							
1.2.2.1	SUPPORT CYLINDERS	4	3	4	4	1	1	23
1.2.2.2	MODULE SUPPORT SHIM RINGS	4	4	4	4	1	1	24
1.2.2.3	CYLNDR SUPPORT END FLANGES	4	3	4	4	1	1	23
1.2.2.4	ASSY SUPPRT COMPNNTS (MACH)	4	3	4	2	1	1	15
1.2.3	SUPERLAYER (S/L) ASSEMBLY							
1.2.3.1	MODULE PREPARATION	3	4	8	2	1	1	18
1.2.3.2	MODULE INSTALLATION	6	6	8	2	1	1	26
1.2.3.3	MODULE ALIGNMENT	8	4	8	2	1	1	28
1.2.3.4	ADHESIVE	1	3	4	2	1	1	9
1.2.4	TRACKER S/L TO S/L ASSEMBLY							
1.2.4.1	EXTERNAL SUPPORT SYSTEM	6	6	4	2	2	1	28
1.2.4.2	S/L TO S/L ASSY AND ALIGNMENT	6	6	8	2	2	1	32
1.2.5	EQUIPMENT,TOOLING,& FIXTURES							
1.2.5.1	MODULE ASSEMBLY TOOLING							
1.2.5.1.1	MODL COMPNNTS ASSY TOOLNG	4	4	8	2	2	1	24
1.2.5.1.2	MODULE ALIGNMENT TOOLING	6	4	8	2	2	1	28
1.2.5.1.3	MODULE FINAL ASSY TOOLING	6	4	4	2	2	1	24
1.2.5.1.4	MODULE FINAL TESTING TOOLING	6	4	4	2	2	1	24
1.2.5.1.5	MODL TRANS. SHIP CONTAINR TOOL	6	6	4	2	2	1	28
1.2.5.2	SUPPORT STRCTRE ASSY TOOLNG							
1.2.5.2.1	MANDRELS FOR CYLNDRS & RINGS	6	4	4	4	2	1	36
1.2.5.2.2	TAPING STATION	8	6	4	2	2	1	32
1.2.5.2.3	STRONGBACK CYLNDR LIFTING FXTR	6	4	2	2	2	1	22
1.2.5.2.4	BANDSAW/MILLING TOOLING	2	1	2	2	2	1	8
1.2.5.2.5	ALIGNMENT TOOLING	2	4	4	4	2	1	20

MODULAR STRAW CENTRAL TRACKER

CONTINGENCY TABLE REV.C

	ACTIVITY	RISK FACTOR			WTG FACTOR			CONTIN.
		TR	CR	SR	TR	CR	SR	%
1.2.5.2.6	MACHINING STATION	6	6	4	2	2	1	28
1.2.5.3	SUPERLAYER ASSEMBLY TOOLING							
1.2.5.3.1	MISC. S/L ASSEMBLY TOOLING	8	6	4	4	2	1	48
1.2.5.4	TRACKER S/L TO S/L ASSY TOOLNG							
1.2.5.4.1	CYLNDR DIAPHRAGM FXTRS(8 TOTAL	4	4	4	4	2	1	28
1.2.5.4.2	TRACKER SUPPORT MOUNTING FXTR	4	4	4	4	2	1	28
1.2.5.4.3	SUPERLAYER ALIGNMENT TOOLING	4	4	4	4	2	1	28
1.2.5.4.4	ADJUSTMENT TOOLING	4	4	4	4	2	1	28
1.2.5.5	FINAL FACTORY ASSEMBLY TOOLING							
1.2.5.5.1	FINAL FACTORY ALIGNMNT TOOLNG	4	4	4	4	2	1	28
1.2.5.5.2	FINAL FACTORY ASSEMBLY TOOLING	4	4	4	4	2	1	28
1.2.5.5.3	FINAL FACTORY TESTING TOOLING	4	4	4	4	2	1	28
1.2.5.6	TRACKER TRANSPORTT'N TOOLING							
1.2.5.6.1	STRONGBACK TRACKER LIFTING FXT	4	4	4	4	2	1	28
1.2.5.6.2	SHIPPING ATMOSPHERE SYSTEM	4	4	4	4	2	1	28
1.2.5.6.3	TRACKER SHIPPING CONTAINER	4	4	4	4	2	1	28
1.2.5.7	ERECTION TOOLING							
1.2.5.7.1	ERECTION ALIGNMENT TOOLING	8	8	8	2	2	1	40
1.2.5.7.2	INSTALLATION FIXTURES	8	4	4	2	2	1	28
1.2.5.7.3	MOUNTING FIXTURES	6	4	4	2	2	1	24
1.2.5.8	ELECTRICAL FNCTN TEST EQUP							
1.2.5.8.1	MODULE TEST EQUIPMENT	3	3	8	2	2	1	20
1.2.5.8.2	FINAL FACTORY TEST EQUIPMENT	6	4	4	4	2	1	36
1.2.5.8.3	SURFACE ASSEMBLY TEST EQUIP	6	4	4	4	2	1	36
1.2.5.8.4	INSTALLED TEST EQUIPMENT	8	4	4	4	2	1	44
1.2.6	FINAL FACTORY ASSEMBLY							
1.2.6.1	INSTALL UTILITIES ASSEMBLIES							
1.2.6.1.1	COOLING UTILITIES	4	3	4	4	2	1	26
1.2.6.1.2	DRIFT GAS UTILITIES	4	3	4	4	2	1	26
1.2.6.1.3	SIGNAL ELECTRONIC UTILITIES	4	4	4	4	2	1	28
1.2.6.1.4	ELECTRICAL POWER UTILITIES	3	3	4	4	2	1	22
1.2.6.2	INSTALL SAFETY DIAGONSTIC SYST							
1.2.6.2.1	DRIFT GAS LEAK DETECTORS	6	6	4	2	2	1	28
1.2.6.2.2	INERTING SYSTEM	4	3	4	4	2	1	26
1.2.6.2.3	THERMAL SAFETY EQUIPMENT	3	3	2	4	2	1	20
1.2.7	FINAL FACTORY TESTING							
1.2.7.1	LEAK TESTING							
1.2.7.1.1	COOLING LOOP	4	3	4	4	2	1	26
1.2.7.1.2	DRIFT GAS LOOP	4	3	4	4	2	1	26
1.2.7.2	FACTORY FUNCTIONAL TESTS							
1.2.7.2.1	FUNCTIONAL TEST EQUIPMENT	6	4	4	4	2	1	36
1.2.7.2.2	FUNCTIONAL TESTING	6	4	4	4	2	1	36
1.2.7.3	FACTORY ALIGNMENT TESTS							
1.2.7.3.1	INTERNAL TRACKER EQUIVLNT WGHT	4	3	4	4	2	1	26

MODULAR STRAW CENTRAL TRACKER

CONTINGENCY TABLE REV.C

	ACTIVITY	RISK FACTOR			WTG FACTOR			CONTIN.
		TR	CR	SR	TR	CR	SR	%
1.2.7.3.2	INTERNAL TRACKER MOUNTS	6	6	8	4	2	1	44
1.2.8	TRACKER TRANSPORTATION SYSTEM	8	6	4	4	2	1	48
1.2.9	ERECTION AT SUPERCOLLIDER SITE							
1.2.9.1	SURFACE ASSEMBLY	6	6	4	4	2	1	40
1.2.9.2	DRIFT GAS SYSTEM	8	6	4	4	2	1	48
1.2.10	FACILITIES							
1.2.10.1	MODULE ASSEMBLY FACILITY	4	3	4	2	2	1	18
1.2.10.2	SUPPORT ASSEMBLY FACILITY	4	3	8	2	2	1	22
	TRACKER CONSTR (W/O PRJT MGMT) SIMPLISTIC AVERAGE							26
1.2.11	PROGRAM MANAGEMENT							
1.2.11.1	DESIGN REVIEWS	2	2	4	2	1	1	10
1.2.11.2	SCHEDULE REVIEW	2	2	4	2	1	1	10
1.2.11.3	REPORTS	2	2	4	2	1	1	10
1.2.11.4	SYSTEMS ENGINEERING	2	3	4	2	1	1	11
1.2.11.5	PROGRAM COORDINATION	2	3	4	2	1	1	11
1.2.11.5.1	PROGRAM MANAGER	2	3	4	2	1	1	11
1.2.11.5.2	COST/SCHEDULE CONTROL	2	3	4	2	1	1	11
1.2.11.6	NOT USED							
1.2.11.7	QUALITY MANAGEMENT	2	3	4	2	1	1	11
1.2.11.8	SAFETY MANAGEMENT	2	3	4	2	1	1	11
1.2.12	R & D EFFORT							
1.2.12.1	CONSTRUCT PROTOTYPE	6	4	4	4	1	1	32
1.2.12.2	OTHER EFFORTS	4	4	2	2	1	1	14
	PROJECT MANAGEMENT SIMPLISTIC AVERAGE							13
8.2.1.1.2	TRACKER HALL INSTALATION							
8.2.1.1.2.1	INSTALL GAS REGENERATION EQUIP	4	3	4	4	1	1	23
8.2.1.1.2.2	LOWER TRACKER INTO HALL	8	4	4	2	1	1	24
8.2.1.1.2.3	INSTALL INTO DETECTOR	8	4	4	2	1	1	24
8.2.1.1.2.4	FINAL CABLING IN DETECTOR	6	6	8	4	1	1	38
8.2.1.1.2.5	LEAK CHECK PLUMBING	4	4	4	2	1	1	16
8.2.1.1.2.6	FINAL TESTING IN DETECTOR							
8.2.1.1.2.6.1	FUNCTIONAL TESTS IN DETECTOR	6	4	8	4	1	1	36
8.2.1.1.2.6.2	ALIGNMENT TESTS IN DETECTOR	8	6	8	4	1	1	46
	TRACKER INSTALLATION SIMPLISTIC AVERAGE							30

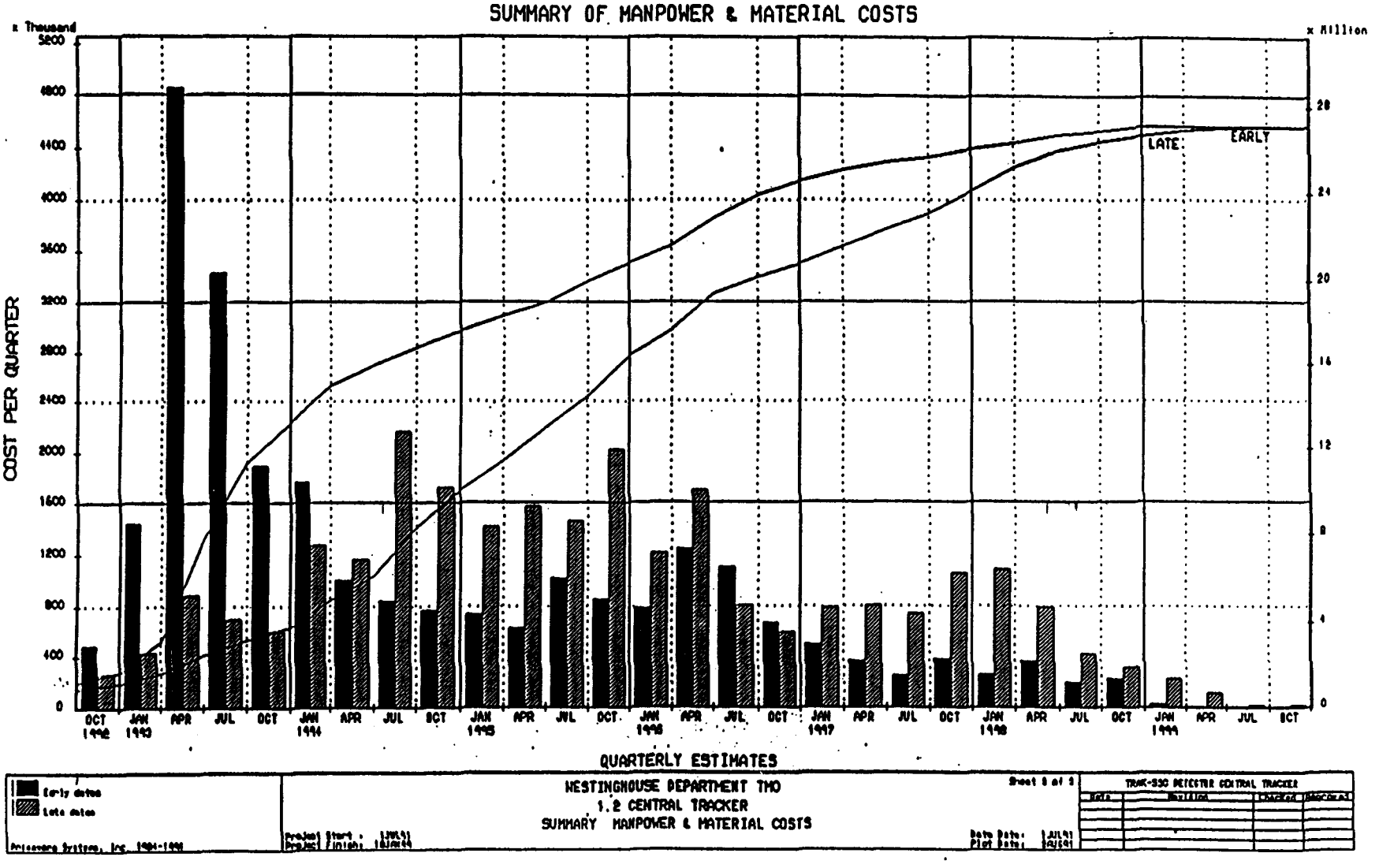
SUMMARY OF MANPOWER & MATERIAL COSTS
x Thousand
x Million
COST PER QUARTER
LATE
EARLY
QUARTERLY ESTIMATES
Early dates
Late dates
WESTINGHOUSE DEPARTMENT TMO
1.2 CENTRAL TRACKER
SUMMARY MANPOWER & MATERIAL COSTS
TRAK-330 DETECTOR CENTRAL TRACKER

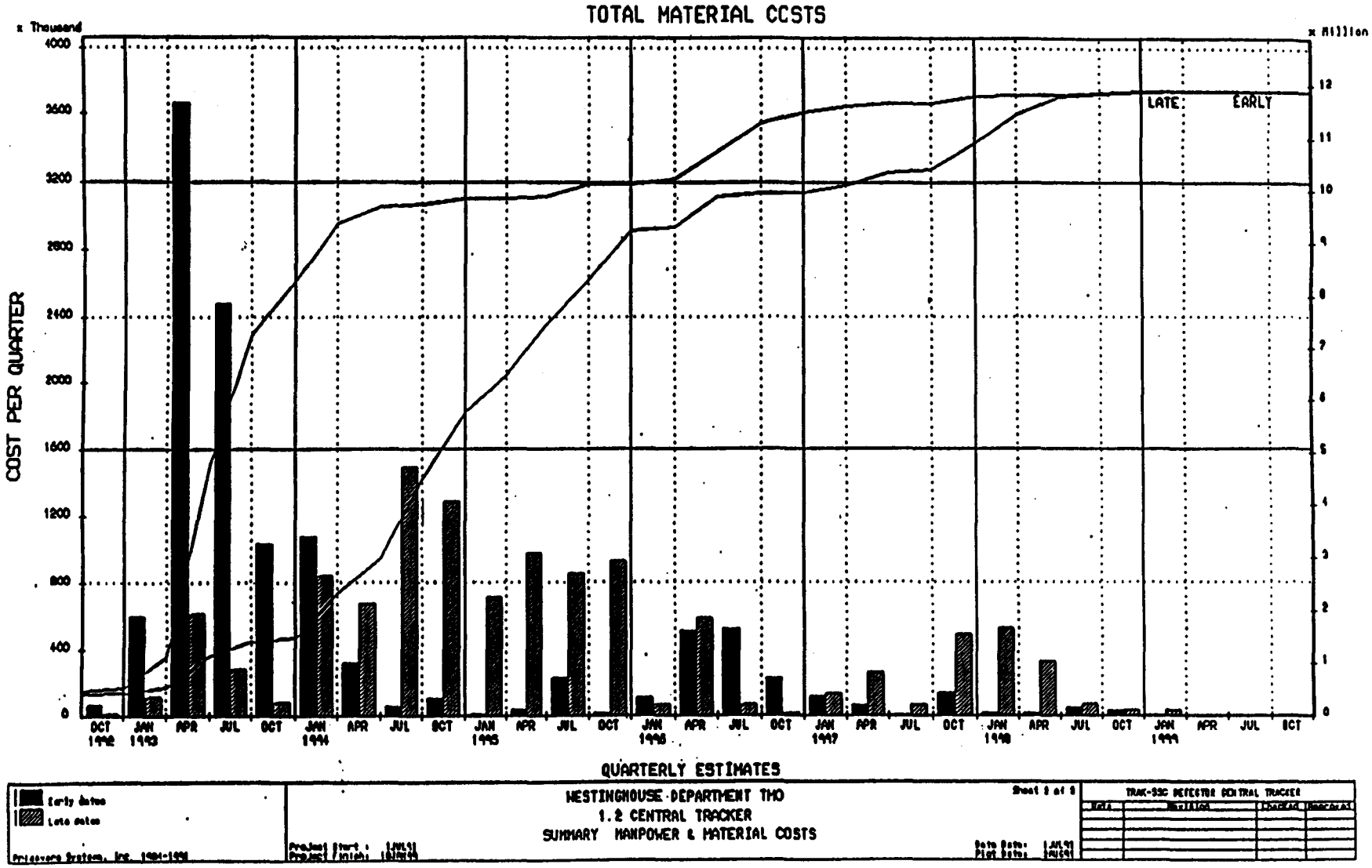
TOTAL MATERIAL COSTS
x Thousand
x Million
COST PER QUARTER
LATE
EARLY
4000
3600
3200
2800
2400
2000
1600
1200
800
400
0
12
11
10
9
8
7
6
5
4
3
2
1
0
OCT 1992
JAN 1993
APR
JUL
OCT
JAN 1994
APR
JUL
OCT
JAN 1995
APR
JUL
OCT
JAN 1996
APR
JUL
OCT
JAN 1997
APR
JUL
OCT
JAN 1998
APR
JUL
OCT
JAN 1999
APR
JUL
OCT
QUARTERLY ESTIMATES
early dates
late dates
WESTINGHOUSE-DEPARTMENT TMO
1.2 CENTRAL TRACKER
SUMMARY MANPOWER & MATERIAL COSTS
TRAK-SSC DETECTOR CENTRAL TRACKER

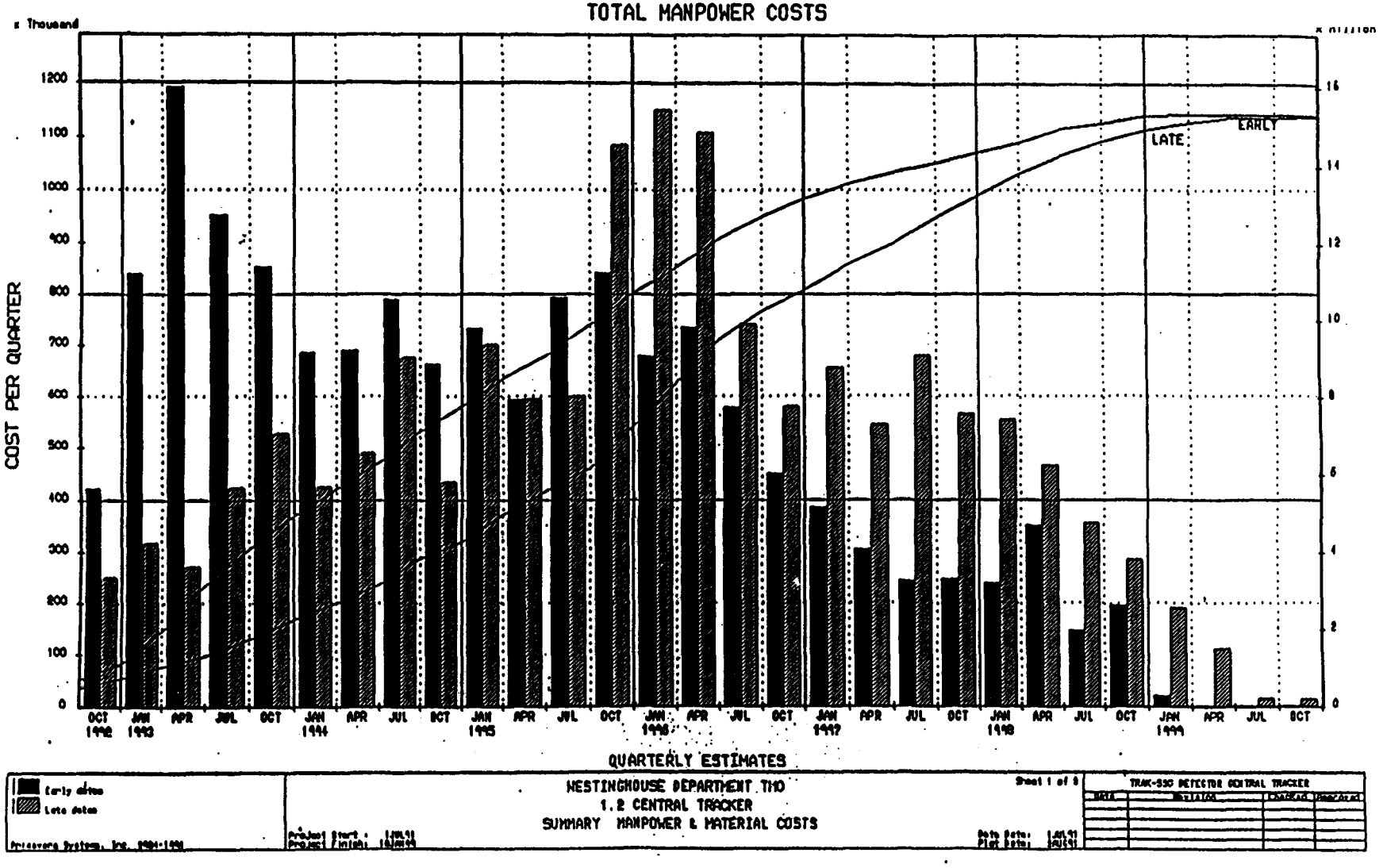
TOTAL MANPOWER COSTS
$ Thousand
$ million
COST PER QUARTER
LATE
EARLY
1200
1100
1000
900
800
700
600
500
400
300
200
100
0
16
14
12
10
8
6
4
2
0
OCT 1992
JAN 1993
APR
JUL
OCT
JAN 1994
APR
JUL
OCT
JAN 1995
APR
JUL
OCT
JAN 1996
APR
JUL
OCT
JAN 1997
APR
JUL
OCT
JAN 1998
APR
JUL
OCT
JAN 1999
APR
JUL
OCT
QUARTERLY ESTIMATES
Early dates
Late dates
WESTINGHOUSE DEPARTMENT TMO
1.2 CENTRAL TRACKER
SUMMARY MANPOWER & MATERIAL COSTS
Sheet 1 of 8
TRAK-550 DETECTOR CENTRAL TRACKER

ENGINEERING MANPOWER

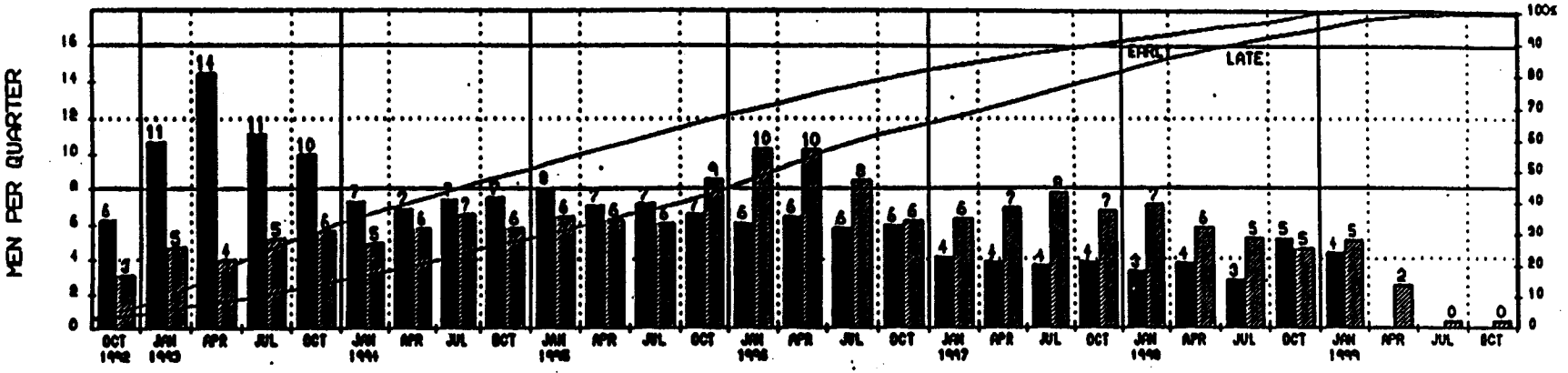

QUARTERLY ESTIMATES

DRAFTING MANPOWER

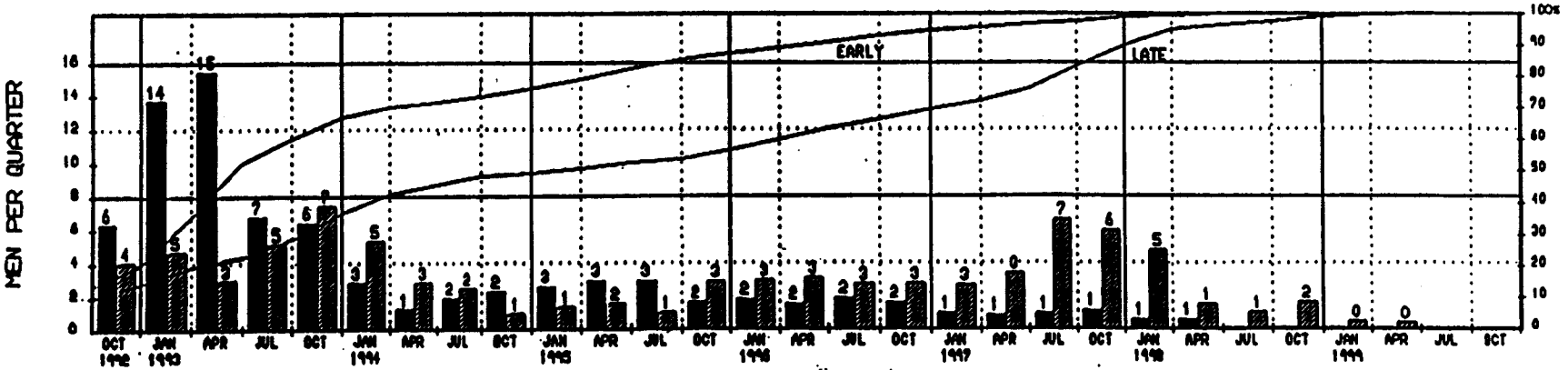

QUARTERLY ESTIMATES

Early dates
Late dates

Primavera Systems, Inc. 1984-1996

WESTINGHOUSE DEPARTMENT TMO
1.2 CENTRAL TRACKER
ENGINEER,DRAFTING,TECHNICIAN,LABORER

Sheet 1 of 2

TRAK-330 DETECTOR CENTRAL TRACKER

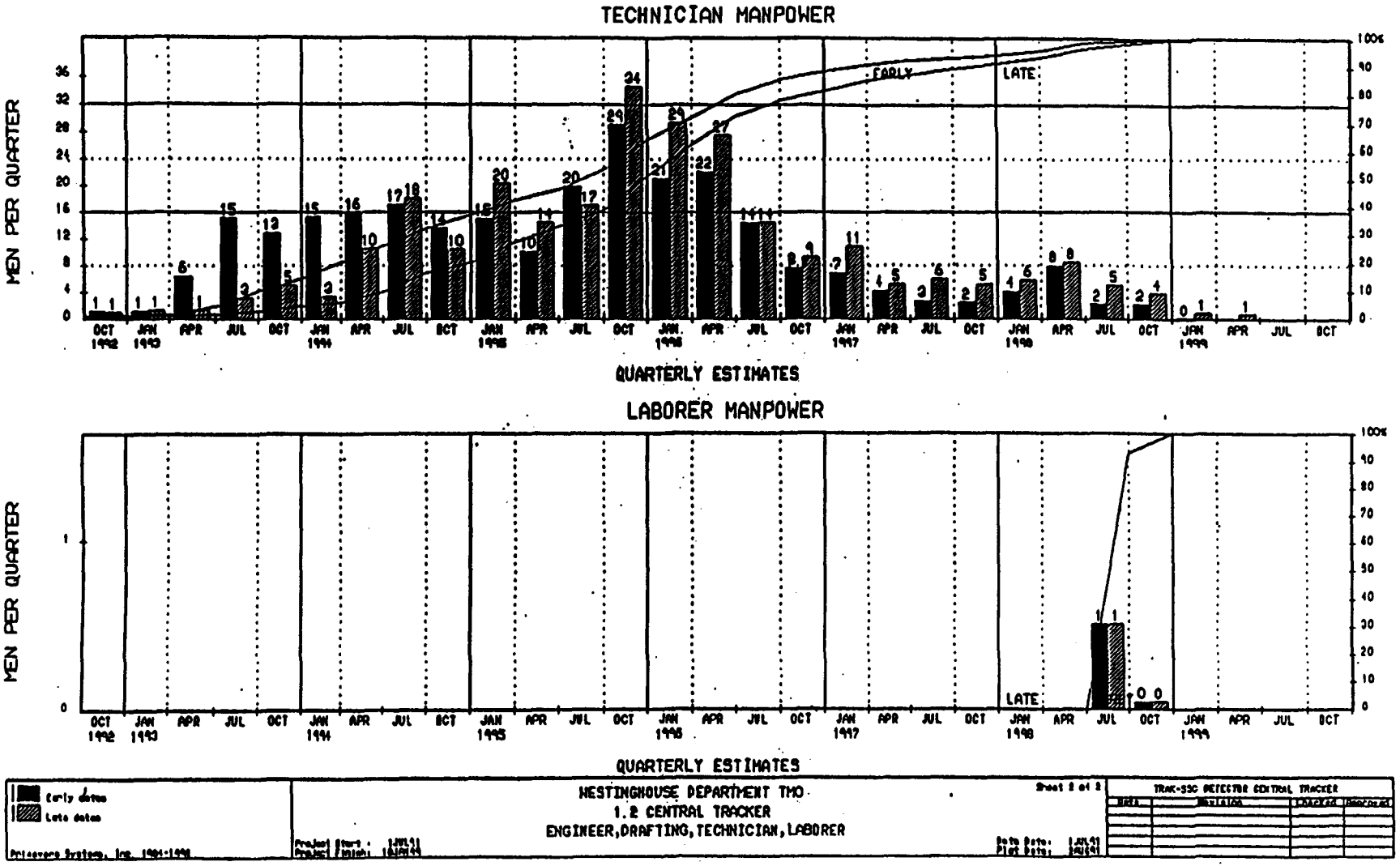
TECHNICIAN MANPOWER
MEN PER QUARTER
QUARTERLY ESTIMATES
EARLY
LATE
LABORER MANPOWER
MEN PER QUARTER
QUARTERLY ESTIMATES
LATE
Early dates
Late dates
WESTINGHOUSE DEPARTMENT TMO
1.2 CENTRAL TRACKER
ENGINEER,DRAFTING,TECHNICIAN,LABORER
TRAK-SSC DETECTOR CENTRAL TRACKER

KAISER
AEROTECH

KAISER AEROTECH
880 DOOLITTLE DRIVE
MAIL ADDRESS: P.O. BOX 1678
SAN LEANDRO, CALIFORNIA 94577-0801 · (415) 562-2456
FAX (415) 568-6420 / TWX 910-366-7014 (KAISERAERSLN)

October 18, 1991

Westinghouse Electric Corporation
Science and Technology Center
1310 Beulah Road
Pittsburgh, Pennsylvania 15235

Attention: Roger L. Swensrud
Electromechanics

Subject: Composite Properties for the Proposed Spaceframe Flange Design

Reference: WECO letter dated October 7, 1991

Dear Roger,

Les Montford and I enjoyed our discussions with you and Warren Barkel and are finding this SCS project very interesting. As we all are discovering, much of the data you want has just not been determined and we would like to determine it.

We hope that the following assists you in getting more confidence in this structure. Our calls to several suppliers did not yield as much as we hoped.

On the 2 x 4 x 0.25 cm rectangular struts, we can assure you that this is a size we can manufacture. If cost is a major concern, however, we suggest that the use of 6:1 warp-to-fill ratio fabric (using P-75 carbon fiber in the warp direction and T-300 carbon fiber in the fill). This would yield an axial modulus of 36 msi. The use of unidirectional tape with P-75 would give 40 million modulus, but it would be more difficult to process. Using the 6:1 fabric, the hoop modulus would be 3 msi. The CTE will have to be determined.

We can, and will, work with Hercules UHM fiber if it is deemed necessary. By utilizing a 6:1 fabric, pitch axial fiber can be used without introducing any bends in the fiber. At this point in time, it is advantageous to not rule out P-75 fiber.

Please find the enclosed data package on Fiberite's 954-3 cyanate ester composite data. Mechanical properties degrade slightly with moisture pick up.

Elongation due to moisture absorption was 17.2 μm/m at 55% R.H. at room temperature, for a total absorption of 0.185%.

Fiberite appears willing to work with us on determining variation in the resin properties. The effects of processing will also be addressed at this time. Current KA SOP in fabricating composite tubes is to maintain axial fiber alignment to ± 5°. Hoop properties are a function of fill fibers and will have a larger variation of approximately ± 10°.

We will continue to address the open questions from your 7 October 1991 letter.

Since the stability of this structure is so critical, we suggest a study to determine the variability of the composite struts. We could use various batches of fiber and resin and different factory personnel to see how much change there is in CTE, moisture induced elongation, and stiffness. A statistically meaningful number of tubes could be made and tested. With the very limited information we have been able to uncover, this may be the only way to ascertain how stable the spaceframe is.

We have attached an article and presentation on cyanate ester resins that Warren Barkel asked to see. Please pass them to him.

This is the situation at the moment, and we will keep you informed of any additional information we find.

Best wishes,

KAISER AEROTECH

Wade H. Brown
Director of Business Development

WHB:pg

Enclosures

KAISER AEROTECH

KAISER AEROTECH
660 DOOLITTLE DRIVE
MAIL ADDRESS: P.O. BOX 1678
SAN LEANDRO, CALIFORNIA 94577-0801 • (415) 562-2456
FAX (415) 568-6420 / TWX 910-366-7014 (KAISERAERSLN)

KA91-081A-RLB-001R
November 4, 1991

Westinghouse
Science and Technology Center
1310 Beulah Road
Pittsburgh, PA 15236

Attention: Mr. Robert Swensrud

Subject: ROM Pricing Fabricate and Assemble Superconductor Super Collider Space Frame Flange

Gentlemen:

Below is pricing for the graphite/cyanate ester space frame including support rings and assembly. The price includes P-75 fiber and cyanate ester resin.

Description of one Space Frame	ROM Pricing for two Space Frames (Lot Price)
160 Struts (2 x 4 x 0.250 cm wall) 64 Connectors 5 Support Rings Assembly Material: 656 Fabric with cyanate ester resin from Fiberite.	$1,900,000

If you should have any questions, please contact the undersigned at (510) 562-2456, extension 238 or Wade Brown at extension 251.

Sincerely,

KAISER AEROTECH

for Ronald L. Bauer
Vice President of Marketing
and Business Development

WHB:pg

HERCULES

Hercules Aerospace Company
Composite Structures
Bacchus Works
Magna, Utah 84044-0098
(801) 250-5911

10 October 1991

In Reply Refer To:
MISC/7300/3-0313

Westinghouse Electric Corporation
Science & Technology Center
1310 Beulah Road
Pittsburgh, Pennsylvania 15235

Attention: Mr. Roger Swensrud
Mail Stop 501 3W62

Subject: Support Cylinders for the Central Tracker for the Super Conducting Super Collider

Reference: Request for Information Letter from Roger Swensrud to Al Vicario, dated October 7, 1991

Dear Mr. Swensrud:

I am pleased to provide information relative to the application of composites to the Central Tracker Support Cylinders for the Super Conducting Super Collider, in response to the questions and information provided in the referenced letter. I have discussed this information with our technical staff and our preliminary thoughts and recommendations follow.

Materials

I assume that the material trade studies shown in your letter are based on technical data sheets that have been provided by the materials suppliers. The data provided in these sheets are usually adequate for trade study purposes, but for detailed design, you will want to use statistically valid materials characterization databases. Hercules has such databases available in-house for most of our own material systems. Hercules has the engineering capability to design these structures, and if Hercules materials could be utilized, the availability of these databases would provide time and cost savings to your program.

We agree with your preliminary selection of UHM as a fiber with high stiffness, high strength, and high strain-to-failure compared to pitch based fibers. Also, Hercules can manufacture UHM into prepreg tapes with thicknesses as low as 1 mil/ply cured thickness.

The only resin on your chart that Hercules manufactures is 3501-6. However, our fiber could be provided to other prepreg manufacturers that offer low moisture resin systems. Some comments on potential low moisture systems:

- PR500-2 - Hercules has done some preliminary work with this 3M product. The early samples that we obtained had no tack and were very boardy. We understand that 3M has solved these workability problems. The moisture absorption is low, and this epoxy based system can be processed like standard structural epoxy systems (assuming the above mentioned problems have been solved).

- Cyanate Esters - Fiberite is a source of these resin systems. They offer somewhat lower moisture absorption than standard structural epoxies and good mechanical properties, but they must be processed at 450° F in a supported condition.

- Hercules Space Resin - Hercules has been developing a low moisture resin system for stability critical spacecraft structures. We have prepregged this material and now have some test results. The moisture absorption is very low, and the material processes like epoxies. We are continuing to develop this system for improved mechanical properties.

The only suggestion I have with respect to your choice of Rohacell foam core is that you may want to consider balsa cores. Balsa is lower in cost, easier to manufacture into a cylindrical configuration, higher in compressive strength, higher in shear modulus, but lower in shear strength compared to Rohacell foam. If you want more information on this product, I suggest you call Joseph Pantalone of Baltek Corporation at (201) 767-1400.

Hercules has a great deal of experience with fabricating sandwich structures with a wide variety of core materials. We have produced these structures using filament winding, fiber placement, and hand layup fabrication processes. Our experience base includes large cylinders similar to the Central Tracker Support Cylinders.

Design

Producibility should be designed into these large structures, either through a design build team cooperative arrangement, or by making the fabricator responsible for designing the structures to a design specification that you would provide. Hercules has complete engineering capabilities and could perform this effort through either arrangement. We have a great deal of experience with the design of large composite cylindrical structures.

Tooling

I believe that if the fabricator is made responsible for the tooling design, this would save time and costs for your program. Hercules has an accomplished tool engineering staff with considerable experience in tool design for similar projects. We have good relationships with several vendors with proven capabilities for fabricating large tools to tight tolerances.

Fabrication

Hercules is interested in working with you on the fabrication of these cylinders. The choice of fabrication process depends heavily on the final design. If an ultra-thin ply material is required, this may restrict the use of our automated processes. If thicker plies could be used, the Hercules fiber placement process offers: a repeatable, automated process that produces high quality laminates and is capable of applying any fiber orientation desired. Hercules has a great deal of experience with both automated and hand layup processes.

Price Estimates

We expect that vendor prices for autoclave quality tools for these large cylinders will be in the range of $100,000 to $150,000. Material prices for ultra-thin UHM/3501-6 prepreg tape are approximately in the following ranges:

- 1 mil/ply cured thickness - $1800 per pound
- 1 1/2 mil/ply cured thickness - $1500 per pound
- 2 mil/ply cured thickness - $ 900 per pound

In order to provide you with a complete Rough-Order-of-Magnitude (ROM) price estimate for a program to fabricate these cylinders, we would need the following information about your program:

- period of performance
- who is responsible for the product design
- who is responsible for the product drawings
- who is responsible for the tooling design
- who is responsible for the tooling procurement
- the density of the Rohacell foam core
- the feasibility of balsa core
- deliverables requirements
- testing and inspection requirements
- Quality Assurance requirements
- tolerances
- key design requirements
- definition of the cylinder end close-outs

I hope this information is helpful to you. For further discussions of this program, please call me at (801) 251-2830.

Sincerely,

Michael Moore

Michael Moore
Senior Marketing Representative

November 5, 1991

Westinghouse Electric Corporation
Science and Technology Center
1310 Beulah Road
Pittsburgh, PA 15235

Attention: Mr. Roger Swensrud

Subject: Preliminary Statement of Work (SOW) and Rough-Order-of-Magnitude (ROM) Pricing for the Central Tracker Support Cylinders Program

Dear Mr. Swensrud:

Hercules is pleased to provide you with the enclosed preliminary SOW and ROM pricing of a program to design and fabricate five large composite cylinders for the Central Tracker for the Superconducting Super Collider. We believe that Hercules is uniquely qualifed to perform this program because of our experience with the design and fabrication of large composite structures and our integrated capabilities which include graphite fiber and prepreg materials production, composite structures design, analysis, tooling design, and composite structures fabrication, assembly, inspection and testing.

The enclosed preliminary SOW and ROM prices are based on the information that you have supplied over the past few weeks and our current assessment of a program to meet your requirements. We understand that you are in the very early stages of defining program requirements. As requirements become better defined, we could provide you with updated scope and pricing. We are also available to review requirements and provide you with input to ensure that the cylinders are designed for producibility.

If you have any questions, please contact me at (801) 251-2830. We look forward to working with you in the future.

Sincerely,

Michael Moore

Michael Moore
Senior Marketing Representative

Enclosures

CC: Al Vicario
Steve Davis
Bob Anderson

PRELIMINARY STATEMENT OF WORK
WESTINGHOUSE CENTRAL TRACKER SUPPORT CYLINDERS PROGRAM

SCOPE:

This preliminary statement of work (SOW) outlines a program for Hercules Composite Structures Group to work with the Westinghouse/Indiana University team in the design and fabrication of five large composite cylinders to be used in the central tracker of the Superconducting Super Collider. The SOW is preliminary in that the total program requirements are not yet completely defined and understood. The purpose of this preliminary SOW is to outline a preliminary program that Hercules and Westinghouse can agree upon, so that reasonably accurate Rough-Order-of-Magnitude (ROM) costing for the program can be performed in support of Westinghouse's proposal activities.

PROGRAM PLAN:

This program will consist of two phases. Phase I is the design of the full-scale composite cylinders and sub-element development testing to support the design. Phase II is the tooling design, tooling fabrication, and fabrication of the full-scale cylinders. For costing purposes, the period of performance of Phase I is assumed to be one year congruent with calendar year 1993, and Phase II is assumed to be one year congruent with calendar year 1994. Each phase consists of the following tasks as outlined below.

PHASE I

Task 1 - Program Administration

Task 1 consists of the effort required to manage Phase I. It includes costs for a program office including a Program Manager and related support efforts, a contracts effort to initiate and maintain the contract, and a cost accounting effort to track all charges to the contract. The Program Manager will be the primary point of contact for Westinghouse, and he will have the authority to manage and direct all effort related to the program.

This task also includes travel costs required to support Phase I. Phase I travel requirements are assumed to be the following:

- One trip to Pittsburgh to initiate the program and to familiarize the Hercules Program Manager and design team with the Westinghouse design efforts to date. The duration of this trip is assumed to be one week.

- Three trips to Dallas for design/program reviews. These meetings will be supported by the Hercules Program Manager and Designer and the duration is assumed to be 2 days each.

Task 2 - Product Design Support to Westinghouse

Task 2 consists of Hercules providing product design support to Westinghouse for the design of the cylinders. A level of effort type support for a composite structures design analyist has been costed for this task. The composite designer will provide Westinghouse with information on accepted composite design practices, composite design codes, and composite material databases; will review Westinghouse drawings and concepts; will support Westinghouse trade studies; will provide recommendations on design concepts and details; will provide Westinghouse with development test plans; and will support Westinghouse design reviews. However, Westinghouse will retain product design responsibility and authority and will produce the product drawings.

Task 3 - Development Testing

In Task 3 Hercules will perform development testing to support the product design effort. This testing will be performed to provide material and design properties to support and verify the design. This task is assumed to consist of defining, performing or subcontracting, and reporting the following tests on composite laminate specimens, sandwich specimens, and sub-element cylinders:

- CTE testing: (5) UHM/3501-6 laminate specimens
  (5) sandwich specimens
- CME testing: (5) UHM/3501-6 laminate specimens
- Strength/modulus testing of sandwich specimens:
  (5) axial strength/modulus
  (5) shear strength/modulus
  (5) bending strength/modulus
- Sub-element cylinder fabrication and testing:
  tooling design and fabrication
  fabrication of sub-element cylinder
  axial strength/modulus of the cylinder
  (5) CTE of tag end specimens

PHASE II

Task 1 - Program Administration

Task 1 consists of the effort required to manage Phase II. It includes a program office consisting of a Program Manager and related support, a contracts effort to initiate and maintain the contract, and a costing effort to track all charges to the contract. No travel costs are assumed to be required to support Phase II.

Task 2 - Tooling

Task 2 consists of the effort required to design, specify, procure, and inspect the tooling required to fabricate the five large composite cylinders. The major tooling consists of five metal mandrels required to fabricate the composite cylinders and to provide support during autoclave curing of the cylinders. Other tooling includes handling aids, fabrication aids, and shipping containers.

Task 3 - Materials

Task 3 consists of the effort required to specify, procure, and inspect the materials required to fabricate the five large composite cylinders. The primary materials required are assumed to be:

- UHM/3501-6 prepreg tape, 1 mil/ply cured thickness
- Rohacell foam core
- Adhesive film to bond the inner and outer composite skins to the foam core

Task 4 - Fabrication

Task 4 consists of the effort required to fabricate, inspect, and deliver five large composite cylinders. This task also includes production verification testing of the cylinders and the effort to produce and deliver associated paperwork.

The fabrication effort includes writing manufacturing procedures, process development, layup and cure of the cylinders including a Quality Assurance program, and packing and shipping of the cylinders. Inspection of the completed cylinders will include dimensional verification and ultrasonic NDE testing to verify laminate and bondline quality.

Production verification testing will be performed on specimens cut from tag ends from each cylinder and will include:

- CTE testing: (5) from each end of each cylinder
- CME testing: (5) from each end of each cylinder
- strength/modulus testing:
  axial strength/modulus from each end of each cylinder
- fiber volume/resin content/void content:
  from each end of each cylinder

WESTINGHOUSE ROM

CENTRAL TRACKER SUPPORT CYLINDERS FOR THE SSC

	ROM PRICE
PHASE I - DESIGN SUPPORT	
Task 1 - Program Administration	$75,000
Program Office	
Program Support	
Contracts	
Travel (1 trip to Pittsburgh/2 men/1 week)	
(3 trips to Dallas/2 men/2 days)	
Task 2 - Product Design Support	$125,000
Design Support Labor	
Task 3 - Development Testing	$125,000
Write Test Plans	
CTE Tests	
CME Tests	
Strength/Modulus Tests	
Sub-element Cylinder Tool	
Sub-element Cylinder Fabrication	
Sub-element Cylinder Tests	
TOTAL PHASE I PRICE =	$325,000

		ROM PRICE
PHASE II - TOOLING AND FABRICATION		
Task 1 -	Program Administration	$125,000
	Program Office	
	Program SUpport	
	Contracts	
	Travel (None)	
Task 2 -	Tooling	
	Tool Design	$1,000,000
	Computer	
	Tool Purchase	
	Tool Specifications	
	Procurement	
	RQC	
Task 3 -	Materials	$975,000
	UHM/3501-6, 1 mil (432 lbs x $1800/lb)	
	Rohacell Foam	
	Adhesives	
	Material Specifications	
	Procurement	
	RQC	
Task 4 -	Fabrication	$3,350,000
	Write Procedures	
	Process Development	
	Fabricate Cylinders	
	Quality Assurance	
	Ship Cylinders	
	Production Verification Testing	
	Status Meetings with Customer	
	Data Reporting	
	TOTAL PHASE II PRICE =	$5,450,000

GROUNDRULES AND ASSUMPTIONS

1. The Phase I price includes travel costs as follows: 1 trip to Pittsburgh/2 men/1 week; and 3 trips to Dallas/2 men/2 days.

2. The Phase II price does not include travel.

3. Phase I is assumed to begin 1 January 1993 and end 31 December 1993.

4. Phase II is assumed to begin 1 January 1994 and end 31 December 1994.

5. Minimal levels of program management, reporting and quality assurance costs are included: when these requirements are defined, these costs can be adjusted to meet the requirements.

6. The design of the cylinders is assumed to be:
   - Inner and outer skins consist of 6 layers of 1 mil/ply cured thickness UHM/3501-6 in a quasi-isotropic layup.
   - Core consists of 0.6" thickness of 51 WF Rohacell foam.
   - Adhesive film bonds the skins to the core.
   - Approximate cylinder sizes are:

Diameter (in)	Length (ft)
52	20
80	23
100	28
112	28
124	28

CHROMIUM INDUSTRIES, INC. • 4645 West Chicago Avenue, Chicago, Illinois 60651-3385 • (312) 287-3716 • FAX (312) 287-5792

CHROMIUM

June 4, 1991

Mr. Roger Swensrud
Westinghouse Electric Corporation
1310 Beulah Rd.
Pittsburgh, PA 15235

Dear Roger:

Thank you for your time and patience as we review and prepare this proposal. The mandrels really are not complicated but the raw size of these and establishing tolerances is the difficulty.

Below is a basic summary of what we have considered, followed by the pricing estimates. We would imagine that the prices are accurate within 10% but changes could impact the price significantly. The considerations such as material type, wall thickness, and the taper have not only an impact on costs but in manufacturing techniques which can cause additional costs.

MATERIALS - The shells would be made of grade A-36 plate that would be rolled and welded into tubing. Both circumferential and longitudinal weld seams will exist.

WALL THICKNESS - For quoting purposes, we have assumed a .75 inch wall. This would have to be reviewed for deflection and deformation so not to "collapse". Also, the shell thickness is critical to the manufacturing processes. A thin wall could cause machining problems.

WALL THICKNESS VARIATION - This is difficult to establish at this point but we currently beleive a specification of ±.125 inch is appropriate.

BALANCING - The mandrels are to be statically balanced for manufacturing reasons.

SHAFTS AND BEARINGS - Shafts and bearings will be supplied for manufacturing and handling reasons. The bearings and shafts will be made so to be removable. The shaft diameters are assumed to be 8" diameter for this quote.

PRICING

GROUP 1

1400mm dia x 6100mm lth	=	$114,970
2000mm dia x 6800mm lth	=	171,210
2268mm dia x 7600mm lth	=	223,260
2532mm dia x 8300mm lth	=	265,100
2790mm dia x 8400mm lth	=	309,250
3064mm dia x 8400mm lth	=	347,125

GROUP 2

2268mm dia x 7600mm lth	=	$245,590
2532mm dia x 8300mm lth	=	291,500
2790mm dia x 8400mm lth	=	339,900
3064mm dia x 8400mm lth	=	381,700

GROUP 3

1400mm dia x 6100mm lth	=	$105,775
2000mm dia x 6800mm lth	=	157,515
2268mm dia x 7600mm lth	=	205,400
2532mm dia x 8300mm lth	=	243,892
2790mm dia x 8400mm lth	=	284,510
3064mm dia x 8400mm lth	=	319,355

GROUP 4

2268mm dia x 7600mm lth	=	$225,940
2532mm dia x 8300mm lth	=	268,180
2790mm dia x 8400mm lth	=	312,708
3064mm dia x 8400mm lth	=	351,100

DELIVERIES - A delivery schedule can be established based on your requirements. We would expect a period between twenty-eight (28) and fifty-two (52) weeks depending on quanitites.

TERMS - We would negotiate the terms with you at a point closer to establishing the actual requirements. We would need to have a downpayment for engineering and materials purchase. We would also like to have a progress payment schedule developed.

We appreciate the opportunity to work with you. If Chromium Industries or I may be of further assistance, please call.

Sincerely,

CHROMIUM INDUSTRIES, INC.

Scott Patterson
General Manager

SP/pf

MACH2.WK3 MACHINING STATION 6-14-91

ITEM	SUPPLIER	COMMENT	PURCHASE $	DESIGN HRS	DESIGN $	DRAFTING HRS	DRAFTING $	MACHINING HRS	MACHINING $	LABOR HRS	LABOR $	TOTAL
BED PLATE PEDESTAL ASSY.	LAKE SHORE INC	10 FT X 20 FT X 8 PCS	$30,000.00	24.00	$1,440.00	20.00	$1,000.00					$32,440.00
BLANK END PEDESTAL												
BASE ASSY												
BURNOUTS		PURCHASED MATERIALS	$1,400.00	80.00	$1,960.00	40.00	$2,000.00	20.00	$1,000.00			$6,760.00
WELDING		TIME & MATERIALS								32.00	$1,600.00	$1,600.00
STRESS ANNEALING		TRANSPORTATION & TIME	$400.00									$400.00
MACHINING		TIME						80.00	$3,000.00			$3,000.00
ASSY		TIME								24.00	$1,200.00	$1,200.00
COLUMN ASSY												
BURNOUTS		PURCHASED MATERIALS	$1,800.00	80.00	$1,960.00	40.00	$2,000.00			80.00	$1,600.00	$6,160.00
WELDING		TIME & MATERIALS								80.00	$1,600.00	$1,600.00
STRESS ANNEALING		TRANSPORTATION & TIME	$400.00									$400.00
MACHINING		TIME						32.00	$1,600.00	16.00	$800.00	$2,400.00
ELEVATING MECHANISM		PURCHASED MATERIAL	$2,000.00	24.00	$1,440.00	32.00	$1,600.00			12.00	$600.00	$5,760.00
ASSY		TIME								40.00	$2,000.00	$2,000.00
TRUNNION BRG HOUSING ASSY												
BURNOUTS		PURCHASED MATERIALS	$1,800.00	80.00	$2,000.00	40.00	$2,000.00	24.00	$1,200.00	16.00	$800.00	$7,800.00
WELDING		TIME								24.00	$1,200.00	$1,200.00
STRESS ANNEALING		TRANSPORTATION AND TIME	$400.00									$400.00
MACHINING		TIME						32.00	$1,600.00	12.00	$600.00	$2,200.00
BEARING ASSY		PURCHASED MATERIALS	$400.00	16.00	$1,040.00	16.00	$800.00			16.00	$800.00	$3,040.00
ASSEMBLY TIME		TIME								32.00	$1,600.00	$1,600.00
SHAFT BRG HOUSING ASSY												
BURNOUTS		PURCHASED MATERIALS	$300.00	16.00	$780.00	16.00	$800.00					$1,880.00
WELDING		TIME								16.00	$800.00	$800.00
STRESS ANNEALING		TRANSPORTATION AND TIME	$300.00									$300.00
MACHINING		TIME						80.00	$1,600.00	8.00	$400.00	$2,000.00
BEARING ASSY		PURCHASED MATERIALS	$2,000.00	12.00	$780.00	12.00	$600.00			8.00	$400.00	$3,780.00
ASSEMBLY TIME		TIME								16.00	$800.00	$800.00
DRIVEN END PEDESTAL												
BASE ASSY												
BURNOUTS		PURCHASED MATERIALS	$1,800.00	80.00	$1,960.00	40.00	$2,000.00	80.00	$1,000.00			$6,760.00
WELDING		TIME								32.00	$1,600.00	$1,600.00
STRESS ANNEALING		TRANSPORTATION AND TIME	$400.00									$400.00
MACHINING		TIME						80.00	$3,000.00			$3,000.00
ASSY		TIME								24.00	$1,200.00	$1,200.00
COLUMN ASSY												
BURNOUTS		PURCHASED MATERIALS	$1,800.00	80.00	$1,960.00	40.00	$2,000.00	40.00	$2,000.00	80.00	$1,600.00	$6,160.00
WELDING		TIME								80.00	$1,600.00	$1,600.00
STRESS ANNEALING		TRANSPORTATION AND TIME	$400.00									$400.00
MACHINING		TIME						32.00	$1,600.00	16.00	$800.00	$2,400.00
ELEVATING MECHANISM		PURCHASED MATERIALS	$2,000.00	24.00	$1,440.00	32.00	$1,600.00			12.00	$600.00	$5,760.00
ASSY		TIME								40.00	$2,000.00	$2,000.00
TRUNNION BRG HOUSING ASSY												
BURNOUTS		PURCHASED MATERIALS	$1,800.00	80.00	$2,000.00	40.00	$2,000.00	24.00	$1,200.00	16.00	$800.00	$7,800.00
WELDING		TIME								24.00	$1,200.00	$1,200.00
STRESS ANNEALING		TRANSPORTATION AND TIME	$400.00									$400.00
MACHINING		TIME						32.00	$1,600.00	16.00	$800.00	$2,400.00
BEARING ASSY		PURCHASED MATERIALS	$400.00	16.00	$1,040.00	24.00	$1,200.00			16.00	$800.00	$3,040.00
ASSEMBLY TIME		TIME								32.00	$1,600.00	$1,600.00
SHAFT BRG HOUSING ASSY												
BURNOUTS		PURCHASED MATERIALS	$300.00									$300.00
WELDING		TIME						12.00	$600.00	12.00	$600.00	$1,200.00
STRESS ANNEALING		TRANSPORTATION AND TIME	$300.00									$300.00
MACHINING		TIME						80.00	$1,600.00	8.00	$400.00	$2,000.00
SHAFT BEARING ASSY		PURCHASED MATERIALS	$2,000.00	12.00	$780.00	12.00	$600.00			8.00	$400.00	$3,780.00
THRUST BEARING ASSY		PURCHASED MATERIALS	$3,500.00	24.00	$1,560.00	32.00	$1,600.00			16.00	$800.00	$7,560.00
DRIVE												
ROTARY ENCODER		PURCHASED MATERIALS	$1,600.00	16.00	$1,040.00	24.00	$1,200.00			16.00	$800.00	$4,440.00
BRAKE ASSY		PURCHASED MATERIALS		12.00	$780.00	16.00	$800.00			16.00	$800.00	$2,380.00
ASSEMBLY TIME		TIME								24.00	$1,200.00	$1,200.00
MACHINING STATION		PURCHASED MATERIALS										
BED PLATE WAYS		PURCHASED MATERIALS	$4,500.00	40.00	$2,600.00	32.00	$1,600.00	40.00		24.00	$1,200.00	$9,900.00
MACHINE TABLE		PURCHASED MATERIALS	$15,000.00	120.00	$7,800.00	120.00	$6,000.00	80.00		40.00	$2,000.00	$30,800.00
MACHINE TABLE WAYS		PURCHASED MATERIALS	$2,000.00	16.00	$1,040.00	24.00	$1,200.00	20.00		20.00	$1,000.00	$5,240.00
SPINDLE CARRIER		PURCHASED MATERIALS	$2,000.00	40.00	$2,600.00	32.00	$1,600.00	40.00		20.00	$1,000.00	$11,000.00
SPINDLE		PURCHASED MATERIALS	$2,000.00	16.00	$1,040.00	16.00	$800.00	20.00		12.00	$600.00	$4,240.00
CONTROL SYSTEM		PURCHASED MATERIALS	$10,000.00	40.00	$2,600.00	20.00	$1,000.00	40.00		40.00	$2,000.00	$15,600.00
		TOTALS	$90,000.00	$40.00	$43,420.00	716.00	$35,800.00	692.00	$22,800.00	830.00	$41,500.00	$233,220.00

MACH1.WK3 TAPING STATION 6-14-91

ITEM	SUPPLIER	COMMENT	PURCHASE $	DESIGN HRS	DESIGN $	DRAFTING HRS	DRAFTING $	MACHINING HRS	MACHINING $	LABOR HRS	LABOR $	TOTAL
BED PLATE PEDESTAL ASSY.	LAKE SHORE INC	10 FT X 20 FT X 8 PCS	$30,000.00	24.00	$1,560.00	20.00	$1,000.00					$32,560.00
BLANK END PEDESTAL												
BASE ASSY												
SUNHOUTS		PURCHASED MATERIALS	$1,800.00	24.00	$1,560.00	40.00	$2,000.00	20.00	$1,000.00			$6,360.00
WELDING		TIME & MATERIALS								80.00	$1,600.00	$1,600.00
STRESS ANNEALING		TRANSPORTATION & TIME	$400.00									$400.00
MACHINING		TIME						60.00	$3,000.00			$3,000.00
ASSY		TIME								24.00	$1,200.00	$1,200.00
COLUMN ASSY												
SUNHOUTS		PURCHASED MATERIALS	$1,800.00	24.00	$1,560.00	40.00	$2,000.00					
WELDING		TIME & MATERIALS								80.00	$1,600.00	$5,160.00
STRESS ANNEALING		TRANSPORTATION & TIME	$400.00							80.00	$1,600.00	$1,600.00
MACHINING		TIME										$400.00
ELEVATING MECHANISM		PURCHASED MATERIAL	$2,000.00	32.00	$1,560.00	20.00	$1,000.00	20.00	$1,000.00	10.00	$400.00	$5,460.00
ASSY		TIME								12.00	$480.00	$3,760.00
TRUNNION BRG HOUSING ASSY										40.00	$1,600.00	$1,600.00
SUNHOUTS		PURCHASED MATERIALS	$1,800.00	24.00	$1,560.00	40.00	$2,000.00	24.00	$1,200.00			
WELDING		TIME								10.00	$400.00	$7,360.00
STRESS ANNEALING		TRANSPORTATION AND TIME	$400.00							80.00	$1,600.00	$1,600.00
MACHINING		TIME										$400.00
BEARING ASSY		PURCHASED MATERIALS	$600.00	16.00	$1,040.00	16.00	$800.00	20.00	$1,000.00	12.00	$480.00	$3,920.00
ASSEMBLY TIME		TIME								16.00	$640.00	$3,160.00
SHAFT BRG HOUSING ASSY										80.00	$1,600.00	$1,600.00
SUNHOUTS		PURCHASED MATERIALS	$600.00	16.00	$780.00	16.00	$800.00					
WELDING		TIME										$1,380.00
STRESS ANNEALING		TRANSPORTATION AND TIME	$300.00							16.00	$640.00	$640.00
MACHINING		TIME										$300.00
BEARING ASSY		PURCHASED MATERIALS	$2,000.00	16.00	$780.00	16.00	$800.00	20.00	$1,000.00	8.00	$320.00	$4,900.00
ASSEMBLY TIME		TIME								16.00	$640.00	$3,720.00
												$640.00
DRIVEN END PEDESTAL												
BASE ASSY												
SUNHOUTS		PURCHASED MATERIALS	$1,800.00	24.00	$1,560.00	40.00	$2,000.00	20.00	$1,000.00			$6,360.00
WELDING		TIME								80.00	$1,600.00	$1,600.00
STRESS ANNEALING		TRANSPORTATION AND TIME	$400.00									$400.00
MACHINING		TIME						60.00	$3,000.00			$3,000.00
ASSY		TIME								24.00	$1,200.00	$1,200.00
COLUMN ASSY												
SUNHOUTS		PURCHASED MATERIALS	$1,800.00	24.00	$1,560.00	40.00	$2,000.00	40.00	$2,000.00	80.00	$1,600.00	$5,160.00
WELDING		TIME								80.00	$1,600.00	$1,600.00
STRESS ANNEALING		TRANSPORTATION AND TIME	$400.00									$400.00
MACHINING		TIME						60.00	$3,000.00	16.00	$640.00	$3,640.00
ELEVATING MECHANISM		PURCHASED MATERIALS	$2,000.00	32.00	$1,560.00	20.00	$1,000.00			12.00	$480.00	$4,740.00
ASSY		TIME								40.00	$1,600.00	$1,600.00
TRUNNION BRG HOUSING ASSY												
SUNHOUTS		PURCHASED MATERIALS	$1,800.00	24.00	$1,560.00	40.00	$2,000.00	24.00	$1,200.00	10.00	$400.00	$7,160.00
WELDING		TIME								80.00	$1,600.00	$1,600.00
STRESS ANNEALING		TRANSPORTATION AND TIME	$400.00									$400.00
MACHINING		TIME						60.00	$3,000.00	16.00	$640.00	$3,640.00
BEARING ASSY		PURCHASED MATERIALS	$600.00	16.00	$1,040.00	24.00	$1,200.00			16.00	$640.00	$3,440.00
ASSEMBLY TIME		TIME								80.00	$1,600.00	$1,600.00
SHAFT BRG HOUSING ASSY												
SUNHOUTS		PURCHASED MATERIALS	$300.00									$300.00
WELDING		TIME						12.00	$600.00	16.00	$640.00	$1,240.00
STRESS ANNEALING		TRANSPORTATION AND TIME	$300.00									$300.00
MACHINING		TIME						60.00	$3,000.00	8.00	$320.00	$3,320.00
SHAFT BEARING ASSY		PURCHASED MATERIALS	$2,000.00	16.00	$780.00	16.00	$800.00			8.00	$320.00	$3,780.00
THRUST BEARING ASSY		PURCHASED MATERIALS	$2,000.00	24.00	$1,560.00	20.00	$1,000.00			16.00	$640.00	$5,200.00
DRIVE												
ROTARY ENCODER		PURCHASED MATERIALS	$1,800.00	16.00	$1,040.00	24.00	$1,200.00			16.00	$640.00	$4,440.00
BRAKE ASSY		PURCHASED MATERIALS		16.00	$780.00	12.00	$600.00			16.00	$640.00	$2,220.00
ASSEMBLY TIME		TIME								24.00	$1,200.00	$1,200.00
MATERIAL SUPPLY STATION												
CUTTING TABLE		PURCHASED MATERIALS	$2,000.00	16.00	$780.00	16.00	$800.00	16.00	$800.00	32.00	$1,280.00	$6,160.00
CHAIN WAYS		PURCHASED MATERIALS	$2,000.00	16.00	$1,040.00	24.00	$1,200.00	24.00	$1,200.00	80.00	$1,280.00	$7,440.00
CHAIN DRIVE SYSTEM		PURCHASED MATERIALS	$2,000.00	16.00	$1,170.00	24.00	$1,200.00	40.00	$2,000.00	16.00	$640.00	$8,210.00
FEEDLOCK ENCODER SYSTEM		PURCHASED MATERIALS	$1,200.00									$1,200.00
TAPING HEAD		PURCHASED MATERIALS	$2,000.00	80.00	$2,340.00	32.00	$1,600.00	60.00	$3,000.00	40.00	$1,280.00	$10,220.00
CONTROL SYSTEM		PURCHASED MATERIALS	$10,000.00	120.00	$7,800.00	60.00	$3,000.00	40.00	$2,000.00	120.00	$3,840.00	$26,640.00
		TOTALS	$80,300.00	976.00	$57,876.00	624.00	$31,200.00	696.00	$31,200.00	962.00	$41,280.00	$220,176.00

SPACE FRAME

MATERIAL

Struts

Item	Section cm	Length cm	Quan
A	4x4x0.2	25.7	16
B	2x4x0.2	52.2	32
C	4x4x0.2	37.9	16
D	2x4x0.2	85.4	32
E	4x4x0.2	49.8	16
F	2x4x0.2	43.6	28
G	2x4x0.2	63.2	12
H	2x4x0.2	34.9	2
I	2x4x0.2	55.9	2
J	2x4x0.2	54.1	2
K	2x4x0.2	41.5	2

Connectors

Style	Quan
1	16
2	16
3	16
4	14
5	2

Rings

Item	Section	Radius cm	Quan
1	1.25x5x.125	65.8	1
2	1.25x5x.125	102.0	1
3	1.25x5x.125	130.0	1
4	1.25x5x.125	144.0	1
5	1.25x5x.125	158.0	1

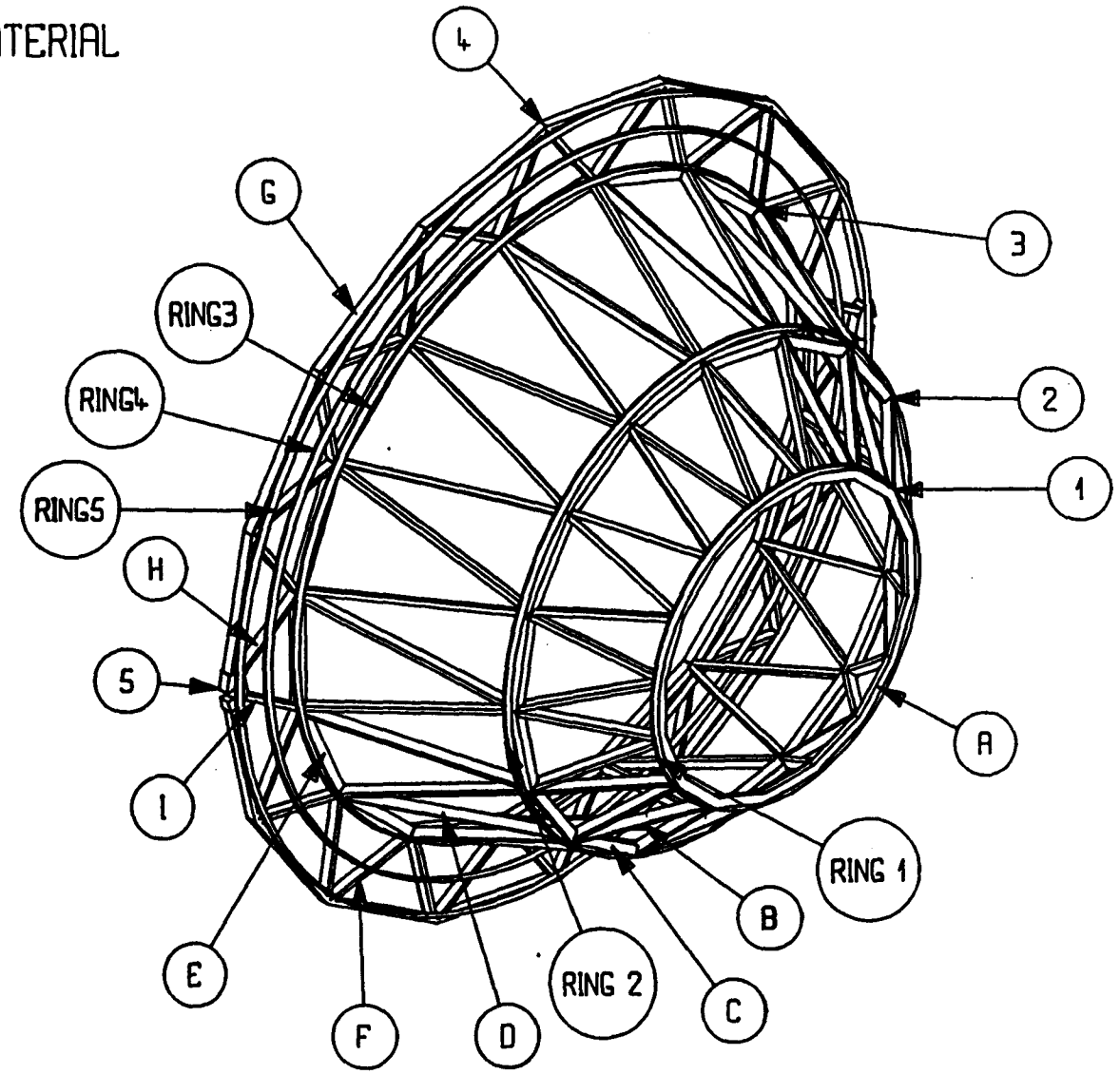

WESTINGHOUSE STC

DM 10-24-91

COMP1.WK3 6-14-91

TRACKER SUPPORT STRUCTURE MATERIAL COST

ITEM	MATERIAL	OD, IN.	ID, IN.	THKNESS,IN.	LENGTH IN.	VOL, CU.IN.	# / IN. CU.	WT, LBS.	COST $ /LB.	MATERIAL $
SUPPORT CYL. SUPERLAYER #3										
OUTSIDE SKIN	GRAPHITE-EPOXY	92.81		0.01	287.4	836.66	0.05	41.84	$2,400.00	$100,665.43
INSIDE SKIN	GRAPHITE-EPOXY	90.81		0.01	287.4	820.62	0.05	41.04	$2,400.00	$98,496.48
FOAM CORE	ROHACELL 71 IG	92.81	90.81		287.4	82988.18	0.0027	224.06	$50.00	$11,203.00
SHIM RINGS (12 PCS)	ROHACELL 71 IG	94.81	92.81		1	295.03	0.0027	0.80	$50.00	$477.94
END FLANGES (2 PCS)	ROHACELL P190 /	101.81	92.81	1	2	2530.87	0.007	35.43	$50.00	$1,771.81
	GR-EPXY	101.81	92.81	0.02*3*2		78.93	0.05	7.89	$2,400.00	$19,222.24
SUPPORT CYL. SUPERLAYER #4										
OUTSIDE SKIN	GRAPHITE-EPOXY	103.27		0.01	314.96	1021.63	0.05	51.09	$2,400.00	$122,619.63
INSIDE SKIN	GRAPHITE-EPOXY	101.27		0.01	314.96	1002.04	0.05	50.10	$2,400.00	$120,245.08
FOAM CORE	ROHACELL 71 IG	103.27	101.27		314.96	101183.66	0.0027	273.22	$50.00	$13,661.18
SHIM RINGS (12 PCS)	ROHACELL 71 IG	105.27	103.27		1	327.87	0.0027	10.81	$50.00	$530.87
END FLANGES (2 PCS)	ROHACELL P190 /	114.63	103.27	1	2	3484.37	0.007	84.44	$50.00	$2,721.79
	GR-EPXY	114.63	103.27	0.02*3*2	2	118.65	0.05	11.86	$2,400.00	$27,995.55
SUPPORT CYL. SUPERLAYER #5										
OUTSIDE SKIN	GRAPHITE-EPOXY	116.69		0.01	318.89	1160.05	0.05	58.45	$2,400.00	$140,283.20
INSIDE SKIN	GRAPHITE-EPOXY	114.69		0.01	311	1120.68	0.05	56.03	$2,400.00	$134,467.42
FOAM CORE	ROHACELL 71 IG	116.69	114.69		311	113033.48	0.0027	305.19	$50.00	$15,259.52
SHIM RINGS (12 PCS)	ROHACELL 71 IG	118.69	116.69		1	366.75	0.0027	11.96	$50.00	$598.87
END FLANGES (2 PCS)	ROHACELL P190 /	128.09	116.69	1	2	3178.43	0.007	44.50	$50.00	$2,224.80
	GR-EPXY	128.09	116.69	0.02*3*2	2	93.95	0.05	9.84	$2,400.00	$22,664.71
SUPPORT CYL. SUPERLAYER #6										
OUTSIDE SKIN	GRAPHITE-EPOXY	127.12		0.01	311	1243.01	0.05	62.10	$2,400.00	$149,040.68
INSIDE SKIN	GRAPHITE-EPOXY	125.12		0.01	311	1222.47	0.05	61.12	$2,400.00	$146,695.99
FOAM CORE	ROHACELL 71 IG	127.12	125.12		311	123823.98	0.0027	332.70	$50.00	$16,635.24
SHIM RINGS (12 PCS)	ROHACELL 71 IG	129.12	127.12		1	402.80	0.0027	13.04	$50.00	$652.05
END FLANGES (2 PCS)	ROHACELL P190 /	132.66	127.12	1	2	2299.00	0.007	31.77	$50.00	$1,588.30
	GR-EPXY	132.66	127.12	0.02*3*2	2	86.07	0.05	8.61	$2,400.00	$16,336.61
									TOTAL	$1,148,943.87

TRACKER SUPPORT STRUCTURE LABOR COST

ITEM	LAYUP DESIGN HRS ENGR	PURCHASING ENGR	MATL CUTTING TECH	LAYUP HRS ENGR	LAYUP HRS TECH	MACHINING HRS	INSPECTION HRS			
SUPPORT CYL. SUPERLAYER #3										
OUTSIDE SKIN	120.00	20.00	40	233.02	466.04					
INSIDE SKIN	120.00	20.00	40	228.01	456.01					
FOAM CORE	160.00	20.00	200	99.89	233.03					
SHIM RINGS (12 PCS)	60.00	20.00	60	48.89	96.30	72.00	180.00			
END FLANGES (2 PCS)	40.00	20.00	40							
SUPPORT CYL. SUPERLAYER #4										
OUTSIDE SKIN	40.00	10.00	40	283.84	567.68					
INSIDE SKIN	40.00	10.00	40	278.35	556.69					
FOAM CORE	55.00	10.00	200	70.96	283.84					
SHIM RINGS (12 PCS)	20.00	10.00	60	55.12	110.24	78.00	190.00			
END FLANGES (2 PCS)	16.00	10.00	40							
SUPPORT CYL. SUPERLAYER #5										
OUTSIDE SKIN	40.00	10.00	40	324.73	649.46					
INSIDE SKIN	40.00	10.00	40	311.27	622.54					
FOAM CORE	55.00	10.00	200	79.17	316.70					
SHIM RINGS (12 PCS)	20.00	10.00	60	62.15	124.29	80.00	200.00			
END FLANGES (2 PCS)	16.00	10.00	40							
SUPPORT CYL. SUPERLAYER #6										
OUTSIDE SKIN	40.00	10.00	40	345.00	690.01					
INSIDE SKIN	40.00	10.00	40	339.57	679.15					
FOAM CORE	55.00	10.00	200	86.25	345.00					
SHIM RINGS (12 PCS)	20.00	10.00	60	67.81	135.21	84.00	210.00			
END FLANGES (2 PCS)	16.00	10.00	40							

VIII.2. SCHEDULE

WBS1	MAJOR ITEM	EARLY START	EARLY FINISH
121	1.2.1 MODULES	10CT92	5DEC96
122	1.2.2 SUPPORT STRUCTURE	10CT92	12OCT95
123	1.2.3 SUPERLAYER (S/L) ASSEMBLY	29DEC94	8JUL97
124	1.2.4 TRACKER S/L TO S/L ASSEMBLY	9APR93	20JAN98
125	1.2.5 EQUIPMENT, TOOLING, & FIXTURES	10CT92	19AUG97
126	1.2.6 FINAL FACTORY ASSEMBLY	25MAR93	3APR98
127	1.2.7 FINAL FACTORY TESTING	25MAR93	21MAY98
128	1.2.8 TRACKER TRANSPORTATION SYSTEM	10AUG95	28MAY98
129	1.2.9 SURFACE ASSY AT SUPERCOLLIDER SITE	21MAY93	8JUL98
12A	1.2.10 FACILITIES	30NOV92	20JAN98
12B	1.2.11 PROGRAM MANAGEMENT	10CT92	18JAN99
12C	1.2.12 R & D EFFORT	15JUL91	30DEC93
821	8.2.1 SUBSYSTEM INSTALLATION IN HALL	28OCT93	18JAN99
822	8.2.2 SUBSYSTEM AND SYSTEM TEST IN HALL	27JUN95	18JAN99

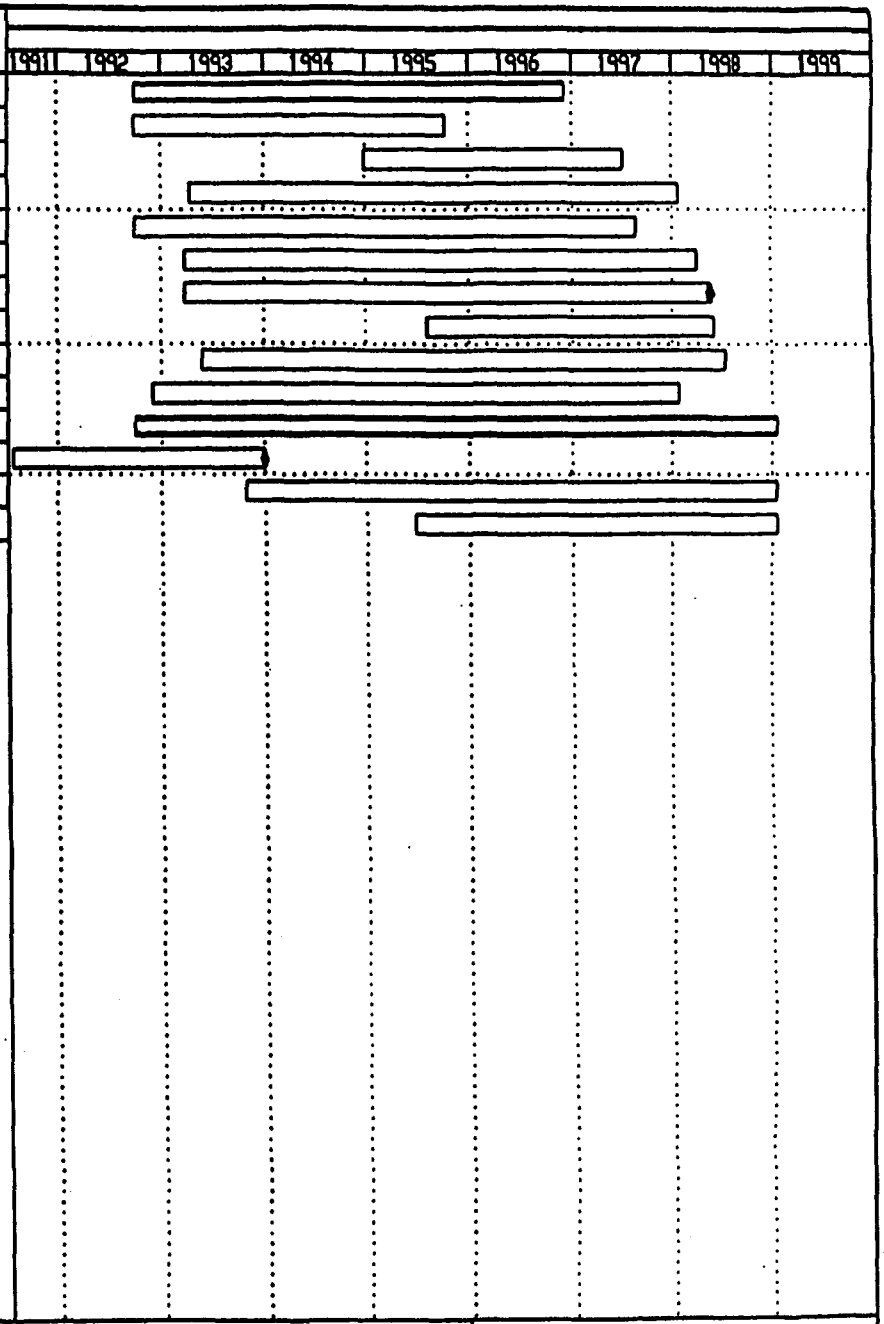

Summary Bar/ Early Dates
Critical Designator
Progress Bar

Primavera Systems, Inc. 1984-1991

Project Start : 1JUL91
Project Finish: 18JAN99

WESTINGHOUSE DEPARTMENT TMO
1.2 CENTRAL TRACKER
WBS LEVEL 3 SUMMARY

Sheet 1 of 1

Data Date: 1JUL91
Plot Date: 16AUG91

TRAK-SSC DETECTOR CENTRAL TRACKER REV.2

Date	Revision	Checked	Approved

ACTIVITY ID	ACTIVITY DESCRIPTION	EARLY START	EARLY FINISH
S001	START MODULE DESIGN	1OCT92	
S004	START MODULE PURCHASING	28JAN93	
S005	START ASSY OF MODULES	28APR93	
F003	FINISH MODULE PURCHASING		6JUL94
F002	FINISH MODULE DSGN ACTIVITIES		14JUN95
F001	FINISH MODULE ASSY ACTIVITIES		18OCT95
F004	FINISH SHIPMENT OF MODULES		5DEC95
S006	START STRUCTURE SUPPORT DESIGN	1OCT92	
S009	START STRUCTURE SUPPORT PURCHASING	15SEP93	
S008	START STRUCTURE SUPPORT FABRICATION	17JAN94	
F009	FINISH STRUCTURE SUPPORT PURCHASING		25FEB94
S007	START STRUCTURE SUPPORT ASSY	12APR94	
F006	FINISH STRUCTURE SUPPORT DESIGN		28DEC94
F007	FINISH STRUCTURE SUPPORT ASSY		9AUG95
F008	FINISH STRUCTURE SUPPORT FABRICATION		5OCT95
S01O	START SUPERLAYER ASSY	6DEC95	
F01O	FINISH SUPERLAYER ASSEMBLY		8JUL97
S011	START TRACKER S/L TO S/L ASSEMBLY	9JUL97	
F011	FINISH S/L TO S/L ALIGNMENT		2OJAN98
S013	START EQUIP, TOOLING DESIGN	1OCT92	
S014	START TOOLING PROCUREMENTS	28JAN93	
S012	START TOOLING ASSY	26APR93	
F014	FINISH TOOLING PROCUREMENTS		16SEP93
F013	FINISH EQUIP, TOOLING DESIGN		21DEC94
F012	FINISH TOOLING & FIXTURES ASSY		2JUN97
S015	START FINAL FACTORY PERIPHERAL ASSY	1MAY96	
F015	FINISH FINAL FACTORY PERIPHERAL ASSY		1APR98
S016	START FINAL FACTORY TESTING	14MAY98	
F016	FINISH FINAL FACTORY TESTING		21MAY98
F017	RECEIVE TRACKER AT SITE		28MAY98
S018	START UNPACKING TRACKER FOR SURFACE ASSY	1JUN98	
F018	COMPLETE CENTRAL TRACKER SURFACE ASSY		8JUL98
B10000.07	#7 MFG,TOOLING & TESTING PRELIM.DESIGN REVIEW	11FEB93	12FEB93
B10000.04	#4 SUPPORT STRUCT.PREL.DSGN REVIEW	11MAR93	12MAR93

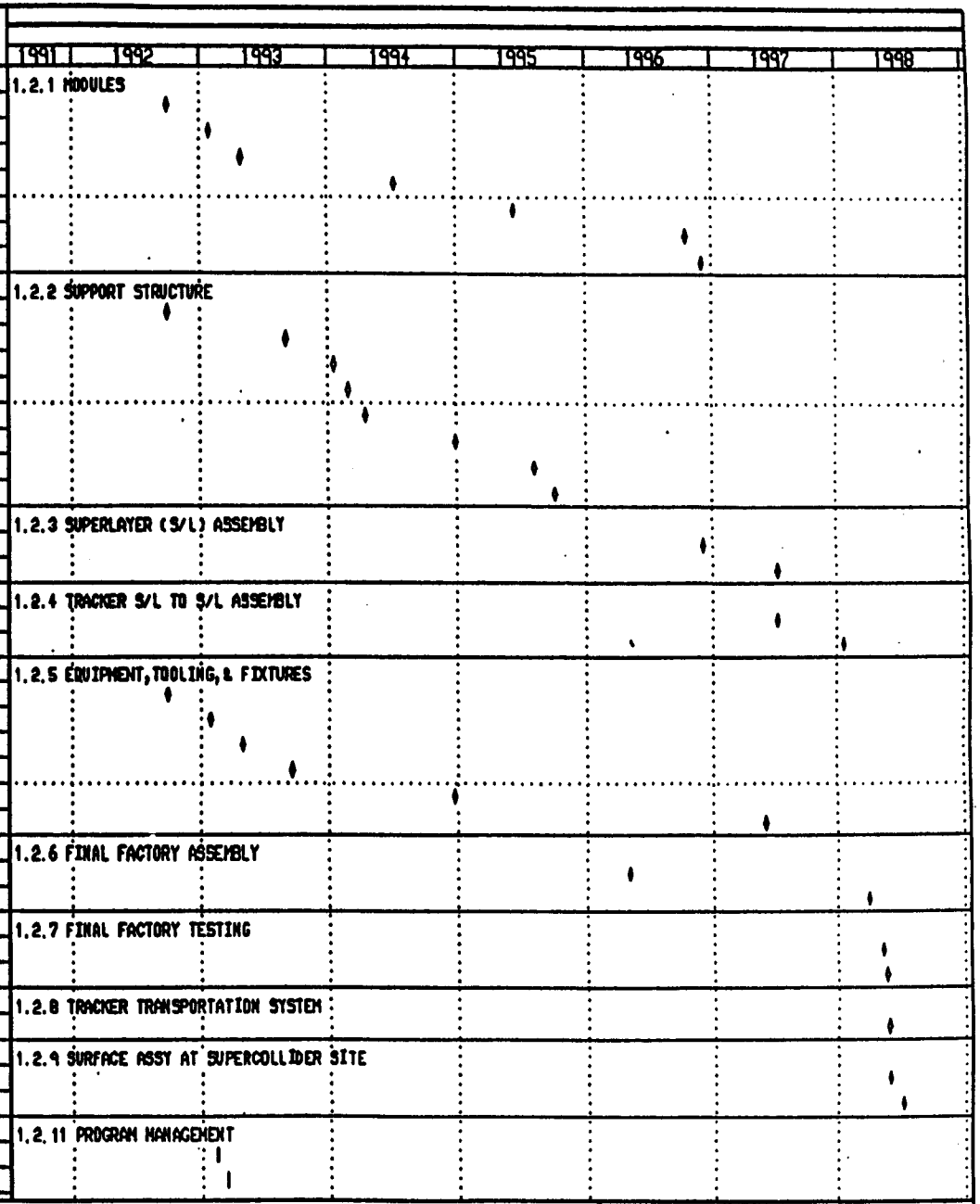

Activity Bar/Early Datas
Critical Activity
Progress Bar

WESTINGHOUSE DEPARTMENT TMO
1.2 CENTRAL TRACKER
MILESTONES

Sheet 1 of 2

Project Start : 1JUL91
Project Finish: 18JAN99

Data Date: 1JUL91
Plot Date: 16AUG91

TRAK-SSC DETECTOR CENTRAL TRACKER REV.2

Date	Revision	Checked	Approved

ACTIVITY ID	ACTIVITY DESCRIPTION	EARLY START	EARLY FINISH
B10000.01	s1 MODULE PREL.DESIGN REVIEW	25MAR93	26MAR93
B10000.05	s5 SUPPORT STRUCT.INTERIM DESIGN REVIEW	27APR93	28APR93
B10000.02	s2 MODULE INTERIM DESIGN REVIEW	11MAY93	12MAY93
B10000.08	s8 MFG,TOOLING & TESTING INTERIM DESIGN REVIEW	9JUN93	10JUN93
B10000.06	s6 SUPPORT STRUCT. FINAL DESIGN REVIEW	21JUN93	22JUN93
B10000.03	s3 MODULE FINAL DESIGN REVIEW	18AUG93	19AUG93
B10000.09	s9 MGF,TOOLING & TESTING FINAL DESIGN REVIEW	6OCT93	7OCT93
B10000.10	s10 TRACKER INST./TEST PREL.DESIGN REVIEW	14DEC95	20DEC95
B10000.11	s11 TRACKER INST./TEST INTERIM DESIGN REVIEW	5FEB96	6FEB96
B10000.12	s12 TRACKER INST./TEST FINAL DESIGN REVIEW	14JUN96	17JUN96
C12000	Dsgn Prototype Modules	15JUL91	23SEP91
S000	START PROTOTYPE DSGN	15JUL91	
C11000	Dsgn Prototype Cylinder	24SEP91	2MAR92
C13000	Dsgn Prototype Cylinder Module Interface	24SEP91	20JAN92
C14000	Dsgn Prototype Support Structure	24SEP91	17FEB92
C1200A	Assy & Test Prototype Modules	23DEC91	30SEP92
C1400A	Assy Prototype Support Structure	18MAY92	30DEC93
C1300A	Assy & Test Prototype Cylinder Module Interface	18OCT92	31AUG93
F000	COMPLETE PROTOTYPES		30DEC93
S020	START OF INSTALLATION	1MAY97	
F020	END CENTRAL TRACKER INSTALLATION & TEST		18JAN99
S021	START SETUP FOR TRACKER TESTING	28OCT98	
F021	FINISH FOR TRACKER TESTING		18JAN99

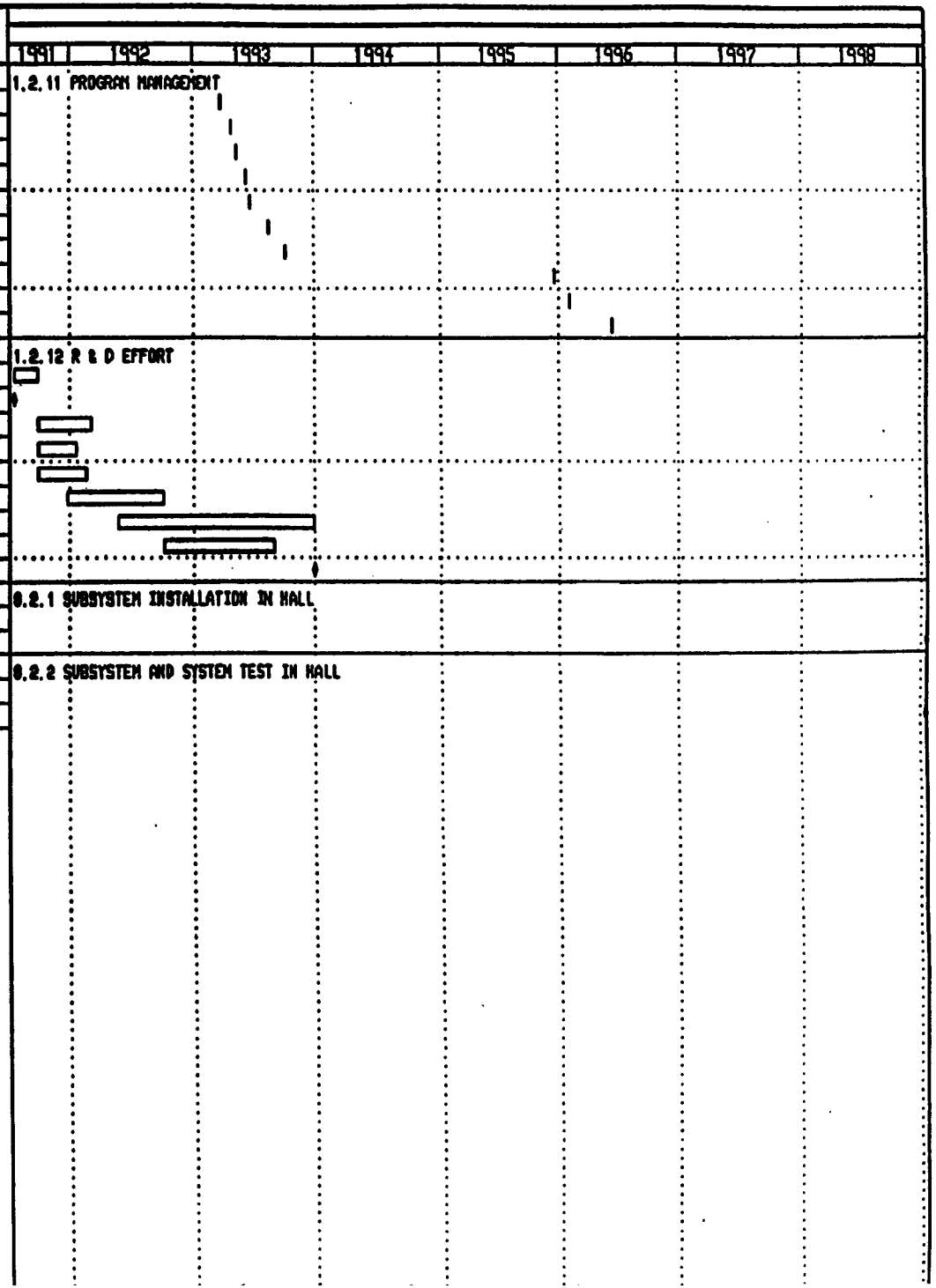

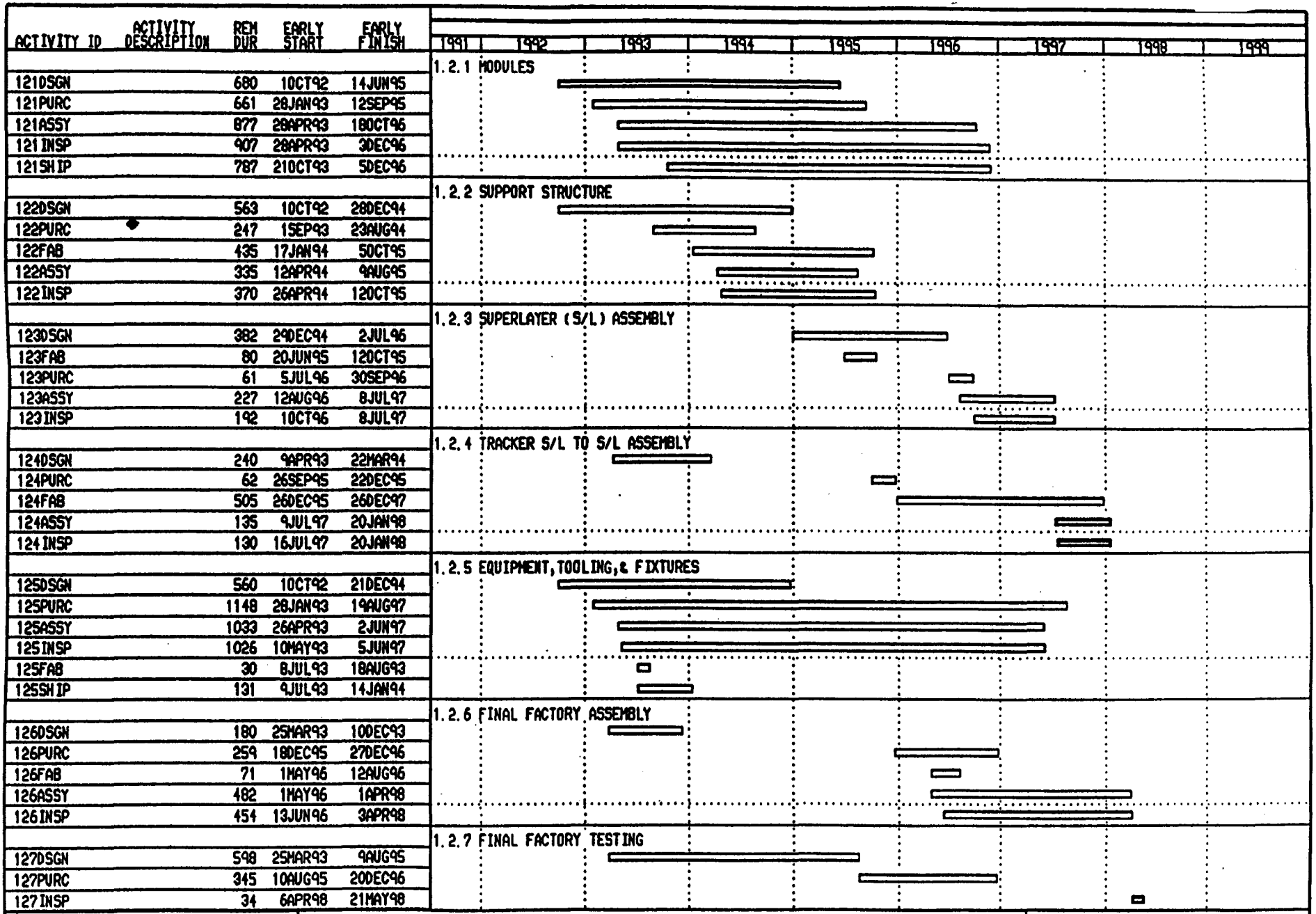

Activity Bar/Early Dates
Critical Activity
Progress Bar

WESTINGHOUSE DEPARTMENT TMO
1.2 CENTRAL TRACKER
WBS LEVEL 3 SUMMARY BY FUNCTION,ES

Sheet 1 of 2

Project Start : 1JUL91
Project Finish: 18JAN99

Data Date: 1JUL91
Plot Date: 16AUG91

TRK-SSC DETECTOR CENTRAL TRACKER REV.2

Date	Revision	Checked	Approved

ACTIVITY ID	ACTIVITY DESCRIPTION	REM DUR	EARLY START	EARLY FINISH
127TST		0	14MAY98	13MAY98
127ASSY		4	14MAY98	19MAY98
127TEST		0	22MAY98	21MAY98
128DSGN		30	10AUG95	21SEP95
128PURC		63	23FEB98	21MAY98
128SHIP		5	22MAY98	28MAY98
129DSGN		608	21MAY93	19OCT95
129PURC		367	24SEP96	10MAR98
129FAB		90	26NOV96	4APR97
129INSP		284	1MAY97	16JUN98
129ASSY		129	6JAN98	8JUL98
12ADSGN		150	30NOV92	6JUL93
12APURC		262	26APR93	9MAY94
12AFAB		50	29JUL93	7OCT93
12AMGMT		1092	17SEP93	20JAN98
12BMGMT		1583	10CT92	18JAN99
12BDSGN		1040	11FEB93	31MAR97
12CDSGN		160	15JUL91	2MAR92
12CPURC		172	24SEP91	26MAY92
12CASSY		509	23DEC91	30DEC93
12CFAB		0	3JAN94	30DEC93
821DSGN		1128	28OCT93	22APR98
821FAB		50	7NOV96	22JAN97
821ASSY		431	1MAY97	18JAN99
821PURC		90	28NOV97	8APR98
821INSP		155	2APR98	9NOV98
822DSGN		180	27JUN95	13MAR96
822ASSY		14	28OCT98	16NOV98
822TST		54	28OCT98	18JAN99
822INSP		49	4NOV98	18JAN99

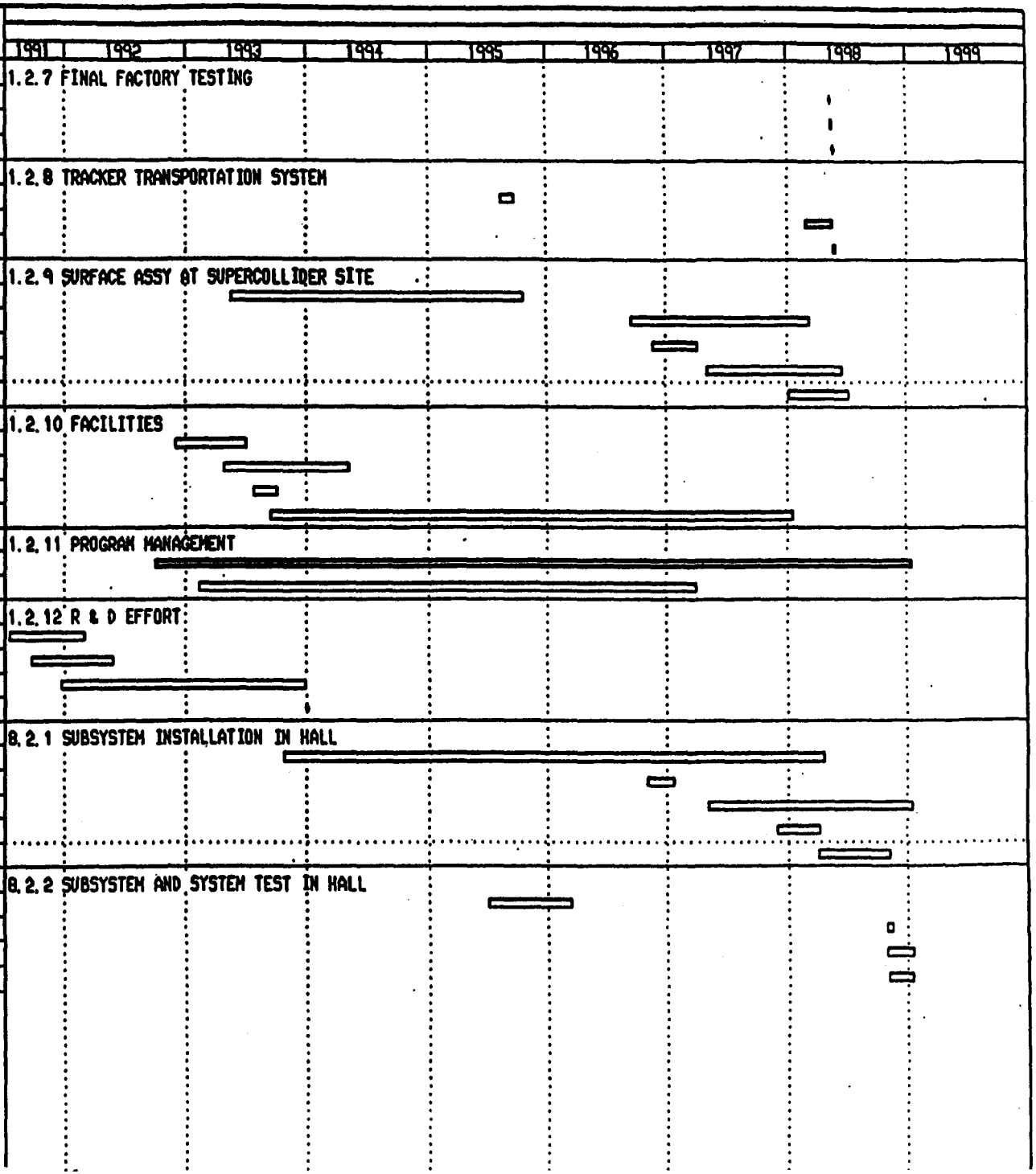

CENTRAL AND FORWARD TRACKING SUBSYSTEM

SCHEDULE AND TASKS IN FISCAL YEAR 1992

ACTIVITY ID	ACTIVITY DESCRIPTION	REM DUR	EARLY START	EARLY FINISH
SA	START PROOF OF PRINCIPLES	0	10CT91	
A11	Module Assembly	80	10CT91	27JAN92
A12	Structural Support Assembly	80	28JAN92	19MAY92
A13	Module to support Assembly	80	10CT91	27JAN92
A14	Surface Assembly (SSCL)	40	20MAY92	15JUL92
A15	Installation (SSCL)	40	16JUL92	9SEP92
A15M	COMPLETE Installation REPORT	0		9SEP92
A2M	COMPLETE CYLINDER REPORT	0		6APR92
A21	Develop Lamina, Compositions, Thickness	45	29OCT91	6JAN92
A22	Develop End Closeouts	45	7JAN92	9MAR92
A23	Develop manufacturing Process	20	10MAR92	6APR92
A31	Develop Alignment Techniques	64	10CT91	3JAN92
A32	Structure, Modules, Interface, SILI, Internal	30	6JAN92	14FEB92
A33	Identify Optical Align Tools/Fixturing	64	17FEB92	15MAY92
A34	Write Procedures and Specs	64	6JAN92	2APR92
A34M	COMPLETE ALIGNMENT METHODS REPORT	0		15MAY92
A41	Develop Trigger Geometry	40	18MAY92	13JUL92
A42	Develop layout Program for Trigger Tracks	50	14JUL92	21SEP92
A5	Fiber Replacement	40	14JUL92	7SEP92
A6	Conceptual Design report	15	1SEP92	21SEP92
AE	END PROOF OF PRINCIPLES	0		21SEP92
A7	SDC meetings - 6 TRIPS	255	10CT91	30SEP92

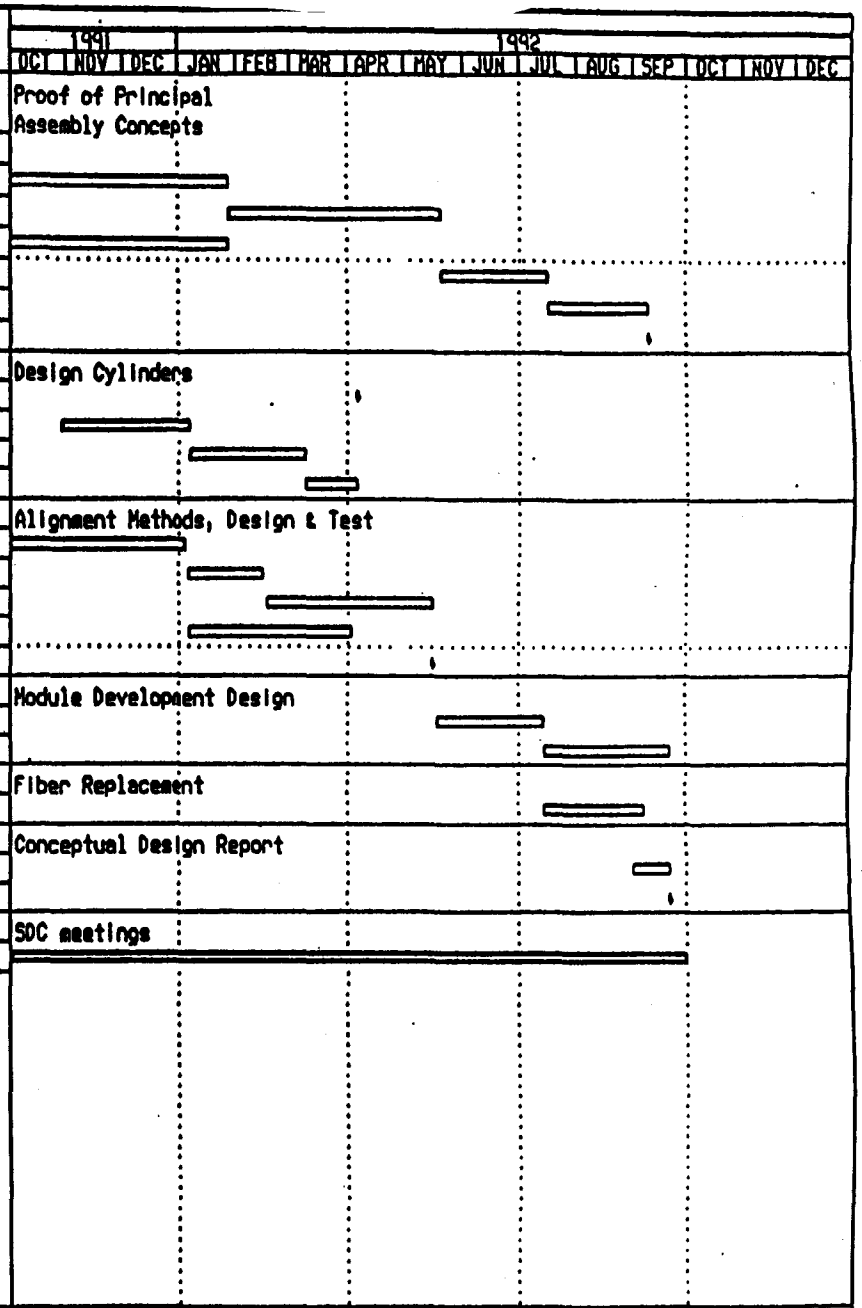

Activity Bar/Early Dates
Critical Activity
Progress Bar

Primavera Systems, Inc. 1984-1991

SUPERCOLLIDER LABORATORY
CENTRAL TRACKER
WORK BREAKDOWN

Project Start : 10CT91
Project Finish: 30SEP92

Sheet 1 of 3

Date Date: 10CT91
Plot Date: 23SEP91

CERT-1992 ENGINEERING EFFORTS

Date	Revision	Checked	Approved

ACTIVITY ID	ACTIVITY DESCRIPTION	REM DUR	EARLY START	EARLY FINISH
SB	START THE SDC PROPOSAL	0	10CT91	
B12	Analysis and documentation of Structure	80	10CT91	27JAN92
B13	FEA, Thermal & Humidity	24	28JAN92	28FEB92
B21	Establish Calorimeter Interface	40	2MAR92	27APR92
B22	Develop Kinimatic Mount System	40	28APR92	22JUN92
B31	Select Strut Material, size & design	20	10CT91	28OCT91
B32	Design Rings and Select Material	25	29OCT91	4DEC91
B33	Develop Flange Cylinder Connections	25	5DEC91	13JAN92
B34	Size Hardware material & design	25	14JAN92	17FEB92
B35	Design for Fabrication & Assy	25	18FEB92	23MAR92
B35M	Complete Efforts for Support Flanges	0	24MAR92	23MAR92
B41	Module Assembly	80	10CT91	27JAN92
B42	Structure and Module Install	80	5NOV91	2MAR92
B51	Internal Onboard Utilities	32	10CT91	13NOV91
B511	Design Plumbing	24	10CT91	1NOV91
B512	Write Spec,Quote,& Schedule	8	4NOV91	13NOV91
B52	External Regeneration Drift Gas System Utilities	53	4NOV91	22JAN92
B521	Concept Regeneration System	15	14NOV91	6DEC91
B522	Concept Plumbing System	10	9DEC91	20DEC91
B523	Write Spec,Quote,& Schedule	20	23DEC91	22JAN92
B6	SDC Proposal Engineering Efforts	83	6JAN92	30APR92
BE	END OF CONCEPTUAL DESIGN FOR PROPOSAL	0	3MAR92	2MAR92
B7	Costing for Proposal	42	3MAR92	30APR92
B7M	Complete costing for Proposal	0		30APR92

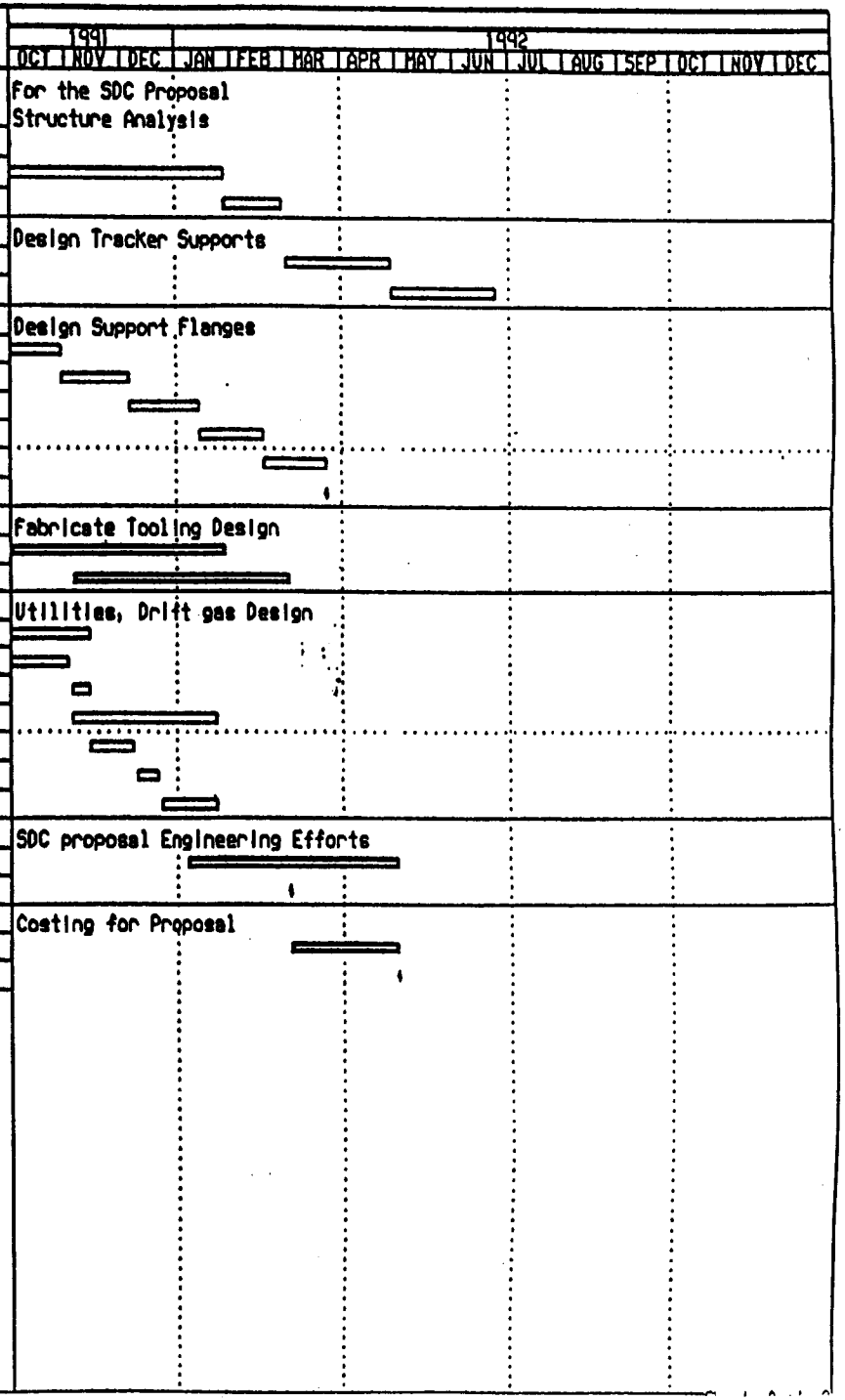

ACTIVITY ID	ACTIVITY DESCRIPTION	REM DUR	EARLY START	EARLY FINISH
C1	Prototype Sector (Build)	120	10CT91	23MAR92
SC	START STAY ON SCHEDULE	0	10CT91	
CE	END	0		23MAR92
C11	Structure Design and Fab	40	10CT91	25NOV91
C12	Flanges Design and Fab	40	26NOV91	27JAN92
C13	Module Interface Attachments	40	28JAN92	23MAR92

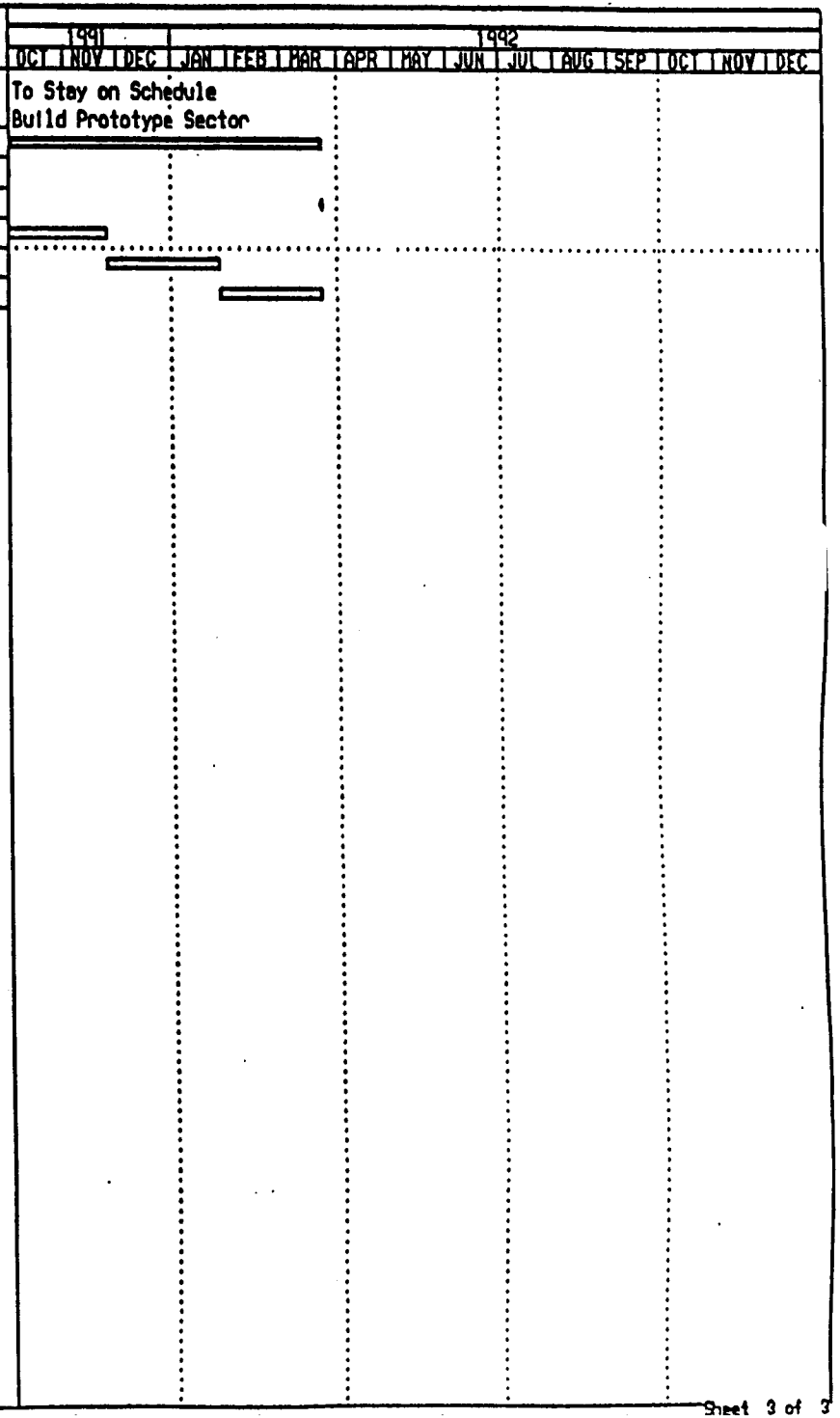

IX. CONCLUSIONS

We have presented the conceptual design for a central outer tracking system for the SDC based on superlayers of straw tube modules. This tracking system is integrated with the silicon inner tracker, and will be integrated with the intermediate angle tracking system once that design has been formulated. Performance studies of the combined silicon and outer tracking system have begun but are by no means complete. This is the goal for the next few months. Based on the studies so far, we believe that this tracking system will meet the requirements for the SDC tracking system.

The straw module tracking system provides a low-mass system with the capability for sufficiently precise alignment of the wires, modular construction, and maintainability over the life of the SDC. The module design has made great progress. Short modules have already been constructed and are being tested at several institutions. A one-meter-long carbon fiber composite shell is almost complete and will be assembled into a working module. A four-meter-long shell will be complete by the end of 1991. By the time of the SDC proposal we expect to have a working four-meter module.

The support structure for the superlayers of modules is composed of carbon fiber cylinders and spaceframe. Considerable engineering has yet to be done on these structures, as well as on the mechanism for attaching the modules to the support structure. Work on these will take place during 1992. We will need to construct prototypes of the elements of the support structure.

Great progress has been made in the front end and trigger electronics, but tests with prototypes on actual straw tube modules are just beginning. We still have quite a bit to learn in this area. One of our main goals for the next year will be to establish a low-gain operating condition for prototype modules with prototype electronics. The connection from the anode wires to the electronics must be made with low cross talk in order to achieve this goal. In addition, we need to construct a prototype system of enough modules to determine whether system electrical interference will be at a tolerable level. We had planned to build a system of approximately two thousand wires for this purpose. Tests of the high-p_T track segment trigger electronics are also progressing but more work is needed there as well.

During the next few months we will also have to make more progress in the design of utilities and addressing the safety aspects of the tracking system. An estimate of the cost has been presented here, but this work is ongoing as better estimates are obtained. We have presented a schedule for the construction of the tracking system.

In summary, the straw module outer tracking system should meet the requirements for the SDC, and we expect to make it a reality during the coming years.

REFERENCES

1. SDC Tracking Group (W. T. Ford, ed.), "Requirements for the SDC Tracking System," SDC-91-XXXXX (1991).

2. A. Seiden, "Systematic Errors and Alignment for Barrel Detectors," SCIPP 91/20, SDC-91-00021, March 1991.

3. H. O. Ogren, "Straw and Module Placement," IUHEE 91-4, SDC-91-xxxx, April 23, 1991.

4. R. Foster *et al.*, "Self Centering Measurement for an 8 Layer Trapezoid," IUHEE 91-7, SDC-91-00056 (1991).

5. J. Matthews, ed., "Report of the Task Force on Impact of Material in Tracking Volume," SDC-91-xxxx, September, 1991.

6 . "Radiation Levels in the SSC Interaction Regions," Task Force Report, ed. D. E. Groom, SSC-SR-1033, SSC Central Design Group (1988).

7. H. Ogren, "Recent Developments in Wire Chamber Tracking at SSC," IUHEE 90-17, SDC-90-00138, *Proceedings of the Symposium on Detector Research and Development for the Superconducting Super Collider, Fort Worth, Texas, Oct. 15-18, 1990, World Scientific Publishing Co.*, p. 40.

8. "Report of the Task Force on R&D Directions for Tracking," SDC-91-00055, April, 1991.

9. "Straw Tube Superlayer Design Concepts," Prepared for SDC Tracker Review, University of Colorado, Duke University, Indiana University, Oak Ridge National Laboratory and Westinghouse Science and Technology Center, SDC-91-00062, May 20, 1991.

10. Silicon Tracking Conceptual Design Report, November, 1991.

11. Martyn Corden's fitter.

12. R. Bouclier, *et al.*, Nucl. Inst. and Methods, **A283** 509 (1990).

13. G. Godfrey, "The Tracking Chamber for the Crystal Ball Detector," unpublished.

14. P. Baringer, *et al.*, Nucl. Inst. and Methods **A254** 542 (1987); W. W. Ash, *et al.*, Nucl. Inst. and Methods, **A261** 399 (1987); W. T. Ford, *et al.*, Nucl. Inst. and Methods **A255** 486 (1987).

15. D. G. Cassel, G. G. Hanson, *et al.*," Report of the Central Tracking Group," *Proceedings of the 1986 Summer Study on the Physics of the Superconducting Supercollider, edited,by R. Donaldson and J. Marx, Snowmass, CO, 1986*, p.377.

16. J. Fischer *et al.*, Nucl. Inst. and Methods **A238** 249 (1985).

17. D. E. Groom, Nucl. Inst. and Methods, **A279** 1 (1989).

18. H. Sadrozinski, Presentation at SDC Collaboration Meeting, 11 Feb 1991; T. Gabriel, Presentation at the same meeting.

19. J. A. Kadyk, J. Va'vra and J. Wise, Nucl. Inst. and Methods **A300** 511 (1991); J. A. Kadyk, J. Wise and J. Va'vra, "Effects of Cathode and Wall Materials and Water Vapor on Straw Tube Aging," SDC note SDC-91-00093.

20. R. Openshaw *et al.*, "Etching of Anode Wire Deposits with CF_4/Isobutane (80:20) Avalanches," *Proceedings of the Symposium on Detector Research and Development for the Superconducting Super Collider, Fort Worth, Texas, Oct. 15-18, 1990, World Scientific Publishing Co., p. 231.*

21. J. Wise, J. A. Kadyk and D. W. Hess, "Chemical Modeling of Aging Processes in CF_4/Isobutane Gases," SDC Note SDC-91-00094.

22. P. LeDu *et al.*, "Experimental Study of High Flux in Multiwire Proportional Chambers,",CERN EP Internal Report 77-11, 7 Sept 1977.

23. H. Ogren *et al.*, "Wire Stability Tests on 4 mm Straw Chambers," SDC Note SDC-90-00055, 9 Feb. 1990.

24. H. Iwasaki, Presentation at SDC Collaboration Meeting, Oak Ridge, 11 Feb 1991.

25. L. G. Christophorou *et al.*, Nucl. Inst. and Methods, **163** 141 (1979); M. S. Naidu and A. N. Prasad, J. Phys. **D5** 983 (1972); S. R. Hunter, J. G. Carter and L. G. Christophorou, J. Appl. Phys. **58** 3001 (1985); B. Schmidt and S. Polenz, Nucl. Inst. and Methods **A273** 488 (1988); J. Va'vra *et al.*, Presented to the Fifth Pisa Meeting on Advanced Detectors, May 26, 1991.

26. R. Openshaw *et al.*,IEEE Trans. Nucl. Sci., **NS-36** 567 (1989); T. Yamashita *et al.*, Nucl. Inst. and Methods **A283** 709 (1989); J. Va'vra, *et al., ibid.*

27. S. R. Hunter, J. G. Carter and L. G. Christophorou, *ibid.*

28. H. Ogren, "Progress Report on 4mm Straw Chambers," Indiana University, IUHEE - 90-9.

29. H. Ogren, "X-Ray Measurements of Straw Tube Modules" SDC note in preparation.

30..R. Foster, *et al.*, 'Self Centering Measurement for 8 Layer Trapezoid", IUHEE-91-7.

31. Y. Arai, H. Ikeda, F. M. Newcomer, R. Van Berg, Y. Watase and H. H. Williams, "SDC Straw Tracking Electronics Preliminary Conceptual Design Report - Draft Version 2.0," 1991.

32. "Progress Report for the Trigger for a Fast Solenoidal SSC Detector," SSC Subsystem Report, Chicago and Michigan, October 1991.

33. SDC Trigger Preliminary Conceptual Design, W. Smith *et al.*, August 1991.

34. J. Chapman and J. Mann, "Triggering in the SDC Using Mean Timer Synchronizers with Straw Drift Tubes," Conference on Electronics for Future Colliders, LeCroy Corporation, May (1991).

35. SDC Task Force Report on the Effects of a Non-uniform Field,
Takahiko Kondo, KEK (1991).

36. J. Chapman, "Drift Tube Synchronizers," University of Michigan Preprint, UM-HE-89-10, June, 1989.

VI.4. Appendices

VI.4.1 Five Superlayer Design Data

VI.4.2 Radation Length Study

VI.4.3 Mandrel Dead Weight Deflection Analysis

VI.4.4 Finite Element Analysis Six Cylinder Tracker

VI.4.5 Finite Element Analysis Five Cylinder Tracker

CENTRAL AND FORWARD TRACKING SUBSYSTEM

FIVE SUPERLAYER MODULE DESIGN DATA

Westinghouse
Science & Technology Center

Table. Central Outer Tracker Design

Superlayer	Radius (m)	Straws/Layer	Modules	Layers/Superlayer	z_{max} (m)	Stereo Angle (°)
1	0.708	1112	84	6	2.80	0
2	1.04	1640	124	6	3.20	+3
3	1.35	2120	160	8 (trigger)	3.90	0
4	1.48	2328	176	6	3.95	-3
5	1.61	2536	192	8 (trigger)	3.95	0

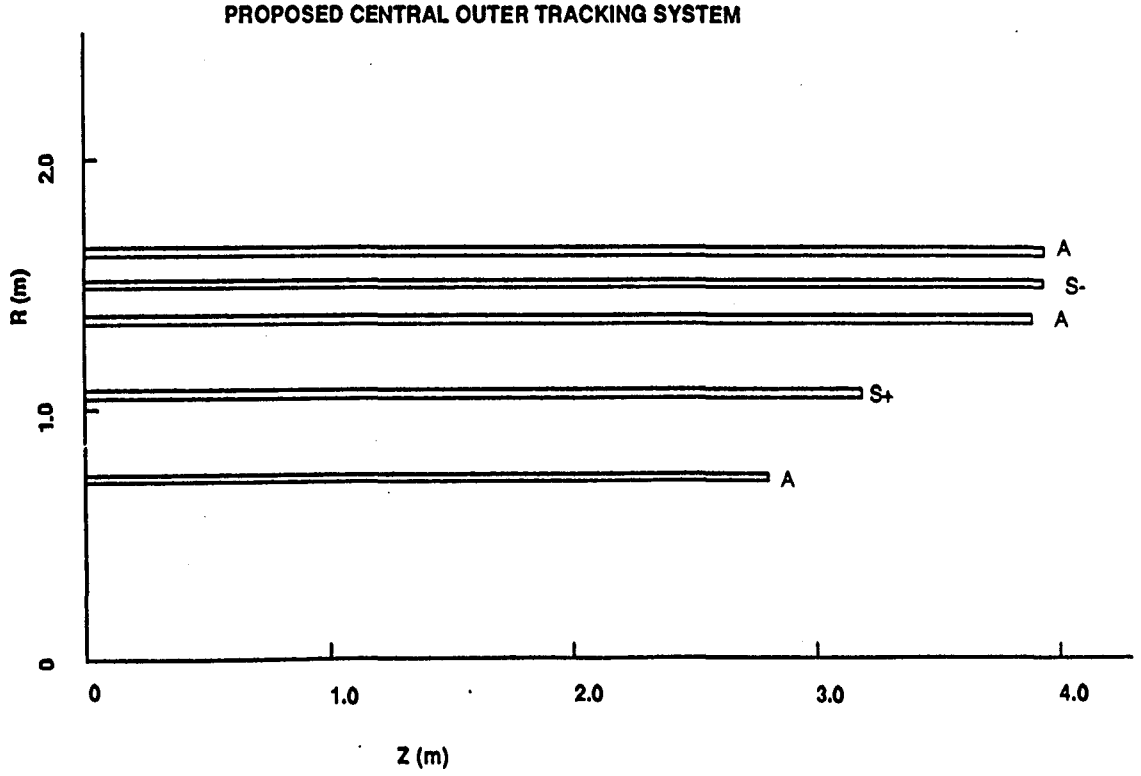

Revised Outer Tracker Parameters

This revision is composed of a of five superlayers of straws and will define these superlayers with minimum radial displacement and minimum module side clearance, this attempt has the modules mounted to shim rings located on concentric cylinders.

Baseline information from Gail relating to this structure

Suprlyr	Radius cm	straws/lyr	rows/mod	zmax	stereo
#1	70.8	1112	6	280.0	0 deg
#2	104.0	1640	6	320.0	+3 deg
#3	135.0	2120	8 trig	390.0	0 deg
#4	148.0	2328	6	395.0	-3 deg
#5	161.0	2536	8 trig	395.0	0 deg

Maximum Tracker radius = 167.5 cm

Point of rotation for stereo layers is now defined as (zmax - zmin) /2.

Description of Flat, Axial Trapezoidal section modules, (superlayer #1)

Each trapezoid is (N) straws wide on the long side and each succeding layer contains one straw less. The height is (L) straws high with the straws nested. The module has a epoxy-graphite wrapper (T) cm thick, (T1) equals the thickness of the top and bottom of the module box. (T2) is the sside wall thickness of the module box. (F1) and (F2) equals the foam core thickness of the top, bottom and sides of the box. The straw diameter is d) cm. These trapezodial modules are alternated in position and are spaced (sp) cm from the adjoining modules. Both the radial position (D) of the alternate modules and the number of straws (N) may be varied to change the superlayer radius. Trapezodial modules must be added in groups of two to make large radius changes such as between superlayers. Each module contains (CH) straws.

Flat Axial Module Defination (superlayer #1)

```
sp := 0.1                    (space between modules, cm)
d := .40437                  (straw diameter, cm)
D := 0.5                     (radial difference of alternating modules,
T := 0.0127                  (Wrapper thickness. cm)
T1 := 0.424                  (thickness top and bottom of module box)
T2 := 0.125                  (thickness sides of module box)
F1 := T1 - (2·T)
F1 = 0.399                   (thickness of box foam core, top and bottom)
F2 := T2 - (2·T)
F2 = 0.1                     (Thickness of box foam core, sides)
N := 29                      (number of straws, long side)
L := 6                       (number of straws high)
H := ((L - 1)·d·.866) + d + (2·T1)
H = 3.003                                  (height of module, cm
LS := N·d + (2·T2)
LS = 11.977                                (length of module long side, cm)
SS := (N - (L - 1))·d + (2·T2)
SS = 9.955                                 (length of module short side, cm)
U := LS + SS + sp - (D·.5774)
U = 21.743                                 (total length of module pair, cm)
```

$$CH := L \cdot \left[N - \frac{L - 1}{2} \right] \qquad CH = 159$$ (straws per module)

Description of Curved Trapezoidal Module, (superlayer #3 and #5)

Superlayers #3 and #5 are trigger layers, their modules are eight straws high. The long and short sides, (top and bottom) are curved to the same radius as their distance from the beam centerline. Other than the curved top and bottom and increased layers of straws these modules are simular to the flat Ones and will be incorporated into the tracker like other axial layers.

Curved Axial Element Definitions that may be different from above.

spc := 0.1 (space between modules, cm)
Dc := 0.0 (radial difference of alternating modules, cm)
Nc := 30 (number of straws, long side)
Lc := 8 (number of straws high)
Hc := ((Lc - 1)·d·.866) + d + (2·T1)
Hc = 3.704 (height of module, cm)
LSc := Nc·d + (2·T2)
LSc = 12.381 (length of module,long side cm)
SSc := (Nc - (Lc - 1))·d + (2·T2)
SSc = 9.551 (length of module, short side)
Uc := LSc + SSc + spc - (Dc·.5774)
Uc = 22.032 (total length of module pr cm)

$$CHc := Lc \cdot \left[Nc - \frac{Lc - 1}{2} \right] \qquad CHc = 212$$ (straws per module)

Description of Trapezodial Stereo Modules, (superlayers #2 & #4)

The need is to generate stereo modules that have a trapezodial cross section and provide uniform spacing between modules.

The rotation of the stereo module is on a line starting at the beam axis and passing through the center of the module. To achieve uniform stereo module spacing the modules with the long side up are rotated 3.00 degrees and the modules with the short side up are rotated 2.714 degrees.

Definitions that may apply only to this set of modules.

sps := .1 (space between modules, cm)
Ds := 0.0 (radial difference of alternating modules, cm)
Ns := 29 (number of straws, long side)
Ls := 6 (number of straws, high)
Hs := ((Ls - 1)·d·.866) + d + (2·T1)
Hs = 3.003 (height of module, cm)
LSs := Ns·d + (2·T2)
LSs = 11.977 (length of module,long side,cm)
SSs := (Ns - (Ls - 1))·d + (2·T2)
SSs = 9.955 (length of module short side,cm)
Us := LSs + SSs + sps - (Ds·.5774)
Us = 22.032 (total length of module pr cm)

$$CHs := Ls \cdot \left[Ns - \frac{Ls - 1}{2} \right] \qquad CHs = 159$$ (straws per module)

Superlayer #1 Axial

a := 20 module pairs

$$is1 := \frac{a \cdot U}{2 \cdot \pi}$$

inside radius (is1), short side up		is1 = 69.21
outside radius (os1), short side up	os1 := is1 + H	os1 = 72.213
inside radius (i11), long side up	i11 := is1 + D	i11 = 69.71
outside radius (o11), long side up	o11 := i11 + H	o11 = 72.713
mean radius (m1),	m1 := .5·(o11 - is1) + is1	m1 = 70.961

Superlayer #2 Stereo

b := 30 module pairs

AT MODULE CENTERS

$$is2 := \frac{b \cdot Us}{2 \cdot \pi}$$

inside radius (is2), short side up		is2 = 105.193
outside radius (os2), short side up	os2 := is2 + Hs	os2 = 108.196
inside radius (i12), long side up	i12 := is2 + Ds	is2 = 105.193
outside radius (o12), long side up	o12 := i12 + Hs	o12 = 108.196
mean radius (m2)	m2 := .5·(o12 - is2) + is2	m2 = 106.695

AT MODULE ENDS Rotated 3.00 degrees, ac := .0524 Radians

module length mlb := 320.0 cm

distance from module centerline at ends to centerline after rotation

$$ABb := \frac{LSs}{2} + \frac{mlb}{2} \cdot \tan(ac) \qquad ABb = 14.38$$

outside radius, (o12r), long side up at the module centerline

$$o12r := \sqrt{(o12)^2 + (ABb)^2} \qquad o12r = 109.148 \quad cm$$

delta radius = delb := o12r - o12 delb = 0.951

inside radius, short side up	is2r := is2 + delb	is2r = 106.145
outside radius, short side up	os2r := os2 + delb	os2r = 109.148
inside radius, long side up	i12r := i12 + delb	i12r = 106.145
outside radius, long side up	o12r := o12 + delb	o12r = 109.148
mean radius, rotated	m2r := m2 + delb	m2r = 107.646

Superlayer #3 Axial Trigger

c := 38 module pairs

$$is3 := \frac{c \cdot Uc}{2 \cdot \pi}$$

inside radius, short side up		is3 = 133.245
outside radius, short side up	os3 := is3 + Hc	os3 = 136.948
inside radius, long side up	i13 := is3 + Dc	i13 = 133.245
outside radius, long side up	o13 := i13 + Hc	o13 = 136.948
mean radius	m3 := .5·(o13 - is3) + is3	m3 = 135.097

Superlayer #4 Stereo
d := 42 module pairs

AT MODULE CENTERS

$$is4 := \frac{d \cdot Us}{2 \cdot \pi} \qquad is4 = 147.27$$

inside radius, short side up		is4 = 147.27
outside radius, short side up	os4 := is4 + Hs	os4 = 150.274
inside radius, long side up	il4 := is4 + Ds	il4 = 147.27
outside radius, long side up	ol4 := il4 + Hs	ol4 = 150.274
mean radius	m4 := .5·(ol4 - is4) + is4	m4 = 148.772

AT MODULE ENDS Rotated 3.00 degrees, ac := .0524 Radians
module length mld := 395 cm
distance from module centerline at ends to centerline after rotation

$$ABd := \frac{LSs}{2} + \frac{mld}{2} \cdot \tan(ac) \qquad ABd = 16.347$$

outside radius, (ol4r), long side up at the module centerline

$$ol4r := \sqrt{(ol4)^2 + (ABd)^2} \qquad ol4r = 151.16 \quad cm$$

delta radius = deld := ol4r - ol4 deld = 0.886

inside radius, short side up	is4r := is4 + deld	is4r = 148.157
outside radius, short side up	os4r := os4 + deld	os4r = 151.16
inside radius, long side up	il4r := il4 + deld	il4r = 148.157
outside radius, long side up	ol4r := ol4 + deld	ol4r = 151.16
mean radius, rotated	m4r := m4 + deld	m4r = 149.659

Superlayer #5 Axial Trigger
e := 46 module pairs

$$is5 := \frac{e \cdot Uc}{2 \cdot \pi} \qquad is5 = 161.296$$

inside radius, short side up		is5 = 161.296
outside radius, short side up	os5 := is5 + Hc	os5 = 165
inside radius, long side up	il5 := is5 + Dc	il5 = 161.296
outside radius, long side up	ol5 := il5 + Hc	ol5 = 165
mean radius, rotated	m5 := .5·(ol5 - is5) + is5	m5 = 163.148

Total number of straws in superlayers 1 through 5, both ends

Total_1 := CH·a·4	Total_1 = 12720
Total_2 := CHs·b·4	Total_2 = 19080
Total_3 := CHc·c·4	Total_3 = 32224
Total_4 := CHs·d·4	Total_4 = 26712
Total_5 := CHc·e·4	Total_5 = 39008

Total number of straws, both ends
Total_s := Total_1 + Total_2 + Total_3 + Total_4 + Total_5
Total_s = 129744

Total number of modules in superlayers 1 through 5, both ends

modules_1 := a·4 modules_1 = 80
modules_2 := b·4 modules_2 = 120
modules_3 := c·4 modules_3 = 152
modules_4 := d·4 modules_4 = 168
modules_5 := e·4 modules_5 = 184

Total_m := modules_1 + modules_2 + modules_3 + modules_4 + modules_5
Total_m = 704 modules

Support Cylinders, graphite-epoxy skin with Rohacell foam core

skin thickness, (skcyl)
skcyl := 0.0176 cm

core thickness, (corcyl)
corcyl := 0.60 cm

cylinder thickness, (cyl)
cyl := (skcyl·2) + corcyl
cyl = 0.635 cm

Shim Rings these rings have a nominal section of 2.5 x 2.5 cm and are constructed from Rohacell foam. Shim rings used for stereo layers have a greater radial dimension at the module ends than at their centers or points of rotation.

sh := 2.5

Support Cylinder #1 (Axial)
Outside Radius S1o := is1 - sh S1o = 66.71
Inside Radius S1i := S1o - cyl S1i = 66.075

Support Cylinder #2 (Stereo)
Outside Radius S2o := is2 - sh S2o = 102.693
Inside Radius S2i := S2o - cyl S2i = 102.058

Support Cylinder #3 (Axial Trigger)
Outside Radius S3o := is3 - sh S3o = 130.745
Inside Radius S3i := S3o - cyl S3i = 130.11

Support Cylinder #4 (Stereo)
Outside Radius S4o := is4 - sh S4o = 144.77
Inside Radius S4i := S4o - cyl S4i = 144.135

Support Cylinder #5 (Axial Trigger)
Outside Radius S5o := is5 - sh S5o = 158.796
Inside Radius S5i := S5o - cyl S5i = 158.161

Shim Rings

Shim Ring set for cylinder #1 (Axial)		
Outside Radius	sh1o := il1	sh1o = 69.71
Inside Radius	sh1i := S1o	sh1i = 66.71
Radial section	sh1r := sh1o - sh1i	sh1r = 3
Shim Ring set for cylinder #2 (Stereo)		
Outside Radius	sh2o := il2 + delb	sh2o = 106.145
Inside Radius	sh2i := S2o	sh2i = 102.693
Radial section	sh2r := sh2o - sh2i	sh2r = 3.451
Shim Ring set for cylinder #3 (Trigger, Axial)		
Outside Radius	sh3o := il3	sh3o = 133.245
Inside Radius	sh3i := S3o	sh3i = 130.745
Radial section	sh3r := sh3o - sh3i	sh3r = 2.5
Shim Ring set for cylinder #4 (Stereo)		
Outside Radius	sh4o := il4 + delb	sh4o = 148.222
Inside Radius	sh4i := S4o	sh4i = 144.77
Radial section	sh4r := sh4o - sh4i	sh4r = 3.451
Shim Ring set for cylinder #5 (Trigger, Axial)		
Outside Radius	sh5o := il5	sh5o = 161.296
Inside Radius	sh5i := S5o	sh5i = 158.796
Radial section	sh5r := sh5o - sh5i	sh5r = 2.5

Radial dimensions of the Support Cylinders and Modules

Space Between Cylinders

outside radius to inside radius of next cylinder

Min to Cyl#1	S1i - 46.5 = 19.575
Cyl#1 to Cyl#2	S2i - S1o = 35.348
Cyl#2 to Cyl#3	S3i - S2o = 27.416
Cyl#3 to Cyl#4	S4i - S3o = 13.391
Cyl#4 to Cyl#5	S5i - S4o = 13.391
Cyl#5 to Max	167.5 - S5o = 8.704

Space Between Superlayer and next Cylinder

Superlayer #1 and Cyl #2	S2i - ol1 = 29.345
Superlayer #2 and Cyl #3	S3i - ol2r = 20.962
Superlayer #3 and Cyl #4	S4i - ol3 = 7.187
Superlayer #4 and Cyl #5	S5i - ol4r = 7.001
Superlayer #5 and Max	167.5 - ol5 = 2.5

Mean Radius of Superlayers, and space between them

Layer #1	m1 = 70.961	
Layer #2	m2 = 106.695	m2 - m1 = 35.733
Layer #3	m2r = 107.646	m3 - m2 = 28.402
	m3 = 135.097	
Layer #4	m4 = 148.772	m4 - m3 = 13.676
	m2r = 107.646	
Layer #5	m5 = 163.148	m5 - m4 = 14.376

Radius of Rolled Rings and Bearing Pads, Position of rolled Rings from Z = 0

Section thickness of
Rolled Rings, axial rra := 0.125
Rolled Rings, radial rrr := 0.125
Bearing pads, radial bpr := 0.125

Length of modules as per Gail
Superlayer #1 mod1 := 280
Superlayer #2 mod2 := 320
Superlayer #3 mod3 := 390
Superlayer #4 mod4 := 395
Superlayer #5 mod5 := 395

Length of cylinders = 2 * module zmax + 10
cyl1 := 10 + (2·mod1) cyl1 = 570
cyl2 := 10 + (2·mod2) cyl2 = 650
cyl3 := 10 + (2·mod3) cyl3 = 790
cyl4 := 10 + (2·mod4) cyl4 = 800
cyl5 := 10 + (2·mod5) cyl5 = 800

Axial location of rolled rings bearing surfaces = length of cylinders /2
Locations are at both + and - Z.
Ring 1 = ra1 := .5·cyl1 + bpr ra1 = 285.125
Ring 2 = ra2 := .5·cyl2 + bpr ra2 = 325.125
Ring 3 = ra3 := .5·cyl3 + bpr ra3 = 395.125
Ring 4 = ra4 := .5·cyl4 + bpr ra4 = 400.125
Ring 5 = ra5 := .5·cyl5 + bpr ra5 = 400.125

Radial position of rolled rings bearing surfaces = Support Cylinder inside radius - bearing pad radial thickness (rrr)
Ring 1 = rr1 := S1i - bpr rr1 = 65.95
Ring 2 = rr2 := S2i - bpr rr2 = 101.933
Ring 3 = rr3 := S3i - bpr rr3 = 129.985
Ring 4 = rr4 := S4i - bpr rr4 = 144.01
Ring 5 = rr5 := S5i - bpr rr5 = 158.036

Axial location of rolled rings mounting surface (back side) = bearing surface position + rrr
Ring 1 = mr1 := ra1 + rrr mr1 = 285.25
Ring 2 = mr2 := ra2 + rrr mr2 = 325.25
Ring 3 = mr3 := ra3 + rrr mr3 = 395.25
Ring 4 = mr4 := ra4 + rrr mr4 = 400.25
Ring 5 = mr5 := ra5 + rrr mr5 = 400.25

Radial position of rolled rings mounting surface (back side) = support cylinder inside radius - (rrr+bpr)
Ring 1 = rm1 := S1i - rrr - bpr rm1 = 65.825
Ring 2 = rm2 := S2i - rrr - bpr rm2 = 101.808
Ring 3 = rm3 := S3i - rrr - bpr rm3 = 129.86
Ring 4 = rm4 := S4i - rrr - bpr rm4 = 143.885
Ring 5 = rm5 := S5i - rrr - bpr rm5 = 157.911

CENTRAL TRACKER STUDY

SECTION I
SUPPORT STRUCTURE RADIATION LENGTH CALCULATIONS
STRAW MODULE RADIATION LENGTHS INCLUDED

SECTION II
SUPPORT STRUCTURE CANDIDATE MATERIAL PROPERTY TABULATION

SEPTEMBER 18,1991
(W)STC
Revised
NOVEMBER 04, 1991

SECTION I

SUPPORT STRUCTURE RADIATION LENGTH CALCULATIONS STRAW MODULE RADIATION LENGTHS INCLUDED

INTRODUCTION

The enclosed report calculates radiation lengths for a candidate design of the support structure for the SDC central tracker for the SSCL. The proposed structure can be readily adapted to except sifi, hybird, or modular straw detectors. The work includes radial and end structure calculations using a variety of materials and thicknesses. Module shell and straw radiation lengths are calculated and with estimates calculated of of module radial transitions and shim ring supports. Results are summarized in Table Number 1 and the detailed calculations follow.

SPACE FRAMES WITH CYLINDERS, RINGS AND MODULES

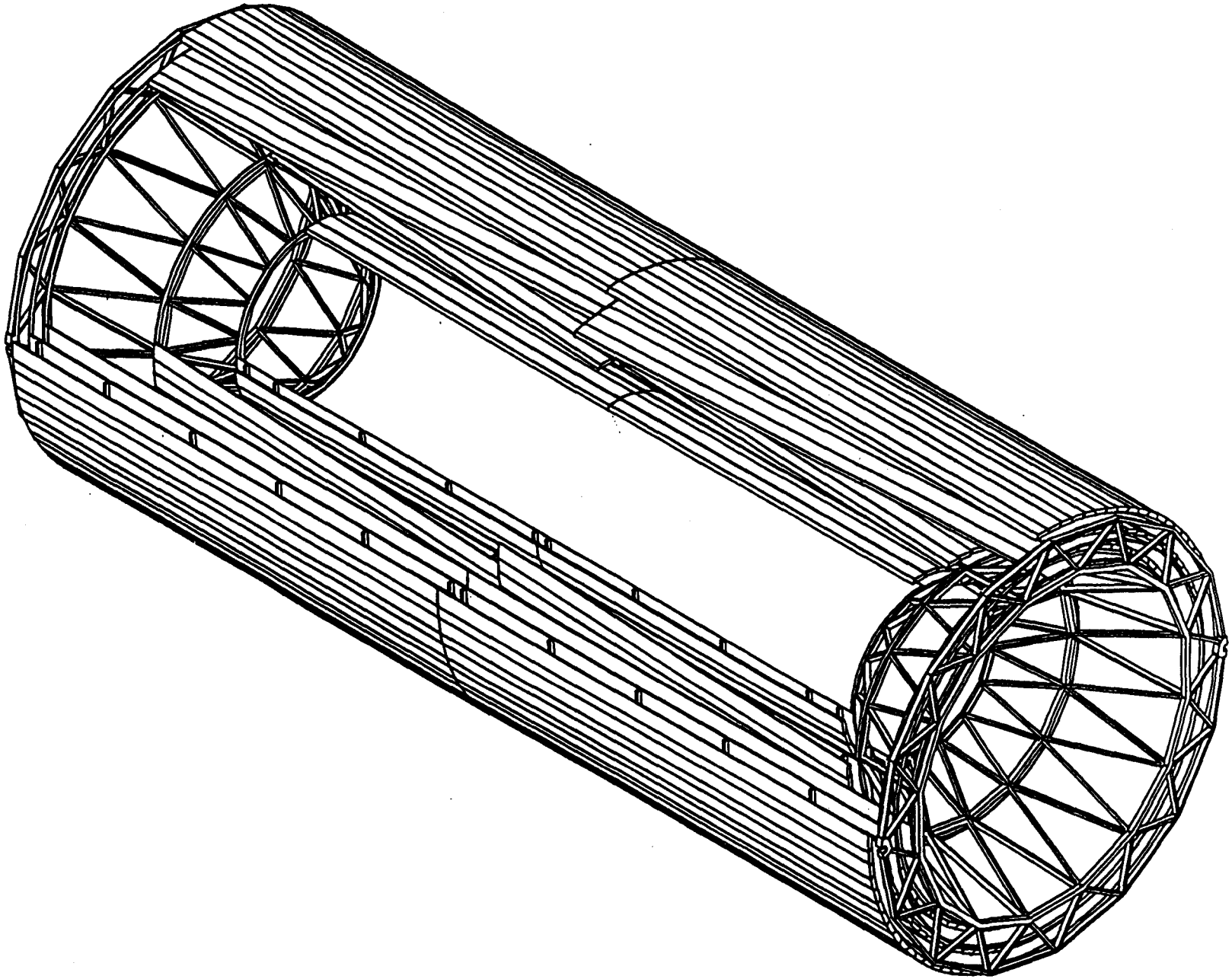

WESTINGHOUSE STC

DM 10-23-91

SUPPORT CYLINDER DIMENSIONS

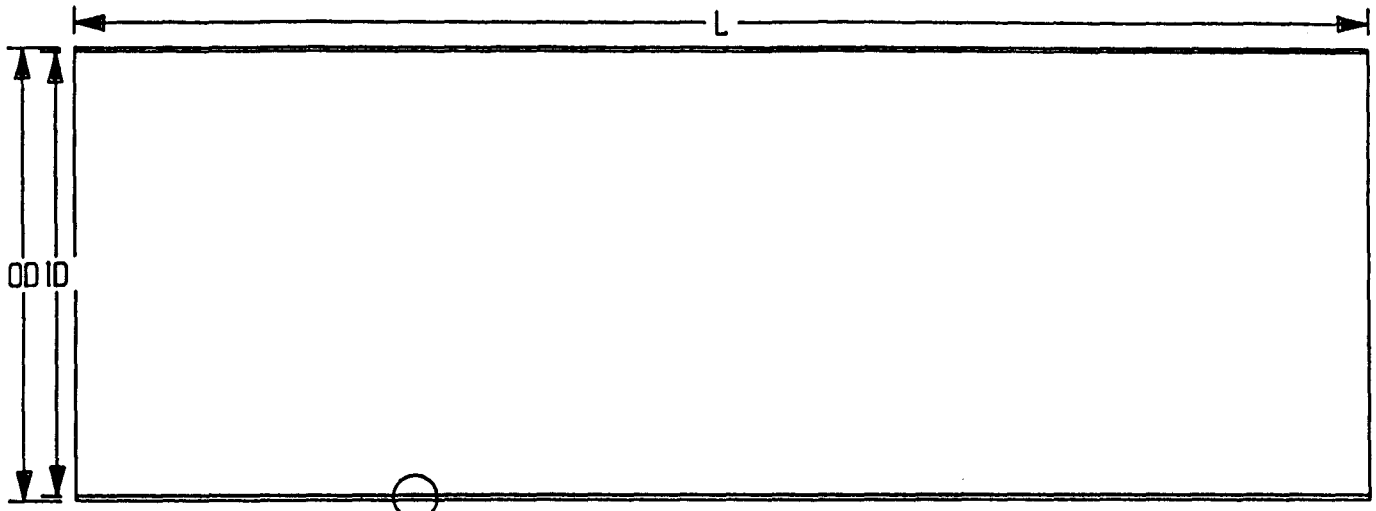

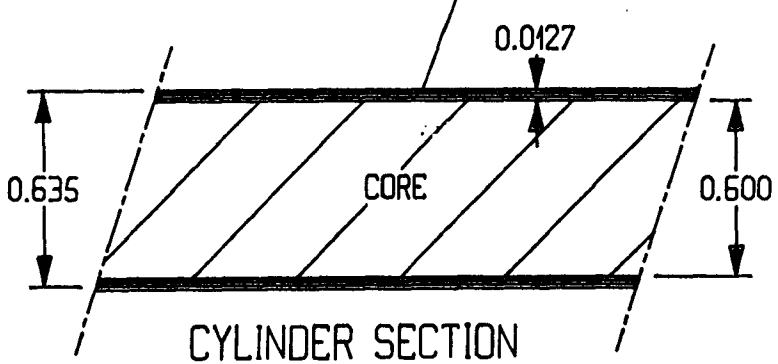

CYLINDER SECTION

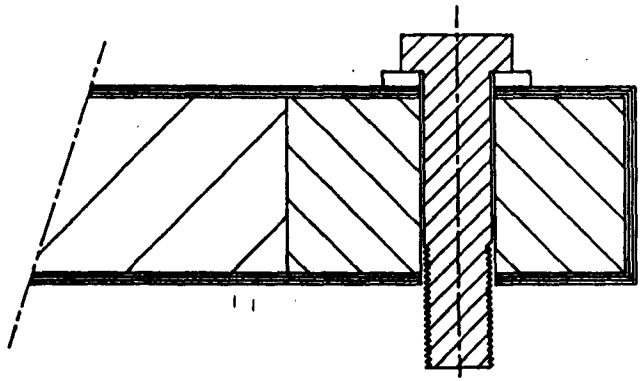

CYLINDER END SECTIONS

CYL	ID	OD	L
1	132.15	133.42	570
2	204.12	205.39	650
3	260.22	261.49	790
4	288.27	289.54	800
5	316.32	317.59	800

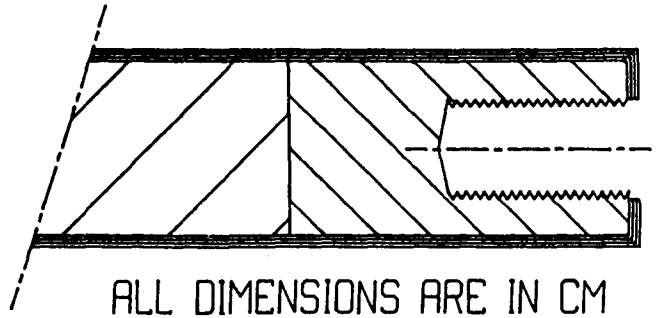

ALL DIMENSIONS ARE IN CM
NOT TO SCALE

WESTINGHOUSE STC

DM 11-5-94

SPACE F..AME

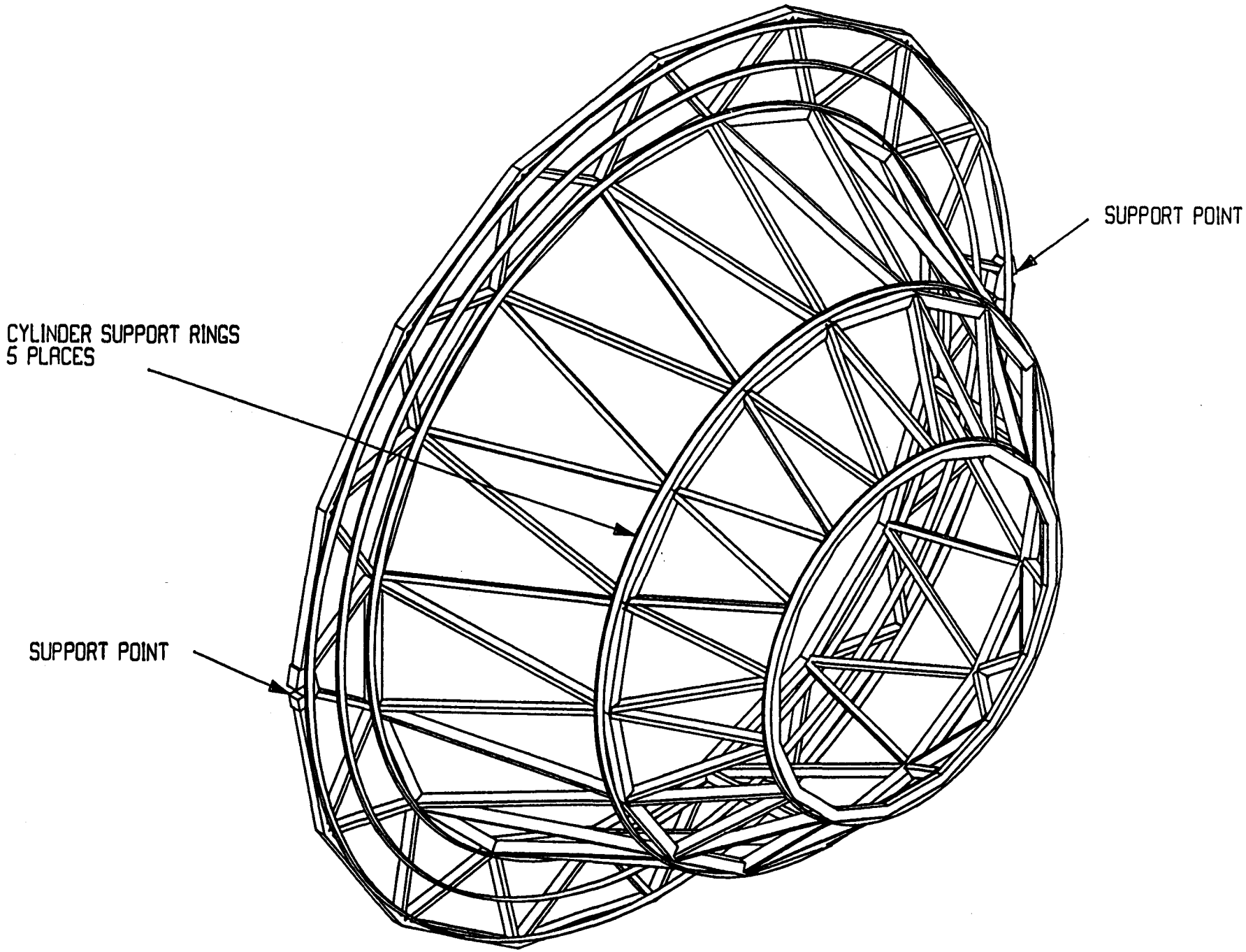

WESTING HOUSE STC

SPACE FRAME OUTSIDE STRUT CONNECTOR

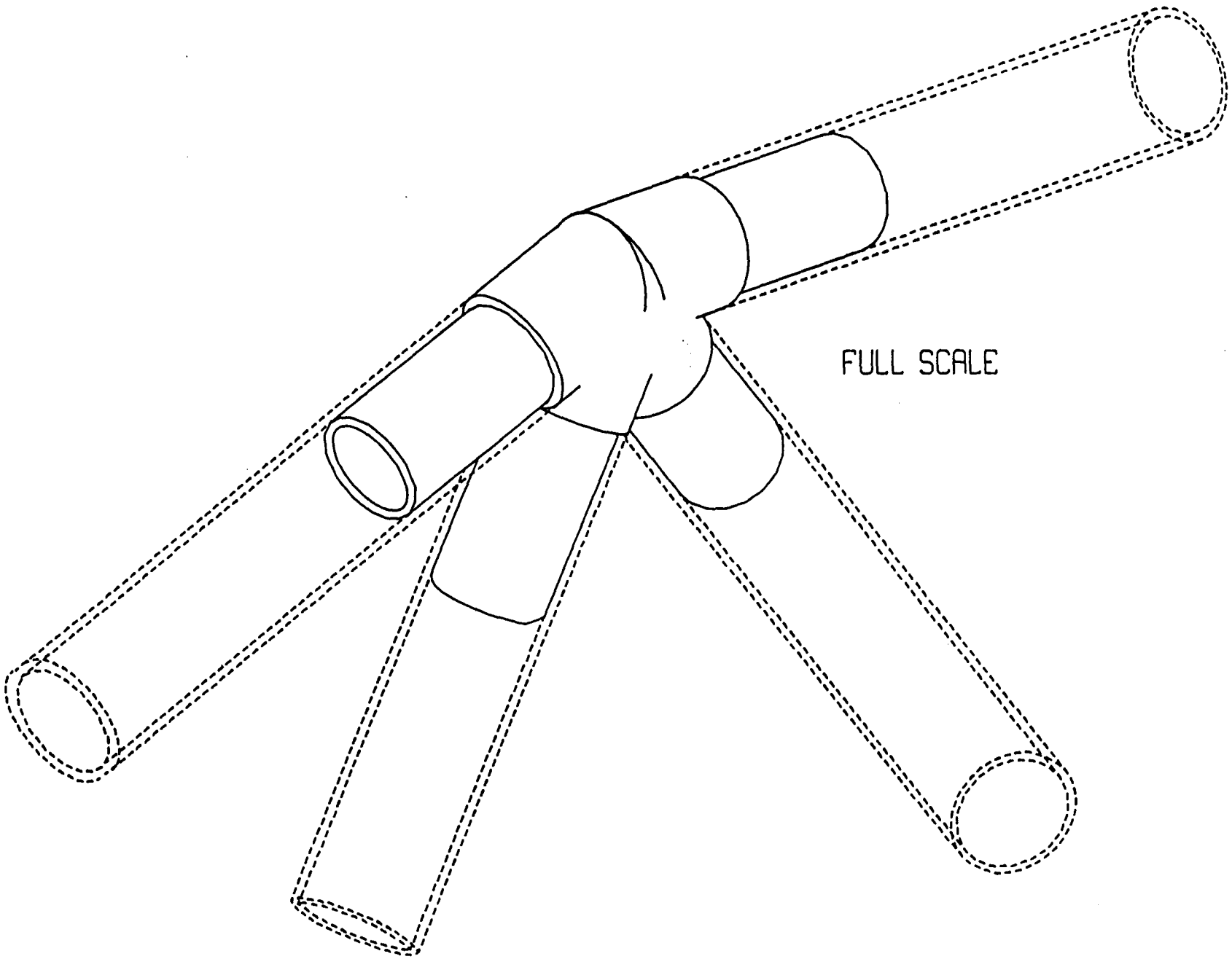

WESTINGHOUSE STC

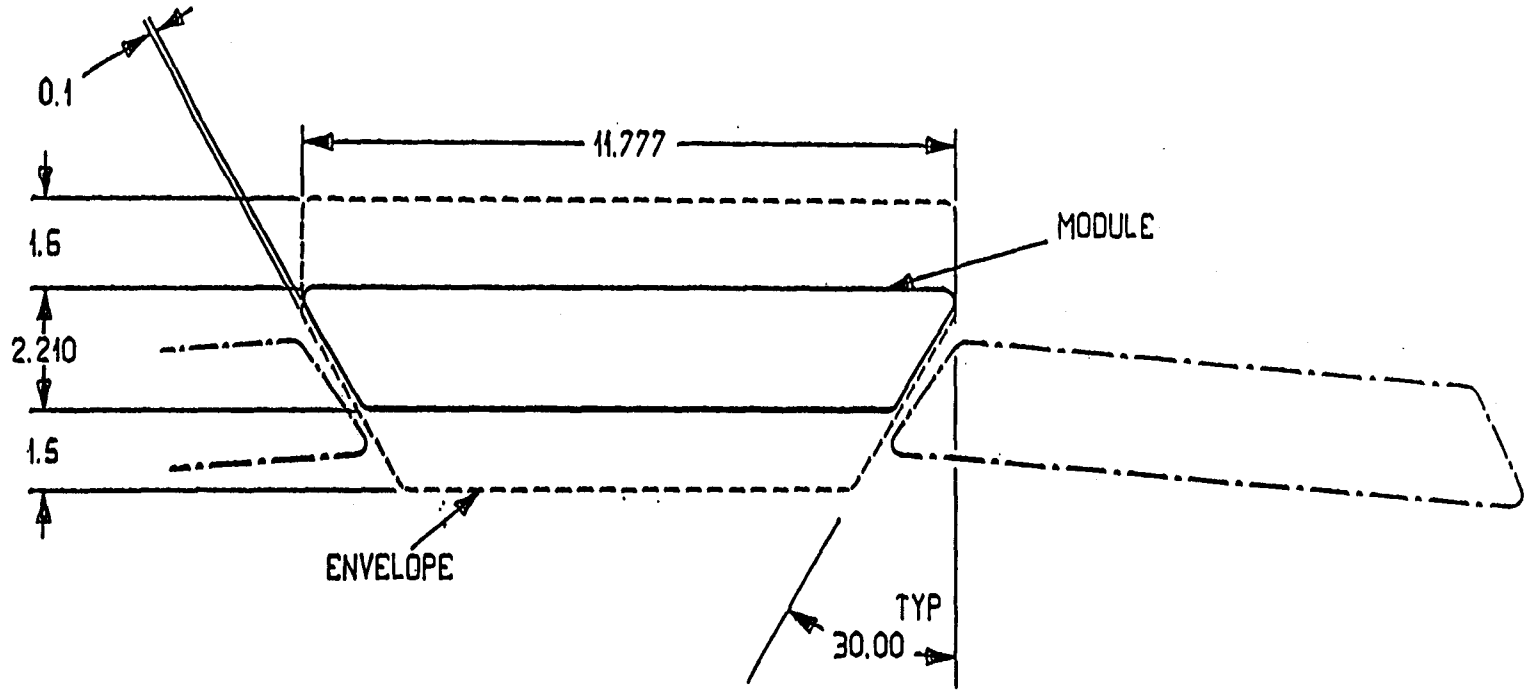

NOTE

1 THE SKETCH ABOVE SHOWS THE ENVELOPE FOR A STANDARD FLAT MODULE AS PER CENTRK18 DATED 7-23-91
(29 STRAWS WIDE BY 6 STRAWS HIGH), 159 STRAWS TOTAL.

2 ASSUMED SHELL WALL THICKNESS OF 0.025 CM

ALL DIMENSIONS IN CM

FLAT MODULE ENVELOPE

W STC DM 7-24-91

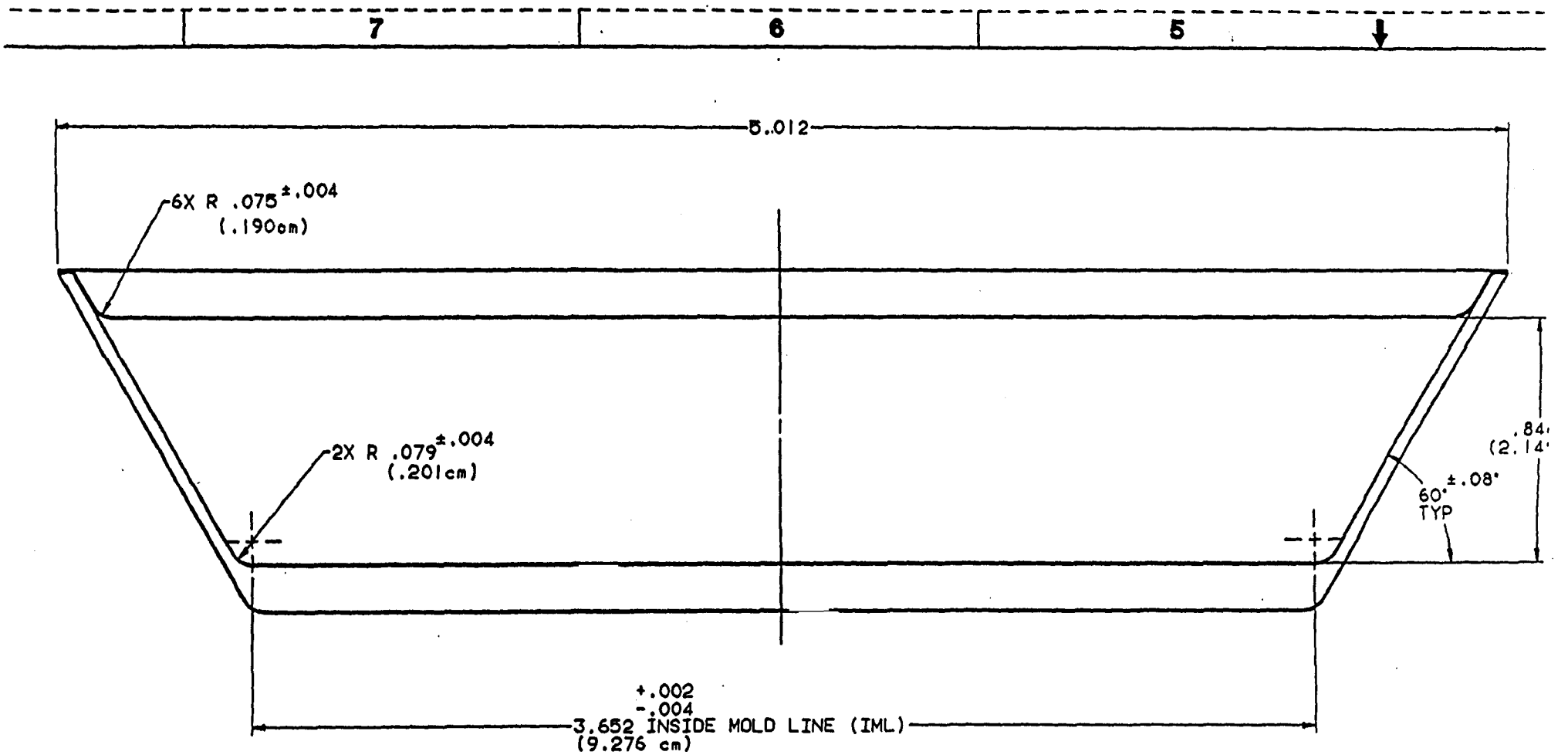

SHELL ASSEMBLY REFERENCE ONLY

SCALE: 4X

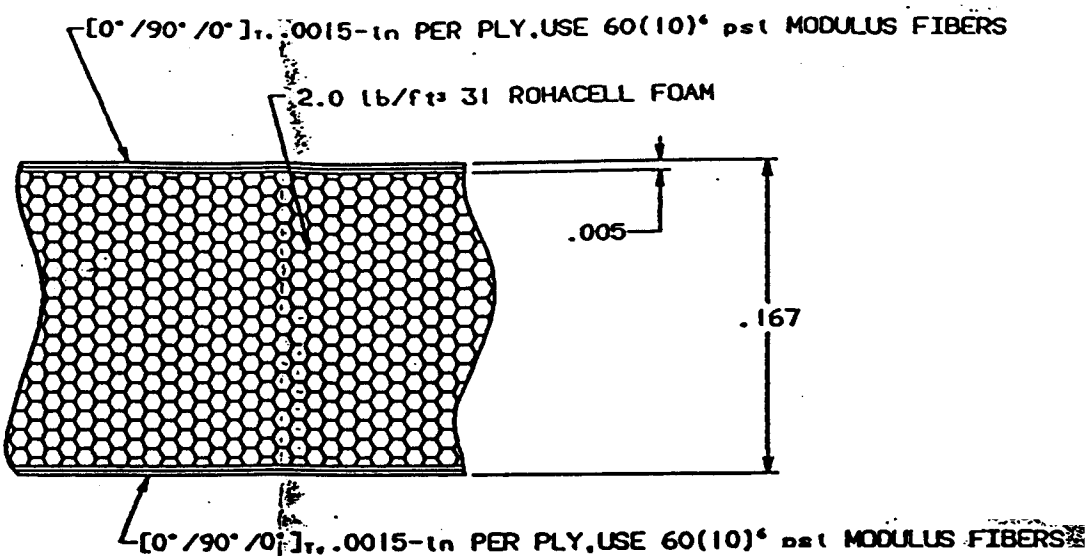

SECTION "A"-"A"

SCALE: 20X

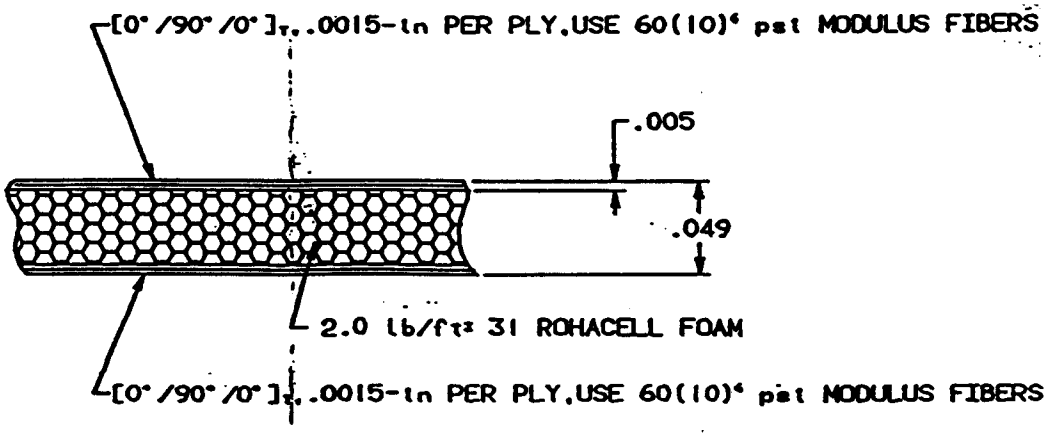

SECTION "B"-"B"

SCALE: 20X

RESULTS SUMMARY

TABLE NUMBER 1

SUMMARY TABLE OF RADIATION LENGTH CALCULATIONS

TABLE #	SUPPORT CYLINDER			SHIM RING EFFECTS	MODULES			MODULE EDGE EFFECTS	PERCENT RADITION LEN/LAYR CM
	GRAPHITE	FOAM			GRAPHITE	FOAM			
	TK/LAYER INCHES	TYPE	TK INCHES		TK/LAYER INCHES	TYPE	TK INCHES		
2	0.0045	31IG	1	NO	0.006	51WF	0.14	NO	0.87
2	0.0045	51WF	1	NO	0.006	51WF	0.14	NO	1.04
4	0.0045	31IG	1	NO	0.0045	51WF	0.14	NO	0.93
5	0.0045	31IG	1	NO	0.0045	31IG	0.14	NO	0.88
6	0.0045	31IG	0.59	NO	0.0045	51WF	0.14	NO	0.83
7	0.0045	31IG	0.59	NO	0.0045	31IG	0.14	NO	0.78
3	0.006	31IG	0.23	NO	0.0045	31IG	0.14	NO	0.71
12	0.006	31IG	0.47	NO	0.0045	31IG	0.14	NO	0.77
11	0.009	31IG	0.23	NO	0.0045	31IG	0.14	NO	0.77
8	0.009	31IG	0.23	NO	0.0045	31IG	0.14	YES	0.79
9	0.009	31IG	0.23	YES	0.0045	31IG	0.14	YES	0.80
9 (SAME AS ABOVE EXCEPT EDA = 1.63)									2.11
10 (SPACEFRAME END DISK SPREAD RADIATION LENGTH CALCULATION)									0.21
0.21 RAD LG IS EQUIVALANT TO 0.007 Inch Thick Aluminum Sheet)									
0.021 Inch Thick Graphite Sheet)									

CONTENTS

TABLE NUMBER 5
CENTRAL TRACKER
SUMMARY RADIATION LENGTH
(Thinned Graphite .0045 inch Support Cylinders
With 1 Inch Thick 311G Lower Density Core)
(Thinned Graphite .0045 inch Module Shells
With 311G Lower Density Core)
TABLE NUMBER 6
CENTRAL TRACKER
SUMMARY RADIATION LENGTH
(Thinned Graphite .0045 inch Support Cylinders
With .59 Inch Thick 311G Lower Density Core)
(Thinned Graphite .0045 inch Module Shells
With 51WF Higher Density Core)
TABLE NUMBER 7
CENTRAL TRACKER
SUMMARY RADIATION LENGTH
(Thinned Graphite .0045 inch Support Cylinders
With .59 Inch Thick 311G Lower Density Core)
(Thinned Graphite .0045 inch Module Shells
With 311G Lower Density Core)
TABLE NUMBER 8
CENTRAL TRACKER
SUMMARY RADIATION LENGTH
MODULE SIDE EFFECTS INCLUDED
(Thinned Graphite .0045 inch Support Cylinders
With .59 Inch Thick 311G Lower Density Core)
(Thinned Graphite .0045 inch Module Shells
With 311G Lower Density Core)
TABLE NUMBER 9
CENTRAL TRACKER
SUMMARY RADIATION LENGTH
SHIM RING EFFECTS INCLUDED
MODULE SIDE EFFECTS INCLUDED
(Thinned Graphite .0045 inch Support Cylinders
With .59 Inch Thick 311G Lower Density Core)
(Thinned Graphite .0045 inch Module Shells
With 311G Lower Density Core)
TABLE NUMBER 10
CENTRAL TRACKER
SUMMARY RADIATION LENGTH
SPACEFRAME EFFECTS
(Hollow Graphite Struts Form the Spaceframe End Disks)
(Silicon Carbide Joints Connect the Struts)
(Thin Graphite Rings Attach the Cylinders to the Spaceframe)
Table Number 10A
SURFACE AREA CALCULATIONS
(For Thickness and Rad Lg Calc See Calculation 5A Above)
Table Number 10B
EFFECTIVE OR SPREAD RAD LG CALCULATIONS

THE SPREADSHEET

1) The Raw Material Properties Are:

1A) B-Stage Unidirectional Fiber — The Raw Material Is (Assumed; Work Done at ORNL):

#	VENDOR	TYPE	RESIN	THICKNSS UNI TAPE INCHES	MODULUS PSI FIBER 0 DEG	MODULUS PSI LAMINATE 0 DEG	MODULUS PSI LAMINATE 90 DEG	DENSITY LBS/IN3	DENSITY gms/CM3	(gms/cm3 *Xo cm = Xogms/cm2) XoGM/CM3	Rad Lg XoCM	COST/LB
1	Hercules	AS4	HMS-	1.5E-03	5.7E+07	3.9E+07	1.3E+06	6.0E-02	1.66	42.7	25.7	$2,200
	(Cylinder)		3501-6									
2	Amaco	p75	250Deg	1.0E-03	5.7E+07			6.0E-02	1.66	42.7	25.7	$600
	(Modules)											
3	Hercules	?	HMS-	1.5E-03	7.5E+07	3.9E+07	1.3E+06	6.0E-02	1.66	42.7	25.7	$2,200
	(Proposed Modules)		3501-6									
4	Kaiser	?	?	1.3E-03	1.0E+08	4.0E+07		6.0E-02	1.66	42.7	25.7	$2,200
	(Struts/Joints)											
5	Kaiser	?	?	2.0E-03	5.0E+07	2.0E+07		6.0E-02	1.66	42.7	25.7	$600
	(Struts/Joints)											

1B) Foam Core — (gms/cm3 *Xo cm = Xogms/cm2)

VENDOR	TYPE	THICKNSS INCHES	MODULUS PSI	COM STRENGTH @250F IN PSI	CTE PPM/F	DENSITY LBS/IN3	DENSITY gms/CM3	XoGM/CM3	Rad Lg XoCM	COST/IN.3
Rohacell	31IG	.12TO 2.6	5.1E+03	40	2.05	1.2E-03	3.2E-02	30	936.6	$0.0361
Rohacell	51WF	.04TO 2	1.1E+04	150	1.83	1.9E-03	5.2E-02	30	576.4	$0.0611
Rohacell	300WF	1.5	5.2E+04	800	?	1.1E-02	3.0E-01	30	99.9	$0.2981

1C) Straws — (gms/cm3 * Xo cm = Xo gms/cm2)

VENDOR	TYPE	THICKNESS INCHES DIAM	THICKNESS INCHES WALL	DENSITY LBS/IN3	DENSITY gms/CM3	XoGM/CM3	Rad Lg XoCM	COST/IN.3
	Mylar	4.0437	0.0014	5.0E-02	1.4E+00	39.9	28.7	
	Tungsten					9.6	0.35	

1D) Spaceframe (End Disk) Components — (gms/cm3 * Xo cm = Xo gms/cm2)

VENDOR	TYPE	THICKNSS INCHES	MODULUS PSI	TENSILE PSI	CTE DEG F	DENSITY LBS/IN3	DENSITY gms/CM3	XoGM/CM3	Rad Lg XoCM	COST/IN.3	COST/LB
DWA	SiC	.05 TO 2	4.7E+07	?	2.23	1.1E-01	3.1E+00	26.64	8.52	11.30	100.00
	Al	(Various)	1.0E+07	6.00E+04	12.89	1.0E-01	2.8E+00	24.93	8.9	0.28	2.75
KAISER	C-C	Bolts	1.6E+07	4.00E+04	-0.11	6.0E-02	1.7E+00	18.8	18.8		

2) The Support Cylinder Radiation Length is:

NOTE:
(Density in gms/cm3 times thickness in cm divided by Xo equals the radiation length for that thickness)
(or 'Material Rad Length' times thickness in cm equals the radiation length for that thickness)

2A) Low Density Foam Support Cylinder 1 Inch Thick:
(Fiber Laminate/Foam/Laminate Construction)

	TYPE	PLYES	THICKNESS INCHES	THICKNESS CM	RAD LGTH CM	PERCENT RAD LGTH
LAMINATE	#1?	0/90/0	0.0045	1.14E-02	4.44E-04	0.0444
FOAM	31IG	1	0.98	2.50E+00	2.67E-03	0.2669
LAMINATE	#1?	0/90/0	0.0045	1.14E-02	4.44E-04	0.0444
TOTAL						0.3594

2B) High Density Foam Support Cylinder 1 Inch Thick:

	TYPE	PLYES	THICKNESS INCHES	THICKNESS CM	RAD LGTH CM	PERCENT RAD LGTH
LAMINATE	#1?	0/90/0	0.0045	1.14E-02	4.44E-04	0.0444
FOAM	51WF	1	0.98	2.50E+00	4.34E-03	0.4338
LAMINATE	#1?	0/90/0	0.0045	1.14E-02	4.44E-04	0.0444
TOTAL						0.5279

2C) Low Density Foam Support Cylinder .59 Inches(15mm) Thick:

	TYPE	PLYES	THICKNESS INCHES	THICKNESS CM	RAD LGTH CM	PERCENT RAD LGTH
LAMINATE	#1?	0/90/0	0.0045	1.14E-02	4.44E-04	0.0444
FOAM	31IG	1	0.59	1.50E+00	1.60E-03	0.1602
LAMINATE	#1?	0/90/0	0.0045	1.14E-02	4.44E-04	0.0444
TOTAL						0.2515

2D) Shim Rings Low Density Estimated Radiation Length:
(Calculate the "Shim Ring Effect" On Radial Rays)
(Shim Dimensions 2.5 Axial 2.5 Radial CM)

	TYPE	PLYES	THICKNESS INCHES	THICKNESS CM	RAD LGTH CM	PERCENT RAD LGTH
COATING			0	0.00E+00	0.00E+00	0.0000
FOAM	31IG	1	0.9843	2.50E+00	2.67E-03	0.2669
COATING			0	0.00E+00	0.00E+00	0.0000
TOTAL						0.2669

2E) Low Density Foam Support Cylinder (6mm) 0.236 Inch Thick:

	TYPE	PLYES	THICKNESS INCHES	THICKNESS CM	RAD LGTH CM	PERCENT RAD LGTH
LAMINATE	#1?	[0/-/+60]s	0.006	1.52E-02	5.92E-04	0.0592
FOAM	31IG	1	0.24	6.00E-01	6.41E-04	0.0641
LAMINATE	#1?	[0/-/+60]s	0.006	1.52E-02	5.92E-04	0.0592
TOTAL						0.1844

2F) Low Density Foam Support Cylinder (6mm) 0.236 Inch Thick:

	TYPE	PLYES	THICKNESS INCHES	THICKNESS CM	RAD LGTH CM	PERCENT RAD LGTH
LAMINATE	#1?	[0/-/+60]s	0.009	2.29E-02	8.89E-04	0.0889
FOAM	31IG	1	0.24	6.00E-01	6.41E-04	0.0641
LAMINATE	#1?	[0/-/+60]s	0.009	2.29E-02	8.89E-04	0.0889
TOTAL						0.2442

2G) Low Density Foam Support Cylinder (12mm) 0.4724 Inch Thick:

	TYPE	PLYES	THICKNESS INCHES	THICKNESS CM	RAD LGTH CM	PERCENT RAD LGTH
LAMINATE	#1?	[0/-/+60]s	0.006	1.52E-02	5.92E-04	0.0592
FOAM	31IG	1	0.47	1.20E+00	1.28E-03	0.1281
LAMINATE	#1?	[0/-/+60]s	0.006	1.52E-02	5.92E-04	0.0592
TOTAL						0.2491

3) Shell Estimated Radiation Length:

(Fiber Laminate/Foam/Laminate Shell Construction)

3A) Nominal Shell Thickness & Higher Density Foam 51Wf

AZMUTHAL SHELL SIDES

	TYPE	PLYES	THICKNESS INCHES	THICKNESS CM	RAD LGTH CM	PERCENT RAD LGTH
LAMINATE	AS4	0/90/0	0.003	7.62E-03	2.96E-04	0.0296
FOAM	51WG	1	0.04	1.02E-01	1.76E-04	0.0176
LAMINATE	AS4	0/90/0	0.003	7.62E-03	2.96E-04	0.0296
TOTAL						0.0776

RADIAL SHELL TOP OR BOTTOM

	TYPE	PLYES	THICKNESS INCHES	THICKNESS CM	RAD LGTH CM	PERCENT RAD LGTH
LAMINATE	AS4	0/90/0	0.003	7.62E-03	2.96E-04	0.0296
FOAM	51WG	1	0.15	3.81E-01	6.61E-04	0.0661
LAMINATE	AS4	0/90/0	0.003	7.62E-03	2.96E-04	0.0296
TOTAL						0.1266
TOTAL (Times 2 For Top and Bottom)						0.2532

3B) Thinner Shell Thickness & Higher Density Foam 51Wf

AZMUTHAL SHELL SIDES

	TYPE	PLYES	THICKNESS INCHES	THICKNESS CM	RAD LGTH CM	PERCENT RAD LGTH
LAMINATE	AS4	0/90/0	0.0045	1.14E-02	4.44E-04	0.0444
FOAM	51WG	1	0.04	1.02E-01	1.76E-04	0.0176
LAMINATE	AS4	0/90/0	0.0045	1.14E-02	4.44E-04	0.0444
TOTAL						0.1076

RADIAL SHELL TOP OR BOTTOM

	TYPE	PLYES	THICKNESS INCHES	THICKNESS CM	RAD LGTH CM	PERCENT RAD LGTH
LAMINATE	AS4	0/90/0	0.0045	1.14E-02	4.44E-04	0.0444
FOAM	51WG	1	0.15	3.81E-01	6.61E-04	0.0661
LAMINATE	AS4	0/90/0	0.0045	1.14E-02	4.44E-04	0.0444
TOTAL						0.1565
TOTAL (Times 2 For Top and Bottom)						0.3131

3C) Thinner Shell Thickness & Lower Density Foam 31IG

AZMUTHAL SHELL SIDES

	TYPE	PLYES	THICKNESS INCHES	THICKNESS CM	RAD LGTH CM	PERCENT RAD LGTH
LAMINATE	AS4	0/90/0	0.0045	1.14E-02	4.44E-04	0.0444
FOAM	31IG	1	0.04	1.02E-01	1.08E-04	0.0108
LAMINATE	AS4	0/90/0	0.0045	1.14E-02	4.44E-04	0.0444
TOTAL						0.1007

RADIAL SHELL TOP OR BOTTOM

	TYPE	PLYES	THICKNESS INCHES	THICKNESS CM	RAD LGTH CM	PERCENT RAD LGTH
LAMINATE	AS4	0/90/0	0.0045	1.14E-02	4.44E-04	0.0444
FOAM	31IG	1	0.15	3.81E-01	4.07E-04	0.0407
LAMINATE	AS4	0/90/0	0.0045	1.14E-02	4.44E-04	0.0444
TOTAL						0.1308
TOTAL (Times 2 For Top and Bottom)						0.2617

3D) Thinner Shell Thickness & Higher Density Foam 51WF

(Calculate the "Side Effect" On Radial Rays)

(Assume 60 Degree Sidewalls)

		AZMUTHAL SHELL SIDES				
			THICKNESS		RAD LGTH	PERCENT
	TYPE	PLYES	INCHES	CM	CM	RAD LGTH
LAMINATE	AS4	0/90/0	0.009	2.29E-02	8.89E-04	0.0889
FOAM	31IG	1	0.02	5.08E-02	8.81E-05	0.0088
LAMINATE	AS4	0/90/0	0.009	2.29E-02	8.89E-04	0.0889
TOTAL						0.1884

4) Straw Bundle Estimated Radiation Length:

4A) Trigger Layer (8 Straws Deep):

	LAYERS	THICKNESS INCHES	THICKNESS CM	RAD LGTH CM	PERCENT RAD LGTH
STRAWS					
Mylar	8	3.52E−02	8.94E−02	3.11E−03	0.3114
Al					
GLUE					
SUPPORTS					
WIRE					
TOTAL					0.3114

4B) Axial or Stereo Layer (6 Straws Deep):

	LAYERS	THICKNESS INCHES	THICKNESS CM	RAD LGTH CM	PERCENT RAD LGTH
STRAWS					
Mylar	6	2.64E−02	6.70E−02	2.34E−03	0.2336
Al					
GLUE					
SUPPORTS					
WIRE					
TOTAL					0.2336

5) Spaceframe Components Estimated Radiation Length:

5A) End Disk Components:

COMPONENT SIZE IN CM

COMPONENT	AXIAL	AZMUTHAL	WALL TK	RADIAL
Struts(Hollow)	4	2	0.25	N/A
Joints(Hollow)	4	4	0.38	4
Rings	0.25	N/A	N/A	1.5

COMPONENT RAD LG (PERCENT)

	MATERIAL	#	THICKNESS INCHES	THICKNESS CM	RAD LGTH CM	PERCENT RAD LGTH
Struts	Graphite	4	1.97E−01	5.00E−01	1.94E−02	1.9438
Joints	Graphite	4	2.99E−01	7.60E−01	2.95E−02	2.9546
Rings	Graphite	4	9.84E−02	2.50E−01	9.72E−03	0.9719

6) Summary Tables

TABLE NUMBER 2
CENTRAL TRACKER
SUMMARY RADIATION LENGTH
(Thinned Graphite .0045 inch Support Cylinders
With 1 Inch Thick 51WF Higher Density and 31IG Low Density Core)
(Thicker Graphite .006 inch Module Shells
With 51WF Higher Density Core)

	CYLINDER		MODULES		TOTAL
	GRAPHITE	FOAM	SHELLS	STRAWS	PERCENT
One Axial Superlayer					
Low Density Foam	0.089	0.267	0.253	0.234	0.843
High Density Foam	0.089	0.434	0.253	0.234	1.009
One Trigger Superlayer					
Low Density Foam	0.089	0.267	0.253	0.311	0.920
High Density Foam	0.089	0.434	0.253	0.311	1.087
Indiana University Design					
Three Axial and Two Trigger					
Low Density Foam					4.369
				Average	0.87
High Density Foam					5.203
				Average	1.04

TABLE NUMBER 3
CENTRAL TRACKER
SUMMARY RADIATION LENGTH
(Thinned Graphite .006 inch Support Cylinders
With .23 Inch Thick 31IG Lower Density Core)
(Thinned Graphite .0045 inch Module Shells
With 31IG Lower Density Core)

	CYLINDER		MODULES		TOTAL
	GRAPHITE	FOAM	SHELLS	STRAWS	PERCENT
One Axial Superlayer	0.118	0.064	0.262	0.234	0.678
One Trigger Superlayer	0.118	0.064	0.262	0.311	0.756
Indiana University Design					3.545
Three Axial and Two Trigger				Average	0.71

TABLE NUMBER 4
CENTRAL TRACKER
SUMMARY RADIATION LENGTH
(Thinned Graphite .0045 inch Support Cylinders
With 1 Inch Thick 31IG Lower Density Core)
(Thinned Graphite .0045 inch Module Shells
With 51WF Higher Density Core)

	CYLINDER		MODULES		TOTAL
	GRAPHITE	FOAM	SHELLS	STRAWS	PERCENT
One Axial Superlayer	0.000	0.000	PERCENT	0.000	0.000
One Trigger Superlayer	0.000	0.000	PERCENT	0.000	0.000
Indiana University Design					0.001
Three Axial and Two Trigger				Average	0.00

TABLE NUMBER 5
CENTRAL TRACKER
SUMMARY RADIATION LENGTH

2a (Thinned Graphite .0045 inch Support Cylinders
With 1 Inch Thick 31IG Lower Density Core)

3c (Thinned Graphite .0045 inch Module Shells
With 31IG Lower Density Core)

	CYLINDER		MODULES		TOTAL
	GRAPHITE	FOAM	SHELLS	STRAWS	PERCENT
One Axial Superlayer	0.089	0.267	0.262	0.234	0.851
One Trigger Superlayer	0.089	0.267	0.262	0.311	0.929
Indiana University Design					4.411
Three Axial and Two Trigger				Average	0.88

TABLE NUMBER 6
CENTRAL TRACKER
SUMMARY RADIATION LENGTH

2c (Thinned Graphite .0045 inch Support Cylinders
With .59 Inch Thick 31IG Lower Density Core)

3b (Thinned Graphite .0045 inch Module Shells
With 51WF Higher Density Core)

	CYLINDER		MODULES		TOTAL
	GRAPHITE	FOAM	SHELLS	STRAWS	PERCENT
One Axial Superlayer	0.089	0.160	0.313	0.234	0.796
One Trigger Superlayer	0.089	0.160	0.313	0.311	0.873
Indiana University Design					4.134
Three Axial and Two Trigger				Average	0.83

TABLE NUMBER 7
CENTRAL TRACKER
SUMMARY RADIATION LENGTH

2c (Thinned Graphite .0045 inch Support Cylinders
With .59 Inch Thick 31IG Lower Density Core)

3c (Thinned Graphite .0045 inch Module Shells
With 31IG Lower Density Core)

	CYLINDER		MODULES		TOTAL
	GRAPHITE	FOAM	SHELLS	STRAWS	PERCENT
One Axial Superlayer	0.089	0.160	0.262	0.234	0.744
One Trigger Superlayer	0.089	0.160	0.262	0.311	0.822
Indiana University Design					3.877
Three Axial and Two Trigger				Average	0.78

TABLE NUMBER 8
CENTRAL TRACKER
SUMMARY RADIATION LENGTH
MODULE SIDE EFFECTS INCLUDED

2c (Thinned Graphite .009 inch Support Cylinders
With .236 Inch Thick 31IG Lower Density Core)

3c (Thinned Graphite .0045 inch Module Shells
With 31IG Lower Density Core)

Superlayer	Total Modules	Circumf Modules	Cylinders		Modules			
			Radius	Total	Total	Total		PerCent
#	#	#	Meters	Circumf	Edges	Centers	Sum	Edges
5	184	92	1.63	403.21	40.02	426.13	466.16	9.39
4	168	84	1.49	368.58	36.54	389.04	425.58	9.39
3	152	76	1.35	333.95	33.06	351.95	385.01	9.39
2	120	60	1.07	264.68	26.10	277.76	303.86	9.40
1	80	40	0.71	175.63	17.40	185.03	202.43	9.40
							Average	9.40
			CYLINDER		MODULES	SHELLS		TOTAL
			GRAPHITE	FOAM	TOP&BOT%	SIDES%	STRAWS	PERCENT
					100.00	9.40		
One Axial Superlayer			0.178	0.064	0.262	0.018	0.234	0.755
One Trigger Superlayer			0.178	0.064	0.262	0.018	0.311	0.833
Indiana University Design								3.929
(Three Axial and Two Trigger)							Average	0.79

TABLE NUMBER 9
CENTRAL TRACKER
SUMMARY RADIATION LENGTH
2d SHIM RING EFFECTS INCLUDED
MODULE SIDE EFFECTS INCLUDED
2c (Thinned Graphite .009 inch Support Cylinders
With .236 Inch Thick 31IG Lower Density Core)
3c (Thinned Graphite .0045 inch Module Shells
With 31IG Lower Density Core)

NUMBER OF SHIM RINGS #	TRACKER LENGTH M	AXIAL WIDTH CM	RADIAL HEIGHT CM	SUPERLAYER CYLINDER LENGTH PERCENT	SHIM RING PERCENT	SHIM RING PERCENT LOCAL RAD LG	EFFECTIVE RAD LG CALC PERCENT SPREAD RAD LG
10	8	2.5	2.5	800	25	ERR	ERR .

	CYLINDER COMPOSI%	SHIM RNG%	MODULES TOP&BOT%	SHELLS SIDES%	STRAWS	TOTAL PERCENT
	100	3.13	100.00	9.40		
One Axial Superlayer	0.244	0.008	0.262	0.018	0.234	0.766
One Trigger Superlayer	0.244	0.008	0.262	0.018	0.311	0.843
Indiana University Design Radial				Total=		3.983
(Three Axial and Two Trigger)Average				Average/layer=		0.80
Indiana U Design (VALUE AT ETA =		1.63)		Total=		10.56
(Three Axial and two Trigger Average)				Average/layer=		2.11

TABLE NUMBER 10
CENTRAL TRACKER
SUMMARY RADIATION LENGTH
SPACEFRAME EFFECTS
(Hollow Graphite Struts Form the Spaceframe End Disks)
(Silicon Carbide Joints Connect the Struts)
(Thin Graphite Rings Attach the Cylinders to the Spaceframe)

Table Number 10A
SURFACE AREA CALCULATIONS
(For Thickness and Rad Lg Calc See Table 5A Above)

SUPERLAY NUMBER	COMPONEN	QUANITY #	AZMUTHA WIDTH INCHES	RADIAL LENGTH INCHES	DISK AREA TOTAL SQ IN	COMPONE TOTAL SQ IN	PERCENT COMPONE COVERS
5 TO 4	STRUTS	16	0.79	5.51	2126.98	69.62	3.273
	JOINTS	16	1.57	1.57	2126.98	39.68	1.866
	RINGS	1	N/A	0.59	2126.98	238.12	11.195
4 TO 3	STRUTS	16	0.79	5.51	1936.10	69.62	3.596
	JOINTS	16	1.57	1.57	1936.10	39.68	2.049
	RINGS	1	N/A	0.59	1936.10	217.66	11.242
3 TO 2	STRUTS	16	0.79	11.02	3299.55	139.23	4.220
	JOINTS	16	1.57	1.57	3299.55	39.68	1.203
	RINGS	1	N/A	0.59	3299.55	197.21	5.977
2 TO 1	STRUTS	16	0.79	14.17	3120.35	179.01	5.737
	JOINTS	16	1.57	1.57	3120.35	39.68	1.272
	RINGS	1	N/A	0.59	3120.35	156.31	5.009
	AVERAGE PERCENT OF AREA STRUT COVERS						4.21
	AVERAGE PERCENT OF AREA JOINT COVERS						1.60
	AVERAGE PERCENT OF AREA RING/(CYLINDER END) COVERS						8.36

Table Number 10B
EFFECTIVE OR SPREAD RAD LG CALCULATIONS
(For Thickness and Rad Lg Calc See Table 5A Above)
(For Area Calc See Table 10A Above)

ITEM	PERCENT LOCAL RAD LG	PERCENT AREA COVERED	PERCENT SPREAD RAD LG
Strut	1.944	4.21	0.082
Joint	2.955	1.60	0.047
Ring	0.972	8.36	0.081
Average Per End			0.21

Or Equal To
0.007 Inch Thick Aluminum Sheet
0.021 Inch Thick Graphite Sheet

TABLE NUMBER 11
CENTRAL TRACKER
SUMMARY RADIATION LENGTH
(Thinned Graphite .009 inch Support Cylinders
With .23 Inch Thick 31IG Lower Density Core)
(Thinned Graphite .0045 inch Module Shells
With 31IG Lower Density Core)

	CYLINDER		MODULES		TOTAL
	GRAPHITE	FOAM	SHELLS	STRAWS	PERCENT
One Axial Superlayer	0.178	0.064	0.262	0.234	0.737
One Trigger Superlayer	0.178	0.064	0.262	0.311	0.815
Indiana University Design					3.841
Three Axial and Two Trigger				Average	0.77

TABLE NUMBER 12
CENTRAL TRACKER
SUMMARY RADIATION LENGTH
(Thinned Graphite .006 inch Support Cylinders
With .47 Inch Thick 31IG Lower Density Core)
(Thinned Graphite .0045 inch Module Shells
With 31IG Lower Density Core)

	CYLINDER		MODULES		TOTAL
	GRAPHITE	FOAM	SHELLS	STRAWS	PERCENT
One Axial Superlayer	0.118	0.128	0.262	0.234	0.742
One Trigger Superlayer	0.118	0.128	0.262	0.311	0.820
Indiana University Design					3.865
Three Axial and Two Trigger				Average	0.77

SECTION II

SUPPORT STRUCTURE CANDIDATE MATERIAL PROPERTY TABULATION

INTRODUCTION

The enclosed report tabulates materials and material properties for use in the SDC central tracker support structure for the SSCL. The proposed spaceframe type structure and materials can be readily adapted to except scintillator fiber, hybird, or modular straw detectors. The work includes radial and end structure materials using a variety of combinations and thicknesses. Module shell, straw, and attachment materials are included.

CONTENTS

THE SPREADSHEET

1) Structural (Cylinder) Materials:

1.1) Raw Materials for Skins and Cores:

1.1.1) Raw Fiber B–Staged Unidirectional Graphite Material Properties:

				THICKNESS	MODULUS PSI				(gms/cm3 * Xo cm = Xo gms/cm2)			
				UNI TAPE	FIBER	LAMINATE		DENSITY			Rad Lg	
#	VENDOR	TYPE	RESIN	INCHES	0 DEG	0 DEG	90 DEG	LBS/IN3	gms/CM3	gms/cm2	CM	COST/LB
A)	Hercules (Cylinder)	AS4	HMS–3501–6	1.5E–03	5.7E+07	3.9E+07	1.3E+06	6.0E–02	1.66	42.7	25.7	$2,200
B)	Japan (Modules)		250Deg	2.0E–03	5.7E+07			6.0E–02	1.66	42.7	25.7	$600
C)	Hercules (Proposed Modules)	?	HMS–3501–6	1.5E–03	7.5E+07	3.9E+07	1.3E+06	6.0E–02	1.66	42.7	25.7	$2,200
D)	Kaiser (Struts/Joints)	?	?	1.3E–03	1.0E+08	4.0E+07		6.0E–02	1.66	42.7	25.7	$2,200
E)	Kaiser (Struts/Joints)	?	?	2.0E–03	5.0E+07	2.0E+07		6.0E–02	1.66	42.7	25.7	$600

1.1.2) Rohacell (Polymethacrylimide) Ridged Foam Material Properties:

(gms/cm3 * Xo cm = Xo gms/cm2)

			THICKNESS	MODULUS	COM STRENGTH	CTE	DENSITY			Rad Lg	
	VENDOR	TYPE	INCHES	PSI	@250F IN PSI	PPM/F	LBS/IN3	gms/CM3	gms/cm2	CM	COST/IN.3
A)	Rohacell (Cylinder and Modules)	31IG	.12TO 2.6	5.1E+03	40	2.05	1.2E–03	3.2E–02	30	936.6	$0.0361
B)	Rohacell (Cylinder and Modules)	51WF	.04TO 2	1.1E+04	150	1.83	1.9E–03	5.2E–02	30	576.4	$0.0611
C)	Rohacell (Module Atachments)	300WF	1.5	5.2E+04	800	?	1.1E–02	3.0E–01	30	99.9	$0.2981

1.2) Graphite Laminate With Foam Core Materials:

(Much of the Basic Composite Material Was Done at ORNL by John Mayhall:

1.2.1) Cylinder Candidate Lamina Foam Core Material Properties:

A) Low Density Foam Support Cylinder 1 Inch (25mm) Thick:

(Fiber Laminate/Foam/Laminate Construction) (gms/cm3 * Xo cm = Xo gms/cm2)

	TYPE	PLYES	THICKNESS INCHES	THICKNESS CM	RAD LGTH CM	PERCENT RAD LGTH
LAMINATE	1.1 A)	0/90/0	0.0045	1.14E-02	4.44E-04	0.0444
FOAM	31IG	1	0.98	2.50E+00	2.67E-03	0.2669
LAMINATE	1.1 A)	0/90/0	0.0045	1.14E-02	4.44E-04	0.0444

0.3594 TOTAL

IN PLANE MODULUS MSI			POISSON RATIO		CTE (IN/IN/DEG F)	
0 DEG	90 DEG	SHEAR	90/0	0/90	0 DEG	90 DEG
0.1203	0.0186	0.0278	1.1107	0.1715	-1.263	16.2332
FLEXURAL MODULUS MSI			POISSON RATIO			
0 DEG	90 DEG	SHEAR	90/0	0/90		
0.3181	0.0353	0.0771	1.4864	0.1649		

B) High Density Foam Support Cylinder 1 Inch Thick:

	TYPE	PLYES	THICKNESS INCHES	THICKNESS CM	RAD LGTH CM	PERCENT RAD LGTH
LAMINATE	#1?	0/90/0	0.0045	1.14E-02	4.44E-04	0.0444
FOAM	51WF	1	0.98	2.50E+00	4.34E-03	0.4338
LAMINATE	#1?	0/90/0	0.0045	1.14E-02	4.44E-04	0.0444

0.5279 TOTAL

C) Low Density Foam Support Cylinder .59 Inches(15mm) Thick:

	TYPE	PLYES	THICKNESS INCHES	THICKNESS CM	RAD LGTH CM	PERCENT RAD LGTH
LAMINATE	#1?	0/90/0	0.0045	1.14E-02	4.44E-04	0.0444
FOAM	31IG	1	0.59	1.50E+00	1.60E-03	0.1602
LAMINATE	#1?	0/90/0	0.0045	1.14E-02	4.44E-04	0.0444

0.2515 TOTAL

IN PLANE MODULUS MSI			POISSON RATIO		CTE (IN/IN/DEG F)	
0 DEG	90 DEG	SHEAR	90/0	0/90	0 DEG	90 DEG
0.3179	0.1739	0.0144	0.0481	0.0263	0.734	2.1638
FLEXURAL MODULUS MSI			POISSON RATIO			
0 DEG	90 DEG	SHEAR	90/0	0/90		
0.9186	0.4727	0.0372	0.0372	0.0199		

1.2.2) Module Lamina Foam Core Material Properties:

A) Nominal 0.006 Inch Shell Thickness & Higher Density Foam 51Wf

AZMUTHAL SHELL SIDES

	TYPE	PLYES	THICKNESS INCHES	THICKNESS CM	RAD LGTH CM	PERCENT RAD LGTH
LAMINATE	AS4	0/90/0	0.006	1.52E−02	5.92E−04	0.0592
FOAM	51WG	1	0.04	1.02E−01	1.76E−04	0.0176
LAMINATE	AS4	0/90/0	0.006	1.52E−02	5.92E−04	0.0592
						0.1375 TOTAL

IN PLANE MODULUS MSI			POISSON RATIO		CTE (IN/IN/DEG F)	
0 DEG	90 DEG	SHEAR	90/0	0/90	0 DEG	90 DEG

(No Data)

FLEXURAL MODULUS MSI			POISSON RATIO	
0 DEG	90 DEG	SHEAR	90/0	0/90

RADIAL SHELL TOP OR BOTTOM

	TYPE	PLYES	THICKNESS INCHES	THICKNESS CM	RAD LGTH CM	PERCENT RAD LGTH
LAMINATE	AS4	0/90/0	0.006	1.52E−02	5.92E−04	0.0592
FOAM	51WG	1	0.15	3.81E−01	6.61E−04	0.0661
LAMINATE	AS4	0/90/0	0.006	1.52E−02	5.92E−04	0.0592
						0.1864 TOTAL
TOTAL (Times 2 For Top and Bottom)						0.3729

IN PLANE MODULUS MSI			POISSON RATIO		CTE (IN/IN/DEG F)	
0 DEG	90 DEG	SHEAR	90/0	0/90	0 DEG	90 DEG

(No Data)

FLEXURAL MODULUS MSI			POISSON RATIO	
0 DEG	90 DEG	SHEAR	90/0	0/90

B) Thinner 0.0045 Inch Shell Thickness & Higher Density Foam 51Wf

AZMUTHAL SHELL SIDES

	TYPE	PLYES	THICKNESS INCHES	THICKNESS CM	RAD LGTH CM	PERCENT RAD LGTH
LAMINATE	AS4	0/90/0	0.0045	1.14E−02	4.44E−04	0.0444
FOAM	51WG	1	0.04	1.02E−01	1.76E−04	0.0176
LAMINATE	AS4	0/90/0	0.0045	1.14E−02	4.44E−04	0.0444
TOTAL						0.1076

RADIAL SHELL TOP OR BOTTOM

	TYPE	PLYES	THICKNESS INCHES	THICKNESS CM	RAD LGTH CM	PERCENT RAD LGTH
LAMINATE	AS4	0/90/0	0.0045	1.14E−02	4.44E−04	0.0444
FOAM	51WG	1	0.15	3.81E−01	6.61E−04	0.0661
LAMINATE	AS4	0/90/0	0.0045	1.14E−02	4.44E−04	0.0444
TOTAL						0.1565
TOTAL (Times 2 For Top and Bottom)						0.3131

C) Thinner 0.0045 Inch Shell Thickness & Lower Density Foam 31IG

AZMUTHAL SHELL SIDES

	TYPE	PLYES	THICKNESS INCHES	THICKNESS CM	RAD LGTH CM	PERCENT RAD LGTH
LAMINATE	AS4	0/90/0	0.0045	1.14E−02	4.44E−04	0.0444
FOAM	31IG	1	0.04	1.02E−01	1.08E−04	0.0108
LAMINATE	AS4	0/90/0	0.0045	1.14E−02	4.44E−04	0.0444
TOTAL						0.1007

IN PLANE MODULUS MSI			POISSON RATIO		CTE (IN/IN/DEG F)	
0 DEG	90 DEG	SHEAR	90/0	0/90	0 DEG	90 DEG

(No Data)

FLEXURAL MODULUS MSI			POISSON RATIO	
0 DEG	90 DEG	SHEAR	90/0	0/90

RADIAL SHELL TOP OR BOTTOM

	TYPE	PLYES	THICKNESS INCHES	THICKNESS CM	RAD LGTH CM	PERCENT RAD LGTH
LAMINATE	AS4	0/90/0	0.0045	1.14E−02	4.44E−04	0.0444
FOAM	31IG	1	0.15	3.81E−01	4.07E−04	0.0407
LAMINATE	AS4	0/90/0	0.0045	1.14E−02	4.44E−04	0.0444
TOTAL						0.1308
TOTAL (Times 2 For Top and Bottom)						0.2617

IN PLANE MODULUS MSI			POISSON RATIO		CTE (IN/IN/DEG F)	
0 DEG	90 DEG	SHEAR	90/0	0/90	0 DEG	90 DEG

(No Data)

FLEXURAL MODULUS MSI			POISSON RATIO	
0 DEG	90 DEG	SHEAR	90/0	0/90

1.2.3) Shim Ring Foam Material Properties:

A) Lower Density Foam 31IG

(Shim Dimensions 2.5 Axial 2.5 Radial CM)

	TYPE	PLYES	THICKNESS INCHES	THICKNESS CM	RAD LGTH CM	PERCENT RAD LGTH
COATING			0	0.00E+00	0.00E+00	0.0000
FOAM	31IG	1	0.9843	2.50E+00	2.67E−03	0.2669
COATING			0	0.00E+00	0.00E+00	0.0000
TOTAL						0.2696

2) Straw Tube Materials:

2.1.1) Raw Production Mylar Material Properties:

		THICKNESS INCHES		(gms/cm3 * Xo cm = Xo gms/cm2) DENSITY		Constant	Rad Lg	
VENDOR	TYPE	DIAM	WALL	LBS/IN3	gms/CM3	(Xo)	CM	COST/IN.3
	Mylar	4.0437	0.0014	5.0E-02	1.4E+00	39.9	28.7	

2.1.2) Raw Production Tungsten Material Properties:

		THICKNESS INCHES		(gms/cm3 * Xo cm = Xo gms/cm2) DENSITY		Constant	Rad Lg		100.00
	VENDOR	TYPE	DIAM	WALL	LBS/IN3	gms/CM3	(Xo)	CM	COST/IN.3	2.75
A)		Tungsten					9.6	0.35		

2.2) Fabricated Straws:

2.2.1) Fabricated Straw Material Properties:

A) Trigger Layer (8 Straws Deep):

	LAYERS	THICKNESS INCHES	THICKNESS CM	RAD LGTH CM	PERCENT RAD LGTH
STRAWS					
Mylar	8	3.52E-02	8.94E-02	3.11E-03	0.3114
Al					
GLUE					
SUPPORTS					
WIRE					
TOTAL					0.3114

B) Axial or Stereo Layer (6 Straws Deep):

	LAYERS	THICKNESS INCHES	THICKNESS CM	RAD LGTH CM	PERCENT RAD LGTH
STRAWS					
Mylar	6	2.64E-02	6.70E-02	2.34E-03	0.2336
Al					
GLUE					
SUPPORTS					
WIRE					
TOTAL					0.2336

(Later)

3) Support Spaceframe Candidate Materials:

3.1) Raw Support Spaceframe Materials (gms/cm3 * Xo cm = Xo gms/cm2)

	VENDOR	TYPE	THICKNESS INCHES	MODULUS PSI	TENSILE PSI	CTE DEG F	DENSITY LBS/IN3	gms/CM3	Constant (Xo)	Rad Lg CM	COST/IN.3
A)	(See 1.1.1 Above) Raw Fiber B–Staged Unidirectional Graphite Properties:										
B)	DWA	SIC	.05 TO 2	4.7E+07	?	2.23	1.1E–01	3.1E+00	26.64	8.52	11.30
C)		Al	(Various)	1.0E+07	6.00E+04	12.89	1.0E–01	2.8E+00	24.93	8.9	0.28
D)	KAISER	C–C	Bolts	1.6E+07	4.00E+04	–0.11	6.0E–02	1.7E+00	18.8	18.8	

3.2) Fabricated Spaceframe:

3.2.1) Fabricated Strut Material Properties:

	Component	Size(cm)	AXIAL	AZMUTHAL	WALL TK	RADIAL
A)	Struts(Hollow)		4	2	0.25	N/A

	Component	Material	#	THICKNESS INCHES	THICKNESS CM	RAD LGTH CM	PERCENT RAD LGTH
A)	Struts	Graphite	4	1.97E–01	5.00E–01	1.94E–02	1.9438

IN PLANE MODULUS MSI			POISSON RATIO		CTE (IN/IN/DEG F)	
0 DEG*	90 DEG	SHEAR	90/0	0/90	0 DEG	90 DEG
40						

FLEXURAL MODULUS MSI			POISSON RATIO	
0 DEG*	90 DEG	SHEAR	90/0	0/90
40				

* Per Composites Horizons,Inc & Kaiser Aerotech use 40 to 50 percent of the Raw Fiber Modulus

3.2.2) Fabricated Joint Material Properties:

	Component	Size(cm)	AXIAL	AZMUTHAL	WALL TK	RADIAL
A)	Joints(Hollow)		4	4	0.38	4

	Component	Material	#	THICKNESS INCHES	THICKNESS CM	RAD LGTH CM	PERCENT RAD LGTH
A)	Joints	Graphite	4	2.99E–01	7.60E–01	2.95E–02	2.9546

IN PLANE MODULUS MSI			POISSON RATIO		CTE (IN/IN/DEG F)	
0 DEG	90 DEG	SHEAR	90/0	0/90	0 DEG	90 DEG

FLEXURAL MODULUS MSI			POISSON RATIO	
0 DEG	90 DEG	SHEAR	90/0	0/90

3.2.3) Fabricated Ring Material Properties:

	Component	Size(cm)	AXIAL	AZMUTHAL	WALL TK	RADIAL
A)	Rings		0.25	N/A	N/A	1.5

	Component	Material	#	THICKNESS INCHES	THICKNESS CM	RAD LGTH CM	PERCENT RAD LGTH
A)	Rings	Graphite	4	9.84E-02	2.50E-01	9.72E-03	0.9719

IN PLANE MODULUS MSI			POISSON RATIO		CTE (IN/IN/DEG F)	
0 DEG*	90 DEG	SHEAR	90/0	0/90	0 DEG	90 DEG
40						

FLEXURAL MODULUS MSI			POISSON RATIO	
0 DEG*	90 DEG	SHEAR	90/0	0/90
40				

* Per Composites Horizons,Inc & Kaiser Aerotech use 40 to 50 percent of the Raw Fiber Modulus

3.2.4) Fabricated Bolt Material Properties:

Bolt		Size	TAP DRILL INCHES	THREAD PSI SS ULT	SHEAR POUNDS @1.5*O.D.
A)	ALUM	1/4-20	0.204	36000	7060
B)	STEEL	1/4-20	0.204	32000	6276
C)	K-KARB	1/4-20	0.204	3640	714
D)	K-KARB	3/8-16	0.316	2640	1242
E)	K-KARB	1/2-13	0.422	1970	1653

ANALYSIS OF DEADWEIGHT DEFLECTIONS OF A STEEL MANDREL FOR FABRICATING A COMPOSITE MODULE-SUPPORT CYLINDER FOR THE CENTRAL TRACKER STRUCTURE

Presented 26 September 1991
Oak Ridge National Laboratory
by R. L. Swensrud

ABSTRACT

It is proposed to fabricate each module support cylinder of the central tracker on a steel mandrel; this mandrel consists of a large cylindrical shell supported internally near its quarter-points by disks which carry its weight to a long shaft with bearings at either end. The gravity-induced deflections of the largest such mandrel were studied to guide its design so as to produce the straightest possible cylinder. Preliminary calculations indicated that the outer shell of a mandrel acts a short, stiff beam whose shear deflections dominate over the bending deflections. Minimizing the gravity sag is sensitive to the axial location of the support disks. More comprehensive calculation, modeling the entire shell-disk-shaft assembly, was carried out using the ANSYS finite-element package.

1

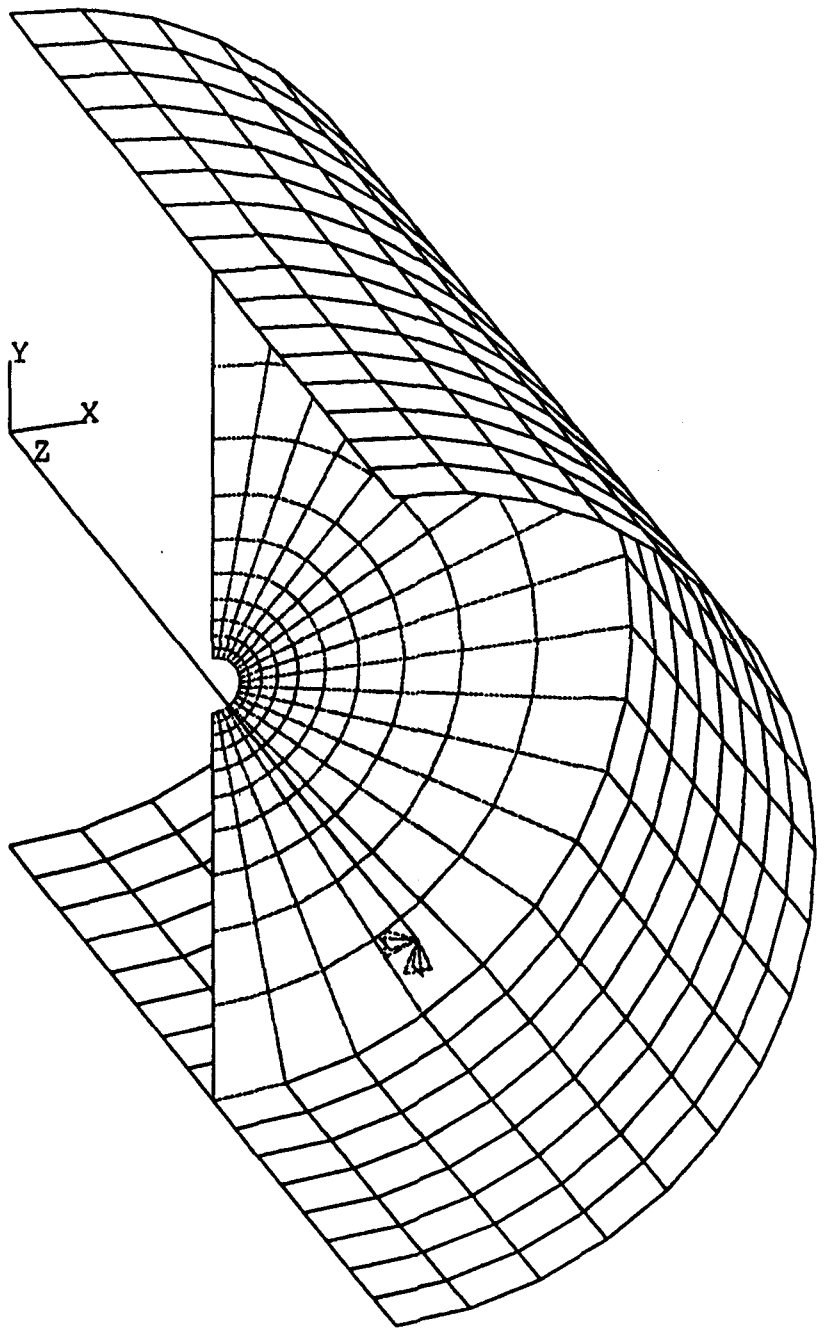

Mandrel Part 06, D=3064 mm Shaft D=8 Disk t=2.0

ANSYS 4.4A
SEP 5 1991
15:49:16
PLOT NO. 1
POST1 ELEMENTS
TYPE NUM

XV =-1
YV =1.4
ZV =3
*DIST=101.549
*XF =29.97
*ZF =87.677
PRECISE HIDDEN

POST1 NODES
TDIS

XV =-1
YV =1.4
ZV =3
*DIST=101.549
*XF =29.97
*ZF =87.677

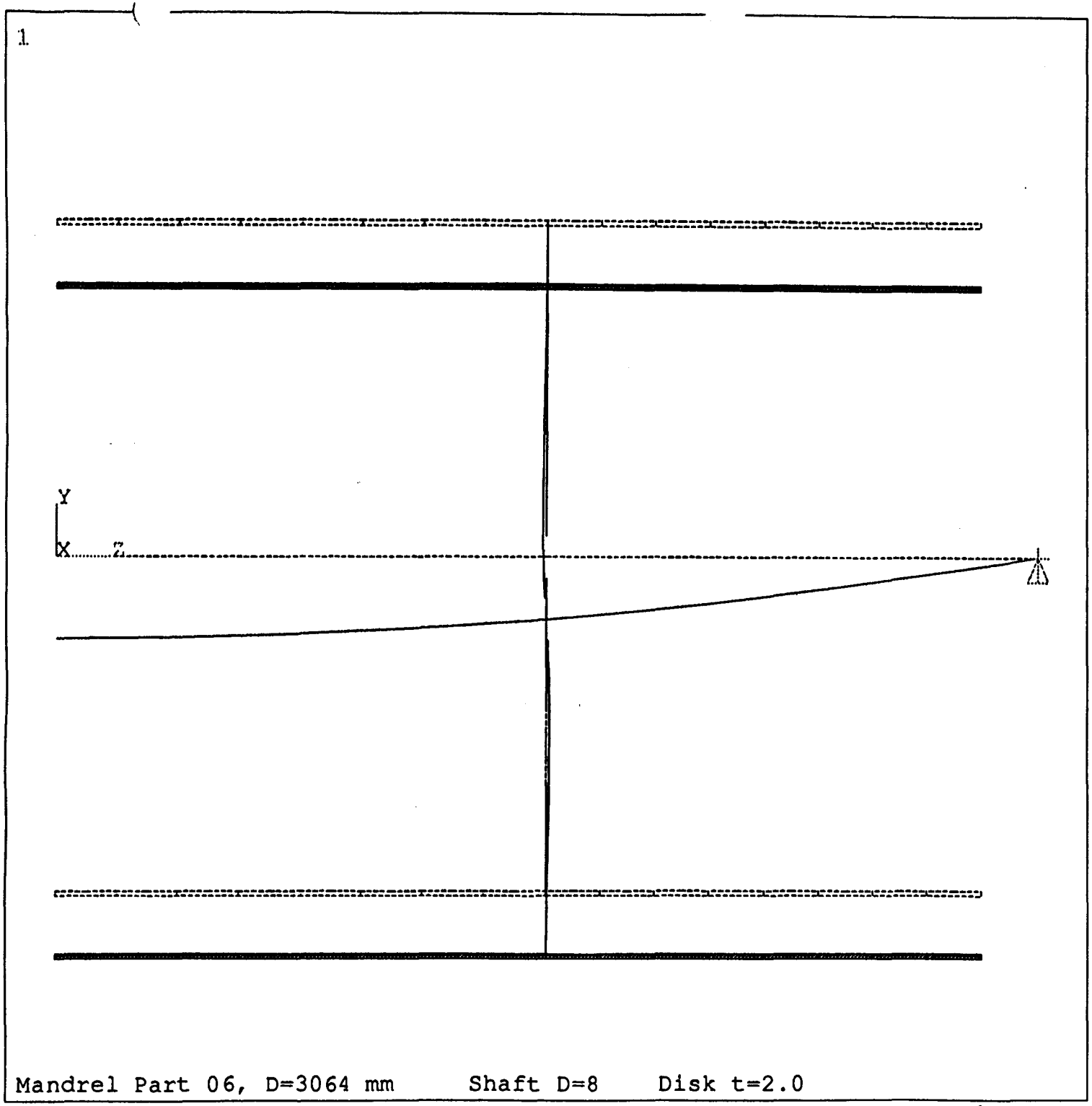

ANSYS 4.4A
SEP 5 1991
15:57:49
PLOT NO. 1
POST1 DISPL.
STEP=1
ITER=1
DMX =1.453
ERPC=0

*DSCA=10
XV =-1
DIST=96.445
XF =5.998
ZF =87.677

POST1 NODES
TDIS

XV =-1
*DIST=96.445
*XF =5.998
*ZF =87.677

CENTRAL AND FORWARD TRACKING SUBSYSTEM

7 MANDREL STRESSES & DISPLACEMENTS FROM FINITE ELEMENT ANALYSIS

Shaft Dia in.	Dsk Tk in.	Disk Nom. kips -in.	Disk Slope	Disk σ_e ksi	Disk σ_r ksi	Displacement Inches				
						Place	Cyl End	Disk	Cyl Midpt	Local Max.	Local Min.
						T/B	2.32452	2.32413	2.32464	2.3259	2.3226
8.0	1.0	179.	0.0186	74.5	83.7	Side	2.32448	2.32441	2.32463		
						Shaft		2.32377			
						T/B	1.61647	1.61655	1.61710	1.6196	1.6137
8.0	2.0	642.	0.0092	67.0	75.1	Side	1.61642	1.61672	1.61715		
						Shaft		1.61634			
						T/B	1.11005	1.10961	1.11011	1.1107	1.088
10.	1.0	93.	0.0091	34.1	38.2	Side	1.11001	1.10988	1.11009		
						Shaft		1.10928			
						T/B	0.89374	0.89371	0.89422	0.8960	0.8916
10.	2.0	494.	0.0062	41.4	46.5	Side	0.89369	0.89388	0.89425		
						Shaft		0.89352			
						T/B	0.60024	0.59978	0.60027	0.6005	0.5994
12.0	1.0	63.	0.0051	17.8	19.9	Side	0.60020	0.60005	0.60024		
						Shaft		0.59948			

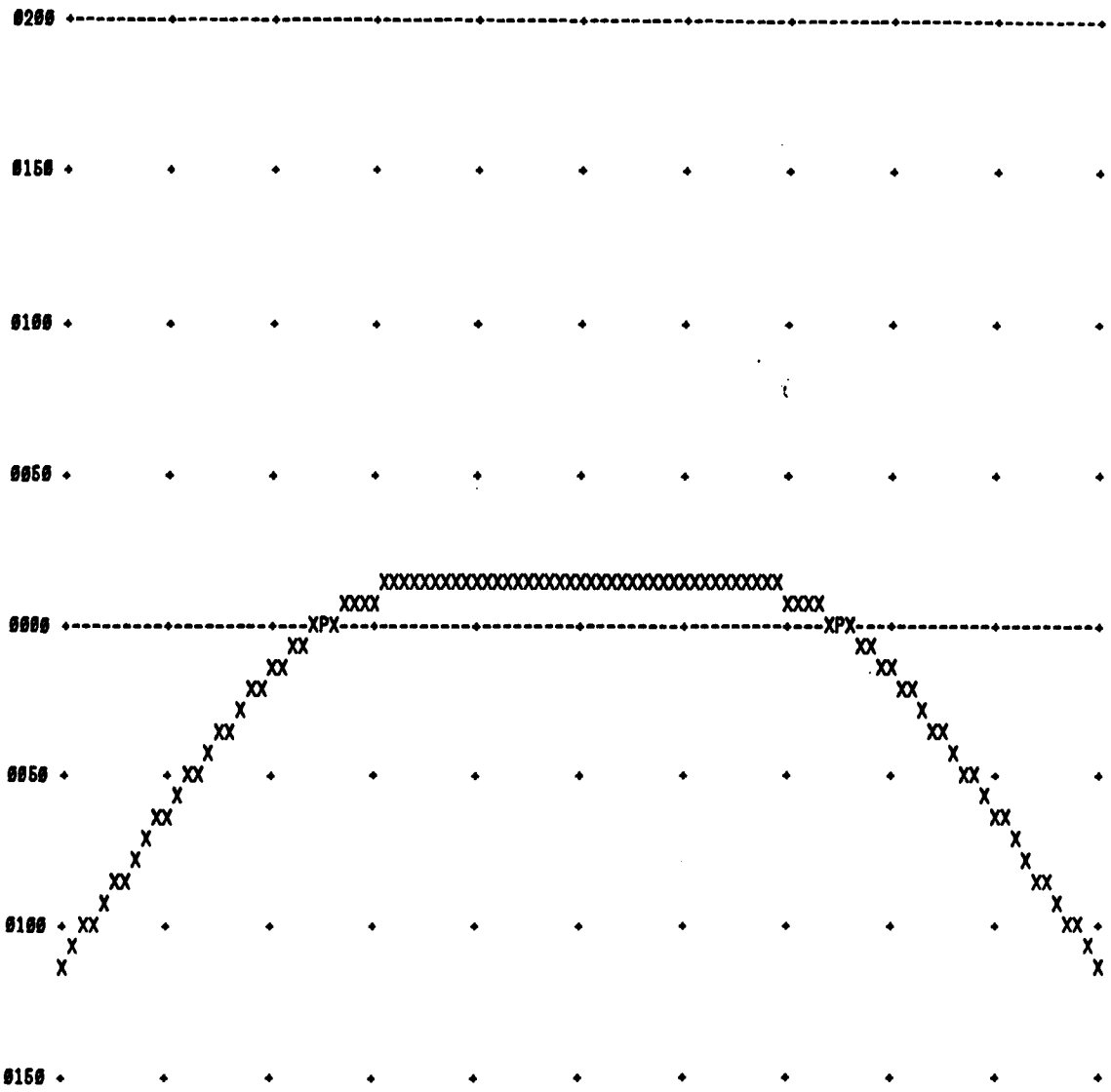

0200
0 10 20 30 40 50 60 70 80 90 100

1 LINE= 18
0.07143

DEFLECTION CURVE

STATIC CALCULATIONS * MANDREL OUTER SHELL DUMMY FOR SUPPORT-POINT PLACEMENT
22 AUG 1991 EI = 1.E9 LC = 25. LS = 50. W/L = 1000.

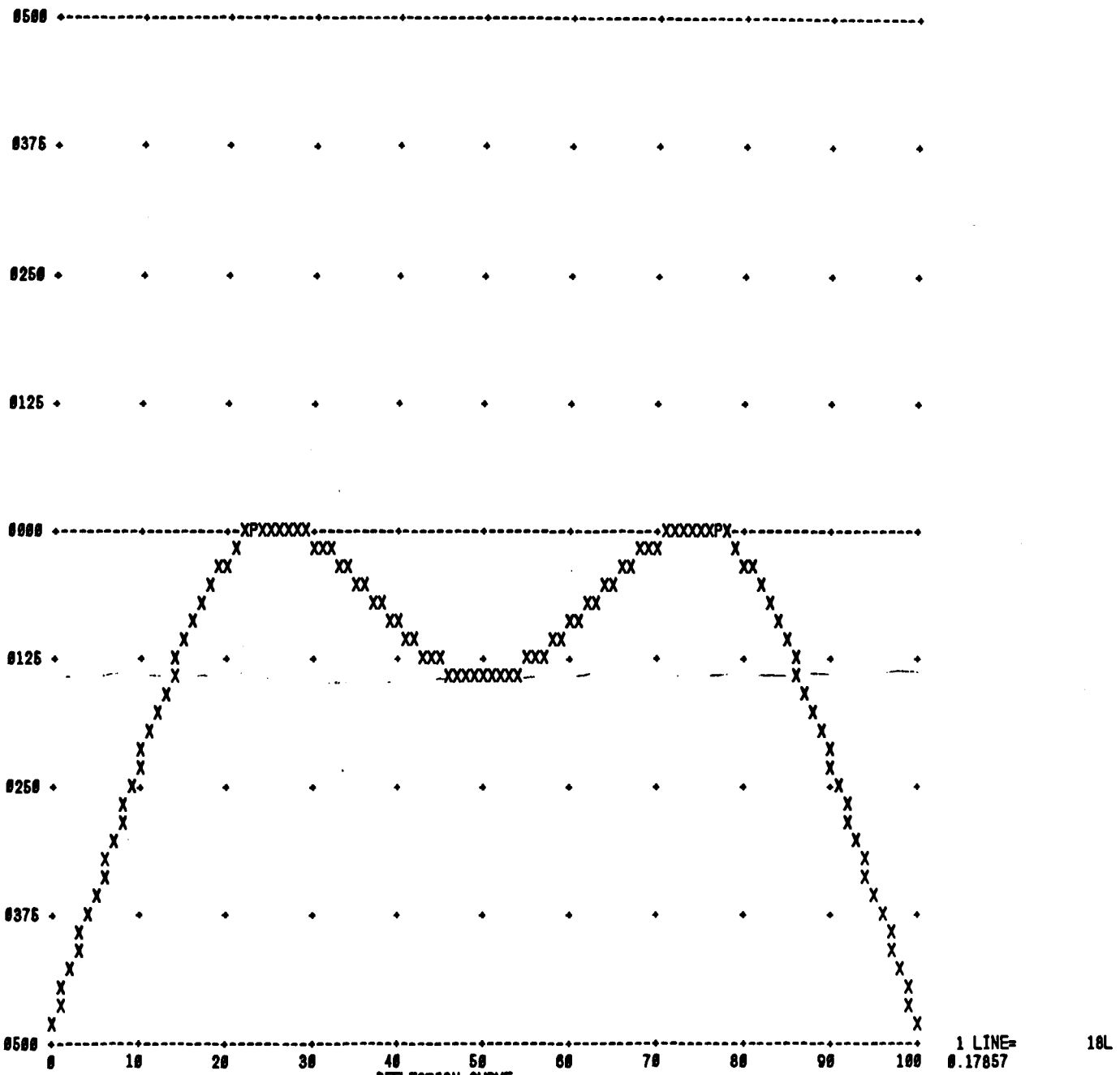

DEFLECTION CURVE

STATIC CALCULATIONS * MANDREL OUTER SHELL DUMMY FOR SUPPORT-POINT PLACEMENT
22 AUG 1991 EI = 1.E9 LC = 23. LS = 54. W/L = 1000.

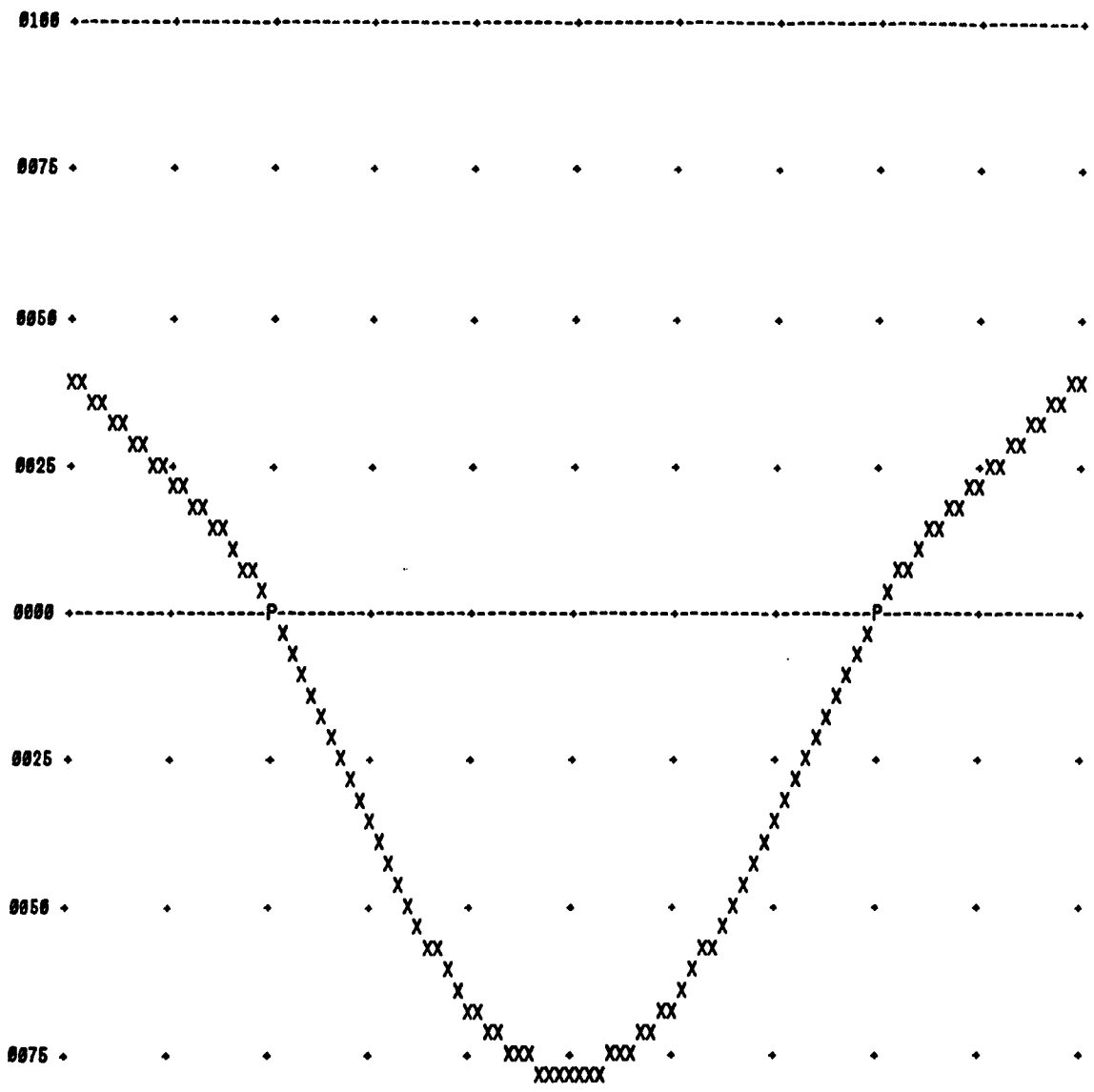

0 10 20 30 40 50 60 70 80 90 100

1 LINE= 18L
0.03671

DEFLECTION CURVE

STATIC CALCULATIONS * MANDREL OUTER SHELL DUMMY FOR SUPPORT-POINT PLACEMENT
22 AUG 1991 EI = 1.E9 LC = 20. LS = 60. W/L = 1000.

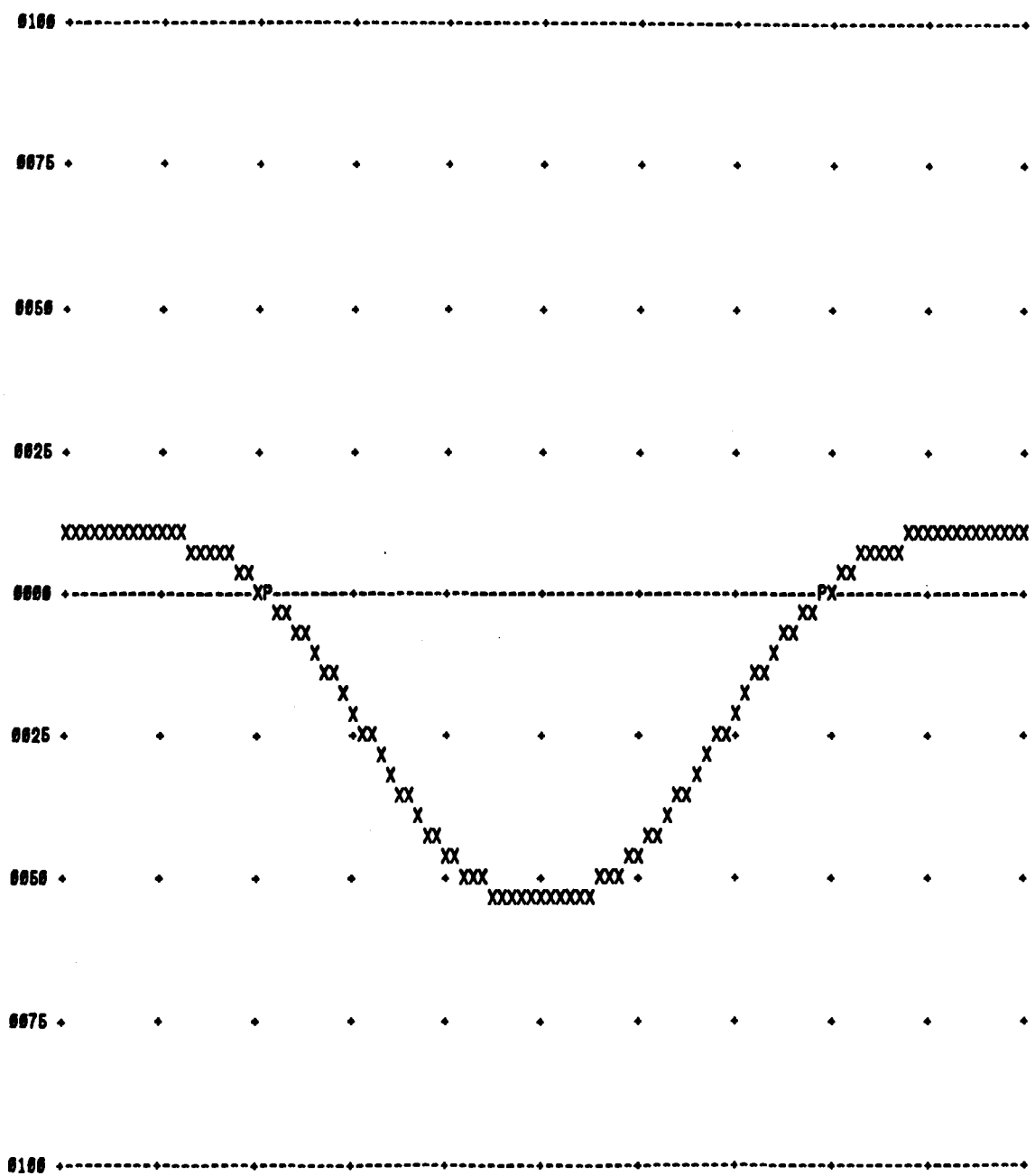

1 LINE= 18L
0.03571

DEFLECTION CURVE

STATIC CALCULATIONS * MANDREL OUTER SHELL DUMMY FOR SUPPORT-POINT PLACEMENT
22 AUG 1991 EI = 1.E9 LC = 21. LS = 50. W/L = 1000.

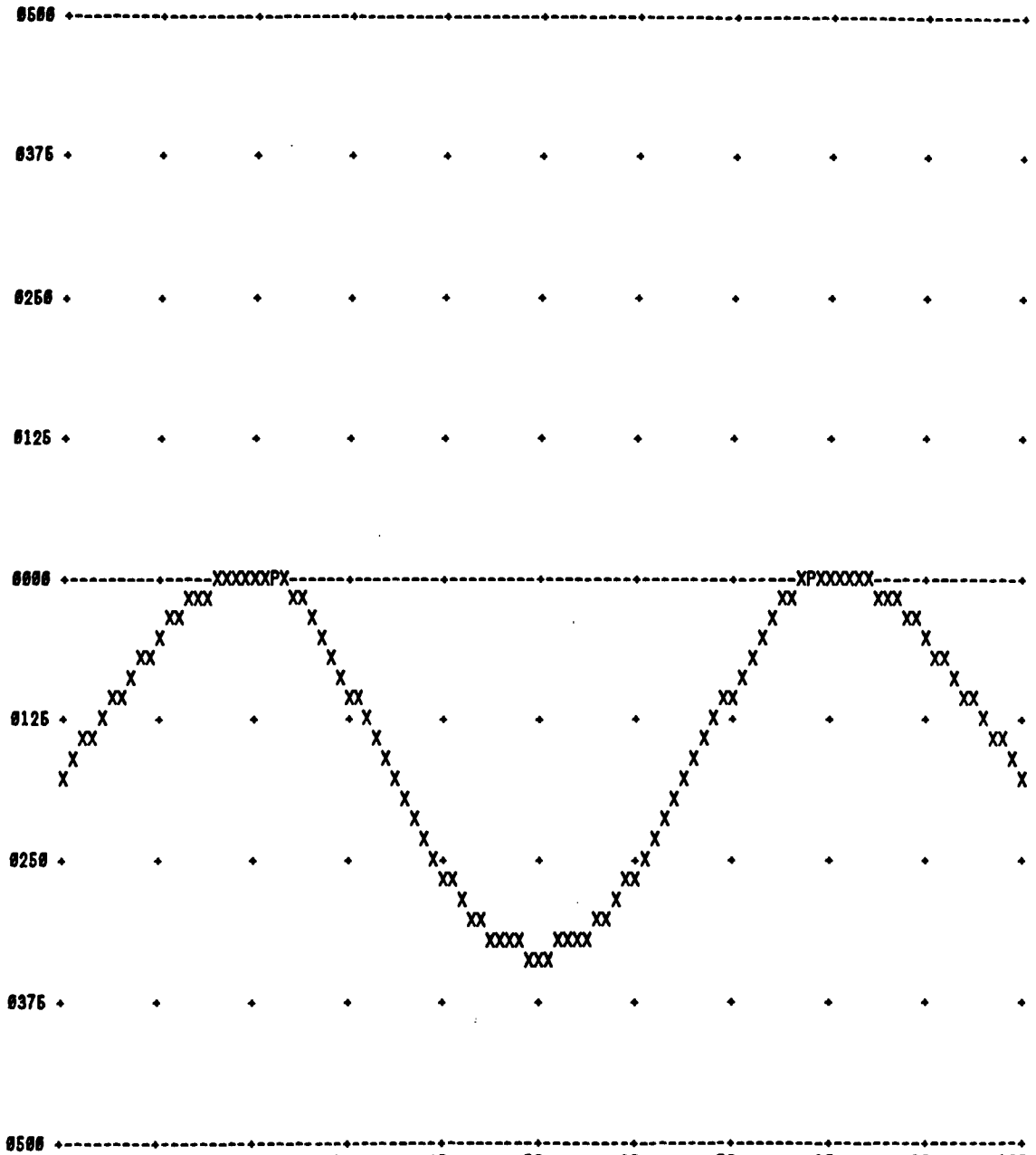

1 LINE= 18L
0.17857

DEFLECTION CURVE

STATIC CALCULATIONS * MANDREL OUTER SHELL DUMMY FOR SUPPORT-POINT PLACEMENT
22 AUG 1991 EI = 1.E9 LC = 22. LS = 66. W/L = 1000.

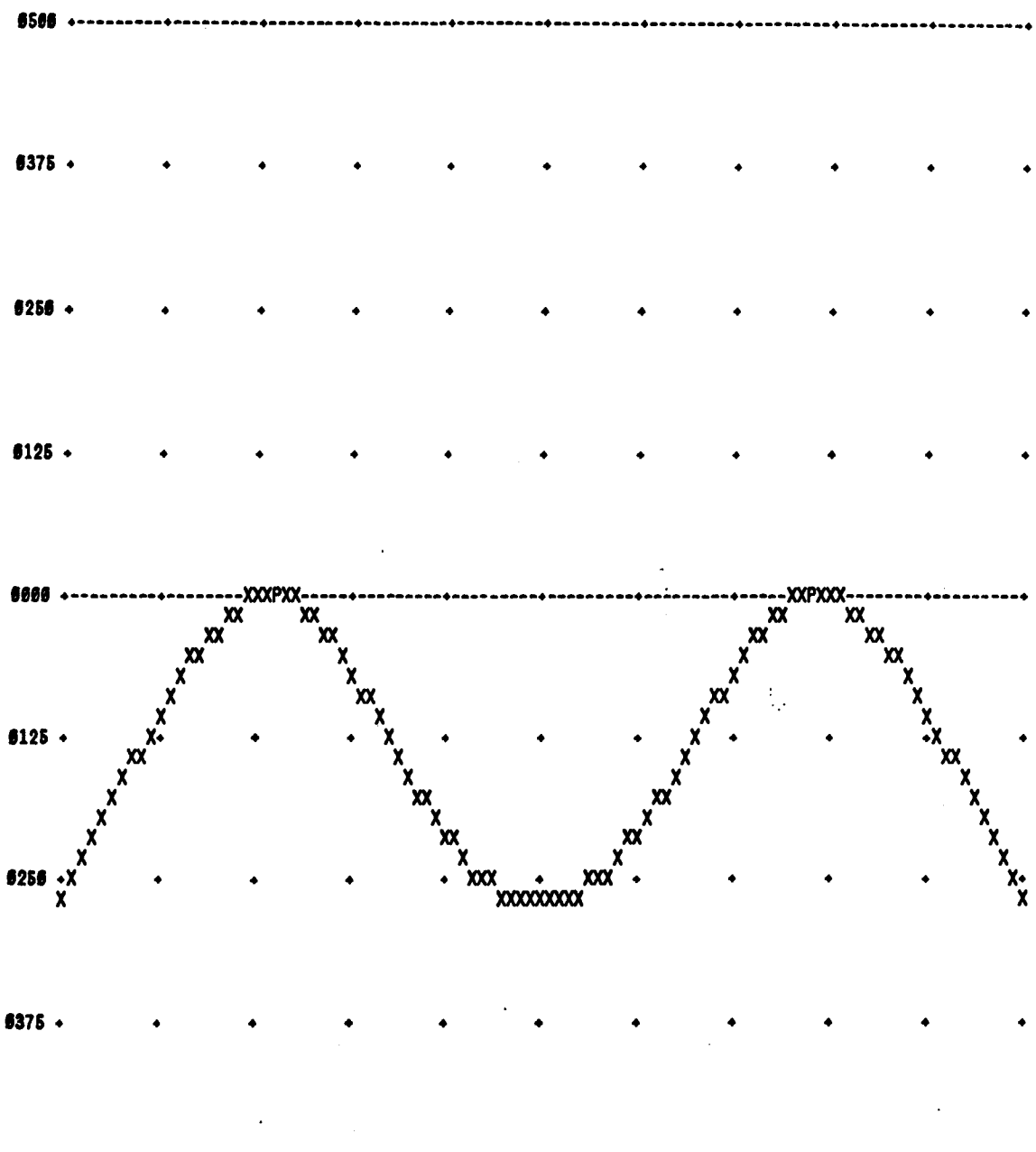

1 LINE= 18L
0.17857

DEFLECTION CURVE

STATIC CALCULATIONS * MANDREL OUTER SHELL DUMMY FOR SUPPORT-POINT PLACEMENT
22 AUG 1991 EI = 1.E9 LC = 22.3 LS = 55.4 W/L = 1000.

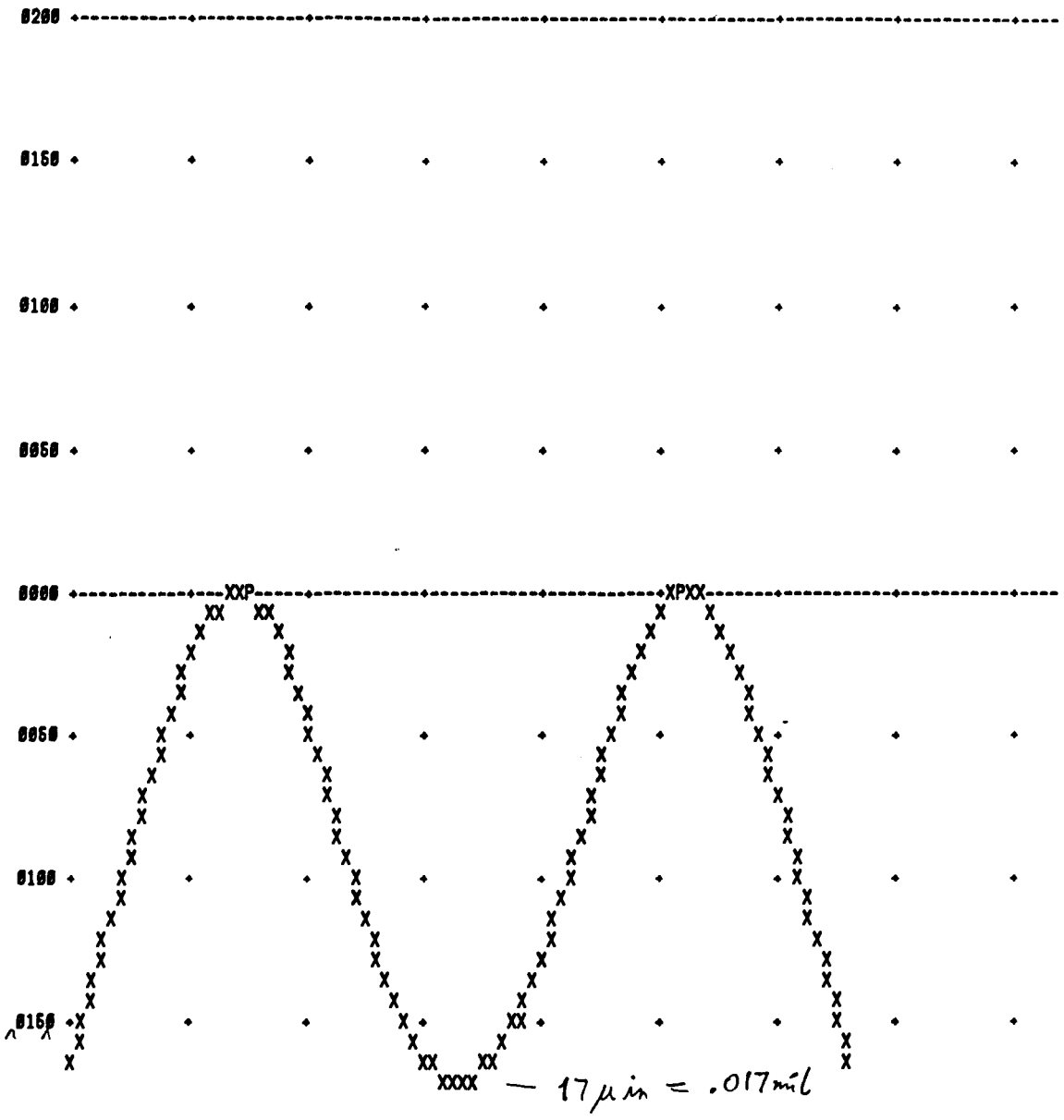

0 50 100 150 200 250 300 350 400

1 LINE= 18L
0.07143

DEFLECTION CURVE

STATIC CALCULATIONS • MANDREL #6 OUTER SHELL (3664 MM) NO SHEAR DISPL
22 AUG 1991 L = 8400 MM = 330.7 IN OD = 120.5 IN ID = 119.0 IN

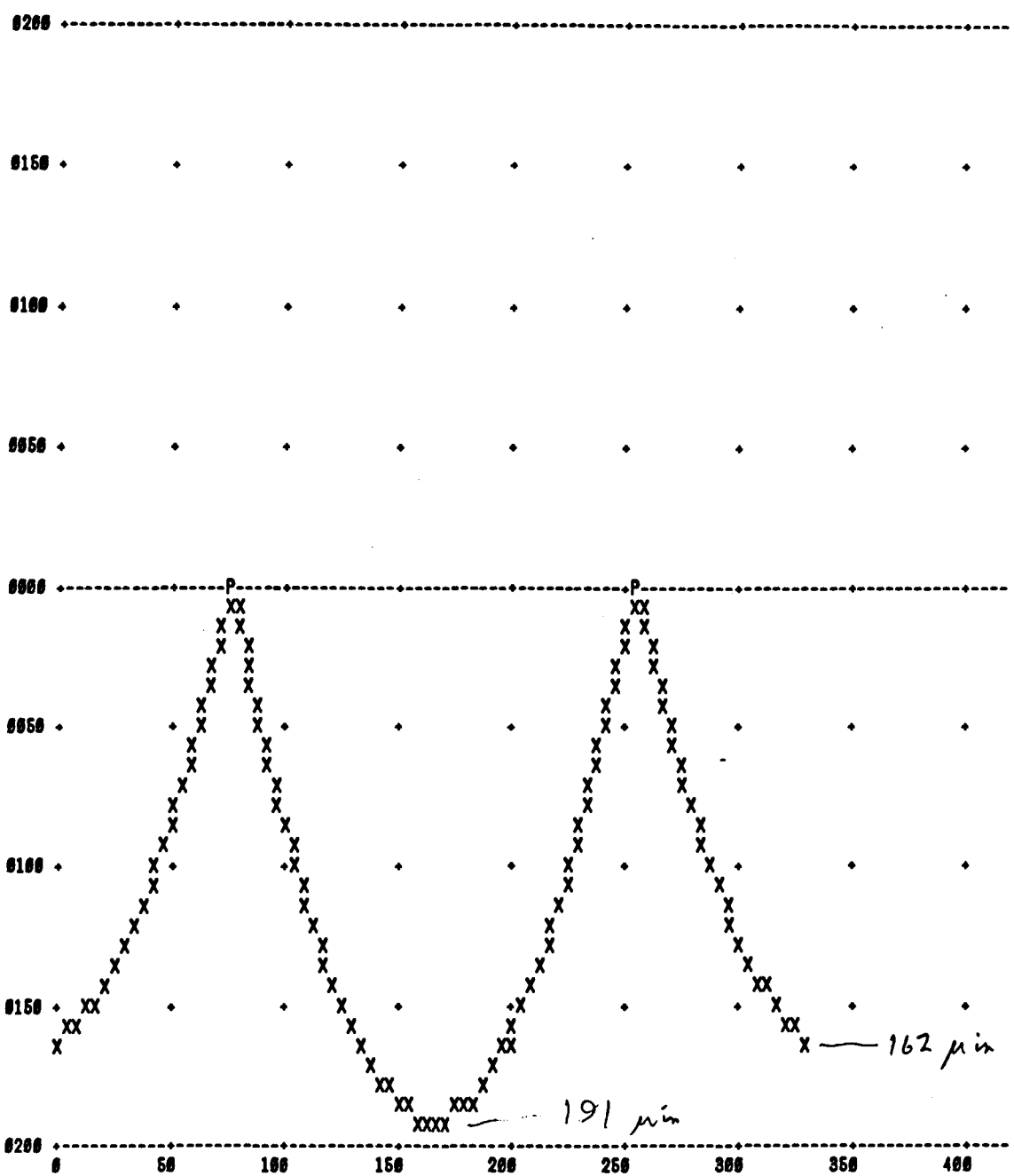

1 LINE= 18L
0.07143

STATIC CALCULATIONS + MANDREL 66 OUTER SHELL (3664 MM) W/ SHEAR DEFL. AT 23-PCT POINTS
23 AUG 1991 L = 8466 MM = 336.7 IN OD = 126.5 IN ID = 119.8 IN

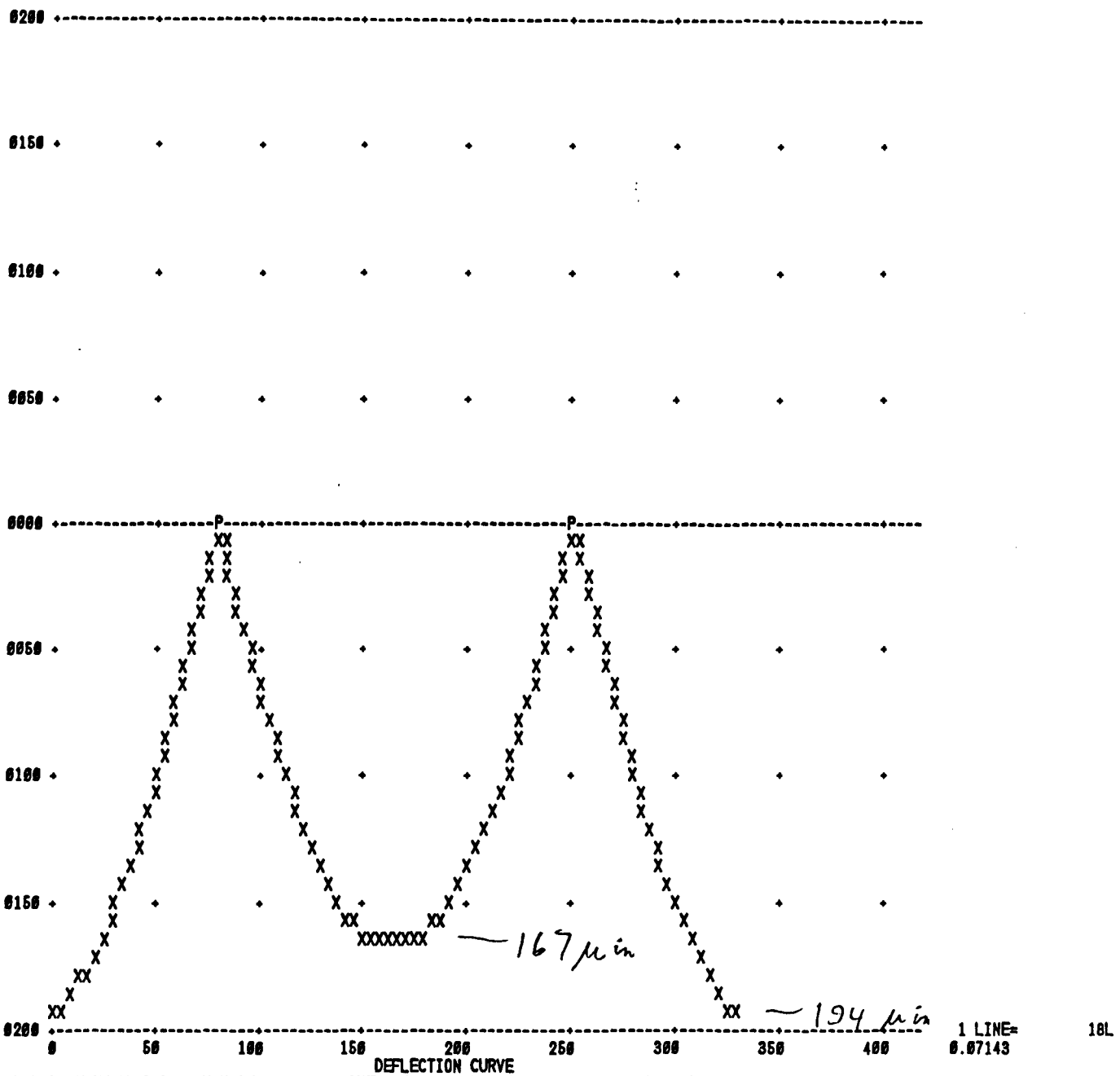

STATIC CALCULATIONS * MANDREL #6 OUTER SHELL (3064 MM) W/ SHEAR DEFL. AT 24-PCT POINTS
23 AUG 1991 L = 8400 MM = 330.7 IN OD = 120.5 IN ID = 119.0 IN

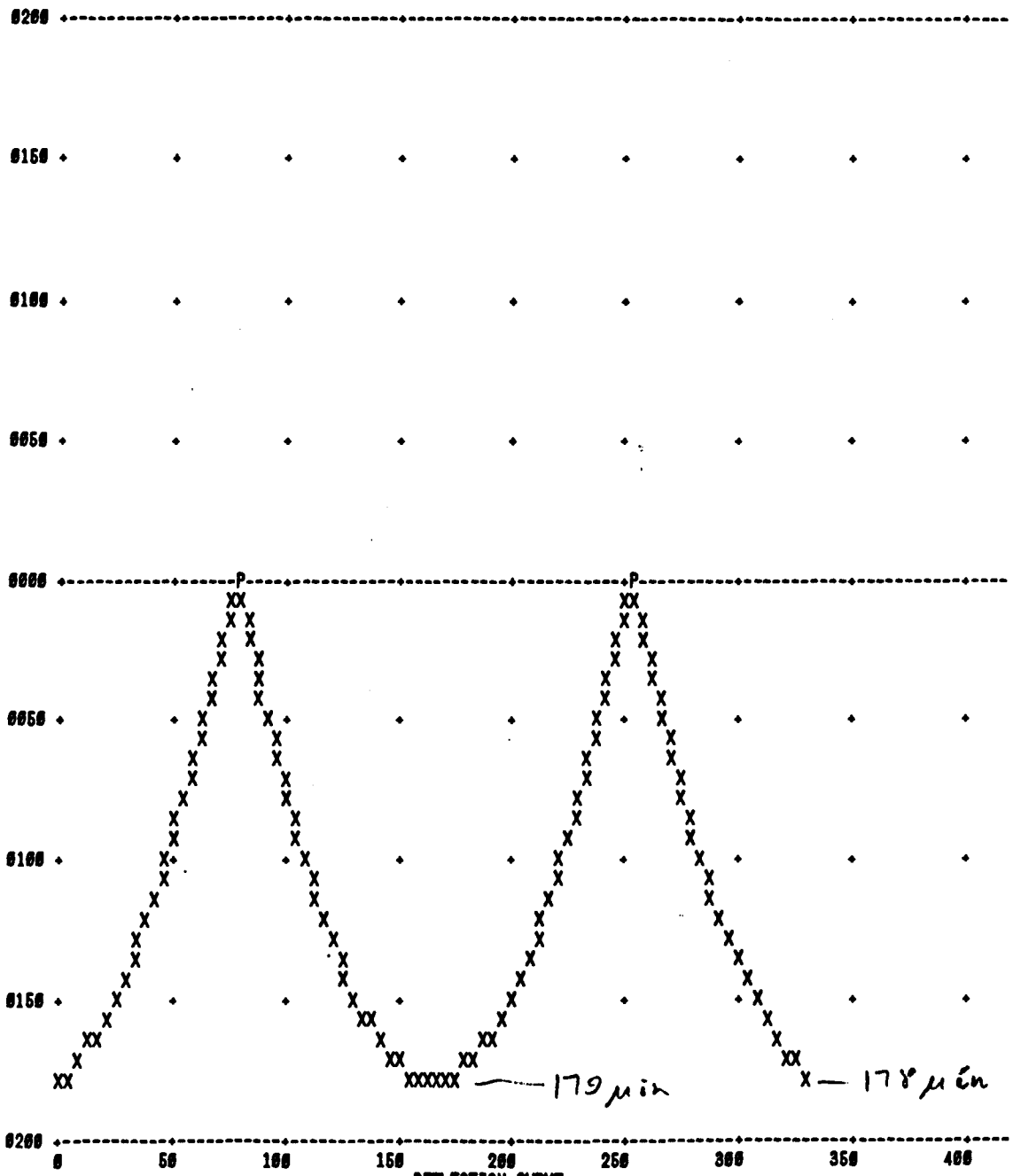

DEFLECTION CURVE

STATIC CALCULATIONS + MANDREL #6 OUTER SHELL (3064 MM) W/ SHEAR DEFL. AT 23.6-PCT POINTS
23 AUG 1991 L = 8400 MM = 330.7 IN OD = 120.5 IN ID = 119.0 IN

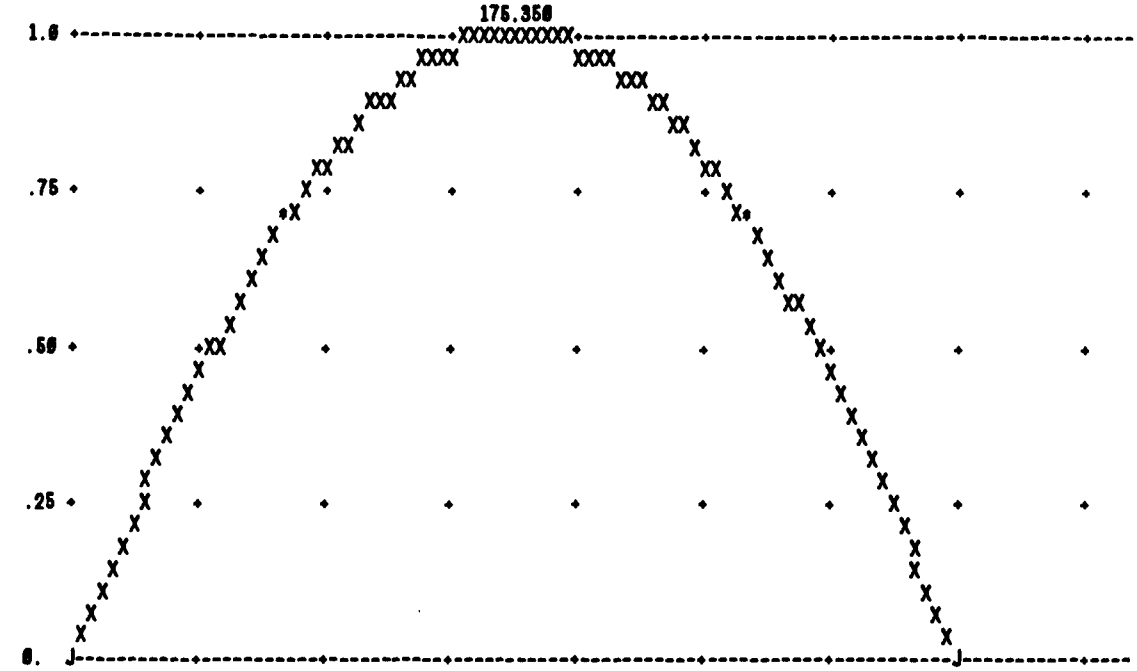

1 LINE= 18L
0.03571

MODE SHAPE RPM= 128.559 (2.1093 HZ)

RIGID CALCULATIONS * MANDREL 06 SHAFT (8-INCH) W/ ADDED WT.
28 AUG 1991 10-INCH EXTENSIONS TO BEARINGS * L = 350.7 IN MODE 1 -4.9D-04
ROTOR MASS= 3.13948E+04 LB GENERALIZED MASS = 1.55354E+04 E.M.=3.04238E+04 -2.8D+10
CALCULATION CUT OFF AFTER FINDING 1 CRITICALS ABOVE 0.0 RPM 04Q

FINITE-ELEMENT ANALYSIS OF DEADWEIGHT DEFLECTIONS OF SIX-CYLINDER CENTRAL TRACKER SUPPORT STRUCTURE WITH SPACEFRAME END SUPPORT

Presented 26 September 1991
Oak Ridge National Laboratory
by R. L. Swensrud

ABSTRACT

The gravity-induced deflections of a six-cylinder central tracker support structure were calculated using the ANSYS package. Two loading variations were considered: with each cylinder supporting a superlayer of detector-straw modules, and with the the innermost two superlayers composed instead of scintillation fiber detectors, roughly quadrupling their weight.

1. INTRODUCTION

The deflections of the central tracker under its own weight have been estimated for the design shown in Figure 1. This design is composed of six concentric structural cylinders, each of which supports one superlayer of detectors, the cylinders being attached at the ends to a space frame of hollow struts. The six cylinders are made of identical symmetrical sandwiches of foam core with outer skin layers of graphite-epoxy laminate. The entire structure is supported at the four corner points indicated in Figure 1: the vertices of the outer ring of the space frame which lie in the horizontal plane through the axis of the structure. Each cylinder is attached at each end to an angle-section ring which connects it to the space frame.

Figure 2 shows some details of the space-frame portion of the structure. Dimensions are given both for the angle section used to attach the cylinders, and for the hollow box section used for all the struts making up the frame itself.

The straw detector module design is shown in Figure 3; modules consist of trapezoidal shells whose interior space is filled with straw detectors 4.0 mm in diameter and weighing 0.5 g/m. The walls of a shell are made of sandwiches of graphite-epoxy skins over a foam core, similar to the structure of the support cylinders.

Each module superlayer is attached to its supporting cylinder by shim rings which are indicated in Figure 4. The modules are more or less loosely attached to these rings. Since the modules are not connected to each other and are not firmly attached to the cylinders, they contribute negligible stiffness to the cylinders. They can therefore be treated as non-structural mass whose dead weight constitutes much of the load on the structure. The module design shown in Figure 3 is estimated to mass 0.2167 kg/m (non-trigger module) and 0.2503 kg/m (trigger module).

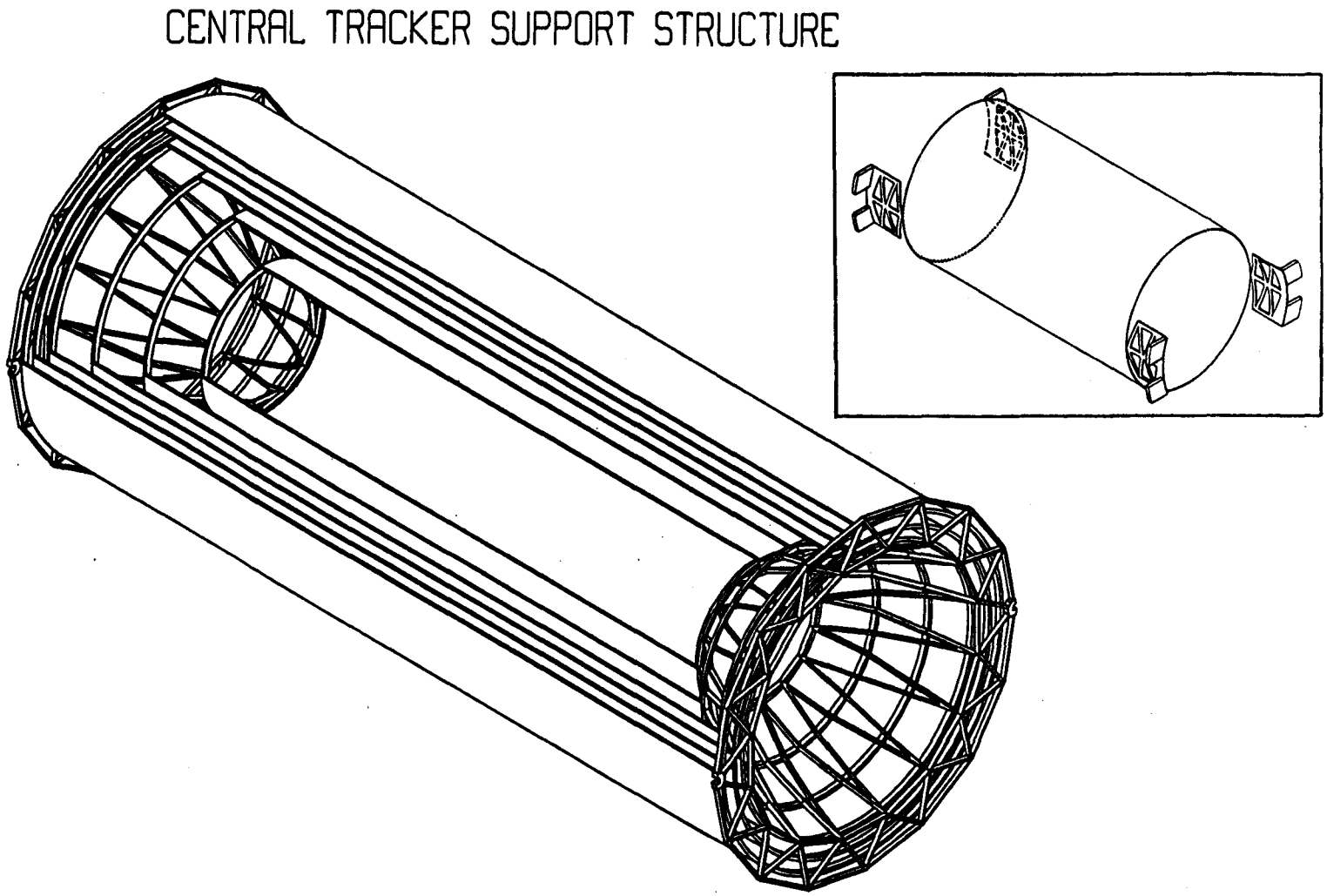

Figure 1: Isometric sketch of tracker structure.
Inset: schematic indication of corner support points.

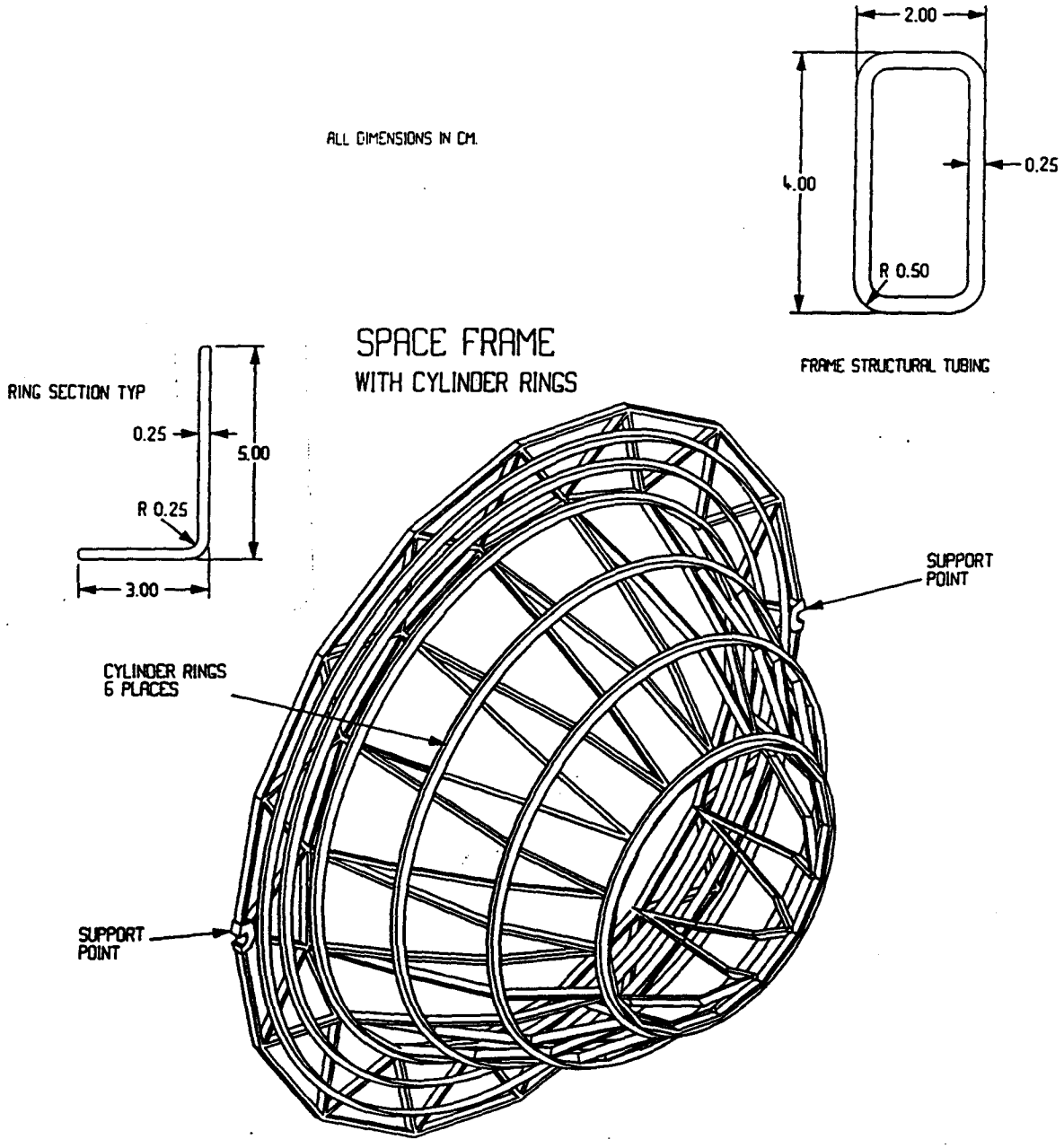

Figure 2: Tracker structure space frame, with dimensions of structural element cross-sections.

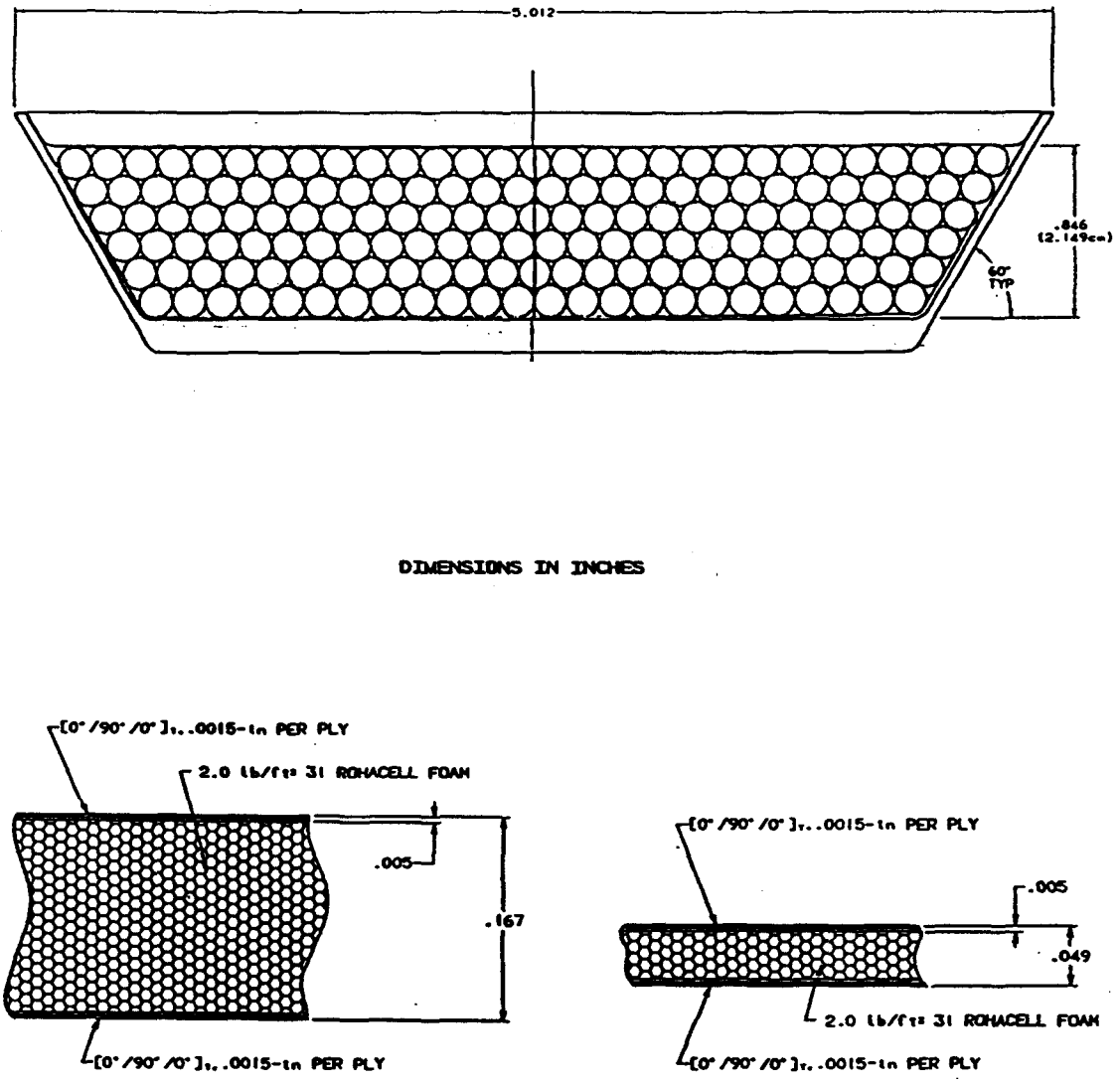

Figure 3: Construction of straw module (non-trigger).

Upper: Overall cross-section.
Lower left: Shell top & bottom construction.
Lower right: Shell sidewall construction.

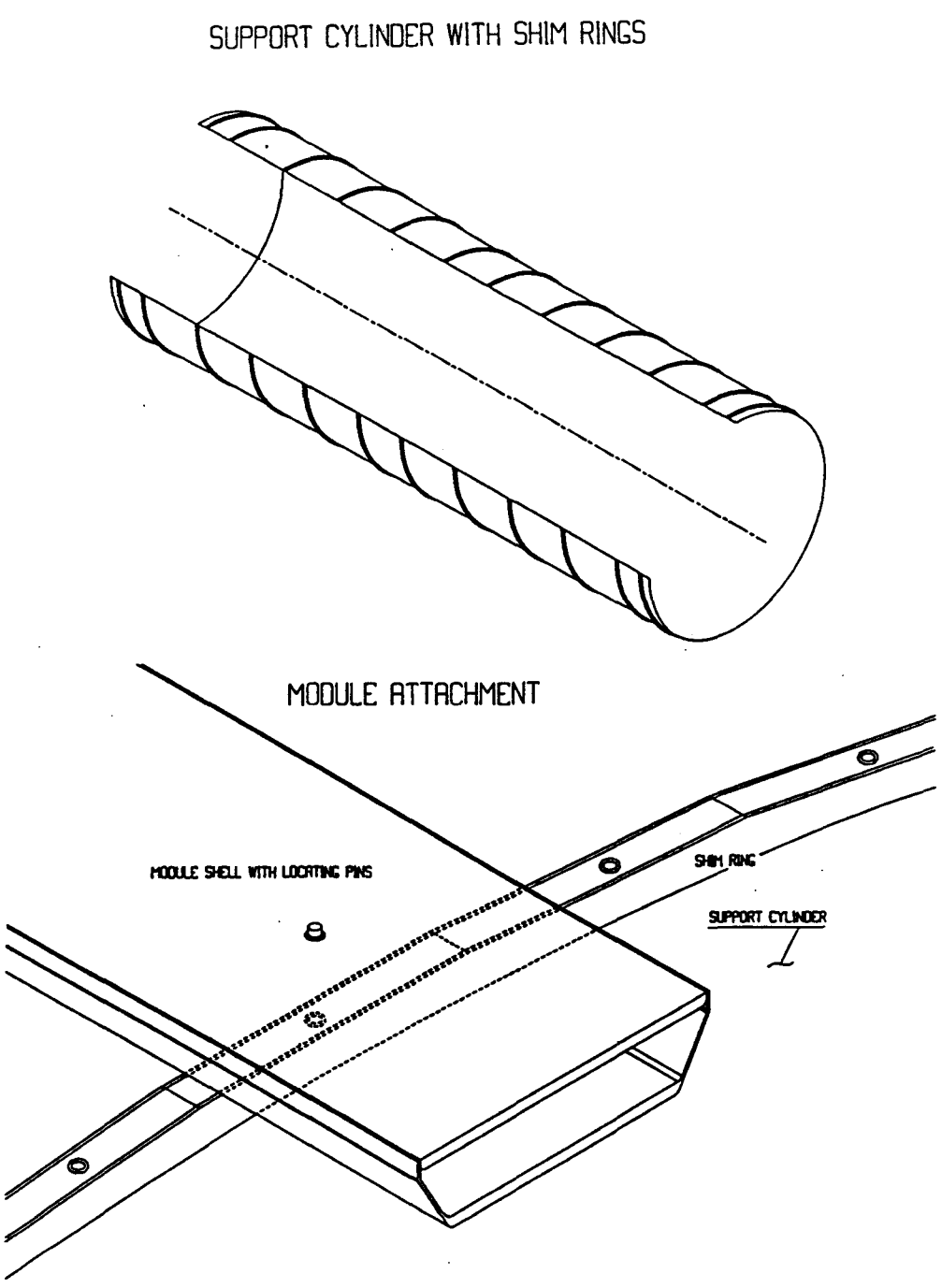

Figure 4: Arrangement of shim rings connecting module superlayer to support cylinder.

The outer four superlayers are always composed of the trapezoidal straw modules described above; for the two innermost superlayers, however, two alternative types of detector have been considered. The lighter option is to make these layers also of straw modules (non-trigger), which load the cylinders pretty uniformly over their surfaces at 2.044 kg per square meter. An alternative design is to make the innermost superlayer of eight layers of scintillation fibers and the second superlayer of twelve layers, introducing superlayer masses of 6.64 and 9.96 kg/m^2 respectively.

To assess the static deflections of this structure due to gravity loading, two families of finite-element model have been constructed using the ANSYS package. These models will be described in the following section.

2. FINITE-ELEMENT MODELS

Figure 1 shows that the structure has two vertical planes of mirror symmetry, dividing it end-to-end and side-to-side. Because of this symmetry, only a quarter of the structure needed to be modeled. Two groups of models were studied: first, models of the end frame alone were run to explore the characteristics of this type of end construction; when feasible frame configurations had been identified, models with the cylinders included were run to get better-detailed pictures of the displacement patterns of the tracker structure. These models will be described in the following sections.

2.1 Modeling of Space Frame

The space frame is modeled with the ANSYS STIF4 3-dimensional beam element, using the two cross-sections indicated in Figure 2: the rectangular box section for the frame proper, and the angle section for the rings to which the cylinders attach. A typical mesh for this model appears in Figure 5; several frame design variations were considered, as will be discussed in a later section.

The nodes in the Y-Z symmetry plane were constrained to have no displacements in the X-direction, and no rotations around the Y or Z axes. The support point on the outer rim was constrained against displacement in the Y direction. The nodes of the rings were constrained against displacement in the Z direction, to approximate the anticipated very stiff character of the cylinders as bending beams; this constraint also prevented the frame from rigid-body rotation about the X-axis.

The weight of the cylinders and their associated modules was included by increasing the density of the material used in modeling the rings, specifying their density as 3.98e-5 kg/mm^3. This is about 24 times the actual 1.63e-6 kg/mm^3 density of the graphite/epoxy, the value input for the box-beam struts. The total masses for one quarter-model were 17.7 kg for the struts and 273.2 kg for the ring/cylinders. Only all-module loadings were calculated with this model; the scintillation-fiber option was not considered.

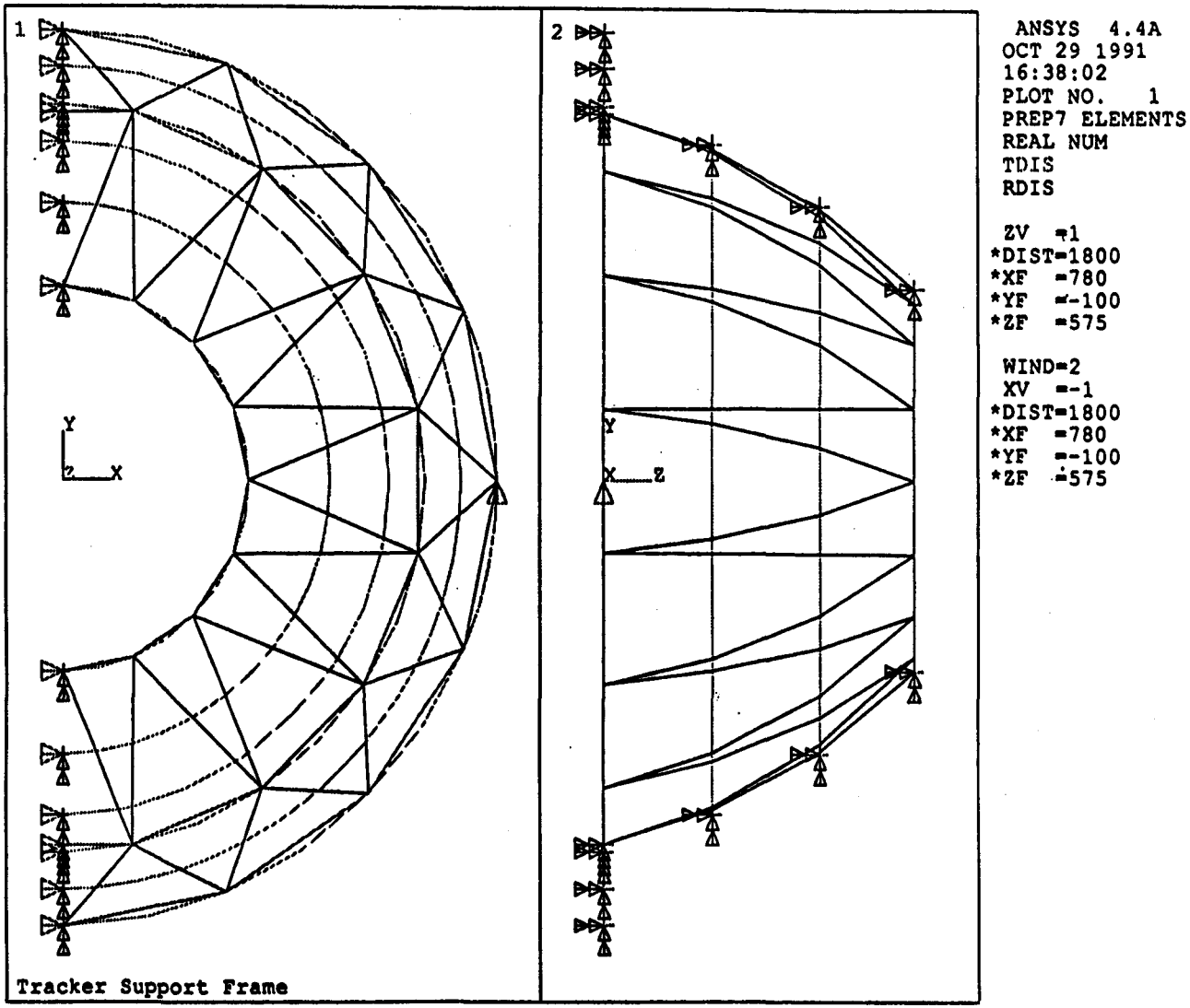

Figure 5: Beam-element model of half of one tracker support frame, approximately representing one quadrant of the structure shown in Figure 1.

Note: the arrowhead symbols indicate nodal constraints; the many axial-displacement constraints are omitted for clarity.

2.2 Modeling of Complete Support Structure

A model mesh of the entire structure (using curved shell elements for the cylinders) is shown in Figure 6. The symmetry of the structure is enforced in this partial model by applying appropriate constraints to the nodes lying in the two vertical symmetry planes. As the figure indicates, the model has been constructed with the origin of global coordinates at the end rather than at the geometrical center of the structure, so that the end-to end symmetry plane is not the global X-Y plane, though the lateral symmetry plane is the global Y-Z plane.

The single-point support indicated in Figure 1 appears as a vertical constraint applied to one node at an outer vertex of the frame.

The model mesh is relatively coarse because only displacements are being sought, and not stresses. Similarly, the application of the dead weight of the modules at the discrete locations of the shim rings has not been considered. Each superlayer has been incorporated into the model of its support cylinder as a sort of nonstructural (but heavy) "cladding."

The cylinder elements shown in Figure 6 are the ANSYS "Layered Shell Element" STIF91, which models a sandwich of various materials all with different thicknesses and material properties. The sandwich for the cylinder element, with a superlayer "cladding" on the outside, is shown in Figure 7. It contains a symmetrical sequence of five materials. The center (no. 4) layer is the structural foam core of the cylinder, a relatively thick layer of "Rohacell 31." The centerline of this layer corresponds to the nominal radius assigned to the shell element. Attached to either surface of the foam (i.e. material layers 3 and 5) are the graphite-epoxy skins of the cylinders, incorporating the combined elastic properties of a multi-ply layup.

Each superlayer of modules is modeled by a layer of nonstructural (very compliant) material, just outboard of the cylinder's outer skin. This module layer (material layer 4) is given a nominal density of 2044 kilograms per cubic meter; non-trigger module layers have a nominal thickness of 1.00 mm, while the heavier trigger module layer is assigned 1.159 mm thickness.

1

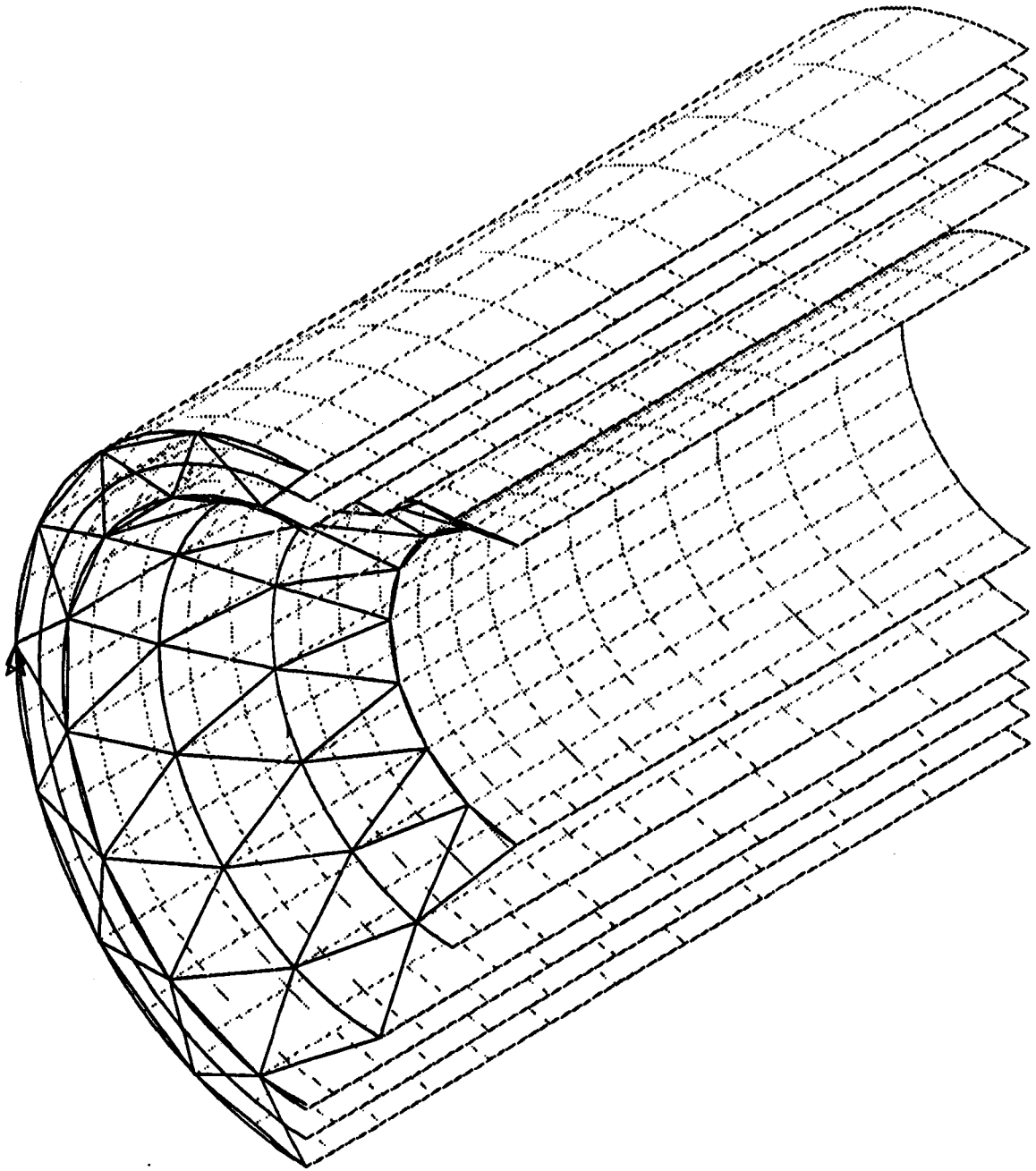

ANSYS 4.4A
OCT 1 1991
17:13:44
PLOT NO. 1
PREP7 ELEMENTS
MAT NUM

XV =-1
YV =1
ZV =-1
*DIST=2604
*XF =861.3
*YF =-290.24
*ZF =1625
PRECISE HIDDEN

PREP7 ELEMENTS
MAT NUM
TDIS

XV =-1
YV =1
ZV =-1
*DIST=2604
*XF =861.3
*YF =-290.24
*ZF =1625

Tracker structure quarter-model (triang. frame) FIGURE 6

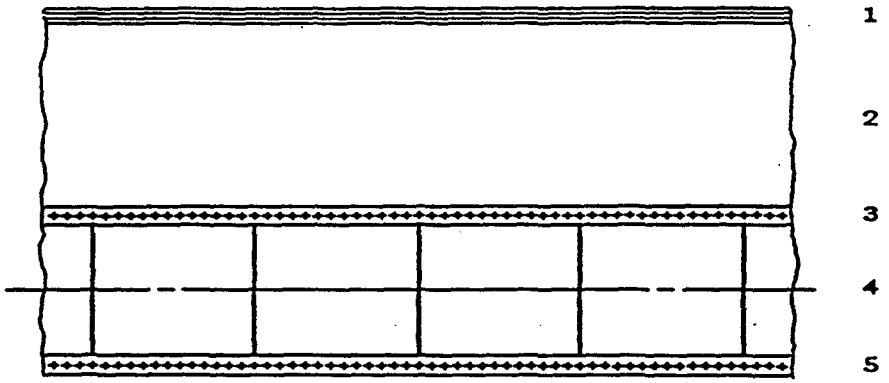

Figure 5: Sandwich of materials specified for layered shell element

1: Nonstructural superlayer of modules with mass included.
2: Dummy nonstructural standoff layer.
3 & 5: Six-ply filament-wound epoxy-graphite skin.
4: "Rohacell-31" foam core.

TRACKER ENDFRAME FINITE-ELEMENT MODEL
MAX DEFLECTIONS (Microns)
DUE TO WEIGHT OF CYLINDERS WITH MODULES
(Straws Only, No Scint. Fibers)

Frame Configuration	Max Deflection for E = 17.4 msi	Max Deflection for E = 40.4 msi
Straight Longerons	62.5	27.2
Straight Longerons (Supported at 45¬Deg Pts)	158.0	(68.7)
Longerons Equally Spaced at Ring 3	53.6	23.3
Fully Triangulated	33.8	(16.9)

N.b.: Parenthesized Values Were Scaled from ANSYS Results for E=17.4 msi.

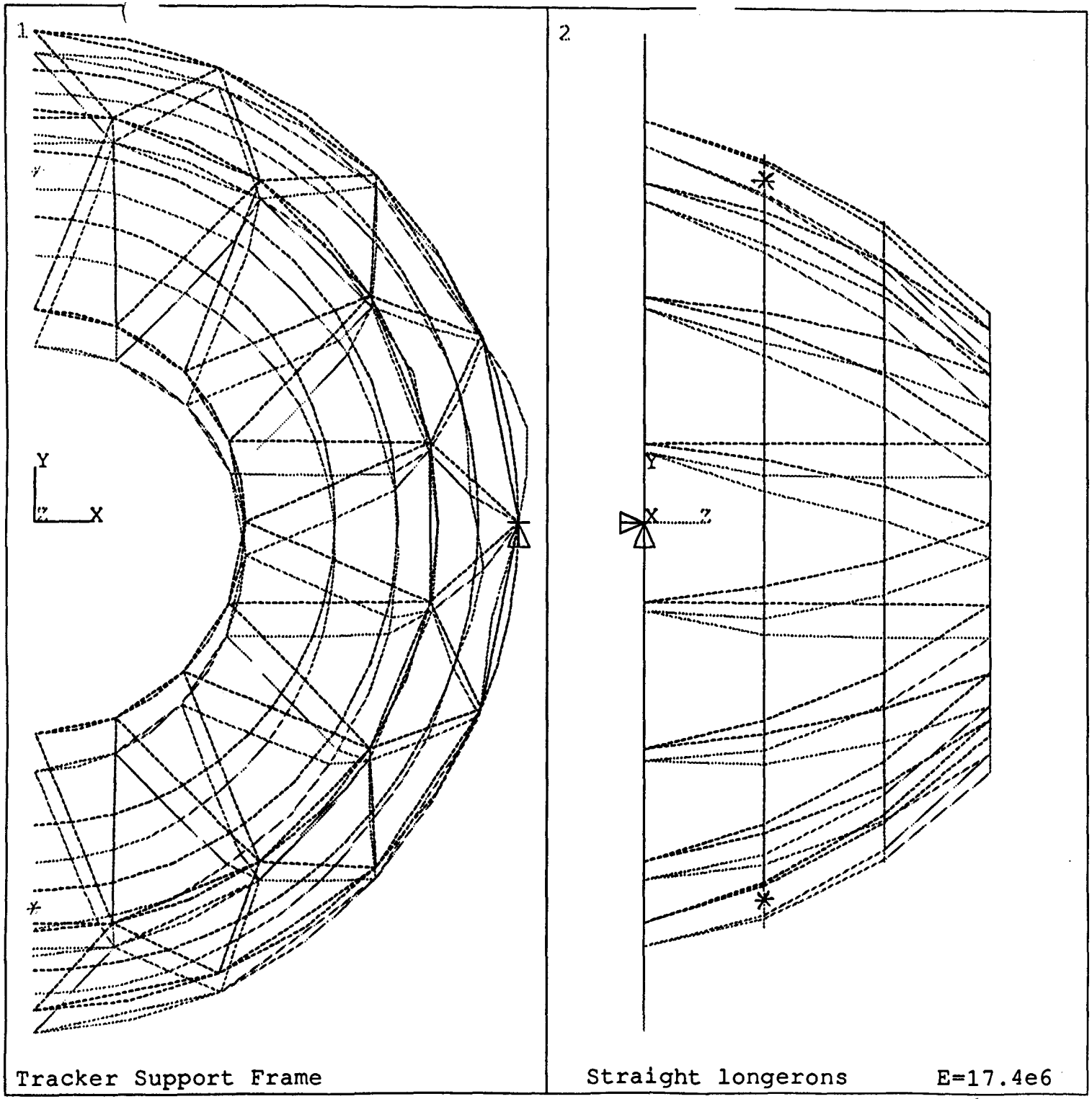


```
 ANSYS  4.4A
OCT  3 1991
17:34:51
PLOT NO.   1
POST1 DISPL.
STEP=1
ITER=1
DMX =0.062519

*DSCA=2000
 ZV  =1
*DIST=1800
*XF  =807
*YF  =-100
*ZF  =575

 WIND=2
*DSCA=2000
 XV  =-1
*DIST=1800
*XF  =807
*YF  =-100
*ZF  =575

 POST1 NODES
 TDIS

 ZV  =1
*DIST=1800
*XF  =807
*YF  =-100
*ZF  =575
```

1

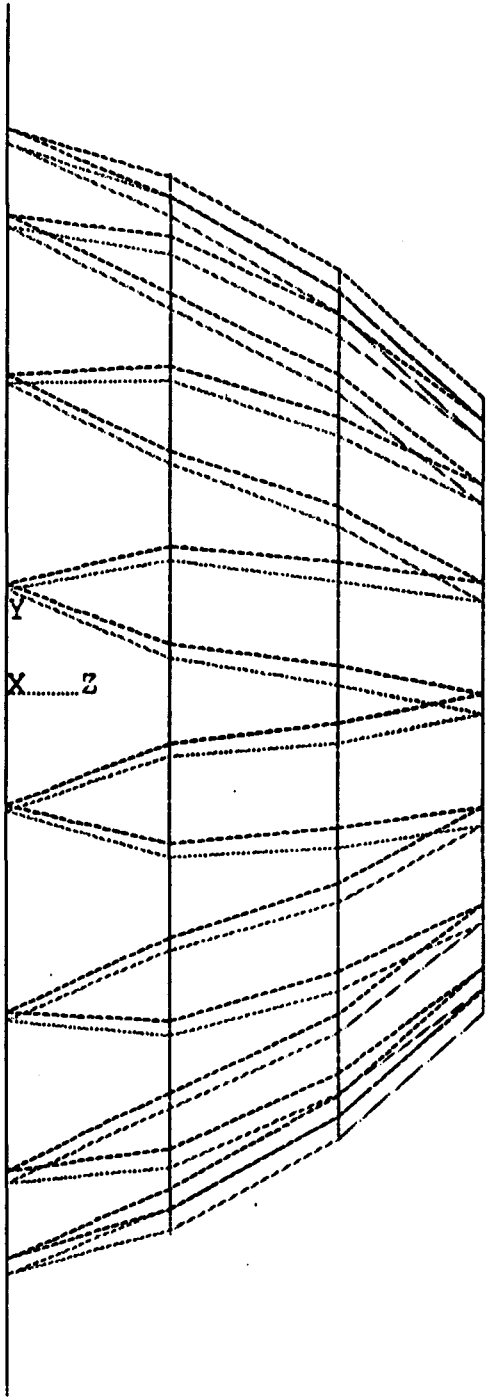

ANSYS 4.4A
SEP 17 1991
18:10:47
PLOT NO. 1
POST1 DISPL.
STEP=1
ITER=1
DMX =0.053456

*DSCA=1000
XV =-1
*DIST=1807
*XF =356.67
*YF =-96.69
*ZF =575

Tracker Support Frame

1

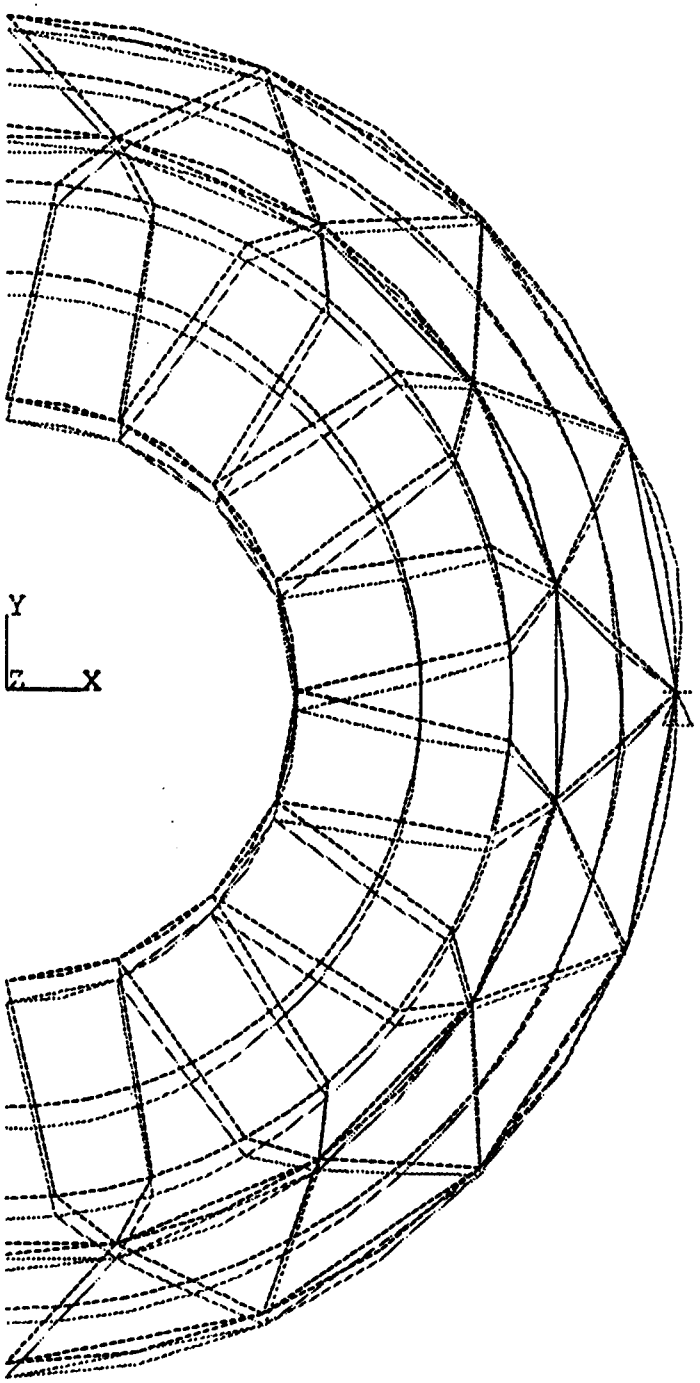

ANSYS 4.4A
SEP 17 1991
18:09:06
PLOT NO. 1
POST1 DISPL.
STEP=1
ITER=1
DMX =0.053456

*DSCA=1000
ZV =1
*DIST=1807
*XF =356.67
*YF =-96.69
*ZF =575

POST1 NODES
TDIS

ZV =1
*DIST=1807
*XF =356.67
*YF =-96.69
*ZF =575

Tracker Support Frame

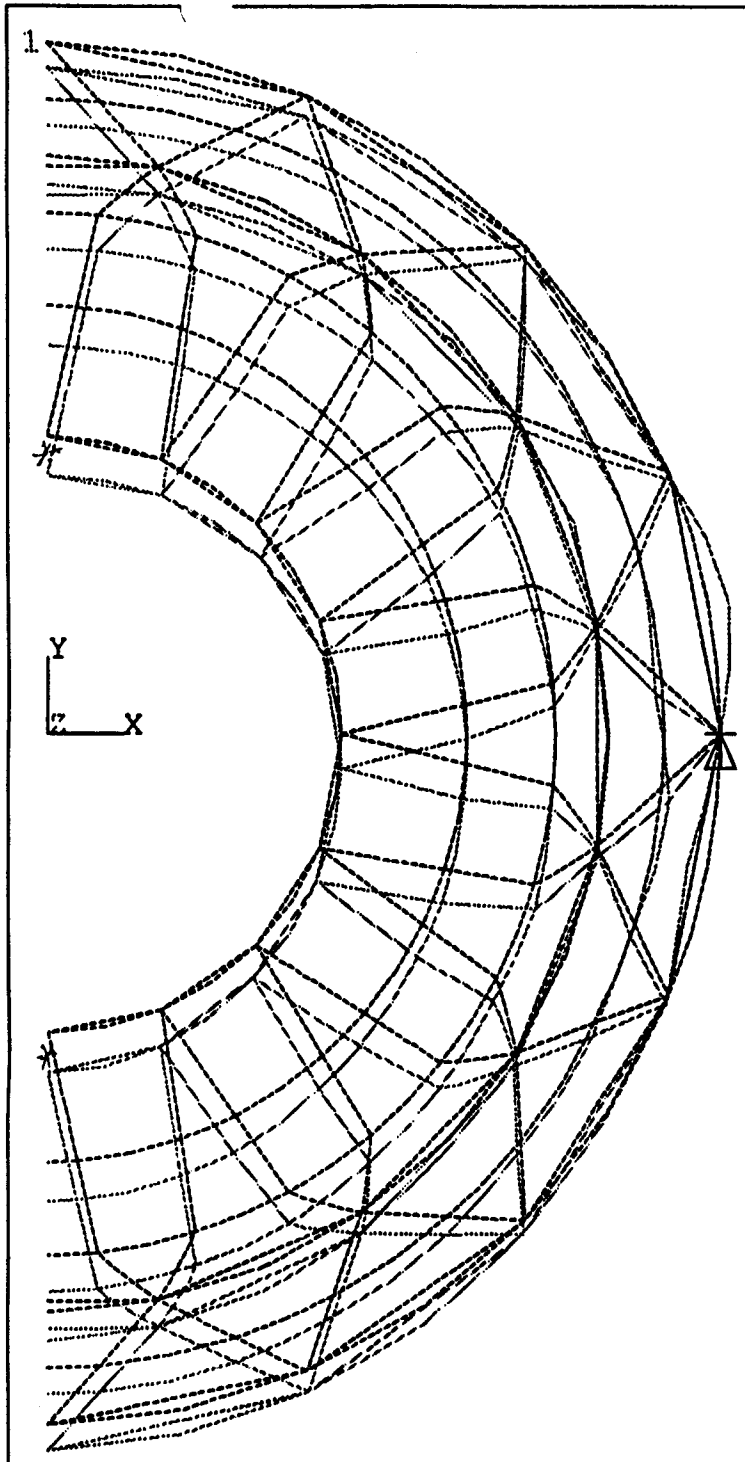

Tracker Support Frame

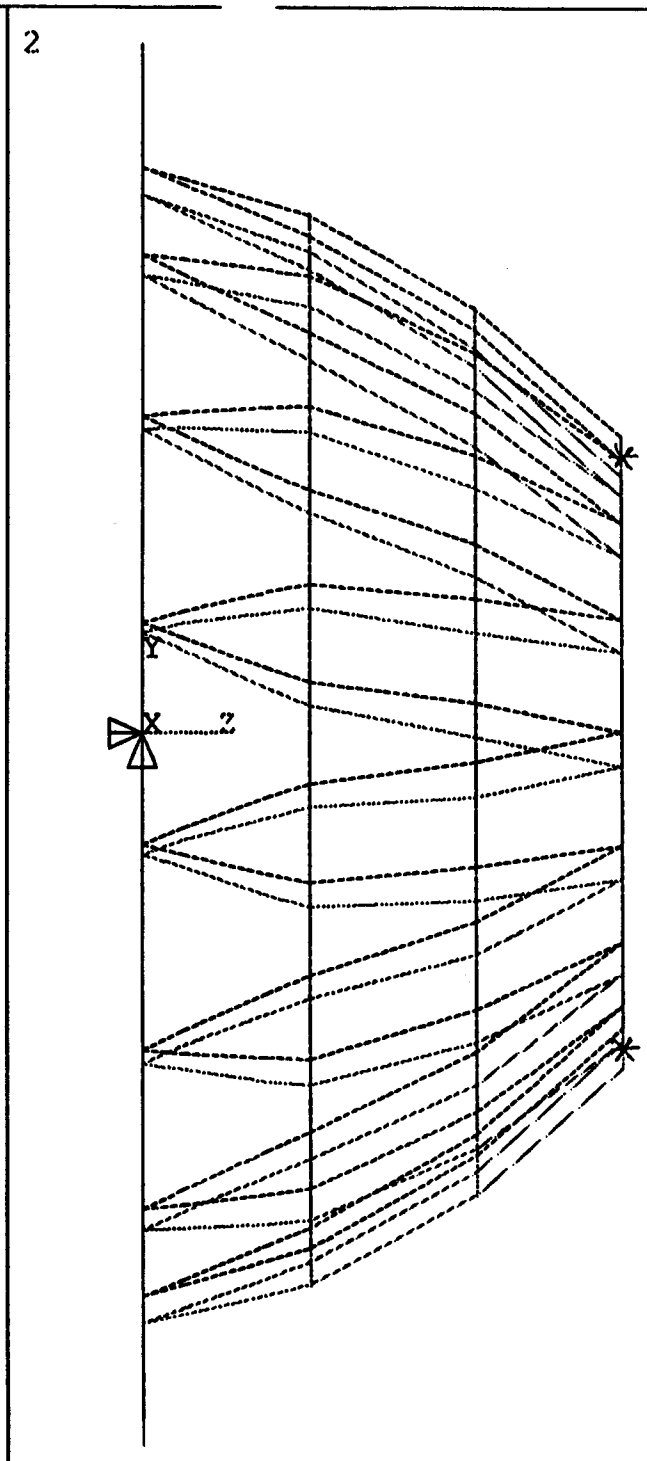

Longerons bent at C3 ring E=40e6

ANSYS 4.4A
OCT 3 1991
17:47:11
PLOT NO. 1
POST1 DISPL.
STEP=1
ITER=1
DMX =0.023325

*DSCA=4000
ZV =1
*DIST=1800
*XF =807
*YF =-100
*ZF =575

WIND=2
*DSCA=4000
XV =-1
*DIST=1800
*XF =807
*YF =-100
*ZF =575

POST1 NODES
TDIS

ZV =1
*DIST=1800
*XF =807
*YF =-100
*ZF =575

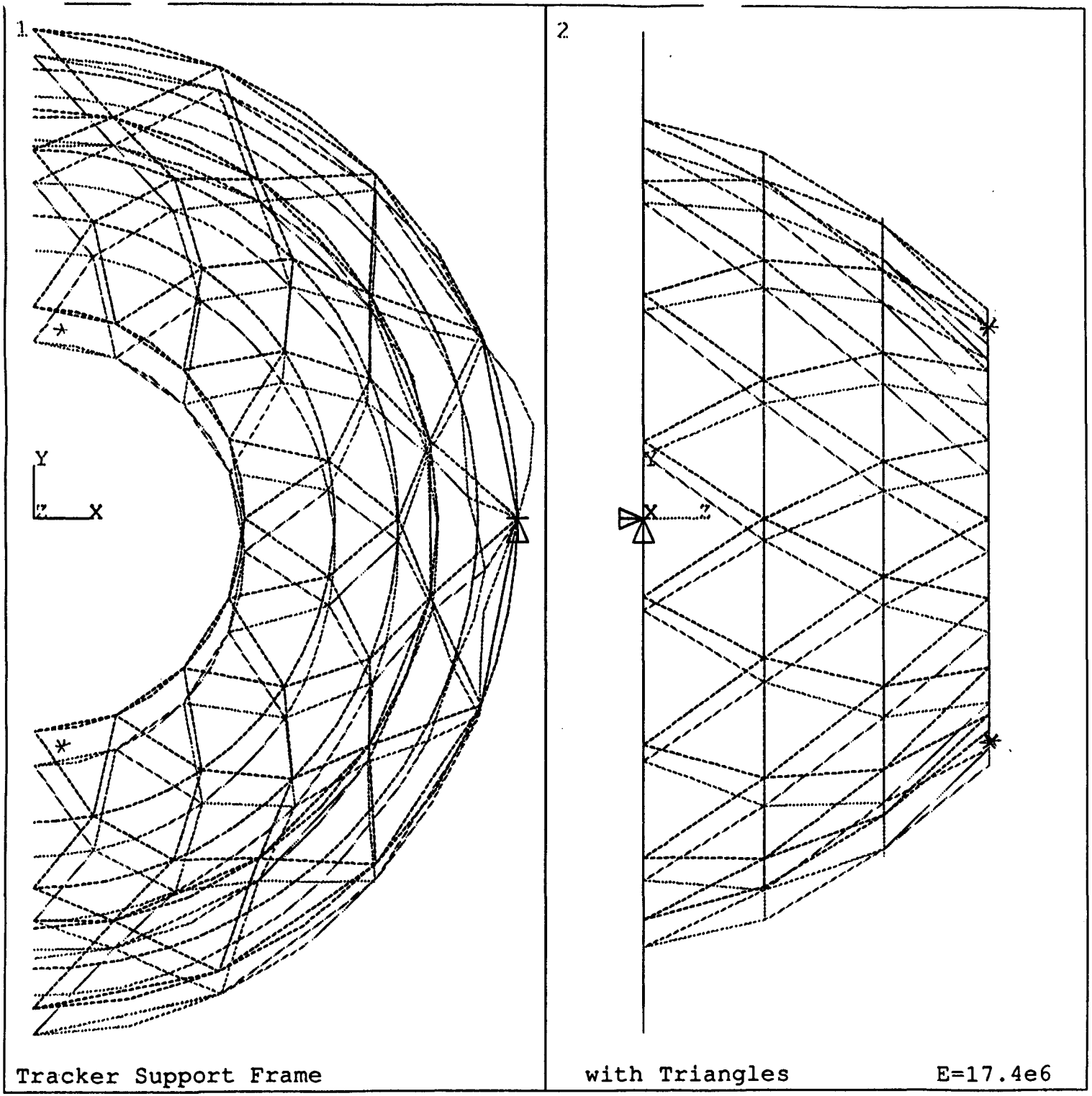

ANSYS 4.4A
OCT 3 1991
18:03:16
PLOT NO. 1
POST1 DISPL.
STEP=1
ITER=1
DMX =0.038768

*DSCA=3000
ZV =1
*DIST=1800
*XF =807
*YF =-100
*ZF =575

WIND=2
*DSCA=3000
XV =-1
*DIST=1800
*XF =807
*YF =-100
*ZF =575

POST1 NODES
TDIS

ZV =1
*DIST=1800
*XF =807
*YF =-100
*ZF =575

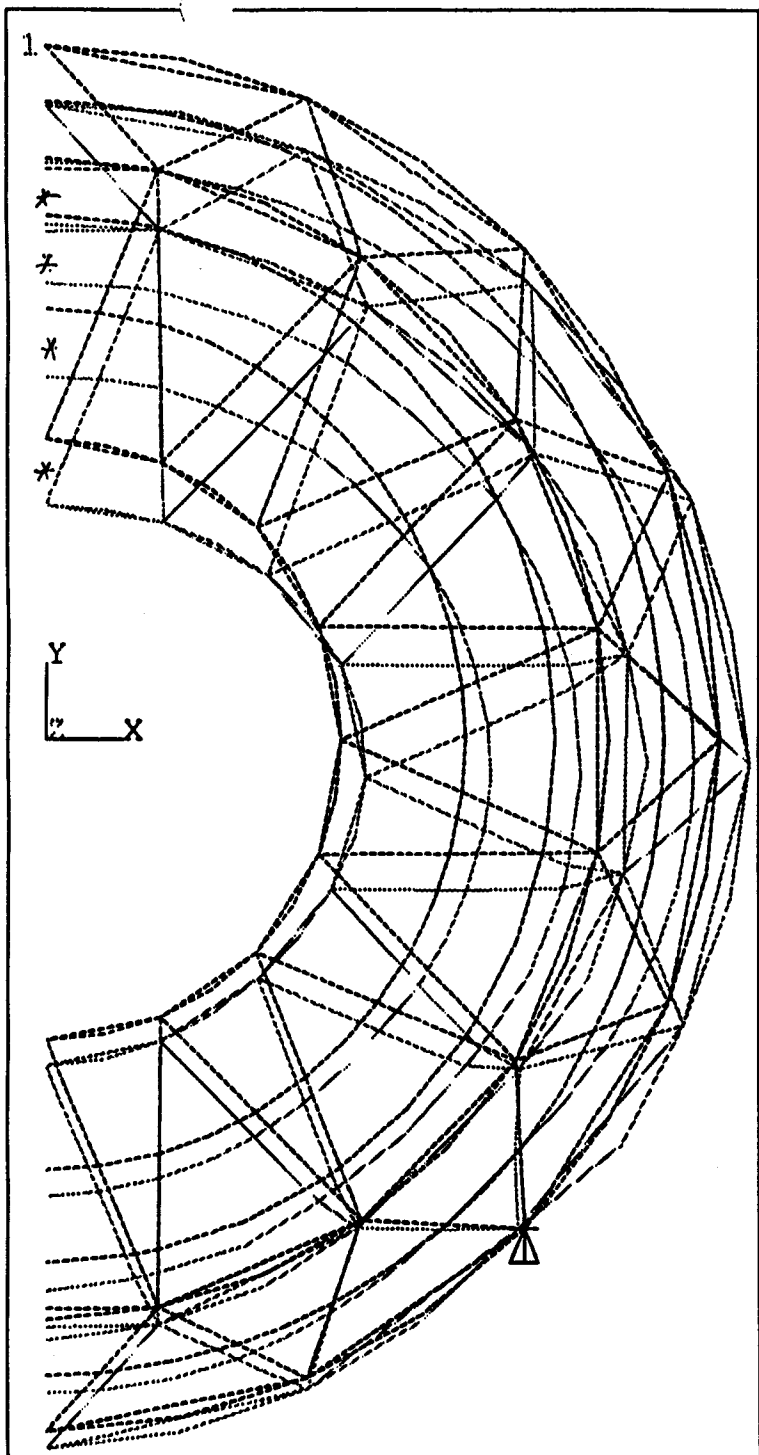

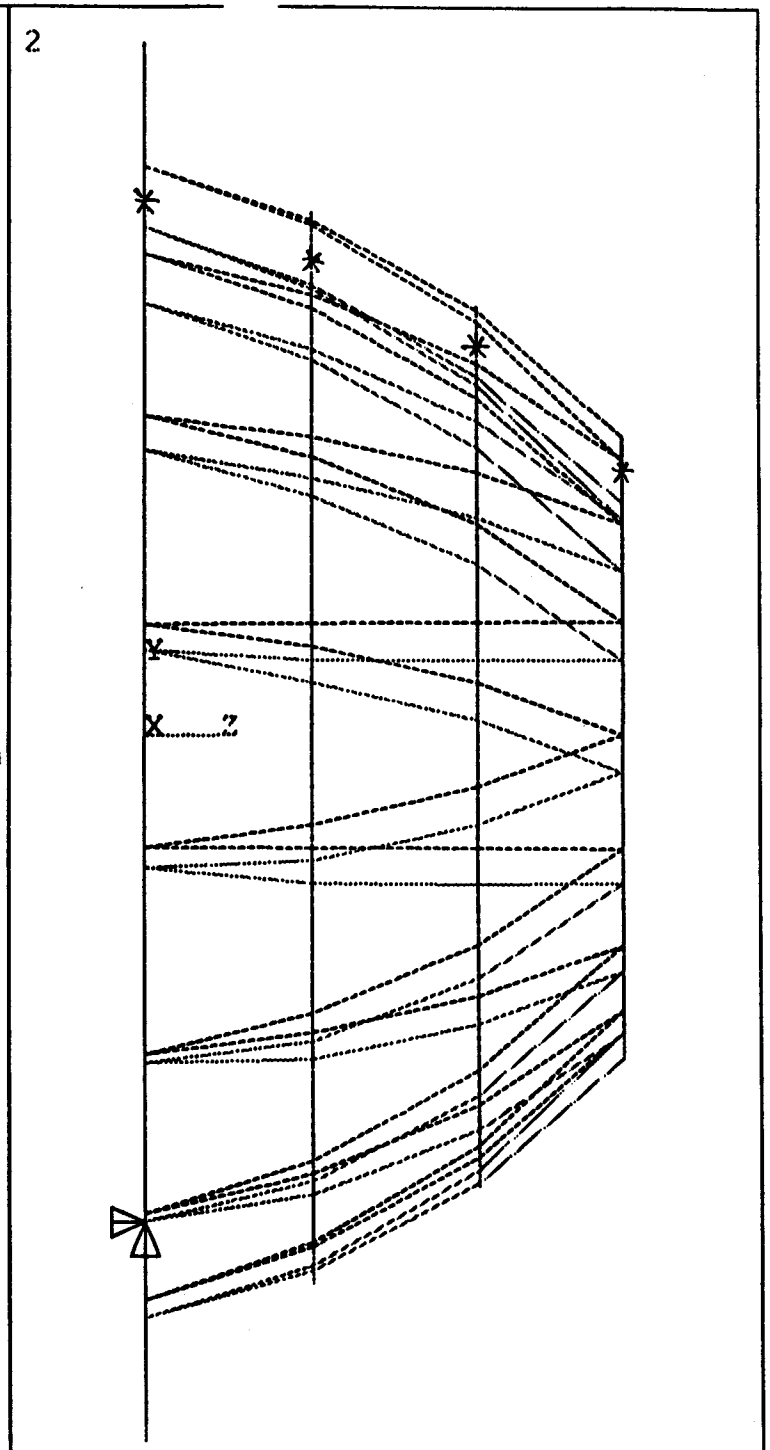

ANSYS 4.4A
OCT 3 1991
17:55:12
PLOT NO. 1
POST1 DISPL.
STEP=1
ITER=1
DMX =0.158005

*DSCA=1000
ZV =1
*DIST=1800
*XF =807
*YF =-100
*ZF =575

WIND=2
*DSCA=1000
XV =-1
*DIST=1800
*XF =807
*YF =-100
*ZF =575

POST1 NODES
TDIS

ZV =1
*DIST=1800
*XF =807
*YF =-100
*ZF =575

Tracker Support Frame

Support at 45-deg pts E=17.4e6

CENTRAL AND FORWARD TRACKING SUBSYSTEM

4

DEFLECTION FEA ANALYSIS
SPACEFRAME AND CYLINDER STRUCTURE

TABLE NUMBER 1
COMPONENT PROPERTY MODEL IN FEA

Cylinders			P-75		Spaceframe		
	Foam Core		Graphite	Composit		Struts	
Foam Core	Thickness	Lamina	Thickness	Thicknes	Modulus	Size	Wall Tk
31 IG	.59 IN.	0/60/60	.0045 IN.	15mm	40 MSI	2 X 4 cm	2.5 mm

TABLE NUMBER 2
MASS SUMMARY OF MODEL FROM COMPUTER

	All Straws Layer1,2,3,4,5,6		Mixed System Straws 3,4,5,6 SiFi 1,2	
Item	Mass Kg	Pound	Mass Kg	Pounds
Cyls With/Modules	1015.5	2239.2	828.4	1826.2
Cyls With/SiFi	0	0 *	613.8	1353.5
Struts & Joints	70.9	156.3	70.9	156.3
Rings	29.3	64.6	29.3	64.6
Pigtails	0.0	0.0	254.0	560.1
TOTAL	1115.7	2460.1	1796.4	3960.7

*(940.5 lbs is 42% less wt for modules)

COMPOSITE MATERIAL PROPERTIES

Materials:

Fiber - Hercules Carbon Fiber Type UHM
Modulus 64.5 M_{psi}

Resin - Hercules 3501-6 (present system)
Hercules 956-3 (proposed for low moisture absorption)

Core - Rohacell foam

Mechanical Properties for Fiber/Resin Layup [0, ±60] sym

Elastic Modulus

E_x (axial) = 14.4 M_{psi}
E_y (hoop) = 14.4 M_{psi}
E_z (radial) = 1.07 M_{psi}

Poisson Ratio

$MU_{xy} = 0.317$ $MU_{yx} = 0.317$
$MU_{yz} = 0.237$ $MU_{zy} = 0.018$
$MU_{zx} = 0.018$ $MU_{xz} = 0.237$

Shear Modulus

$C_{xy} = 5.45\ M_{psi}$
$G_{yz} = 0.5\ M_{psi}$
$G_{xz} = 0.5\ M_{psi}$

Composite Construction Values

Inner Composite Ply	0.009 inches
Foam Core	0.236 inches
Outer Composite Ply	0.009 inches
TOTAL	0.254 inches

Westinghouse
Science & Technology Center

COMPLETE TRACKER FEA ANALYSIS

MAX DEFLECTIONS - MICRONS

Spaceframe	Straws Only Straight	Straws 4 Layers SiFi 2 Layers Straight	Straws 4 Layers SiFi 2 Layers Triangle
[0 90 0 3 layers] Graphite 0.0045" tk Core 15 mm (0.59")	393	---	865
	Real OK Rad Lg - But N/G		
[0+60-60-60-+60 0] Graphite 0.009 tk Core 25 mm (1.00")	57	126	92
	Real But N/G Rad Lg		
[0+60-60-60+60 0] Graphite 0.0045" tk Core 15 mm (0.59")	126	317	268
	Not Real - Ok Rad Lg		
[0+60-60-60+60 0] Graphite 0.009 tk Core 6 mm (0.236")	91	---	172
	Real - OK Rad Lg		

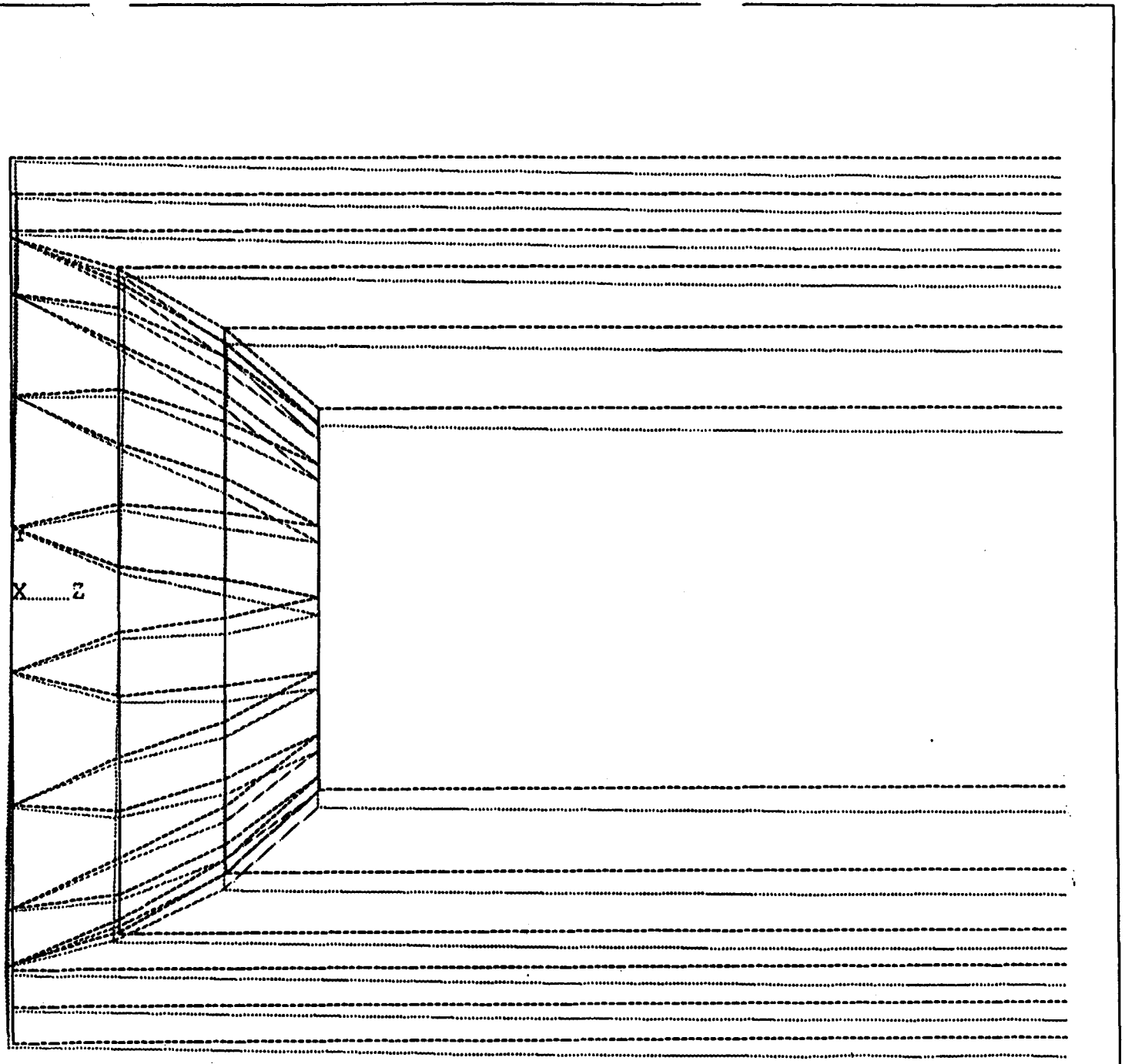

ANSYS 4.4A
SEP 26 1991
17:09:48
PLOT NO. 1
POST1 DISPL.
STEP=1
ITER=1
DMX =0.091624

*DSCA=1000
XV =-1
DIST=2172
XF =807.5
ZF =1975

Straight frame * All straw modules * 6-ply 0/±60 UHM skin, 6 mm foam

1

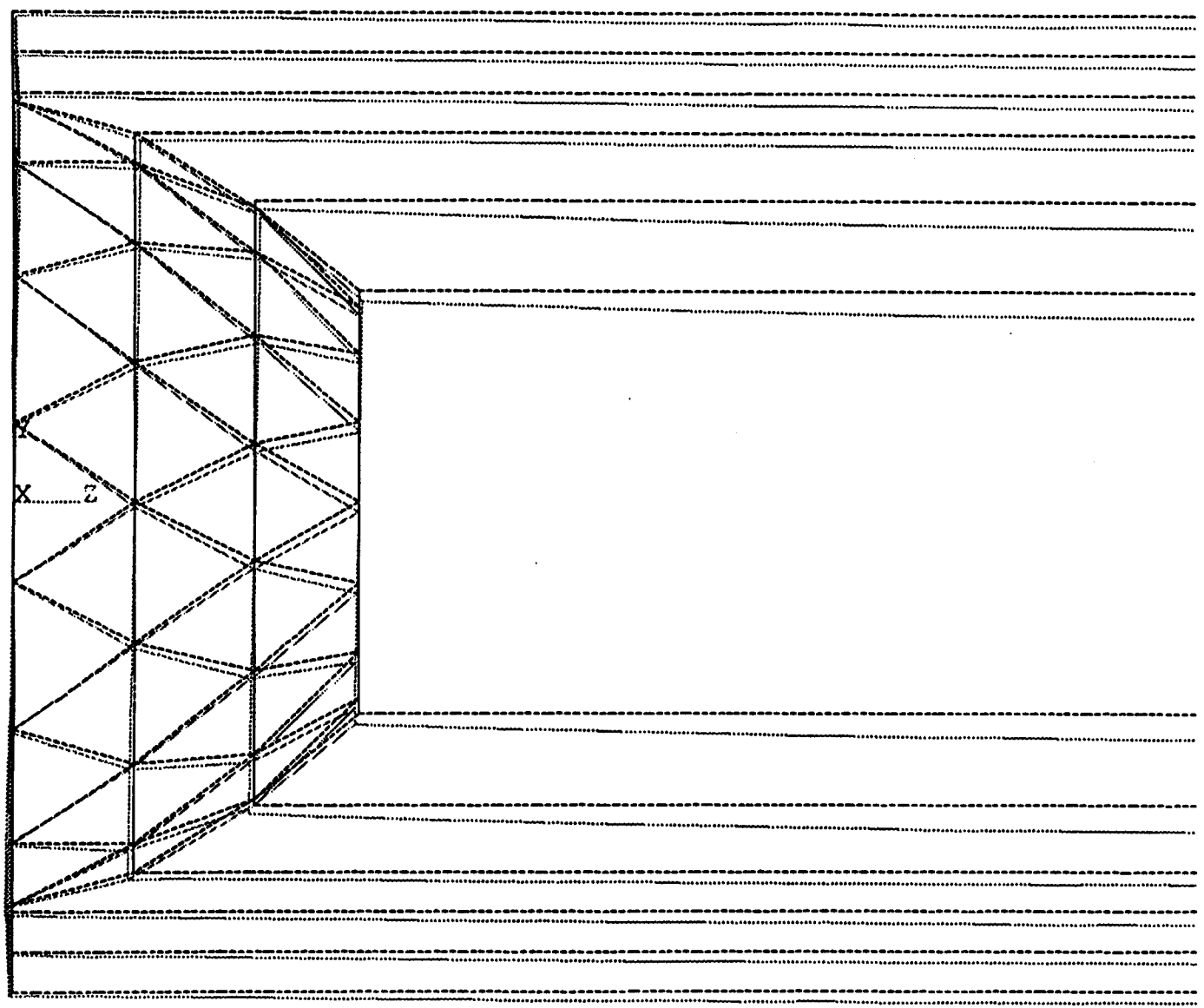

ANSYS 4.4A
SEP 26 1991
15:25:30
PLOT NO. 1
POST1 DISPL.
STEP=1
ITER=1
DMX =0.171596

*DSCA=500
XV =-1
DIST=2172
XF =807.5
ZF =1975

Triang. frame * Scint. fiber wt. * 6-ply 0/+_60 UHM skin, 6 mm foam

STC Memo No. 91-1TM3-ADEMS-M1 Date May 21, 1991

Title **FINITE-ELEMENT ANALYSIS OF DEADWEIGHT DEFLECTIONS OF FIVE-CYLINDER CENTRAL TRACKER SUPPORT STRUCTURE**

Author(s) Donald A. Hoecker

Department Advanced Electromechanical Systems

APPROVED:

Carl J. Heyne, Manager
Advanced Electromechanical Systems

Westinghouse STC
1310 Beulah Road
Pittsburgh, Pennsylvania 15235

Table of Contents

List of Figures

FINITE-ELEMENT ANALYSIS OF DEADWEIGHT DEFLECTIONS OF FIVE-CYLINDER CENTRAL TRACKER SUPPORT STRUCTURE

Donald A. Hoecker
Advanced Electromechanical Systems

Westinghouse Science & Technology Center
1310 Beulah Road
Pittsburgh, PA 15235

ABSTRACT

The gravity-induced deflections of the five-cylinder central tracker support structure were calculated using the ANSYS package. The loading included the eight "superlayers" of detector-straw modules, but omitted the silicon tracker inside the innermost cylinder.

1. INTRODUCTION

The deflections of the central tracker under it own weight have been estimated for the design shown in Figure 1. This design is composed of five concentric structural cylinders which support eight "superlayers" of trapezoidal modules which are packed with straw-shaped detectors. The five cylinders are made of identical sandwiches of foam core symmetrically sandwiched between layers of graphite-epoxy skin.

The entire structure is supported at the four corner points indicated in Figure 1: the points where the circular ends of the outermost cylinder intersect the horizontal plane through the axis of the structure. Each of the four inner cylinders is supported at each end by a ring-shaped plate which connects it to the next-outer cylinder; these end rings are of the same sandwich construction as the cylinders, but with the foam core twice as thick. Figure 2 shows the structure in cross-section.

The detector modules which are supported by the structure are shown in cross-section in Figure 3; an arc of one superlayer made up of these modules is sketched in Figure 4. Each superlayer is attached to its supporting cylinder by a number of "hanger" rings which can be seen in Figures 1 and 2. The modules pass more or less loosely through trapezoidal holes in these rings (and in the structural end-rings). Since the modules are not connected to each other and are not firmly attached to the cylinders, their contribution to the stiffness of the structure is negligible when compared to the stiffness of the cylinders. They can therefore be treated as nonstructural mass whose dead weight contributes to the loading of the structure. The modules shown in Figure 3 are estimated to weigh 0.0100 lb/in (non-trigger module) and 0.0125 lb/in (trigger module).

To assess the static deflections of this structure due to gravity loading, a finite-element model was constructed using the ANSYS package. This model will be described in the following section.

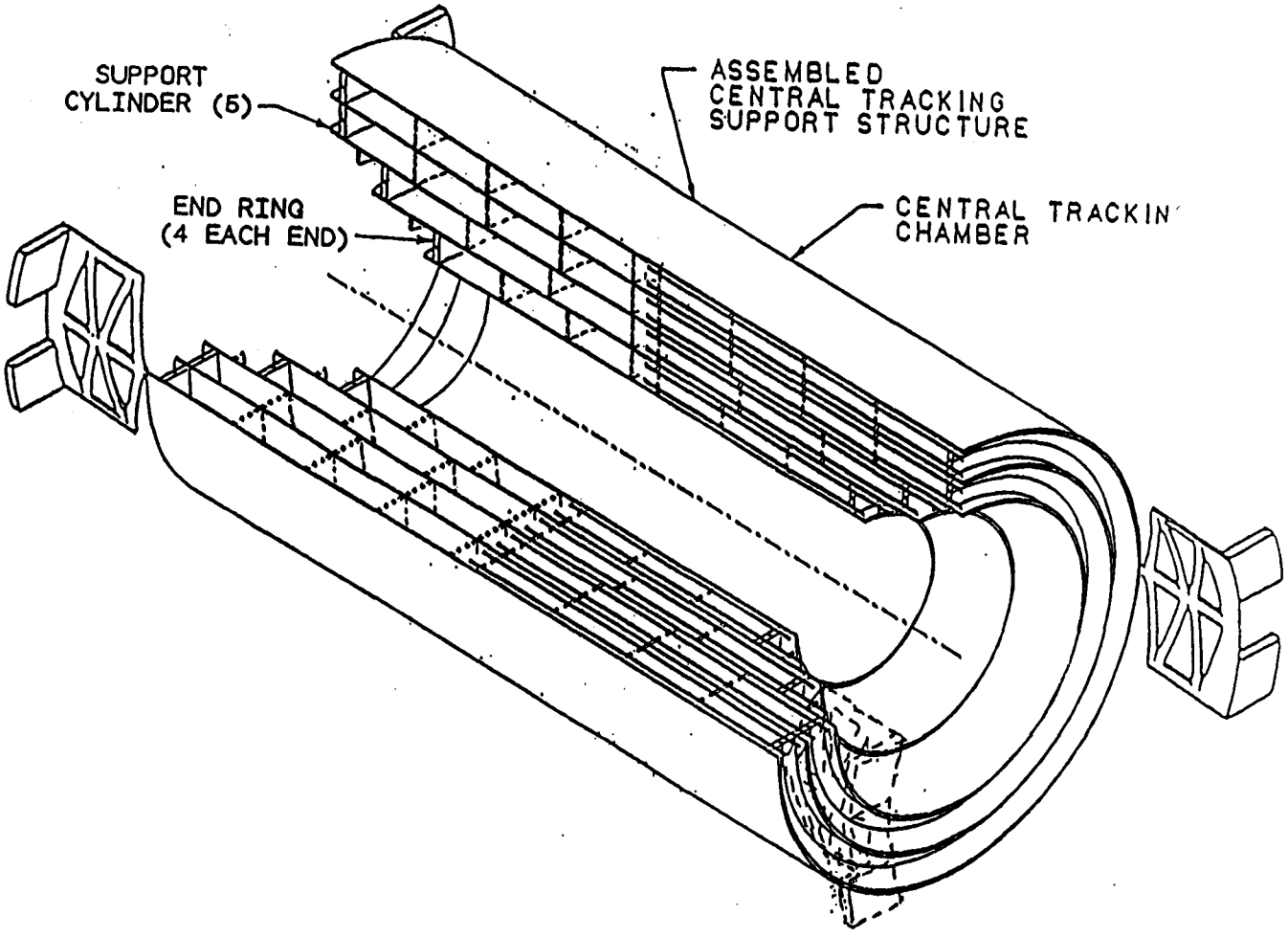

Figure 1: Isometric sketch of tracker structure, including corner support points; module superlayers have been omitted from the left half to show the structural elements more clearly.

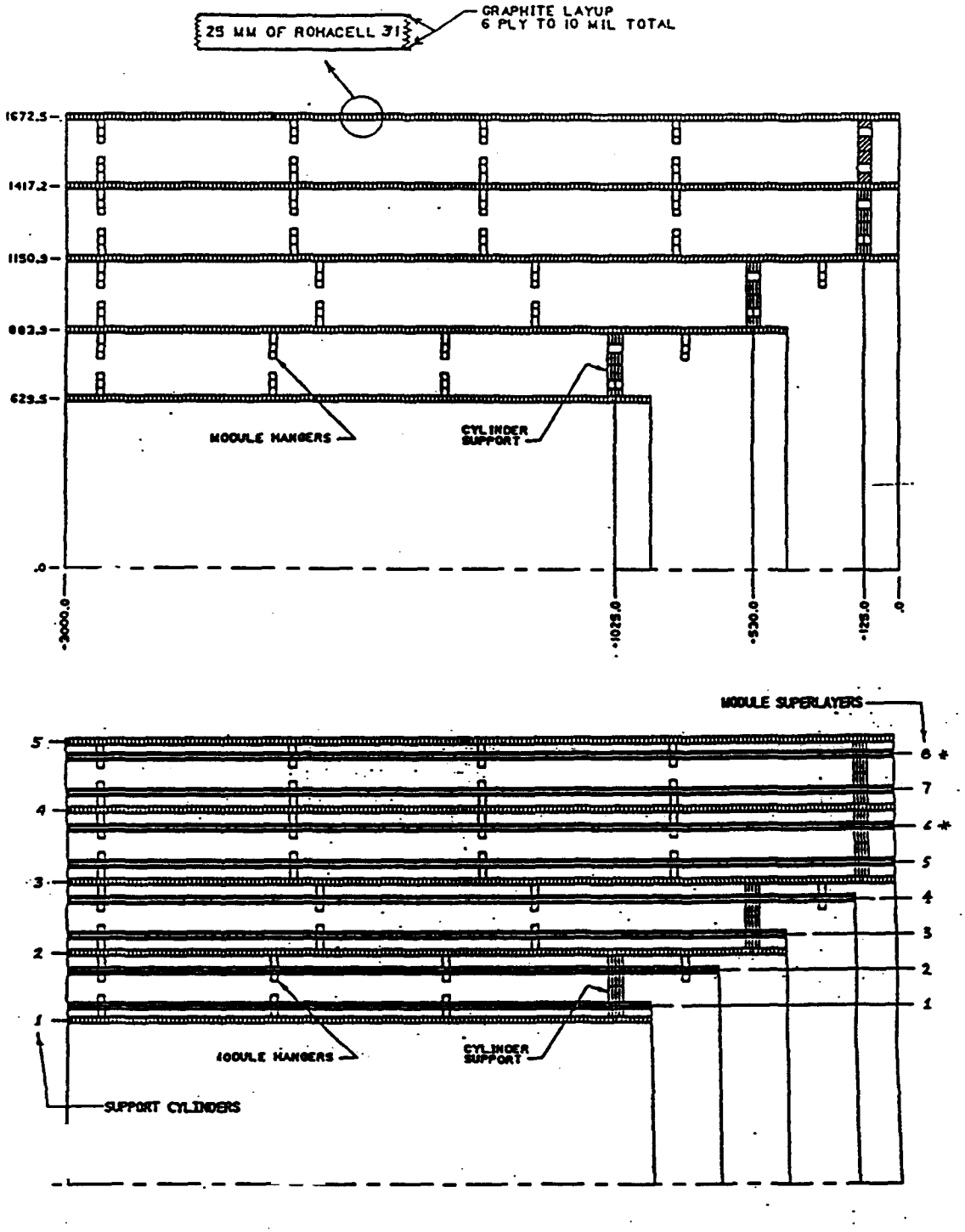

Figure 2: Cross-section of the tracker structure.

Upper: Dimensions of structural elements.
Lower: Attachment of superlayers to structure;
layers 6 & 8 (*) contain the heavier trigger modules.

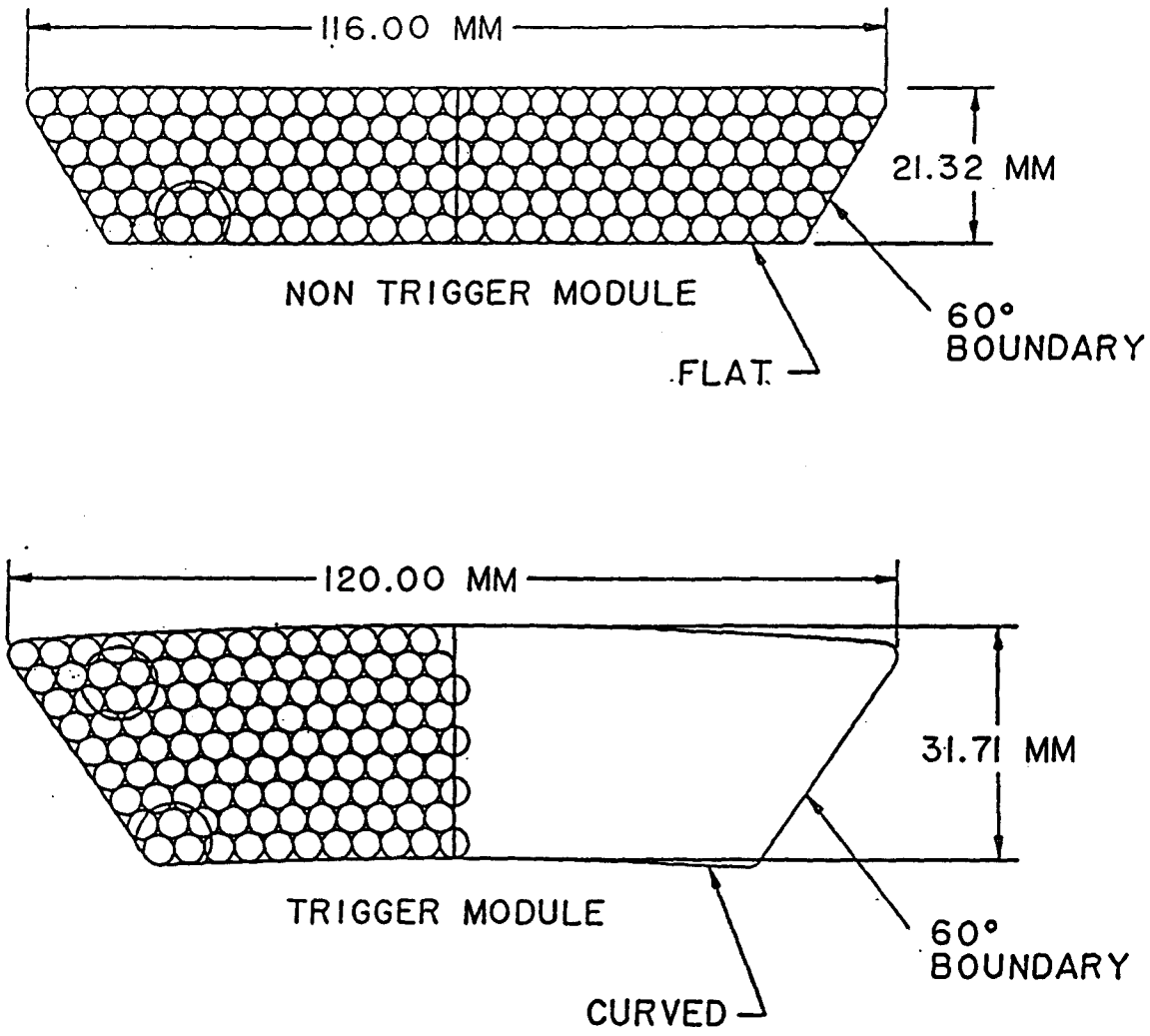

Figure 3: Cross-sections of the modules incorporated in the superlayers.

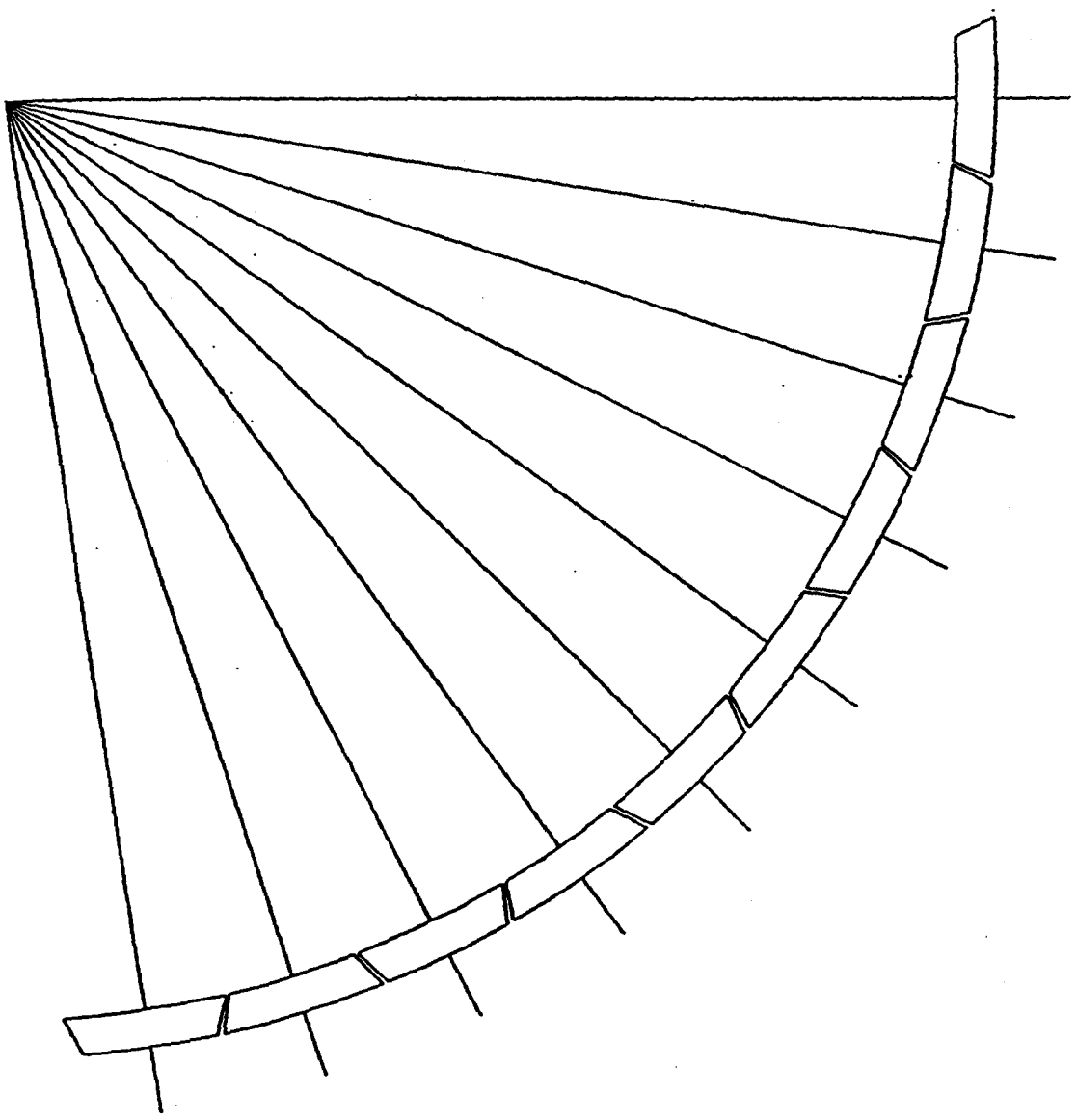

Figure 4: Schematic cross-section of a superlayer arc.

2. FINITE-ELEMENT MODEL

Figure 1 shows that the structure has two vertical planes of mirror symmetry, dividing it end-to-end and side-to-side. Because of this sym- metry, only a quarter of the structure needed to be modeled; the model mesh (using curved shell elements) is shown in Figure 5. The symmetry of the structure is enforced in this partial model by applying appropriate constraints to the nodes lying in the two vertical symmetry planes. As the figure indicates, the model has been constructed with the origin of global coordinates at the geometrical center of the structure, so that the symmetry planes are the global X-Y and Y-Z planes.

The single-point support indicated in Figure 1 is spread into a vertical constraint applied to five nodes along the edge of the outermost cylinder, in order to avoid the unrealistic creation of a point-load singularity in the problem.

The model mesh is relatively coarse because only displacements are being sought, and not stresses; this is why the simple five-node repre- sentation of the corner support is acceptable. Similarly, the application of the dead weight of the modules at the discrete locations of the hanger rings has not been considered. Each superlayer has been incorporated into the model of its support cylinder as a sort of nonstructural (but heavy) "cladding." Thus, each superlayer is considered to be exactly as long as its support cylinder. The short extensions of the cylinders beyond the structural end-rings, which can be seen Figures 1 and 2, were omitted from the model.

The elements shown in Figure 5 are the ANSYS "Layered Shell Element" STIF91, which models a sandwich of various materials all with different thicknesses and material properties. The sandwich for the most general cylinder element, with a superlayer "cladding" both inside and outside, is shown in Figure 6. It contains a symmetrical sequence of seven materials. The center (no. 4) layer is the structural foam core of the cylinder, a 25-mm layer of "Rohacell 31." The centerline of this layer corresponds to the nominal radius assigned to the shell element,

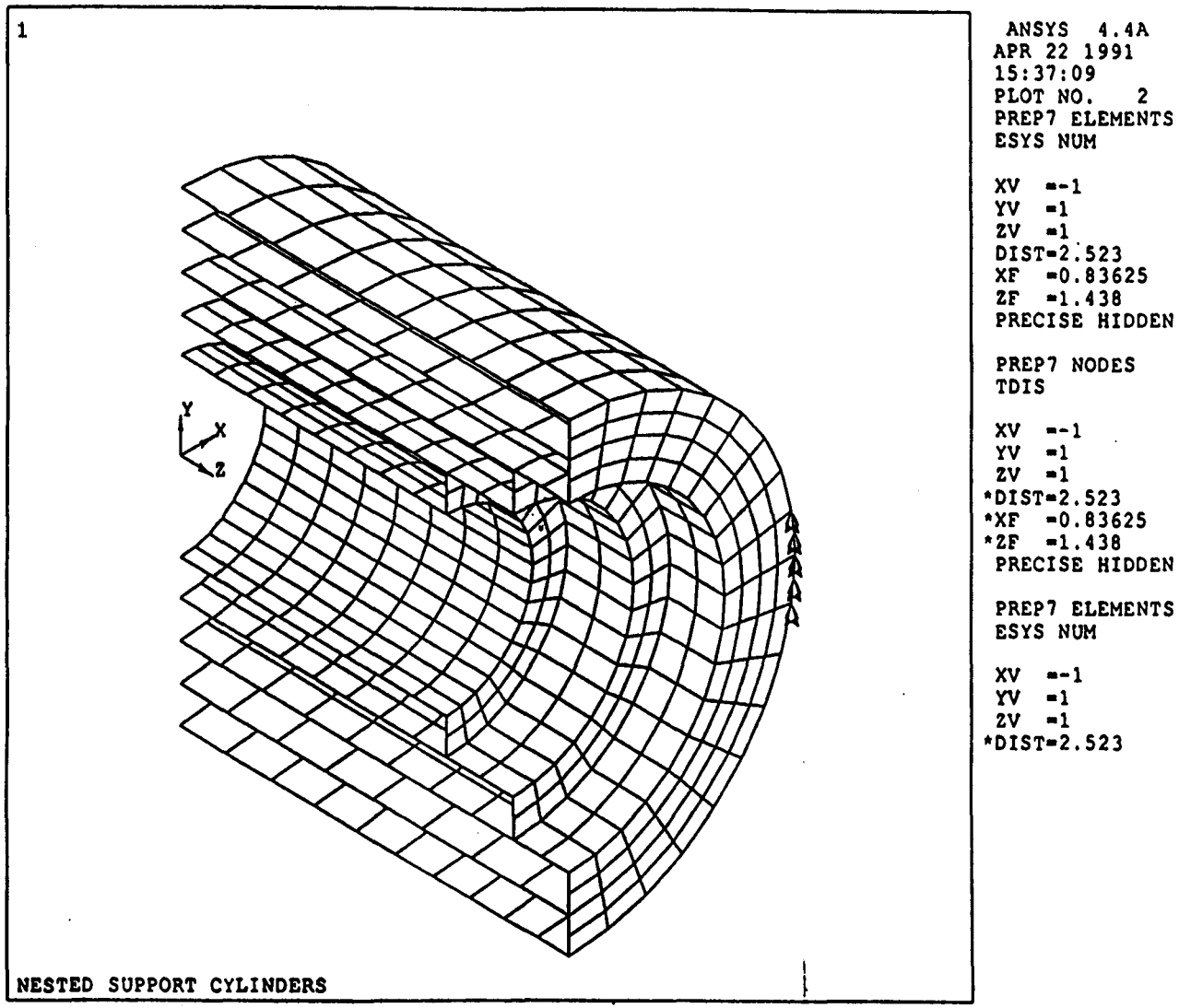

Figure 5: ANSYS shell-element model of the tracker, representing one quadrant of the structure shown in Figure 1.

using the values shown in Figure 2. Attached to either surface of the foam (i.e., material layers 3 and 5) are the graphite-epoxy skins of the cylinders, with a 0.229-mm (9-mil) thickness and incorporating the combined elastic proper- ties of a six-ply filament-wound layup with filaments oriented along the zero-degree (circumferential) direction, +60 degrees, and -60 degrees.

Each superlayer of modules is modeled by a two-layer sandwich of nonstructural (very compliant) materials. Just outboard of the skins (material layers 2 and 6) are dummy standoff layers whose density is negligible as well as its stiffness. These layers are present only to space the layers representing the modules themselves to the correct midline radius, and in most cases are 67 mm thick.

The module layers (material layers 1 and 7) are given a nominal density of 1678 kilograms per cubic meter; non-trigger module layers have a nominal thickness of 1.00 mm, while the heavier trigger module layers (numbered 6 and 8 in Figure 2) are assigned 1.256 mm thickness.

The innermost and outermost cylinders are modeled by a slightly different shell element; since these cylinders each support only one module superlayer, they need only a five-layer shell element. The standoff layer is also reduced in thickness from 67 mm to 53 mm; this closer separation between cylinder and superlayer can be seen in the lower half of Figure 2.

The end rings are modeled with a three-layer STIF91 element, using materials 3, 4, and 5 from Figure 6, but with the thickness of the foam doubled to 50 mm.

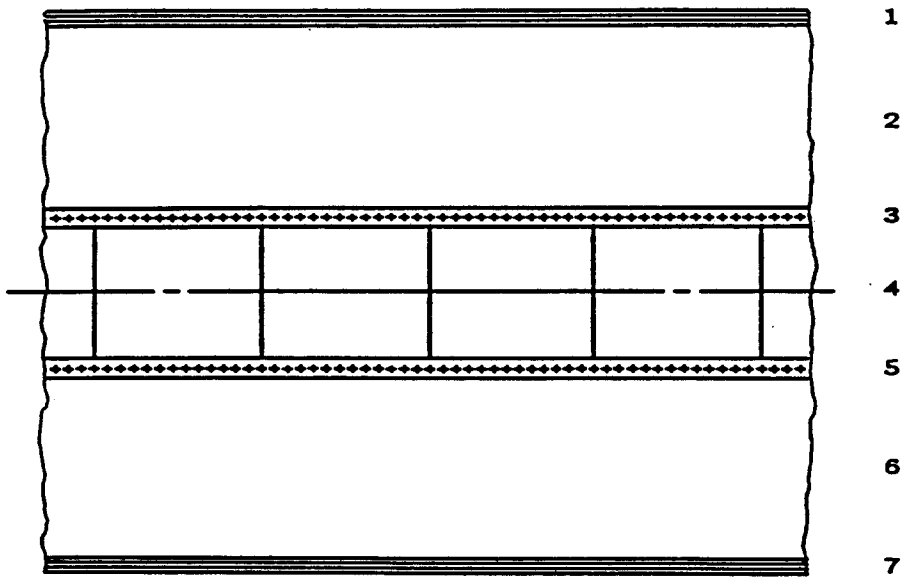

Figure 6: Sandwich of materials specified for layered shell element modeling a general-case (numbered 2, 3, or 4 in Figure 2) structural cylinder with its attached module superlayers.

1 & 7: Nonstructural superlayer of modules with mass included.
2 & 6: Dummy nonstructural standoff layer.
3 & 5: Six-ply filament-wound epoxy-graphite skin.
4: "Rohacell-31" foam core.

3. DISPLACEMENT RESULTS

Figures 7-9 display the element displacements calculated by ANSYS for gravity loading on the model described in the previous section. The original element positions are indicated in dashed lines, and the deflected elements are drawn in solid lines. The displacements have been exaggerated by a factor ("DSCA") which ANSYS selects automatically for each display; as appears in the annotations to the right of the plot frame, its value varies between 2126 and 2626. The value "DMX" gives the vector-sum displacement (in meters) of the largest nodal displacement associated with the display; the value 0.899E-04 shown on Figures 7 and 8 corresponds to 0.0899 mm, or about 3.6 mils. As the end-view in Figure 7 suggests, the displacements are predominantly in the vertical direction.

Figures 7 and 8 exhibit significant local deformation around the five-node support constraint, which contributes to the absolute vertical motion of the rest of the structure. These figures also show some warping of the outermost cylinder and end-ring in the vicinity of their common edge. This is the only area where any of the cylinders depart noticeably from their original circular shape.

Figure 9 displays only the displacements in the Y-Z symmetry plane, and has been annotated with the values of downward vertical displacement at the corner and end nodes. Examining these values gives an idea of how much each cylinder sags out of its original straight profile. For example, the innermost cylinder sags about (0.0859-0.0692) = 0.0167 mm, or about 0.67 mil. Similarly, the inner span of the second cylinder sags (0.0878-0.06905) = 0.01875 mm, while the stub end of that same cylinder, which carries a shear load of most of two cylinders including three superlayers, undergoes a relative displacement of (0.06905-0.05545) = 0.0136 mm over a rather short length.

The maximum-displacement ("DMX") value in this figure is given as 0.878E-04 meters, or 0.0878 mm, and occurs at the top and bottom nodes in the mid-section of the second cylinder. The maximum displacement in the

whole model, the 0.0899 mm mentioned above, also occurs in this cross-section, but in the horizontal X-Z plane; its direction is almost exactly vertical.

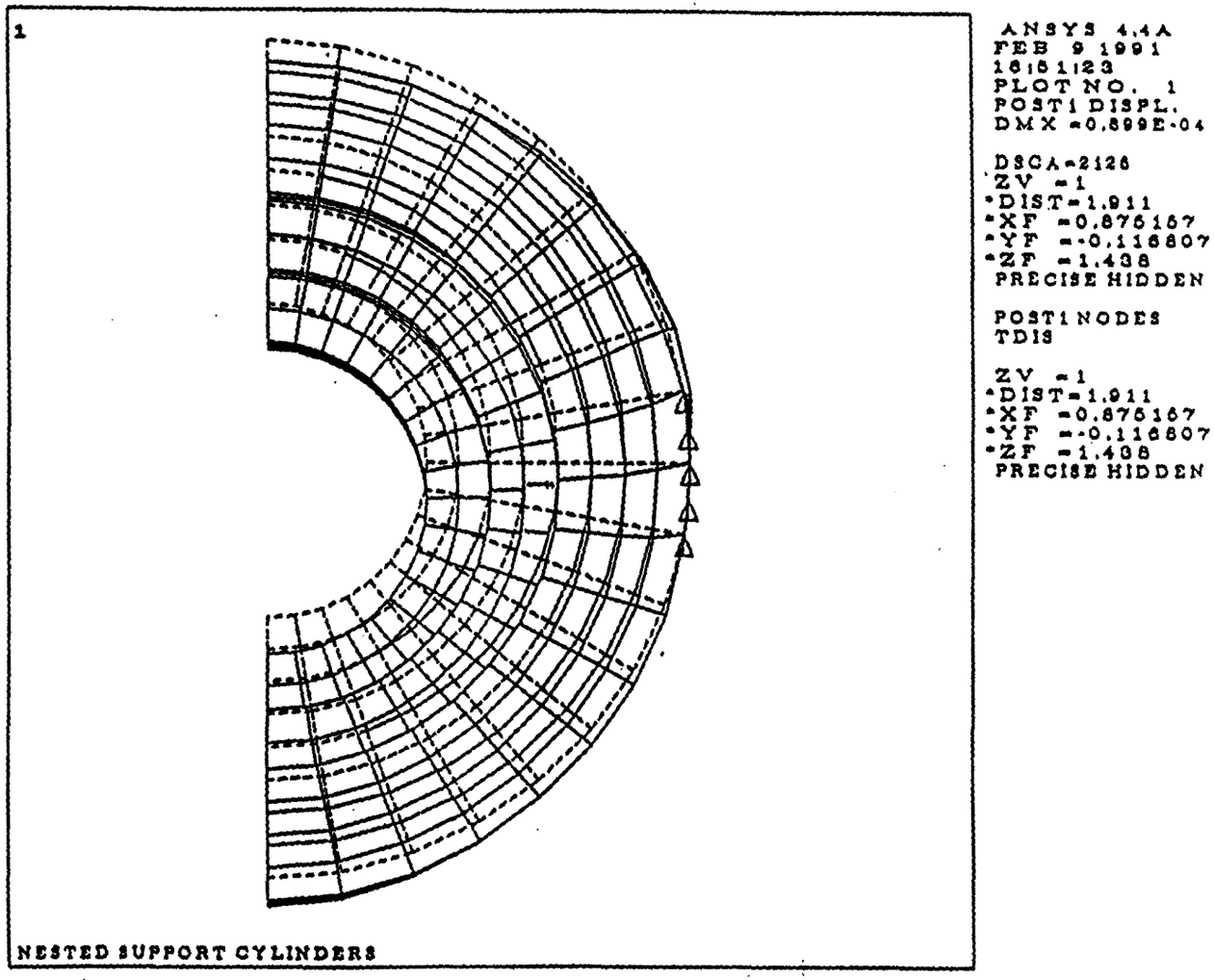

Figure 7: End view of elements displaced by gravity load.

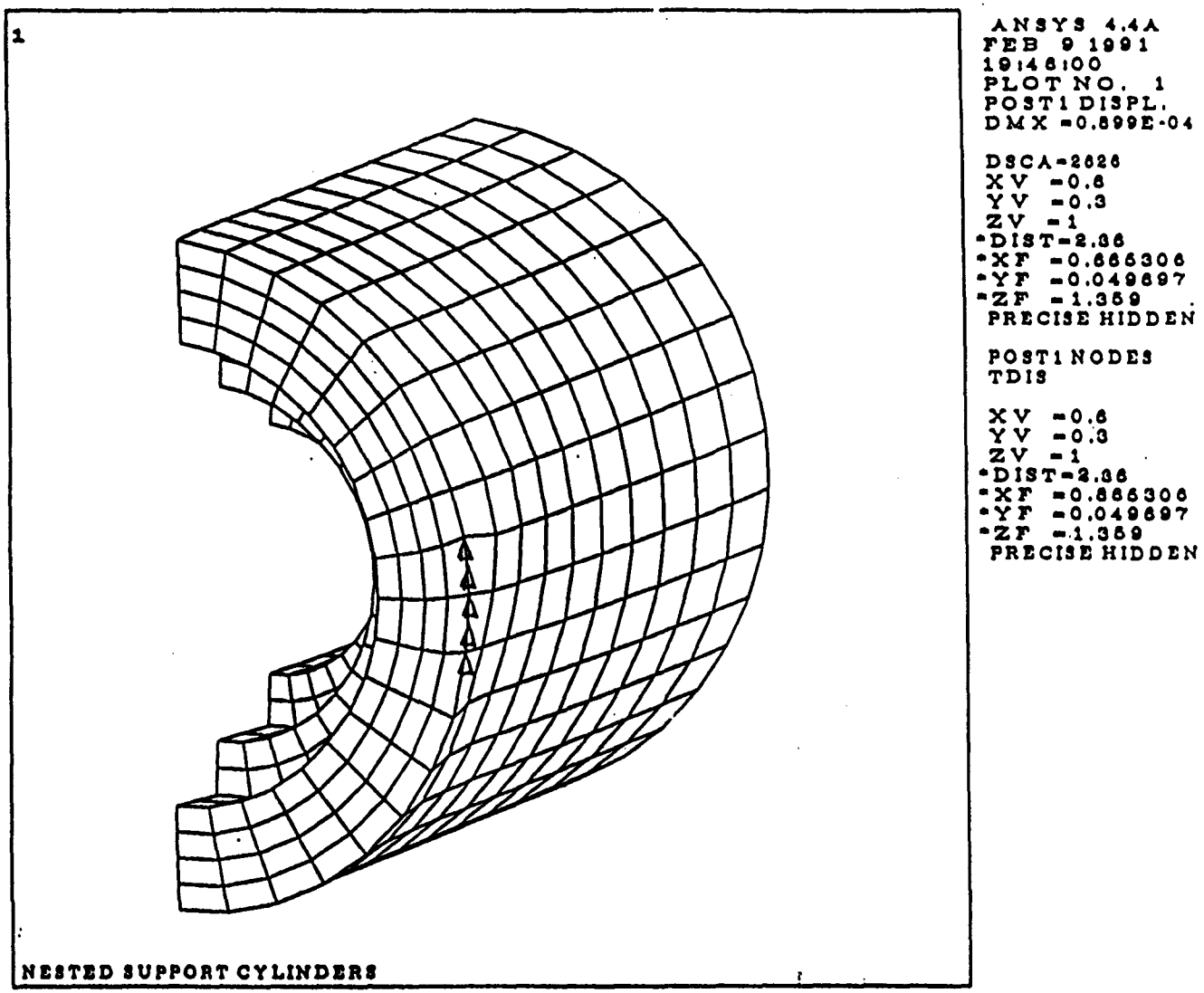

Figure 8: Isometric view of elements displaced by gravity load.

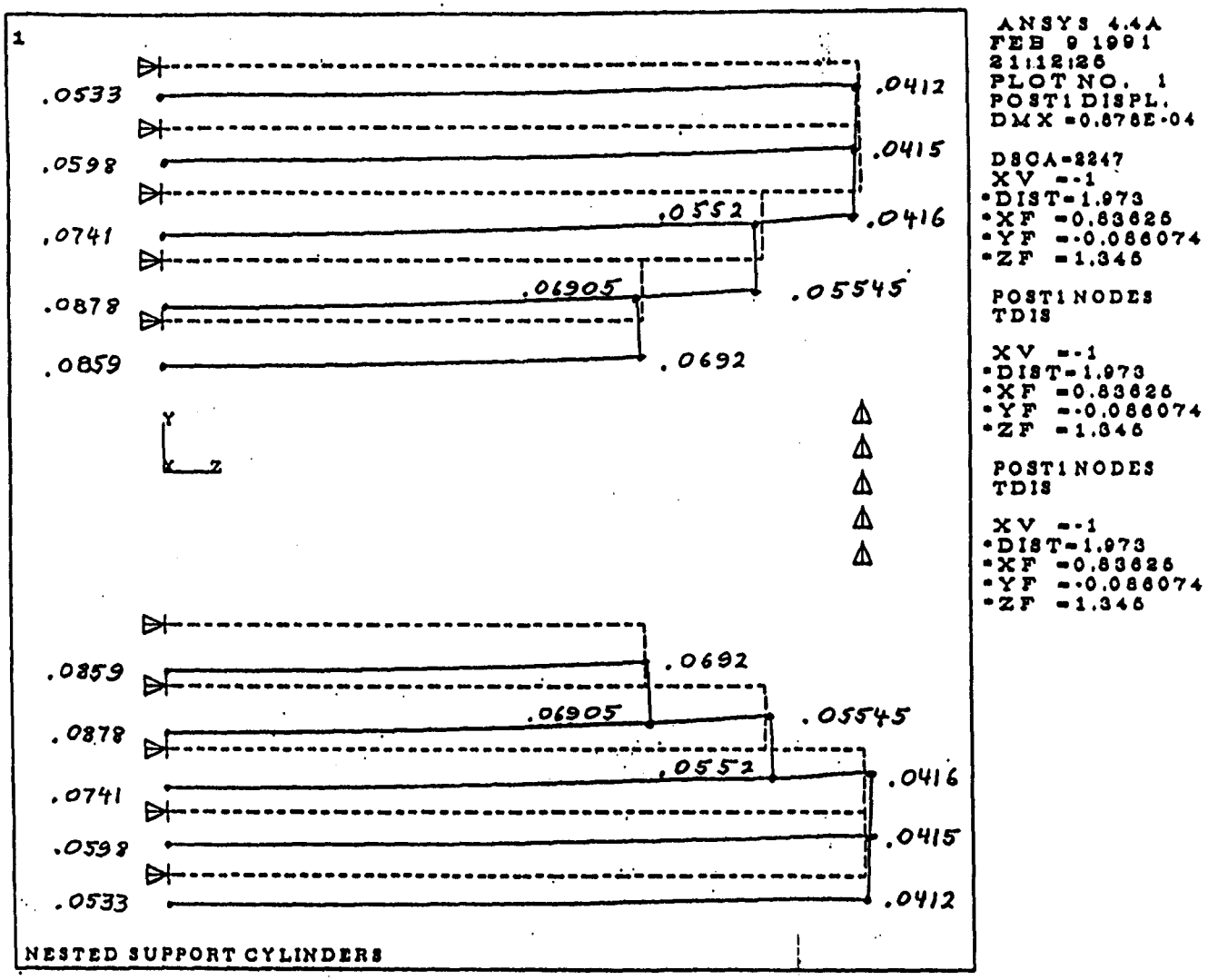

Figure 9: Deadweight displacements (mm) in the Y-Z plane.

FORM S-50-10

Science & Technology Center

TECHNICAL DOCUMENT SUMMARY

Proprietary Class 2

Distribution only within the company. Copies of this document cannot be given or shown to anyone outside the company.

Destroy by tearing into several pieces.

REPORT NO. (RN)	2. PROPRIETARY CLASS (PC)	3. AVAILABILITY (AV)
91-1TM3-ADEMS-M1	2	STC-LIB

4. ORIGINATING SOURCE (OS)	5. CONTRACT NO. (CN)
STC	

6. FUNDING SOURCE/SPONSOR (FS)	7. NOTES (NT)
Corporate	

8. AUTHOR/S (AU)

Hoecker, Donald A.

9. TITLE (TI)

FINITE-ELEMENT ANALYSIS OF DEADWEIGHT DEFLECTIONS OF FIVE-CYLINDER CENTRAL TRACKER SUPPORT STRUCTURE

10. DATE (DA) - YYMMDD	11. PAGES. REFS.. TABLES. FIGS. (PA)
910521	14 p. 0 ref. 0 tab. 9 figs.

12. KEYWORDS (KW)

TRACKING. FINITE ELEMENT. ANSYS. DETECTORS. STRUCTURE. SUPPORT. CYLINDERS

13. ABSTRACT (AB) - PURPOSE. SCOPE. APPROACH. RESULTS. CONCLUSIONS. SIGNIFICANCE

The gravity-induced deflections of the five-cylinder central tracker support structure were calculated using the ANSYS package. The loading included the eight "superlayers" of detector-straw modules, but omitted the silicon tracker inside the innermost cylinder.

TO STC LIBRARY

SEND COPY OF DOCUMENT NO. 91-1TM3-ADEMS-M1 TO:

Name _____

Plant/Div. (Complete Name) _____

Location (City & State) _____

Charge No. _____

(print plainly; this is your mailing label)

☐ Hard Copy* ☐ Microfiche

*No charge until out of stock. Then, hard copy will be furnished only when you request it and include your complete charge number to cover the $0.50/page charge and a $1.00 service charge. Otherwise, once hard copies are gone microfiche copies will be furnished routinely, at no cost.

DISTRIBUTION LIST

STC

S. D. Harkness
C. J. Heyne
D. T. Hackworth
R. L. Swensrud
D. Marschik
J. W. Barkell
R. L. Fuller
H. W. Shaffer
T. L. Michaels
Library (3)

*TDS CARD ONLY